DISSERTATION

THE ROLE OF VITAMIN A AND MYCOBACTERIAL LIPIDS IN THE IMMUNOPATHOGENESIS OF *MYCOBACTERIUM TUBERCULOSIS* INFECTIONS

Submitted by

Macallister C. Harris

Department of Microbiology, Immunology and Pathology

In partial fulfillment of the requirements

For the Degree of Doctor of Philosophy

Colorado State University

Fort Collins, Colorado

Summer 2023

Doctoral Committee:

Advisor: Brendan Podell

Mark Zabel
Marcela Henao Tamayo
Elizabeth Ryan
Randall Basaraba

ABSTRACT

THE ROLE OF VITAMIN A AND MYCOBACTERIAL LIPIDS IN THE IMMUNOPATHOGENESIS OF *MYCOBACTERIUM TUBERCULOSIS* INFECTIONS

Until recently Tuberculosis (TB), *c*aused by *Mycobacterium tuberculosis (Mtb)*, was the deadliest and most ubiquitous infectious disease in the world, infecting an estimated 1.7 billion people as of 2018 and killing 1.6 million people in 2021[1,2]. However, recently COVID-19 has displaced this disease as the most fatal disease, and in the process of doing so has disrupted integral structural apparatuses meant to monitor and treat TB in endemic countries. This degradation has led to an unprecedented rise in disease transmission with a 4.3% rise in infection, with 10.6 million new infections in 2021[3]. Further compounding the problem of this wave of Mtb infections is the rise of multidrug resistant infections, accounting for 3.9% of all new infections and responsible for 14% of Mtb fatalities in 2017[2,4]. With an upsurge in case incidence, faltering antibiotic regimens and a variably effective 100-year-old vaccine, there is a new push in understanding disease comorbidities and alternative treatments for TB.

Although over 1 billion people are presumed to be infected with Mtb, though not all of these patients have clinical TB. In fact, the WHO estimates that 1/3 of infections results in latent disease, a non-clinical phase of the infection which can last in definitively or eventually progress into active, clinical apparent TB. Patient comorbidities have become an intense area of study for further defining the delineating factors that direct infected individuals into either active infection, latent infection, or overcoming the infection. Two defining comorbidities, HIV status and diabetes have been correlated to an increased risk for having progressive TB. HIV infections in itself has been demonstrated to cause a 20 to 30 fold increase risk in clinical manifestations of a Mtb infection, leading to 187,000 deaths in 2021[3,5].

An equally prolific area of Mtb research lies in developing new, efficacious prophylactic and active infection treatment regimens. As previously mentioned, current first line drugs regimens, such as rifampicin and isoniazid, are faltering against multidrug resistant Mtb. Additionally, the only widely available vaccine, the Bacillus Calmette-Guerin vaccine, has high efficacious against several forms of TB, like adolescent TB meningitis, but has variable to low efficacy in control of classic pulmonary TB. These factors are driving research of novel treatments and vaccines that utilize niche characteristics of Mtb, host immunity and overall TB disease pathogenesis to prevent clinical disease manifestation. This thesis centers at the intersection of these two areas of this immunologic research, Mtb comorbidities and investigating a novel branch of immunology, by investigating the immunopathogenesis of TB in relation to a newly recognized comorbidity, vitamin A deficiency, and examining the utility of harnessing a niche lipid-based branch of immunology, CD1 lipid restricted immunology, to combat TB disease progression.

In chapter one, this thesis, stemming from the foundational epidemiological work of Dr. Megan Murray, endeavored to investigate the pathophysiology of vitamin A deficiency and TB in a highly translatable guinea pig model. This novel vitamin A animal model demonstrated that vitamin A deficiency leads to a dysregulated immune system with atypically granulomatous lesions, skewed inflammatory population and contradicting inflammatory gene profiles. These changes lead to progressive clinical disease with increased pulmonary bacterial burden and splenic lesion burdens. Additionally, this chapter was able to demonstrate the ability to partially alter the detrimental effects of vitamin A deficiency during the course of an active Mtb infection via reintroduction of a vitamin A sufficient diet.

In chapter two, this thesis aimed to establish the kinetic expression of CD1 glycoproteins, the lipid antigen presenting molecule homologous to MHC I and the linchpin to lipid-restricted immunology, within tissues of infected guinea pigs. This work demonstrated

CD1b upregulation during the early adaptive immunology phase of infection by profiling of CD1 glycoproteins via flow cytometric analysis, immunohistochemical tissue evaluation, and CD1 specific qPCR profiling. This study went further by not only establishing kinetic expression of this molecule but correlating that expression back to a functional cytolytic response driven by CD1-restricted T cells.

Lastly, chapter three of this thesis aimed to build on the CD1 work in chapter two by assessing the role CD1 lipid restricted immunity plays in the disease pathogenesis of Mtb infections. To performed this work CD1 glycoprotein invivo modulation techniques were perfected via the use of CD1 ortholog specific synthetic antisense RNA, morpholinos, to down regulate CD1 protein translation. To stimulate CD1 expression upregulation, a pleotropic growth factor, FLT3-L, previously shown to upregulate CD1, was utilized. This chapter demonstrated that these compounds were able to alter CD1 expression *in vivo* when evaluated via flow cytometric analysis, immunohistochemically, and via altered qPCR profiles. Additionally, this chapter showed the ability to hamper the functional cytolytic activity of CD1-restricted T cells via CD1 down regulation. Although CD1 glycoprotein expression was altered, disease progression of Mtb in the guinea pig, as measured by lesion and bacterial burden, remained unaltered.

Collective these aims serve as the beginning investigative studies into two unique and potential promising arenas of translational Mtb research. The discovery that vitamin A resupplementation mitigates vitamin A deficiency within chapter 1 has launched a host of different investigations examining the ability of this essential micronutrient to not only prevent clinical TB but to also serve as an immunologic boost to enhance the efficacy of a variety of Mtb treatment regimens. Chapters 2 and 3 reexamined CD1 immunity and the utility of the guinea pig for lipid immunologic work. Though much work has yet to be done in this niche branch of immunology, these chapters lay the ground work and provide the new tools for future studies into potential efficacious and translatable lipid-based vaccination schemes. Tuberculosis,

caused by *Mycobacterium tuberculosis*, is a disease with global ramifications that requires innovative research to meet the new challenges on the horizon. This dissertation looked to meet those challenges by contributing new knowledge to two developing fields of immunologic research while also laying out the tools for future groundbreaking work.

ACKNOWLEDGEMENTS

The work in this dissertation was made possible due to the collective effort of the Podell lab, anatomic pathologists, key collaborators and my committee members. Since joining the Podell lab in 2018, Dr. Brendan Podell has served as a steadfast, and inspirational, mentor. Under his guidance I gained expertise in a host of different arenas of immunologic research and animal model development. His drive for excellence and cutting-edge research pushed me to strive for my best, while allowing for the opportunity to work with leaders in the field of *Mycobacterium tuberculosis* research. I would also like to say thank you to Sarah Cooper, Hadley Gary, Forrest Ackart and James DiLisio. These key individuals taught me the necessarily skills and knowledge in Visiopharm, immunohistochemistry and statistical analysis to complete the heavy bench top work required to complete this dissertation.

Thank you to the CSU anatomic pathology service, for the excellent training and interest you took in my career. This world-renowned training program provided key knowledge for pathology focused diagnostics and research that was not only instrumental for this dissertation, but will carry me into my future profession as a pathology orientated research collaborator and diagnostician. I am especially thankful to my residency mentor, Dr. Paula Schaffer. Dr. Schaffer's interest in my career, both as a diagnostician and leading researcher, have been essential to my journey to become a board-certified anatomic pathologist and in completing this dissertation. Her tireless work ethic and dedication to pathology and resident training served as a daily inspiration for me, and always pushed me to strive for nothing less than excellence.

Thank you to all the collaborators that I met through my work on this dissertation. In particular, I would like to thank Dr. Branch Moody. Dr. Moody, a true leader in CD1 immunology, has taught me so much about this niche branch of immunology while also demonstrating how to

develop and perform world renowned research. Additionally, his novel CD1 reagents, synthetic Mtb lipids and funding were nothing less than instrumental to my own research and the completion of this dissertation.

Thank you to the members of my doctoral committee: Drs. Marcela Henao-Tamayo, Mark Zabel, Randall Basaraba and Elizabeth Ryan. I appreciate the time and interest you invested in my project, and the insightful questions and guidance you provided. Thank you to the NIH T32 training program and the NIH TL1 training program for funding support which made this work possible. Finally, thank you to my resident mates, lab mates, friends and family for the relentless support and inspiration.

TABLE OF CONTENTS

INTRODUCTION

Vitamin A Deficiency and *Mycobacterium Tuberculosis* Infections:

Vitamin A metabolism:

In 2017 Dr. Megan Murray demonstrated, through a nested case-control study design of household contacts, that vitamin A deficient patients correlated with a 10 fold increase in clinical active TB[6]. This correlation, and the inequitable distribution of this micronutrient deficiency, has made it an important risk factor for further investigation[7]. Vitamin A is a pleotropic, fat soluble, micronutrient that is well known for its instrumental role in epithelial homeostasis, vision and organogenesis; however, its role in immunology, and in particular infectious immunology, has yet to be fully elucidated. In collaboration with Dr. Murray, the Podell lab created a vitamin A deficient guinea pig model that replicates human subclinical vitamin A deficiency. Utilizing this novel animal model this dissertation aimed to answer key questions about this comorbidity including: changes in lesion burden, lesion morphology, ability of the bacteria to systemically spread, and overall bacterial burden. Additionally, we aimed to monitor the status and movement of vitamin A in sufficient animals to comprehend how and where vitamin A is utilized kinetically during a Mtb infection. By understanding the intricates of the immunopathogenesis of this essential vitamin we can aim to mitigate negative effects, or potentially harness vitamin A to aid in vaccinations or treatment regimens to provide a boost in immunologic functionality in a time of need. However, to accomplish this aim a basic understanding of vitamin A metabolism and functionality was needed.

Vitamin A, functionally known as retinol, is a lipid soluble vitamin that is essential for several different systems within the body. The body has evolved a complex system of metabolic pathways and mechanisms of movement in order to delivery retinol to cell of need and facilitate its essential functions. The only sources of vitamin A are dietary and include retinyl palmitate or

beta-carotene, which enterocytes can convert into retinol[8]. Once ingested by enterocytes the retinol is brought and stored in hepatic stellate cells in the form retinyl ester in lipid droplet formation[9]. When systemically needed retinyl ester is converted back to retinol, bond to retinol binding protein 4 (RBP4), a small molecular weight protein, and released into circulation. Importantly, RBP4 is highly regulated and linked to levels of retinol release, providing a potential monitoring of vitamin A movement[10]. Once released holo-RBP4 binds with transthyretin, which prevents filtration of holo-RBP4 through kidney glomeruli. Retinol is then brought to a variety of extra-hepatic cells via Stra6 with the apo-RBP4 dissociating from transthyretin and thus excreted through the kidney- providing another parameter for monitoring vitamin A movement.

After entering the cytoplasm of target cells, retinol needs to be converted into a biologically functional form. This required a series metabolic steps involving the conversion of retinol to retinal via retinol alcohol dehydrogenase, and then the rate limiting conversion of retinal to either all trans-retinoic acid (ATRA) or 9-cis retinoic acid (9-cis) acid via retinal aldehyde dehydrogenase[11]. ATRA and 9-cis are the biologically active form of vitamin A, with ATRA being the predominant form, working at the level of the nucleus to stimulate cellular effects

Once ATRA or 9-cis transmigrates from the cytoplasm to the nucleus they induce cellular change via enhancement of transcription of genes via the binding to retinoic acid receptors (RAR), that can bind to ATRA, or retinoic X receptors (RXR), that can bind with 9-cis[12]. Once these heterodimers are formed, they can go to bind with retinoic acid receptor elements (RARE) to induce increase target gene expression. Several isoforms of RAR and RXR exist to diversify the role that vitamin A can play in cellular function, growth and overall homeostasis **(Fig. 1)**.

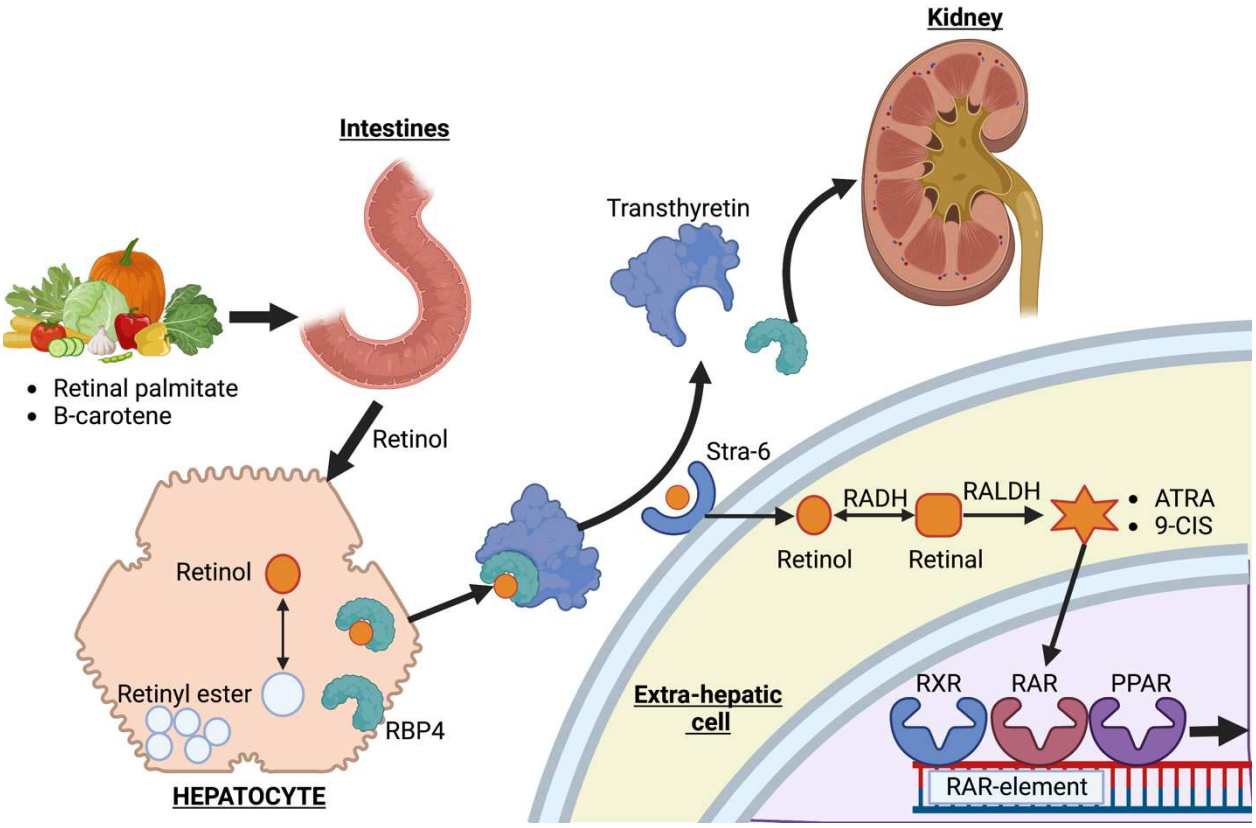

Figure 1. **Retinol metabolism and movement.** Dietary sources of vitamin A are absorbed by intestinal enterocytes, converted in to retinol and brought to the stellate cells and hepatocytes in the liver. Hepatic retinol is then either stored, as retinyl ester, or released into circulation via binding to retinol binding protein (RBP). Once in circulation RBP binds to tranthyretin to prevent premature filtration in the kidney. The RBP-transthyretin complex deposits retinol to the cytosol of target cells via stra-6. Once in the cytoplasm retinol is converted, in a 2-step enzymatic reaction, to biologically functional forms ATRA or 9-cis. These functional forms of retinol then transmigrate to the nucleus to dictate transcriptional modification via DNA located retinol receptors (RAR, RXR or PPAR). Figure made utilizing Biorender.

Vitamin A immunological functionality:

Although the intricacies of vitamin A metabolism and its role in vision and cellular growth has been established its role in immunology is still an area of investigation. However, vitamin A has been found to have a key role to T cell diversity, maturation, and migration. Specifically, vitamin A has been found to be essential for Th17 cell differentiation and CD4+ T cell mediated

adaptive immune responses[13]. Not only does vitamin A seem to be an essential driver for Th17 differentiation but it also seems to skew inflammatory T helper cells from a Th1 to Th2 lineage[14,15]. In additional retinol is essential for T cell functionality, with several studies demonstrating retinol is critical for CD4+ T cells processes. In one study, T cells in a vitamin A deficient state are less efficient in polyclonal activation and T cell receptor interactions[16].

Vitamin A has profound effect on histiocytic cell lineages, with dendritic cells and macrophages acting as major producers of ATRA at sites of inflammation with studies demonstrating RXR heterodimerization being essential for macrophage survival and pathogen killing[17]. Retinol acts as a major regulator for dendritic maturation and inflammatory functions. Under non-inflammatory environments retinol signals induce dendritic apoptosis. However, under the influence of inflammatory cytokines retinol drives the maturation of dendritic cells and increased expression of MHC II complexes[18]. Despite this knowledge there is an ongoing debate within the literature as to whether retinol is acts as a pro-inflammatory or anti-inflammatory mediator[19,20].

Retinol not only serves as an important nuclear factor for cellular differentiation and overall functionality, but has also plays a role in cellular migration, particularly in mucosal associated immunity. Retinol binding to RARX nuclear receptors in T cells displays increased expression CCR9 and $\alpha 4\beta 7$ integrins, essential for mucosal homing of inflammatory cells. Retinol binding protein itself has been shown to act as a potent chemokine for CXCR3 and CXCR5 on dendritic cells, driving them to the site of inflammation and retinol use[21].

Cumulatively the literature demonstrate that vitamin A plays a complex, and at times varied, role in immunology. Retinols driving of both T cell and dendritic cell differentiation and functionality and its potent chemotactic abilities no doubt plays a complex role in infectious and bacteria disease pathogenesis. In fact, several studies have shown a precipitous decrease in retinol serum levels in the face of acute immunity[22,23]. Whether that corresponds to utilization of

retinol at the site of inflammatory or lack of movement from hepatic storage needs further investigation. By further exploring retinol's complex role in immunologic processes, the better we can understand the effects of vitamin A deficiency for a myriad of infectious process.

Vitamin A role in *Mycobacterium tuberculosis* infections:

In-depth investigation of the intricate relationship of vitamin A status and Mtb infections is just now becoming an intense area of research. However, several studies have further investigated the role of vitamin A plays in the pathogenesis of TB. Invitro studies illustrate that ATRA inhibits the growth of Mtb of intracellular macrophages via the upregulated of NPC2 gene, a cholesterol regulator[24]. *In vivo* models of transgenic mice furthered this work, establishing the increased efficacy of anti-tuberculosis drugs with ATRA coadministration[25]. Lastly, several observational human cohort studies found that healthy individuals had a significantly higher retinol serum levels compared to TB infected vitamin A sufficient individuals[26]. Collectively, these findings indicate that while vitamin A deficiency may serve as a major comorbidity to clinical active TB, correct supplementation of vitamin A may not only mitigate this comorbidity but act as a synergistic component to current and developing Mtb treatment regimens.

CD1 Immunology and *Mycobacterium Tuberculosis* Infections:

CD1 immunology background:

A hallmark of cellular immunity is the key interaction of antigen presenting cells (APCs) with T cells via MHCII glycoproteins and costimulatory molecules to drive leukocyte proliferation, cellular recruitment, and systemic changes via cytokine and chemokine release. The linchpin to this immunologic cascade, is the detection of protein antigens followed by loading of those proteins on to MHC complexes to stimulate T cells, via MHC class II, or allow for cytotoxic targeting of potentially infected cells, via MHC class I. This well-established dogma of protein based immunologic detection and response was, until recently, thought to serve as the only

source of APC driven T cell stimulation, primarily functioning under the adaptive immune umbrella. However, in the early 1990s CD1 glycoproteins were discovered, shifting that dogma and further expanding our understanding of immunologic detection of immunogenic antigens[27].

CD1 glycoproteins represent a family of antigen presenting, membrane bound proteins with homologous structuring to MHC class I found on a variety of APCs with the ability to present antigens to a variety of CD1-restricted T cell subsets. In contrast to MHC, CD1 is uniquely able to load and present a host of exogenous and endogenous lipid-derived antigens[28,29,30]. Further contrasting MHC complexes, CD1 glycoproteins have a highly conserved tertiary structure, binding motifs, and ability to present antigens to CD1-restricted T cells[31–33]. This non-polymorphic characteristic allows for a unique opportunity as we investigate and try to harness this branch of immunity for both infectious and autoimmune disease processes. First, the conserved nature allows for clear identification of specific CD1 isoforms with specific and conserved binding grooves, and how these binding capacities interact, load and present specific lipid antigens (**Table 1)**. Second, the highly conserved nature allows for the possibility of particularly efficacious, population wide, therapies with little individual to individual variability.

Since the initial discovery of CD1 glycoproteins five isoforms have been discovered CD1a-e in humans[34–36]. These isoforms have been divided into 2 functions groups, group 1 including CD1a-c and group 2 CD1d. In brief, group 1, found on APCs, thymocytes and specialized endothelium, have been correlated to infectious agent responses, such as *Mycobacterium tuberculosis* (Mtb), and exhibit inducible expression when lipid antigen is detected[37–40]. Group 2, constitutively expressed on a variety of cells types, is correlated to primarily endogenous lipid detection; though new studies indicate a potentially larger role in microbial surveillance[41–43].

A major blockade to investigations into this distinctive branch of immunology is the relative lack of a highly translatable animal model. Small rodent models, under the suborder of myomorpha, rats and mice, lack the CD1 group 1 isoforms making these frequently utilized animal models ineffective for in-depth and translatable CD1 investigations. However, suborders lagomorphs, represented by rabbits, and cavia, represented by guinea pigs, have both functional groups with a similar isoform repertoire to humans[44–46]. Several studies have utilized the guinea pig to further elucidate the functionality of CD1-restricted lipid immunology and the role of CD1 in several disease processes, particularly the lipophilic bacteria *Mycobacterium tuberculosis*.

In this review, we will evaluate the current comparativeknowledge base of CD1 glycoproteins both in humans and in the guinea pig. We then will examine the current understanding of CD1-restricted immunology, emphasizing CD1 protein to CD1-restricted T cell interaction and CD1 T cell diversity and functionality. Finally, we will discuss the current understanding of CD1 immunology in relation to Mycobacterium tuberculosis infection in the human and guinea pig as well as highlighting the current gaps in knowledge in relation to CD1 immunopathogenesis.

Table 1. Currently known lipid specific antigens for individual CD1

CD1a		CD1b		CD1c		CD1d	
Antigen	**Origin**	**Antigen**	**Origin**	**Antigen**	**Origin**	**Antigen**	**Origin**
Sulfatide	Self	Sulfatide	Self	Sulfatide	Self	Sulfatide	Self
Phosphoglycerolipids	Self/ foreign	Gangliosides (GM1, GD1a, GD1b, GT1b, GQ1b	Self	Mannosyl-β1-phosphodolichol	Self	Isoglobotrihexosylceramide	Sef
Didehydroxymycobactin	Mtb	Glucose monomycolate	Mtb	Unknown antigen on human APC	Self	α-galactosylceramide	Self
wax ester	Self	Lipoarabinomannan	Mtb	Mannosyl-β-1 -phosphomycoketide	Mtb	α-galacturonosylceramide,	Bacteria
squalene	Diverse	Phosphatidylinositolmannosides	Mtb			α-glucuronosylceramide	Bacteria
		Diacylsulfoglycolipid	Mtb			1,2-diacyl-3-*O*-α-galactosyl-*sn*-glycerol	Bacteria
		Sphingomyelin	Self			phenyl-pentamethyldihydrobenzofuran sulfonates	Bacteria
		Mycolic accid	Mtb			Sphingomyelin	Self
		Lipomannan	Mtb			Gangliosides (GM1, GD1a, GD1b, GT1b, GQ1b	Self
						Cardiolipon	Self
						Phosphoglycerolipids	Self/ foreign
						Lyso-phospholipids	Self/ foreign
						Ether lyso-phospholipids	Self
						α-Glucosyldiacylglycerol	Bacteria
						Pentamethyl-dihydrobenzofuran sulfonate	Chemical

CD1 structure and assembly:

Structurally all isoforms in humans have homologous structuring to MHC class 1 molecules with three extracellular domains composed of a heavy chain, composed of α_1, α_2 and α_3 that non-covalently bind β_2 microglobulin (**Fig, 2A)**[28,47]**.** One of the main questions initially posed is how these genetically non-polymorphic glycoproteins bind to a large array of endogenous and exogenous lipids; while in contrast MHC glycoproteins rely on genetic polymorphism for diverse antigen surveillance. This question was answered via creation of the crystal structure of each CD1 isoform. It was determined that each isoform has a binding channels A' and F'. With CD1b having two additional binding units the channel C' and connecting tunnel T'. Regardless of composition, all channels are found deep within the α_1, α_2 molecules, in contrast to the superficial binding apparatus of MHC complexes[48] (**Fig. 2C)**. These binding channels bind and hold varyingly long hydrophobic alkyl tails, while typically leaving a hydrophilic head group exposed for possible T-cell receptor (TCR) interaction. These hydrophilic head groups are commonly composed of carbohydrate, phosphate, sulfate or peptide moieties. To aid in binding of a variety of lipid antigens, the CD1 glycoproteins utilize endocytic environments to expose key structures of lipids and assist in loading of large hydrophobic lipid tails into binding grooves[49–51]. To further direct their cellular trafficking many CD1 isoforms in the human, CD1b, c and d, have intracytoplasmic YXXZ tyrosine motifs. Whereas the Y would represent a tyrosine, and the Z representing a large hydrophobic amino acid[47,52,53].

Guinea pigs have both group 1 and group 2 CD1 glycoprotein functional groups, homogenous to humans. Further investigation reveals that guinea pigs have the CD1 isoforms; CD1b, CD1c, CD1d and CD1e, missing the CD1a isoform that are found in both humans and rabbits. Additionally, and in contrast to humans, guinea pigs have 4 orthologs of CD1b, CD1b1-4, and 3 orthologs of CD1c, CD1c1-3 **(Fig. 2C)**. 6 of the 7 of these group 1 orthologs CD1

complexes have equivocal tyrosine motifs[54,55]. Several studies have identified structural differences in these orthologs, leading to functional differences and thus presenting plausible reasoning for why the guinea has such a wide group 1 CD1 repertoire[56,57].

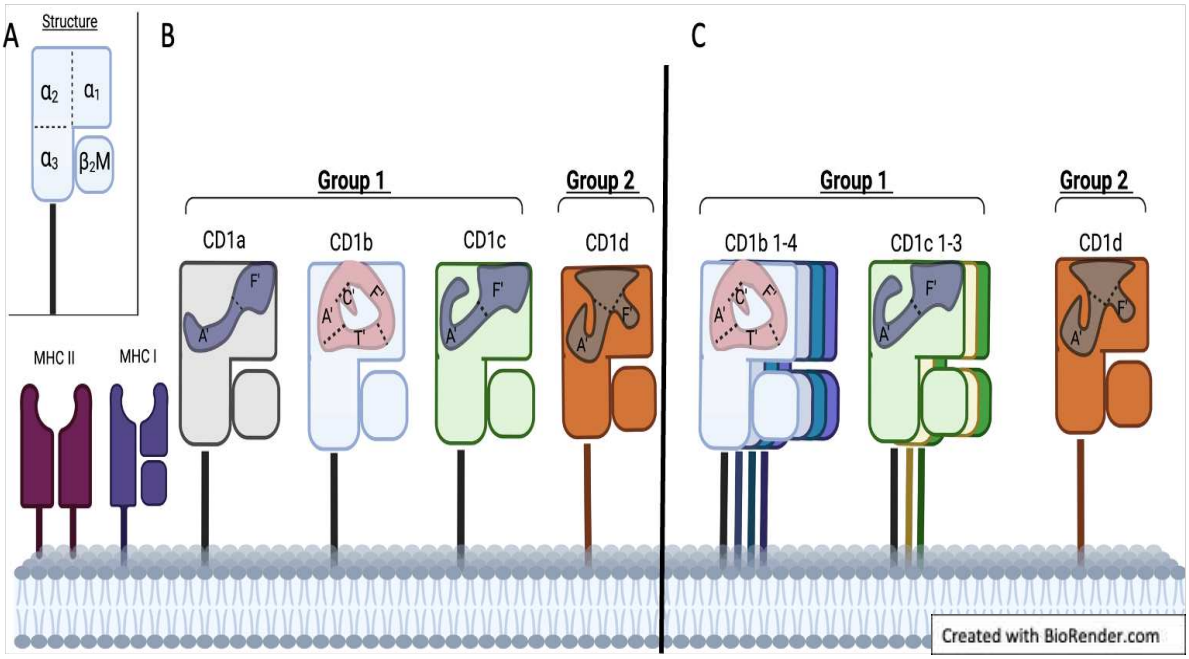

Figure 2. Human CD1 structure and isoform binding grooves. A) CD1 is homologous to MHC I and composed of a cytoplasmic tail, 3 α subunits and heavy β2 microglobulin. B) each CD1 isoform has a different binding groove composed of a combination of A', F' and C' Channels with CD1b having a tunnel connects the A' and F' channels. Each isoform has a different binding capacity with CD1a having the smallest capacity and CD1b having the greatest capacity. C) Guinea pigs have similar CD1 isoforms and propose binding grooves to humans. However, guinea pigs have additional orthologs of CD1b, CD1b1-4, and CD1c, CD1c1-3, compared to humans. Additionally depicted in B) and C) are the two known function groups of CD1, group 1 composed of CD1a-c and group 2 composed of CD1d. These functional groups differ in overall expression and specific T cell subset that they interact with. Created using Biorender

CD1b:

CD1b isoforms in all species have the largest binding apparatus, measuring 2230Å, of all CD1 complexes, allowing for binding of large carbon alkyl tails up to 80c[58]. The binding region contains three 3 binding channels A', F', C'. Channels A' able to hold 17.3 carbons, in α2, and F' able to hold 12 carbons, in α1, are connected by a tunnel structure T' able to hold 23 carbons.

The T' channel connecting the deep aspect of the A' channel to the superficial aspect of F' channel allows for escape of large alkyl tails through the F' portal[28,59–61]. The unique C' channel allows for binding smaller lipids molecules, 16 carbons. Adding to the complexity of the binding groove of CD1b is a secondary entry and exit portal, C' portal, at the end of the C' channel. This double opened channel has been coined an "escape hatch" for large alkyl chain lipids that can't fit within the confines of the A', F' and C' channels. This hydrophobic channel complexity allows for CD1b to have a large diversity in binding potential of exogenous and endogenous lipids. In essence, CD1b unlike other CD1 isoforms is not confined to the volume of the binding groove due to its multiple escape routes of large alkyl tails[59–61]. Lipid antigen detection and binding is broad, including phospholipids, glycosphingolipids, lipoglycans, mycolates, and diacylated sulfoglycolipids.

Guinea CD1b and the related orthologs, CD1b1-3, have similar binding channel structuring and binding potential as human counterparts. However, it has been exhibited that guinea pig CD1b4 lacks a cysteine amino acid in positions 131 and 145, which make up the functional structure of the C' portal; likely indicating an inability of this ortholog to bind large alkyl chain lipids like the human CD1b isoform. This difference of structure requires further investigation to determine differences in lipid binding ability and overall functionality[48,54].

CD1c:

Compared to other CD1 isoforms CD1c has an intermediate size binding capacity of 1780Å[62]. The binding apparatus is composed of two binding channels A' and F'. The F' channel along the superficial aspect of α1 has the largest portal opening, likely allowing for presentation of potentially larger head groups and lipoproteins[63]. The A' binding channel has a convoluted, coiled shape that has been demonstrated to be essential for positioning alkyl tails appropriately for presenting the head group through the F' portal and interaction with CD1c-restricted T cell receptors[64]. This structure allows for binding and presentation of glycosphingolipids,

phospholipids, mycoketides, phosphatidic acids and a host of un-defined headless lipids. Structurally no differences in the guinea pigs three CD1c orthologs have been appreciated or reported in the literature.

CD1d:

CD1d has been identified in a variety of species, including humans and mice. It is the newest discovered CD1 isoform for the guinea pig. Like CD1c the binding channels include A' and F', with F' being superficial and in the α1 glycoprotein. In the human the overall binding groove is smaller than CD1b and CD1c with a total volume of 1650Å[63,65]. The A' channel has a counter clockwise orientation, and may have a similar function to the A' channel in CD1c for ensuring properly orientated of the hydrophilic head of the lipid. Maximally the A' channel can bind a 24-carbon alkyl chain. The F' channel in contrast is straight in configuration, and can maximally bind 18 carbon alkyl chain[28,65]. This asymmetry allows for high affinity binding of certain lipids such as glycolipids such as α-galactosylceramide, an extensively studied stimulatory lipid, and sphingolipids[65,66]. Functional CD1d genes have been established within the guinea pig; however, the crystal structure of this species has yet to be investigated within the literature[67].

Isoform specific cd1 cellular trafficking:

Assembly and initial membrane presentation of CD1 glycoproteins is conserved among all isoforms and orthologs regardless of species. Initial assemble of CD1 occurs within the endoplasmic reticulum, requiring endogenous hydrophobic lipid chaperones to occupy the binding grooves, loaded via microsomal triglyceride transfer protein, to mediate proper folding and maturation[68,69]. Following maturation, CD1 glycoproteins are glycosylated which allows for the association of CD1 with ER chaperone proteins calnexin and calreticulin[49,70,71]. Once associated with these chaperone proteins CD1 quickly transmigrates from the ER to the Golgi

apparatus and then to the plasma membrane surface. Once at the cellular membrane each CD1 isoform in the human, and to a degree each ortholog in the guinea pig, have their own unique intracellular endosomal trafficking pattern.

Once at the cell membrane all CD1 isoforms enter the endosomal and endosomal recycling apparatuses, via clathrin coated pits. Although there is evidence that while on the cellular surface CD1 glycoproteins can bind to extracellular lipids within the cellular milieu, via CD1a and c[72,73]. It has been determined that some isoforms such as CD1b and d have significantly lower efficacy of binding of antigen at the cell membrane when compared to binding within the intracellular environment[74–76]. Several studies have examined the need of endosomal compartmentalization for highly effective lipid binding. Several studies postulate this being due to the need for intracellular processing of lipid antigens to allow for the loading to non-variant binding sites, the needed mechanism to remove the preloaded endogenous lipids during CD1 maturation in the endoplasmic reticulum, or in the case of late endosomes the need of an acidic environment to aid in the loading of the lipid antigens via denaturing of the CD1 binding groove. This ability to survey for lipids both on the cellular membrane and heighted surveillance via endocytic and phagocytic pathways allows complete monitoring of both endogenous and exogenous cells throughout the cellular compartments[77–80].

This type of cell surface-endosomal trafficking of CD1 glycoproteins is unique when compared to MHC class II proteins. In immature dendritic cells MHC class II is typically found in unique intracellular lysosome termed MHC class II compartment (MIIC), where several CD1 isoforms are also found. Upon activation and maturation of dendritic cells MHCII has a significant shift from MIIC to the cell surface with relatively little reinternalization into the intracellular space. However, upon activation CD1 isoforms in dendritic cells were still observable on the cell surface, in recycling endosomes, in early endosomes, in late endosomes and in MIIC[81,82]. These studies indicate that CD1 traffics via independent mechanisms to MHCII

and may indicate the overt importance of CD1 distribution throughout many cellular compartments to provide complete lipid surveillance[52,83].

As mentioned, each CD1 isoform within the human has its own cellular-endosomal trafficking patterns after reaching the cellular surface **(fig. 3)**. These unique trafficking patterns centers on previously eluded to cytoplasmic tail tyrosine YXXZ motif. This endosomal tagging motif binds to the U-subunit of adaptor protein-2 (AP-2), which directs the glycoprotein to early endosomal structures. Certain CD1 isoforms can further be distributed via the hydrophobic amino acid on the cytoplasmic tail motif allowing for association of the U-subunit in the AP-3 complex. AP-3 directs proteins to the late endosome, MIIC, or phagolysosome. Regardless of the distribution within endosomal compartments all CD1 isoforms make their way back to the cellular surface with either the inert endogenous ER loaded lipid or a lipid antigen that is permissive for interaction with the CD1-lipid restricted TCRs[48,57,84]. Guinea pig CD1 isoforms has similarly cell trafficking; however, individual orthologs within CD1b and CD1c isoform families have trafficking differences which leave questions about the functionality of these orthologs.

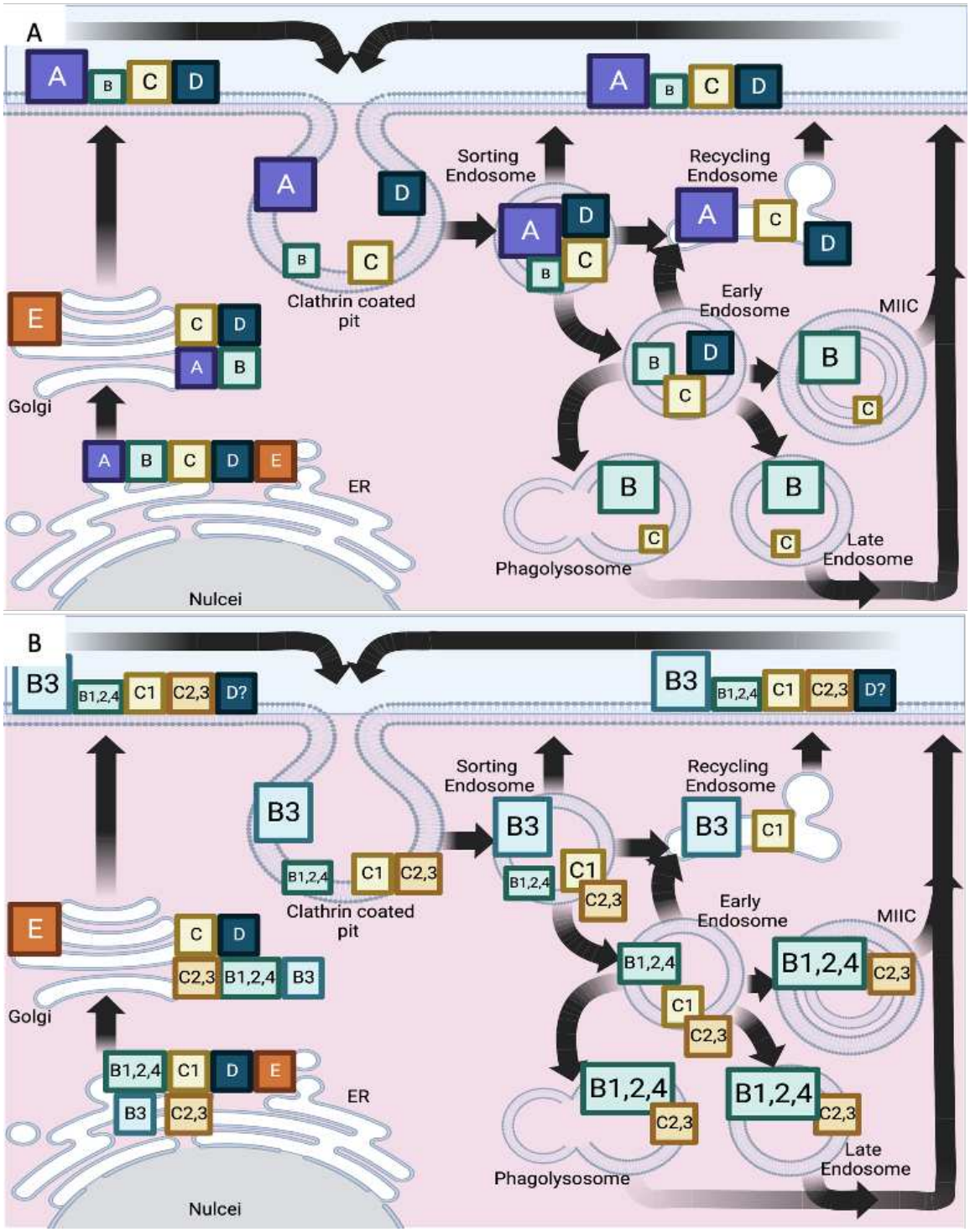

Figure 3. ***Human and guinea pig specific isoform specific cellular trafficking.*** A) Human CD1 isoform specific trafficking into early endosomes, late endosomes, phagolysosome or MIIC compartments. B) Guinea pig isoform and corresponding ortholog specific cellular trafficking into early endosomes, late endosomes, phagolysosomes, or MIIC compartments. Regardless of trafficking all CD1 complexes return to the membrane surface for interaction with CD1-restricted T cells. Created using Biorender.

CD1b:

In humans, that only have one CD1b ortholog, CD1b has the tyrosine YXXZ motif that can interact with both AP-2 and AP-3. Thus, CD1b has been observed on the cellular surface, as well as within early and late endosomes. This isoform favors late endosomal localization, with a relatively small ratio of proteins appreciated on the surface or in early endosomes **(Fig. 3A**). This late endosomal distribution seems to be essential for CD1b lipid loading due to its large binding groove. Several studies have demonstrated CD1b relative inability to load large alkyl chain lipids along the cell surface. This efficacy dramatically changes within the late endosome within an increasingly acidic environment leading to denaturing of the CD1 binding groove. The denaturing seems essentials for large lipid hydrophobic tails to properly access and bind to the large hydrophobic groove of CD1b[74,76].

In contrast to human's guinea pigs have 4 CD1b orthologs, CD1b 1-4. Three of the four CD1b orthologs, CD1b1, CD1b2 and CD1b4, have similar YXXZ motifs to humans and have been demonstrated to have similar late endosomal trafficking patterns. Specific studies examining CD1b1 find this ortholog colocalizing with MHC class II proteins within late endosomes[71](Fig. 3B).

Uniquely, CD1b3 lacks this essential tyrosine motif and has unique cellular trafficking pattern. The change in the motif is due to a single point mutation from TAT, codon for tyrosine, to TGT, a codon for cysteine. CD1b3, lacking the tyrosine motif is found almost exclusively on cellular surface and superficial recycling endosomal structures. This type of trafficking mimics that of human CD1a, which is the only CD1 glycoprotein lacking the tyrosine motif in humans. Interestingly, guinea pigs lack CD1a, which may indicate an evolutionary adaption of CD1b3 for increased surface and recycling endosomal lipid antigen surveillance, like human CD1a. In humans, it has been demonstrated that CD1a shifts from the cell surface to predominately early

endosomal compartment during Mtb infections[85]. Additional studies are needed to investigate if a similar shift with stimulation is appreciated in the guinea pig CD1b3[54,55,71].

Further contrasting gpCD1b3 from other orthologs is its high, constitutive expression on B cells in naïve animals[71,86]. Although CD1 expression has been documented in humans B cells, this type of uniform expression is unique to guinea pig CD1b3 glycoproteins. The function of this expression and type of trafficking, with such a large binding groove, needs further investigation to elucidate overall significance.

CD1c:

In humans CD1c has the YXXZ motif and thus are found both on the cell surface and withinendosomal compartments. Unlike CD1b, CD1c does not interact with AP-3 thus is primarily observed within the early endosome before returning to the cell surface via the early endosome compartments[62,87]. Additionally, when compared to CD1b, CD1c had a high ratio of cell membrane to endocytic localization; whereas CD1b demonstrates an antithetical distribution. Interestingly, A small subset of CD1c is found in late endosomes, and colocalizing with MHC class II. This finding likely points to a secondary, though unknown, mechanism for endosomal distribution of CD1c[57,62]. Studies have investigated the need of endosomal location of CD1c and the ability of CD1c to present lipid antigens. This included blocking endosomal acidification and observing that antigen presentation via CD1c was relatively unaffected, while decreasing CD1b presentation. This study further adds to the credence that CD1b and CD1c survey different cellular compartments, and that like CD1a, CD1c can effectively bind lipids within the cellular milieu[88].

Less is understood about guinea pig CD1c cellular trafficking, with one major limitation being limited antibodies to colocalize all three CD1c orthologs[89]. However, two studies were able to determine that CD1c2 and 3 have similar trafficking to human CD1b[54,71]. This could

indicate that these guinea pig CD1c orthologs are able to interact with AP-3, or rely heavily on an unknown mechanism to descend into deeper intracellular compartments. Additional studies to localize CD1c1 trafficking as well as the significance of deeper trafficking of CD1c2 and 3 are needed.

CD1d:

CD1d has been most extensively studied in the mouse and human, and is the most recently identified CD1 glycoprotein in the guinea pig. Within humans CD1d contains a tyrosine motif that lacks the inability to bind to the AP-3 endosomal tag that drives late endosomal distribution. This indicated that human CD1d is predominately found on the cell surface and early endosomes matching a similar CD1c distribution[90,91]. Several studies have affirmed this functional distribution with loading and presentation of endogenous lipid not being affected by endosomal trafficking[56]. However, exogenous lipid presentation does require some degree of endosomal trafficking, and is markedly decreased when the tyrosine tail motif is removed[88].

This trafficking stands in marked contrast to mice, which have a motif that can bind to the AP-3 endosomal tag, thus allowing for late endosomal trafficking. Studies in the mouse found that both endogenous and exogenous lipid presentation required endosomal trafficking. There is speculation on the ability of mouse CD1d to traverse all endosomal compartments to compensate for the lack of other group 1 isoforms of CD1[65,92]. For the guinea pig, and other animals, one study by Lorringh Van Beeck Et al, found functional CD1d transcripts; however, additional studies are required to elicit the cellular trafficking and functionality of this CD1 isoform in the guinea pig[67].

CD1e:

Relatively little is known when comparing human and guinea pig CD1e glycoproteins. In brief for what has been established in humans, CD1e has been shown to have a unique trafficking

pattern compared to other CD1 isoforms. Unlike CD1a-d, CD1e never migrates to the cellular surface to be continually cycled through endosomal pathways; but rather accumulates within the Golgi apparatus after transmigrating from the ER. Only in maturing and/or activated antigen presenting cells does this accumulation shift from the Golgi apparatus to late endosomal compartments[93,94]. This continual internalization and movement to endosomes adds to the theory that both insoluble and soluble CD1e could play an invaluable role in the lipid loading process for CD1b and Cd1d glycoproteins[95,96].

Lipid-antigen presentation and TCR interaction:

Several different antigen presentation models have been proposed and validated to address the central question of how highly conserved antigen presenting proteins, such as CD1, can present a diverse array of lipids and stimulate polyclonal CD1-restricted T cells. The first discovered model, examining CD1b and CD1d, is akin to the MHC antigen presentation dogma. In this model CD1b loads a lipid antigen via the lipid's hydrophobic alkyl tails, which exposing its unique head group. A heterodimer TCR would interact with this unique head group and CD1 protein to stimulate antigen specific T cell activation[97–99]**(Fig. 4D)**.

A second validated TCR interaction model, is the model of interference. This model examines CD1a binding ability and noted that many of CD1a loaded lipids lack large head groups for TCR interactions[100,101]. Further investigation of the crystal structure of the TCR and CD1a interaction suggested that the TCR interacts with CD1a protein itself and not the specific lipid antigen. In anthesis to the head group TCR model, it was discovered that lipids with large head groups interfere with TCR CD1a interaction. The key to this theory lies in the asymmetry of the F' portal for antigen binding (**Fig. 4A)**. Small lipids with little to no head groups bind, without protruding headgroups from the F' portal on the left of α1, leaving α2 exposed for TCR

interaction; however, a large lipid with a prominent head group will protrude from the F' portal and block intimate associate of α2 subunit of CD1a with the TCR[98,100,101].

A final and emerging TCR interaction model relies on the theory of CD1 remodeling. This theory is based on antigen presentation from CD1c. It postulates that binding of a lipid in the CD1c binding groove modifies CD1c, opening a new portal on the right side of α2, the G' portal. This structure change to CD1c allows for speculation that the lipid antigen structures changes CD1c leading to the ability to interact with CD1c restricted TCRs, with no need for specific lipid antigen interaction[98,102–104].

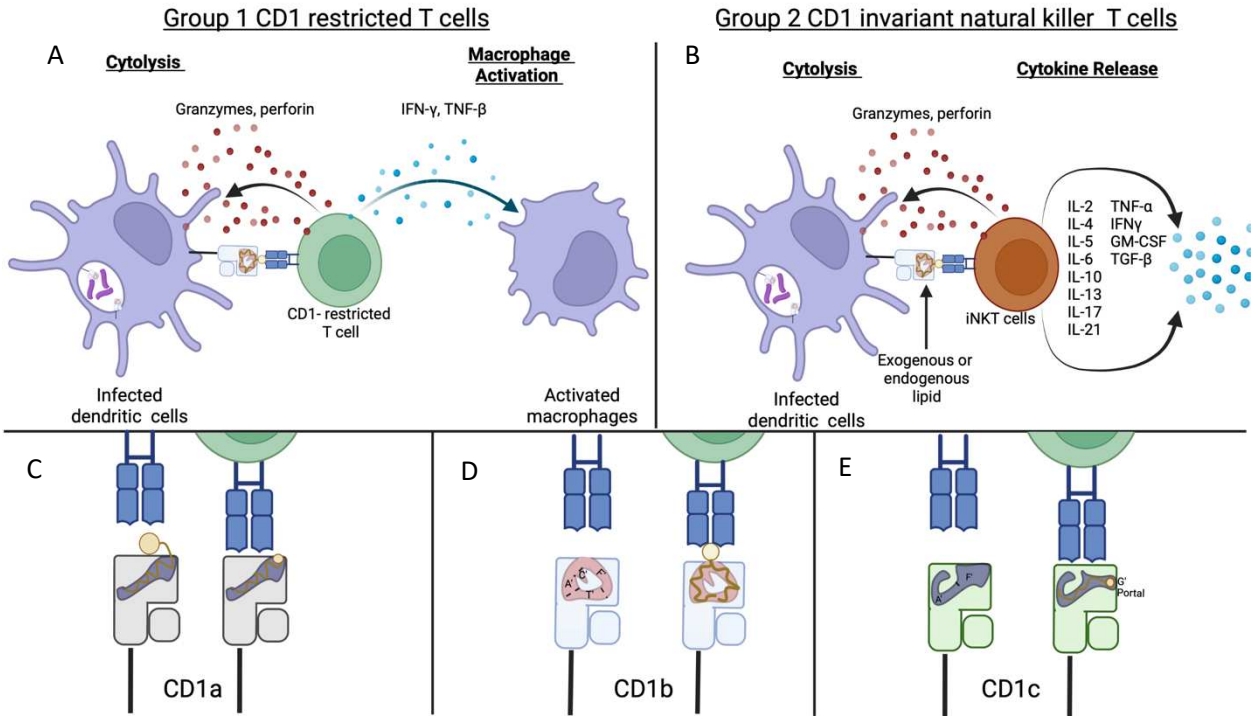

Figure 4. **T cell- CD1 complex interaction.** A) Hypothesized mode of T cell activation, and release of corresponding cytokines and granzymes follow interaction with lipid CD1 group 1 complexes. B) Hypothesized mode of iNK T cell activation, and release of corresponding cytokines and granzymes follow interaction with lipid CD1 group 2 complexes. C-D) hypothesized/validated methods of TCR-CD1 interaction. C) Proposed method of TCR CD1a interaction, interference method. Lipid antigens with large head groups block interaction of the TCR with CD1, while lipids with small head groups are permissive. D) Head group interaction method, the heterogenous headgroup acts a specific source of T cell interaction. E) Complex modulation, Lipid antigen structurally modifies the complex all for direct TCR complex interaction.

CD 1- restricted t cells:

Knowledge of CD1-restricted T cells have been limited compared to the foundational work done on the actual lipid antigen presenting protein, CD1. However, recently advances in CD1 isoform tetramers, and synthetic lipids, have allowed for innovative work leading to a marked expansion of knowledge regarding these cells and their related TCR structures. It has been established that each functional group of CD1 proteins, group 1 and 2, have their own subset of T cell population and thus deviate in their functional immune responses.

Group 1 CD1 T cells:

Group 1 CD1-restricted T cells are composed of variable polymorphic $\alpha\beta$ TCR T cells and rarely $\gamma\delta$ TCR T cells with a distribution of CD4+ and CD8+, double positive and double negative cells (DN)[105]. These lipid restricted T cells are homologous to MHC restricted counterparts and have been shown to differentiate into both T helper cells or into Th1 or Th2 cells. Upon activation and proliferation many of these cells have been shown to produce large quantities of IFN-γ and TNF-α. A large portion of these activated cells show a propensity for cytolytic actions[106,107].

Human CD1 tetramers have allowed for a degree of investigation of the proportion of these specialized T cells subsets within the generalize T cell population and distribution of the cells within tissues[103,108,109]. Initially group 1 CD1-restricted T cells were thought to be rare, to a percentage deemed potentially biologically insignificant; however, CD1-restricted T cells have been appreciated in the peripheral blood ranging from 0.01 to 10% of the total T cell population[87,110,111]. Additionally, high numbers of auto-reactive and allergen induced CD1a T cells have been appreciated within the dermis, potentially indicating a specialized role of CD1a to lipid surveillance and immunopathogenesis within the skin[112,113].

The use of tetramers has also allowed for evaluation of the previous dogma that all group 1 CD1 T cells have polymorphic TCRs. CD1b tetramer isolated T cell subsets reactive to Mtb glucose monomycolate, coined GEM T cells, have a relative invariant α chain, TRAV1-2, which is similar to the invariant NK cells which will be discussed with CD1d[31,114]. Further investigation found that slight variation in the β chain allows for differentiation of antigen selection between glucose monomcyolate and mycolic acid. This highly conserved TCR, found to be conserved in all donors from polyclonal T cells populations, has exciting implication for mycobacterial immunology, diagnostics and treatment methodologies that will be discussed in later sections[31,115].

As mentioned beforehand, there is a consistent endosomal CD1 trafficking regardless of dendritic cell maturation, which is in contrast to MHC proteins[82]. Given this difference, there is evidence that CD1-restricted T cells may be able to detect and proliferate faster than MHC-restricted T cells. This potential stark difference in activation abilities of immature dendritic cells may allow for proliferation of CD1-restricted T cells at the site of inflammation rather than tertiary lymphoid structures such as regional lymph nodes. Proliferation at the local site of inflammation may explain the relatively small populations of peripheralized group 1 CD1 restricted T cells appreciated in individuals regardless of their clinical state[81].

Much of the Group 1 T cell work has been done within *in vitro* human cell culture or transgenic mice. A few studies have examined T cell responses in the guinea pigs assessing cellular proliferation abilities and cytotoxic effect[116]**(Fig. 4A)**. However, more *in vivo* and ex-vivo studies are needed within the guinea pig to establish the role of group 1 T cells, and establish any true species differences between the guinea pig and what has been establish in human cell culture and observational clinical studies. One promising technique, which has been utilized in humans, and is now available for the use in the guinea pig are CD1 isoform and homology specific tetramers via the NIH tetramer core. Utilizing these tetramers, one could examine CD1-

restricted T cells in a lipid antigen specific manner *in vivo* via immunohistochemistry, ex-vivo via flow cytometry, and isolate these population via a cell sorter. However, to the knowledge of the authors there is limited use of these innovative guinea pig specific tetramers in the literature. Investigative studies are still required for the innovative guinea pig tetramers such as creating and validating tetramer lipid binding protocols, establishment of a validated guinea pig CD1-restricted T cell line for use a tetramer loading and binding control, as well as making a robust measure of guinea pig T cell activation, such as IFN-γ Elispot or quantitative IL-2 assay.

Group 2 CD1-restricted T cells:

Group 2 CD1-restricted T cells are driven solely by CD1d lipid antigen presentation and termed either type 1 natural killer cells, invariant natural killer cells (iNKT cells), or type 2 natural killer cells. Type 1 iNKT cells, representing 0.3-1.5% of peripheral T cells in the mouse, have semi-invariant TCR with a highly conserved α chain, TRAV, and limited variable β chain, TRBV[117,118]. This invariant TCR allows for a highly conserved binding motif that is not only conserved in humans, but also in many mammalian species that possess CD1d proteins[119,120]. Besides the invariant TCR iNKT cells have a number of unique properties. First, iNKT cell positive selection occurs via thymocyte mediated mechanism rather than the classic thymic cortical epithelium mechanism. This deviation in maturation allows for antigen mature T cells rather than traditional naïve T cell populations. Additionally, iNKT cells have the ability to rapidly respond to TCR interaction leading to almost immediate and copious cytokine response **(figure 4B).** This rapid TCR-mediated response leads to iNKT cells to commonly be referred to as the cross road of innate and adaptive immunity[35]. Depending on the iNKT cell subset the cell can produce a large range of cytokines including: IL-2, -3, -4 , -5, -6 , -9, -10, -13, -17 and -21, IFN-γ, TNF-α, granulocyte monocyte-colony stimulating factor and several chemokines[121]. Compared to type I NKT cells relatively little is known about type 2 NKT, with the expectation

that upon activation they are thought to play a regulatory role for type NKT, other T cells subsets and B cells activation.

CD1d has been shown to respond to a host of endogenous lipids as well as exogenous microbial lipid to stimulate these NK cell subsets. One proposed reason of self-lipid detection by CD1d proteins is the lipid composite placed within the CD1d proteins will shift, from endogenous glycophospholipids to lysoglycophospholipids, when a cell is in an inflammatory environment or infected with a viral etiology. This shift in endogenous lipid composition can be detected by both type 1 and 2 NK cells and in congruence of a cytokine rich environment, such as IL-12 production, would lead to NK cell activation, iNKT cell cytokine production and proliferation[122].

CD1 immunity and Mycobacterium tuberculosis:

As indicated throughout this review CD1 lipid-based immunity have been shown to play an essential role in surveying for foreign microbial lipids in the cellular milieu and within intracytoplasmic endocytic compartments. This niche branch has been shown to have an out-size role in the immunopathogenesis of *Mycobacterium tuberculosis* infection and tuberculosis[123,110,124]. Many observational studies and invitro experiments have been performed in humans predominately on peripherally derived CD1 restricted T cells and histiocytic cellular populations. Many of these foundational studies found T cell activation, via IFN-γ ELIspots, and proliferation from infected individuals[125–127]. Other investigations demonstrated that Mtb infections of dendritic cells augmented overall CD1 expression ex-vivo[128–130].

In the early 2000s the field of CD1-restricted T cells was revolutionized with the creation of CD1 specific tetramers. These reagents allowed for identification, isolation and study of antigen specific T cell populations in both healthy and Mtb infected individuals. Specific T cell subset have now been observed, with populations including Mtb lipid antigen specific T cells to

glucose monomycolate, mycolic acid, phosphomycoketides, and sulfoglycolipids. In several of these studies these populations were detected in MTB infected patients and not healthy individuals, indicating a proliferation of these T cell subset populations in the face of active Mtb infections[131–133]. However, little is known about this branch immunology in the face of Mtb infection at the tissue level and how these lipid presenting proteins direct disease pathogenesis. This limitation stems directly from the fact that relative few rodent lab animals possess both group 1 and group 2 CD1 proteins. A transgenic mouse model, possessing orthologs of human CD1 isoforms, has been created but are not a natural model and have less translatable Mtb lesions.

The guinea pig, having a similar CD1 repertoire to humans and translatable Mtb lesions, served a perfect CD1 MTB model, with a plethora of studies performed in the early to mid 2000s performed by Steve Porcelli, Branch Moody, and Christopher Drascher[33,134,135]. These innovative investigations and experiments lead to an understanding of lipid specific cellular cytotoxicity of CD1-restricted T cells and proliferation in guinea pigs immunized to the Bacillus Calmette-Guerin vaccine. These studies went further than the human literature performing interventional studies with Mtb lipid vaccines that demonstrated immunized guinea pigs with whole lipid Mtb extractions lead to decreased pulmonary pathology. Furthermore, these studies lead to the foundational creation of isoform and ortholog specific anti-guinea pig CD1 monoclonal antibodies, and CD1 isoform specific transfected guinea pig fibroblasts. However, the difficulty working with the guinea pig tissue and cells, as well as lack of a wide breadth of immunological reagents for this animal model have left many investigations yet to be performed to fully understand the role of CD1 lipid-based immunity in relation to Mtb infections and overall disease pathogenesis.

Concluding remarks:

Since the discovery of CD1, a myriad of understanding within this niche branch of immunity have been achieved; however, many gaps within this field remain to be answered. Though we understand the basics of CD1 cellular trafficking and lipid loading we still need to come to terms with the complex interaction of CD1-restricted T cells with CD1 molecules, such as what co-stimulatory molecules, like CD28 and CD40, lead to CD1- T cell activation. We also need to comprehend where these T cells interact with lipid antigen presenting cells and how they respond in an *in vivo* environment. Lastly, and most importantly we need to assess whether harnessing CD1 glycoproteins or CD1 restricted T cells can be utilized to aid in the control of a host of diseases ranging from infectious etiologies to autoimmune processes.

The guinea pig can play an outsized role in filling in the essential gaps of knowledge in the field of CD1 immunlogy, particularly in relation to Mtb infections. As mentioned, the guinea has been utilized to demonstrate that lipid vaccination effects pulmonary lesion burden with Mtb infected animals. However, many of these studies were performed using whole-lipid extract from bacteria, which have the high potential of protein-antigen contamination potentially confounding findings. It is the opinion of these authors that the guinea pig model should first be utilized to appreciate the basics of CD1 lipid immunity at the tissue level of Mtb infected animals. This includes solidifying our understanding of the role of CD1 within the adaptive immunity via kinetic studies of CD1 APCs and CD1-restricted T cells at the tissue level. Then we can utilize this knowledge to assess the importance of CD1 in Mtb pathogenesis and whether this unique immune system branch can be exploited for prophylactic vaccine approach or mid-infection intervention.

If a CD1 lipid-based treatment is found to be efficacious for decreasing Mtb disease burden CD1 immunology has several advantages that may aid to make it a more potential treatment compared to other vaccine routes. This lies in the basis of CD1 glycoproteins non-

polymorphic characteristics. These highly conserved CD1 proteins are invariant from individual human to human, and in large part from humans to animals. This nature could allow for one, highly translatable animal model studies, and two, a degree of efficacy of these treatments throughout the otherwise diverse human population. It is the authors hope that renewed interest in the guinea pig, and advancement of immunologic guinea pig reagents, will allow for additional investigation that will no doubt lay the groundwork for the assessment of Mtb lipid-based vaccines, and treatment schemes that could have profound effects of controlling deadly Mtb infections.

CHAPTER 1: The role of Vitamin A in the immunopathogenesis of Mycobacterium tuberculosis infection in a guinea pig model[1]

[1] Parts of this chapter have been previously published and are reprinted here with permission from: Podell, B. K., Aibana, O., Huang, C. C., DiLisio, J. E., Harris, M. C., Ackart, D. F., ... & Murray, M. B. (2022). The Impact of Vitamin A Deficiency on Tuberculosis Progression. *Clinical Infectious Diseases*, *75*(12), 2178-2185.

This chapter contains new, never-before published, data including reanalyzed histologic quantification, retinol binding protein 4 quantification, and Nanostring gene expression work.

Summary:

Vitamin A deficiency is one of the most common micronutrient deficiencies in developing countries, with up to 50% of preschool-aged children deficient of this essential vitamin. Vitamin A serves a host of biological functions through its transcriptional nuclear activity and need for vision physiology. However, the role of this vitamin in immunology and a host of disease pathogeneses is still debated in the literature. In 2017, Dr. Murray, discovered that vitamin A deficiency is one of the predominate micronutrient comorbidity for clinically active *Mycobacterium tuberculosis* infections. This study aimed to build on this groundbreaking work to understand the interplay of vitamin A and disease pathogenesis of tuberculosis in a vitamin A deficient guinea pig model. Three treatment groups were infected with *Mycobacterium tuberculosis,* a vitamin A sufficient group, a vitamin A deficient group, and a vitamin A deficient group with reestablishment of a vitamin A sufficient diet during infection. Results demonstrated a breakdown of normal granuloma structuring, increased splenic lesion burden and increased splenic bacterial burden in deficient animals. Further cellular examination revealed a marked proliferation of lymphocytic populations, with skewed CD4 to CD8 T cell ratios, and aberrant genetic expression of key inflammatory mediator in deficient animals compared sufficient animals. Interestingly, vitamin A resupplemented animals are partially rescued from detrimental effect observed in vitamin A deficient animals. Collectively, these study shows dysregulation of

the complex inflammatory environment elicited in *Mycobacterial tuberculosis* infections, which furthers our understanding of Vitamin A deficiency as an important comorbidity for tuberculosis.

Introduction:

Mycobacterium tuberculosis (Mtb) the causative agent of tuberculosis (TB) was, until recently displaced by COVID-19, the leading cause of death for infectious diseases, causing an estimated 1.6 million fatalities in 2021[3,136]. As with other diseases, pandemic disruption caused a precipitous breakdown in surveillance and treatment Mtb apparatuses leading to a 4.3% in infection rate of 10.6 million people in 2021. This rise in cases and fatalities coupled with the rise of multidrug resistant Mtb and a 100-year-old, variably efficacious, Bacillus Calmette-Guerin vaccine has steered Mtb investigators to reexamine TB comorbidities related to active disease states.

As of 2018, the WHO estimated that 1.7 billion people were infected but several studies classify up to 1/3 of these patients to be in a latent, non-clinical, phase of the disease. An intense area of study is focused on the comorbidities that cause a patient to either present as an active, clinical, infection or a latent non-clinical state. Several known comorbidities have been established such as a patient's HIV status and whether a patient is diabetic. HIV is the greatest known risk increasing the risk of active or reactivated infection 20 to 30 fold compared to non-HIV infected individuals, leading to 187,000 deaths in 2021[3,5]. Other comorbidities have become of increasing interest for research to further help prevent clinical Mtb, such as malnutrition and in particular micronutrients. In 2017, Dr. Megan Murray, assessing disease status with micronutrient status discovered vitamin A deficiency led to a 10-fold increase in active TB[6].

Vitamin A, retinol, is a fat-soluble micronutrient that undergoes hepatic and target cell metabolism to form retinoids including 9-cis-retinoic acid and all-trans retinoic acid (ATRA), the most biologically active form. The linchpin of retinoic acid functionality is based on the ability to

interact with nuclear retinoic acid receptors (RAR) and RA-X receptors (RXR) to enhance transcriptional activity of target genes. Through this action, vitamin A plays a multitude of roles to ensure physiologic homeostasis for bodily processes, particularly for epithelial cell integrity, organogenesis and vision. This micronutrient has essential roles within the immune system including, dendritic cell maturation, T cell differentiation and functionality as well as acting as an ant-inflammatory molecule via inhibiting M1 macrophage differentiation[137,138].

Vitamin A deficiency is known to cause a host of pathologic changes in children and adults, including multiorgan metaplasia and hyperkeratosis, nyctalopia, growth/dental abnormalities, and potential infertility. Unfortunately, vitamin A deficiency is considered to be one of the major nutritional deficiencies worldwide, with 190 million preschool and 19 million pregnant women considered to be deficiency as of 2005[139,140]. Further compounding the problem is the unequitable distribution of this deficiency with prevalence being highest in regions with low socio-economic status[141]. Inopportunely, the distribution of this essential nutrient deficiency closely aligns with the region's most heavily affected by Mtb infections, which speaks to the relative importance of this comorbidity correlation[2]. Although many symptoms of vitamin A deficiency are known, the interaction of vitamin A deficiency in relation to Mtb and the pathophysiology of progressive TB is unknown.

Utilizing our expertise of Mtb infected Dunkin Hartley guinea pig models, our lab designed a vitamin A deficient animal model to evaluate the pathophysiology of Mtb infections in the face of a subclinical vitamin A deficiency. This includes assessing changes in lesion morphology, bacterial burdens and changes in gene expression profiles from deficient and sufficient animals. By further understanding the interplay of this micronutrient deficiency and TB disease pathogenesis we may be able to prevent a portion of the population from having clinical disease, thus lowering the burden on already strained health care systems while potentially also stemming the rise of multidrug resistant strain of *Mycobacterium tuberculosis*.

Methods:

Vitamin A deficient diet administration:

Specific diet administration and diet composition is described in Podell et al., 2017[22]. In brief, to limit retinol liver storage capacities, neonatal Dunkin-Hartley guinea, 9 to 12 days in age. were obtained from Charles Rivers Laboratories (Wilmington, Ma). Guinea pigs were divided into 3 groups: vitamin A sufficient (VAS), vitamin A deficient (VAD) and Vitamin A resupplemented (VAD resupp.) (n=5 per group). All guinea pig received a similar dietary composition from (Dyet Inc., Bethlehem, PA). However, vitamin A, in the form of retinyl palmitate, was devoid in the diet composition fed to VAD and VAD resupp. animals. Quantification of vitamin A levels, evaluated via high-performance liquid chromatography, demonstrated 25,100 IU/kg and 100IU/kg of retinoid activity in sufficient and deficient diets respectively. Both VAD and VADresup animals were given oral doses of 100 units of retinyl palmitate to prevent clinically evident vitamin A deficiency, presenting as multiorgan metaplasia and hyperkeratosis. In the infection model, VAD resupp. animal's diets were switch at day 30 post infection to the retinyl palmitate diet in line with that VAS animals were receiving to allow for reestablishment of a vitamin A sufficient status.

Monitoring vitamin A deficient status of animals:

Assessment of vitamin A status from all guinea pigs was performed via biweekly evaluation of blood plasma obtained via intrathoracic blood draw. In depth procedures have been validated by Podell et. al[22]. In short, Guinea pigs were anesthetized via positive pressure intrapulmonary administration of 5% isoflurane. Once anesthetized, animals were positioned into dorsal recumbency and an 18-gauge needle was inserted into the 2nd to 3rd intracostal space to collect blood from the cranial vena cava, brachiocephalic artery or associated arterial offshoot. 1.5 to 3

mls of blood was collected and placed in an EDTA 7ml Monoject tube (Coviden, Dublin, Ireland). Blood was centrifuged at 1000X g for 10 minutes and plasma collected off the top of the cell pack and frozen at -80°C. Plasma retinol concentrations were quantified by HPLC via Michigan State University Veterinary Diagnostic Laboratories, with protocols detail in Podell et al[22]. Guinea pigs were considered to be in a vitamin A deficient state is plasma retinol level were at or below 20 ug/dl.

Mycobacterium infection and euthanasia:

Infection was performed with H37Rv obtained from BEI Resources (ATCC) and passaged in animal infections, grown to phase growth as pellicle in Proskauer-Beck broth, then explained to log-phage single cell suspension in Proskauer-Beck broth. Infection protocols follow previously described laboratory protocols[142,143]. Low-dose, 20 bacilli, aerosol exposure of guinea pigs to *M. tuberculosis* was performed using the Madison chamber aerosol generation device (College of Engineering Shops, University of Wisconsin, Madison, WI). Infections were carried to 60 days post initial infection, ending with guinea pig euthanasia. Euthanasia was performed by anesthetic induction with 40 mg of ketamine and 6 mg of xylazine before intraperitoneal injection with an overdose of 3 mL/kg of sodium pentobarbital.

Tissue collection:

Once euthanized, animal tissues and cells were harvested which included alveolar macrophages by bronchoalveolar lavage, PBMCs from anticoagulated peripheral blood, and cell suspensions derived from lung parenchyma, as previously reported[144,22]. In brief, one lung lobe was clamped off and removed and processed for PCR via RNAlater solution (Thermofisher, cat #: AM7020), protein extraction, or for bacterial enumeration by colony forming units (CFU).

Alveolar macrophages were collected via post mortem bronchoalveolar lavage utilizing an 18-gauge catheter and flushing with 25 ml of HBSS containing 0.01 μM EDTA solution in 5 ml intervals. Following bronchoalveolar lavage, the remaining lung was perfused with 5 ml of collagenase at 5μg/ml (Sigma-Aldrich, Cat#: C9263) and incubated for 30 minutes in a 37°C water bath. The digested lung parenchyma was processed through 40 μm cell strainers. Once strained, all samples were subjected to erythrocyte lysis solution for 20 to 45 seconds. PBMCs were collected via a left ventricular intracardiac blood draw directly following euthanasia, diluted 1:2 in HBSS and separated on a density gradient using Lympholyte mammal (Cedarlane, cat#: CL5110) per manufacturer's instructions. In brief, up to 6mls of obtained blood was diluted 1:1 in HBSS solution. The diluted blood was added to a 15ml conical tube containing 3mls of Lympholyte at a 45° angle as to maintain separation of blood and the Lympholyte. Samples were than centrifuged at 800XG for 20 minutes with no decelerating brake. Lastly the separated buffy coat, PBMCs, were collected and washed.

Histologic assessment and quantification:

Sections of lung, liver and spleen were fixed in 4% paraformaldehyde for 24 to 72 hours then transfer to PBS solution for long term storage. Trimmed specimens were routinely processed, sectioned at 5 microns, collected on charged slides, and stained with hematoxylin and eosin (HE) for evaluation by light microscope. Cut sections were digitized at 20X magnification via an Olympus VS120 (Olympus, Shinjuko, Japan) or a Vectra Polaris spectral imaging scope (Akoya, Boston, MA). Histologic morphology and burden quantification were quantified via Visiopharm software (Visiopharm, Medicon Valley, Denmark). Quantification relied on area lesion and lesion characteristics including necrosis, fibrosis, lymphoid aggregates, and mineralization as compared to whole lesion area and/or whole tissue area.

RNA extraction and nanostring gene expression analysis.

Freshly isolated lung tissue from all guinea pigs was minced in RNALater (Sigma, Cat#: R0901), incubated at 4°C for 24 hours, then frozen at -80°C until RNA extraction. Tissues were thawed at room temp and ~50 mg of tissue homogenized using Lysing Matrix A tubes (VWR, cat# 75784-610) in a bead beater instrument at full speed for 20 seconds twice (MP Biomedical, C321001). Proteinase K was added to the homogenate, incubated at 55°C for 15 minutes, then RNA was extracted with the RNeasy mini kit (Qiagen cat. 74106) per manufacturer's instructions. After Qiagen protocol completion nucleic acid was eluted from the column, digested with DNase-I for 30 minutes at 37°C, then purified again using the RNeasy mini kit protocol. Sample concentration and 260/280 ratios were measured using a Nanodrop spectrophotometer. Isolated samples with an RNA concentration of greater than 100ng/ul and 260/280 ratio of between 2 and 2.2 were deemed acceptable and saved at -80°C. Once all tissue RNA extraction was complete sample were sent on dry ice over night to the University of Utah for Nanostring gene expression quantification. The gene list and associated accession filing are provided in supplemental material (sup. table 1). Received data was analyzed utilizing Nanostring nSolver, providing fold change volcano plots. Unsupervised heatmaps were generated using Shiny's reactivity with built-in functions using R version 4.2.1, created in part by Forrest Ackart[145].

Assessing retinol binding protein 4 liver and plasma concentrations

Isolated tissue sections frozen at -80°C are thawed and placed in a lysis matrix A tube (VWR, cat# 75784-610) with 600ul of IP buffer (ThermoFisher, cat # 87787) and homogenized using a bead beater (MP, cat# C321001) at full speed for 10 secs. Samples were then centrifuged at 10,000x G at 4°C for 10 minutes, followed by isolation of protein supernatant. All samples were

then quantified utilizing Pierce BSA protein assay kit (ThermoFisher, cat# 23225) following manufacturer instruments and read on a spectra max plate reader M2 (Molecular devices, San Jose CA) at an absorption of 562nm. All sample were standardized to 10ug/ul. 5ul of XT 4X sample buffer (Biorad, cat# 1610791) was added to samples which were denatured via a boiling of solution for 10 minutes at 95°C. While samples were boiled SDS page criterion XT Bis-Tris page gels (Biorad, cat# 3450124) were prepared in a criterion vertical electrophoresis cell (Biorad, cat# 1656020) with 1X mops running buffer (Biorad cat# 1610788). After denaturing, samples were pipetted into gel wells followed by 1ul of chemiluminescent magic mark ladder (ThermoFisher, cat# LC5602) and 5ul of chromogenic ladder (Biorad, cat# 1610394) to the last well. Gel electrophoresis was run by PowerPac (Biorad, cat# 1645052) at 180V constant. Once gel electrophoresis was complete protein samples were transferred to a PVDF protein membrane (Biorad, 1620177). Membrane transfer was performed via criterion blotter (Biorad, 1704070) onto PVDF at 100V constant for 45 minutes. Following transfer, the membrane was then blocked-in block buffer (1X TBST, 0.05% 20tween, 5% BSA) for thirty minutes on rocker at room temperature. Block was then decanted and retinol binding protein 4 antibody (Proteintech, cat# 11774-1-AP) was added to the membrane at 1:300 in block buffer on a rocker overnight at 4°C. The next day the membrane was washed in wash buffer (1X TBST, 0.05% 20tween) 3 times. Membranes were then incubated with the secondary HRP antibody (ThermoFisher, cat# 31460) for 2 hours at room temperature on a plate rocker. Lastly the membrane chemiluminescence was developed (ThermoFisher, cat# P132106) according to manufacturer instructions. Membranes were imaged on a ImageQuant LAS 4000 biomolecular imager (GE, Boston MA) at an exposure time ranging from 10-30 seconds. Image analysis and band density quantification was performed via imageJ (NIH) freeware.

Flow cytometry:

Flow cytometry was performed as described in the Podell et al. 2022 manuscript[22]. In short, Pulmonary leukocytes, collected via bronchoalveolar lavage, granuloma-associated leukocytes were collected, counted, processed and assessed. The conjugated monoclonal antibodies described in (Supp. Table 1[22]). Non-viable cells were excluded using the Zombie Yellow viability dye (BioLegend). After labeling, cells were fixed with 4% paraformaldehyde for 10 minutes and data was collected using the Aurora spectral cytometer (Cytek). Leukocyte phenotypes were identified after gating on scatter, single cells, viable cells, and CD45 positive leukocytes (Supplementary Figure 5). Phenotypes are expressed as percent of total leukocytes, lymphocytes, or myeloid cells.

Enumeration of bacterial burden:

Lung, and spleen bacterial burden was quantified as previously described[146]. In brief, tissue homogenate was plated on 7H11 agar quad plates in 5-fold serial dilution and colonies counted after 8 weeks of incubation. Colony-forming units were $\log_{10}$-transformed and expressed as colony-forming units per gram of tissue.

Statistical analysis:

Statistical analysis on flow cytometric and CFU enumeration are described in Podell et al., 2022. Statistical analysis for quantitative histologic analysis was performed via a one-way ANOVA with Dunnet correction for multiple comparisons. Analysis of RBP western blot data was performed using a two-way ANOVA with a Sidak correction for multiple comparison. Statistical significance

for fold change of gene expression was performed and calculated utilizing Nanostring Nsolver V4.0.

Results:

Guinea pigs are able to become vitamin A deficient through dietary modifications.

All neonatal animals are considered to have a vitamin A deficient state at time of arrival from Charles River Laboratories, when compared to older VAS guinea pigs (Sup. fig 1A). Following 12 weeks of a vitamin A deficient diet all VAD guinea pigs reach the limit of detection for retinol serum and hepatic levels, indicating a deficiency (Sup. fig. 1B & 1C). Unfortunately, pilot initial studies found this level of vitamin A level to have clinical manifestations of vitamin A deficiency including systemic metaplasia and keratosis of visceral organs (Sup. fig. 2). To correlate to sub-clinical vitamin A deficiency seen in humans, a subset of guinea pigs were supplemented with a weekly dose of 100 units of retinyl palmitate VAD sup.

Vitamin A sufficient animals lose serum retinol in the face of acute Mtb infection

Retinol serum values were assessed on a biweekly basis to measure changes of retinol status of all three treatment groups **(Fig. 5A[22])**. As expected, VAD animals, who obtained deficiency prior to infection, maintained their deficient state throughout infection being below detectable limits, 20ug/dl, by 20 days post infection. Unexpectedly, results were observed in VAS guinea pigs. During the innate immunity and extending well into the adaptive immunity VAS animal serum retinol drops, with a peak reduction of 40% reduction in retinol levels (13.94 ug/dL$\pm$ 6.73, P= 0.24[22]) by 20 days post infection. Serum retinol is able to rebound as VAS animals enter the early adaptive time point, day 30 post infection, reaching peak recover by day 40 post infection.

VAD guinea pigs lose vitamin A storage capacity in liver tissue.

To evaluate the effect of a vitamin A deficient diet on retinol storage capacity in the face of a Mtb infection samples of liver were submitted for retinol quantification from both naïve and infected animals. In both naïve and infected guinea pig groups VAD animals had significantly depleted liver retinol storage ($P \leq 0.01$[22]). In conjunction with VAS retinol serum levels, the overall retinol storage capacity of infected VAS guinea pigs was decreased when comparing VAS naïve animals **(Fig. 5B**[22]**)**.

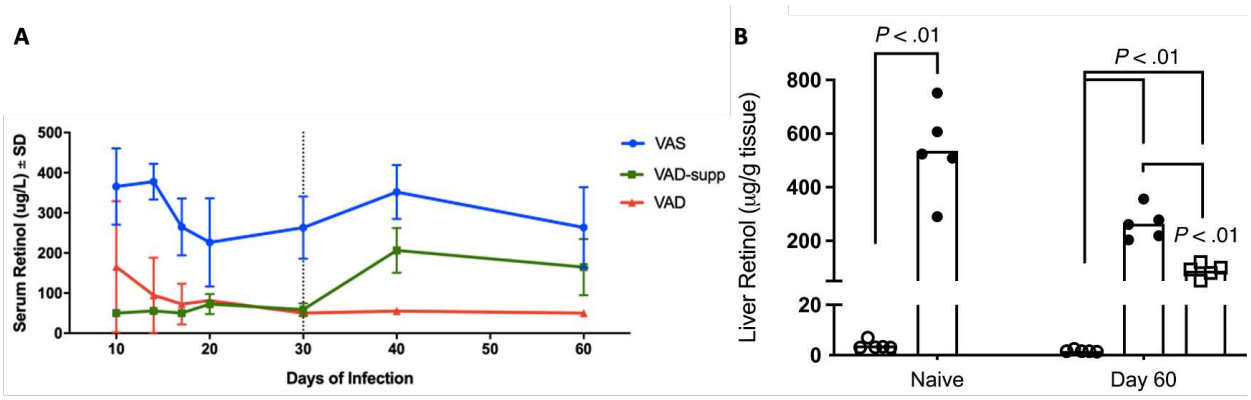

Figure 5. ***Impact of Mycobacterium tuberculosis infection of serum and liver retinol levels.*** *A)* Serum retinol concentrations measured in duplicative experiments over the course of infection. B) Liver retinol stores measured at day 60 of infection compared with liver retinol concentrations in age-matched naive guinea pigs. Open circle, vitamin A deficient animals; close circle, vitamin A sufficient animals; open squares, vitamin A re supplementation animals. Reproduced from Podell et al. 2022[22].

Retinol binding protein 4 distribution shifts in vitamin A deficient guinea pigs

To further comprehend the changes of retinol metabolism and movement during an infection we assessed and quantified retinol binding protein 4 (RBP4). This essential protein for retinol circulatory movement is synthesized in the stellate cells and hepatocytes and is released into circulation with retinol (holo-RBP4). In congruence with retinol serum data, RBP4 distribution shifts are observed in VAD to VAS guinea pigs in both naïve and infected groups. Based on western blot analysis there is a significant decrease in terminally collected serum distribution of retinol binding protein in both VAD naïve ($P \leq 0.01$) and infected animals ($P \leq 0.001$) compared to VAS animals. Interestingly, the resupplemented animals although able to partially recover serum retinol, still had significantly decreased serum RBP4 concentrations ($P \leq 0.05$) **(Fig. 6A)**. In stark contrast to the serum RBP4, liver RBP4 VAD animals were significantly higher than VAS in both naïve animals ($P < 0.0001$) and infected animals ($P < 0.001$). In concordance with terminal serum data is the alignment of the VAD resupp. treatment group with the VAS animals rather than the Deficient as observed **(Fig. 6B)**. Images of western blot analysis are provided in the data supplement (Sup. Fig 3).

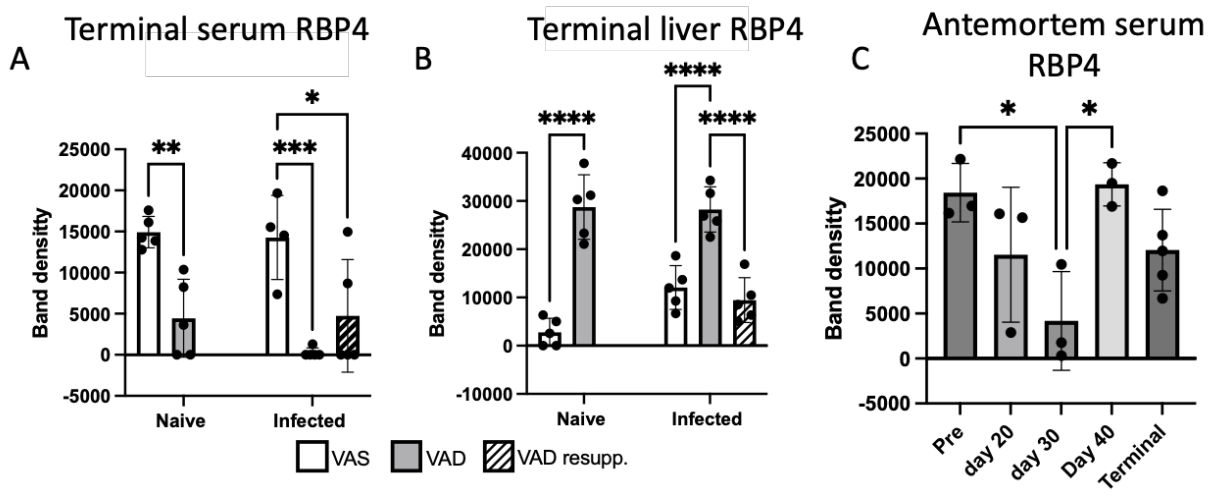

Figure 6. Impact of Mycobacterium tuberculosis infection on retinol binding protein 4 levels. Retinol binding protein 4 (RBP4) protein concentration was assessed via western blot techniques. A) Terminal serum RBP4, 60 days post infection, concentrations between naive and infected VAS, VAD and VAD resupp. animals. B) Terminal liver RBP4, 60 days post infection, concentrations between naïve and infected VAS, VAD, and VAD resupp. animals. C) Antemortem RBP4 concentrations of VAS animals throughout the course of the study. Naïve animal cohort had no VAD resupp. treatment group. *P≤0.05, **P≤0.01, ***P≤0.001, ****P≤0.0001; two-way ANOVA and Sidak correction test.

Retinol binding protein 4 shifts kinetically during Mtb infection in vitamin A sufficient guinea pig.

To investigate the observed, and unexpected, significant drop in serum retinol levels in infected VAS animals during the innate and early adaptive immunity of Mtb infections, serum RBP4 concentrations were analyzed via obtained antemortem blood draws. As with the terminal RBP4 serum levels, the antemortem RBP4 closely mirrors the findings of aberrant loss of serum retinol, with the largest loss of RBP4 protein at day 30 post infection. Preinfection sufficient RBP4 is significantly higher than day 30 post infection RBP4 protein concentration (P≤0.05). RBP4 returns to or above pre-infection levels swiftly, in line with observed rebounding of retinol serum, at 40 days post infection. The recovery of RBP4 is significantly higher than day 30 post infection RBP4 level (P≤0.05) **(Fig. 6C)**.

Vitamin A status changes lesion morphology but not overall lesion burden at the primary site of infection.

To assess the effect of Vitamin A status on tissue pathology H&E slides were cut processed and analyzed via quantitative software, Visiopharm. Lung tissue sections were analyzed for overall lesion burden and lesion morphology, including degree of lymphocytic infiltration, and degree of lesion necrosis. Regardless of vitamin A status, all animals had relatively consistent lesion burden of approximately 15% of the whole lung section **(Fig. 7A)**. Lesion morphology both quantitatively and visually were vitamin A status dependent. Necrosis is significantly higher in VAS animals than both VAD and VAD resupp animals ($P \leq 0.01$) **(Fig. 7B)**. Interestingly, and of unknown significance, VAD resupp. animals had increased lymphocyte infiltration in the granuloma compared to both VAD and VAS animals, being significantly higher than VAD animals ($P \leq 0.05$) **(Fig. 7C)**.

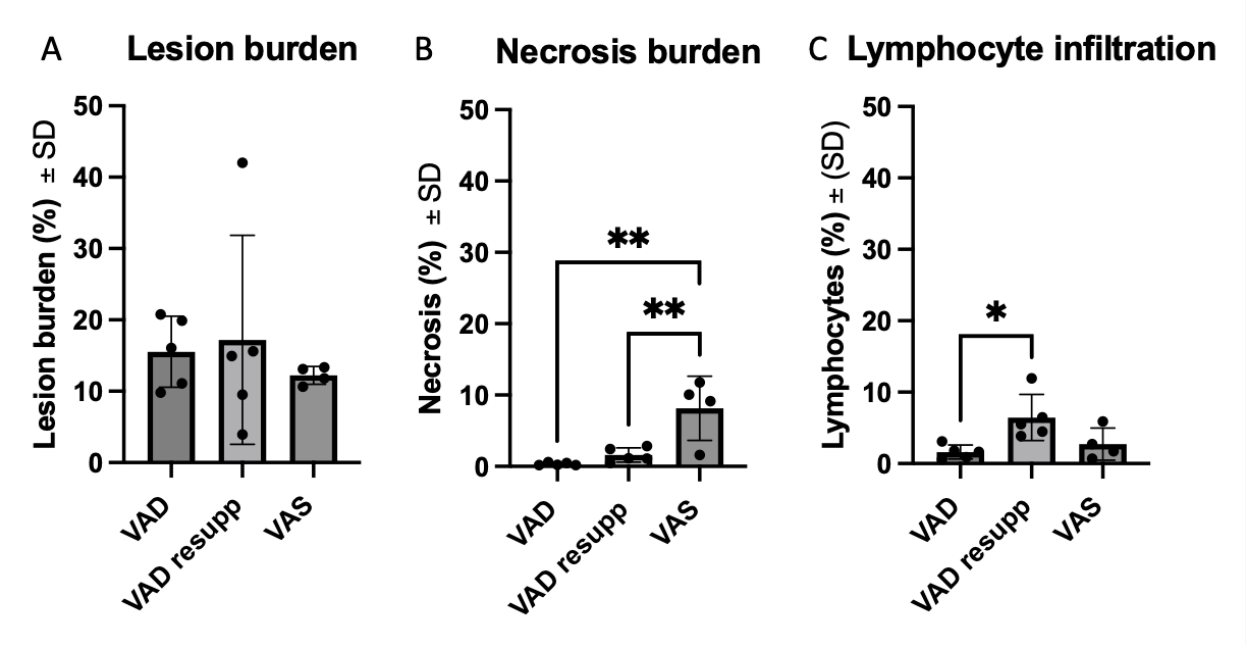

Figure 7. Impact of vitamin A status on Mtb lung lesion burden and morphology. Quantification of lesion burden and lesion morphology in the lung between vitamin A groups. A) Percentage of overall lesion burden based on overall lesion area compared to the area of the whole tissue. B) Percent of necrosis within lesions based on all necrosis area vs whole lesion area. C) Percent of lymphocytic infiltration based on overall lymphocytic population area vs the whole lesion area. *P≤0.05,**P≤0.01; one-way ANOVA and Dunnet correction test.

On microscopic examination there is an appreciable difference in morphology of Mtb granulomas. VAS animals had numerous well-demarcated lesions circumscribed by variable degree of fibrosis and outer ring of lymphocytes, inner foamy to epithelioid macrophages with central caseous necrosis, representing a classic Mtb granuloma for guinea pig models **(Fig. 8A-B)**[147]. VAD guinea pigs had poorly delineated inflammatory aggregations with collapse of distinct structuring leading to a lesion composed of randomly distributed clusters of lymphocytes and macrophages **(Fig. 8C-D)**. Intriguingly, VAD resupp. animals demonstrate a mixed phenotype with some poorly demarcated, non-classic, granulomas and others forming discrete classic granulomas, demonstrating a potent shift of lesion morphology with vitamin A reintroduction **(Fig. 8E-F)**.

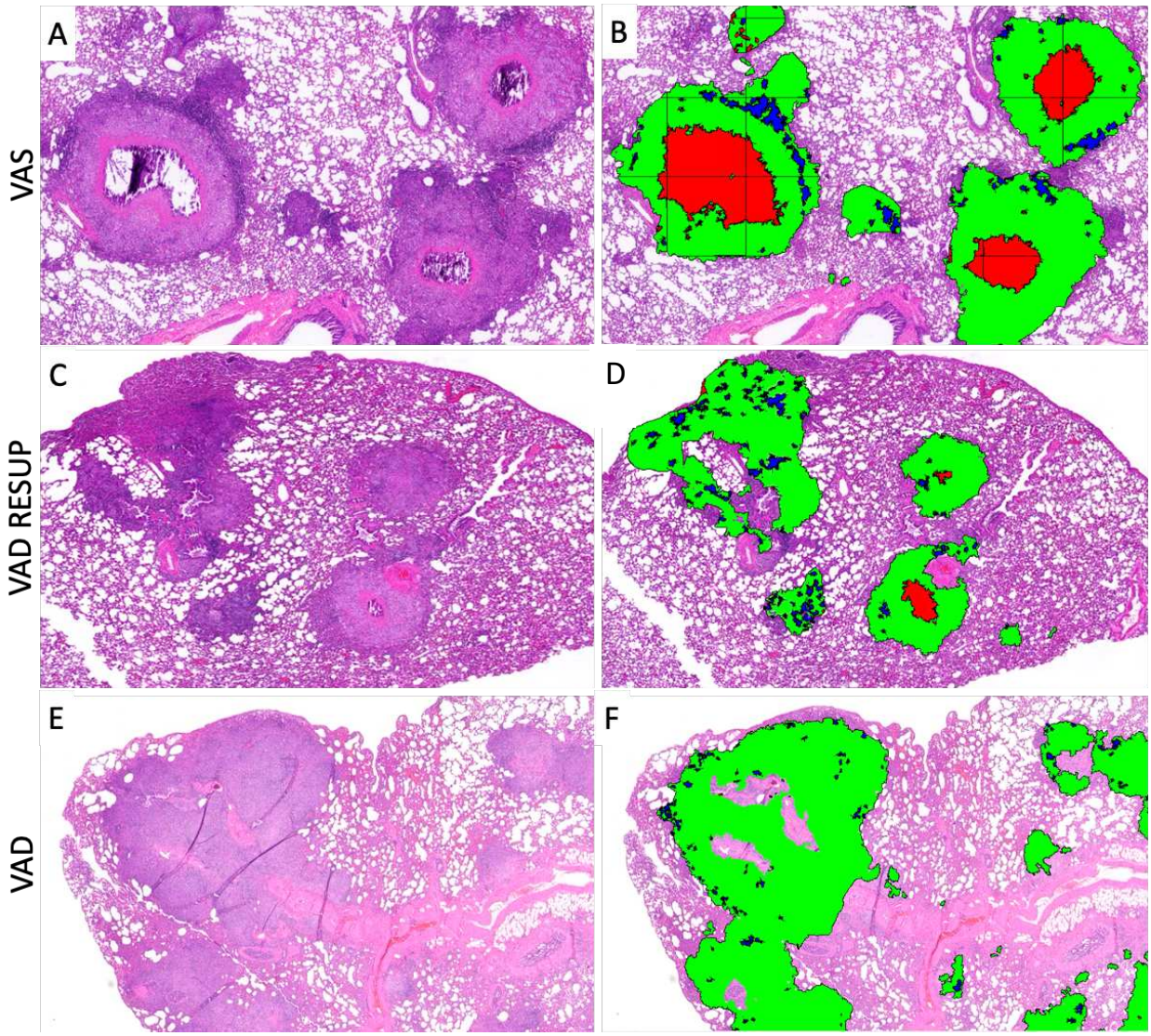

Figure 8. Vitamin A status effects lung morphology. Representative sections of lung from guinea pigs 60 days post infection of varying vitamin A status with or without visiopharm analysis. A-B) Lung sections from vitamin sufficient animals with prominent discrete granulomas. C-D) Lung sections from vitamin A re supplemented animals demonstrating a mosaic of lesion morphology. E-F) Lung sections from vitamin A deficient animals demonstrating poorly delineated granulomatous lesions.

Vitamin A status effects distant organ lesion burden.

Lesion burden in visceral organs, other than the lung, serve as an indication of bacteria spread and overall disease progression. To assess this, lesion burden was quantitatively measured in

both the liver and splenic parenchyma **(Fig. 9A-B)**. In the liver both VAD resupp. and VAS guinea pigs burden trends lower than VAD animals **(Fig. 9C)**. In the spleen, VAS animals had a significant decrease in lesion burden compared to VAD animals($P \leq 0.05$). Vitamin A resupplementation is able to partially reverse the effects of vitamin A deficiency, with VAD resupp. guinea pigs cutting lesion burden within the liver almost in half compared to the VAD treatment group **(Fig. 9D)**.

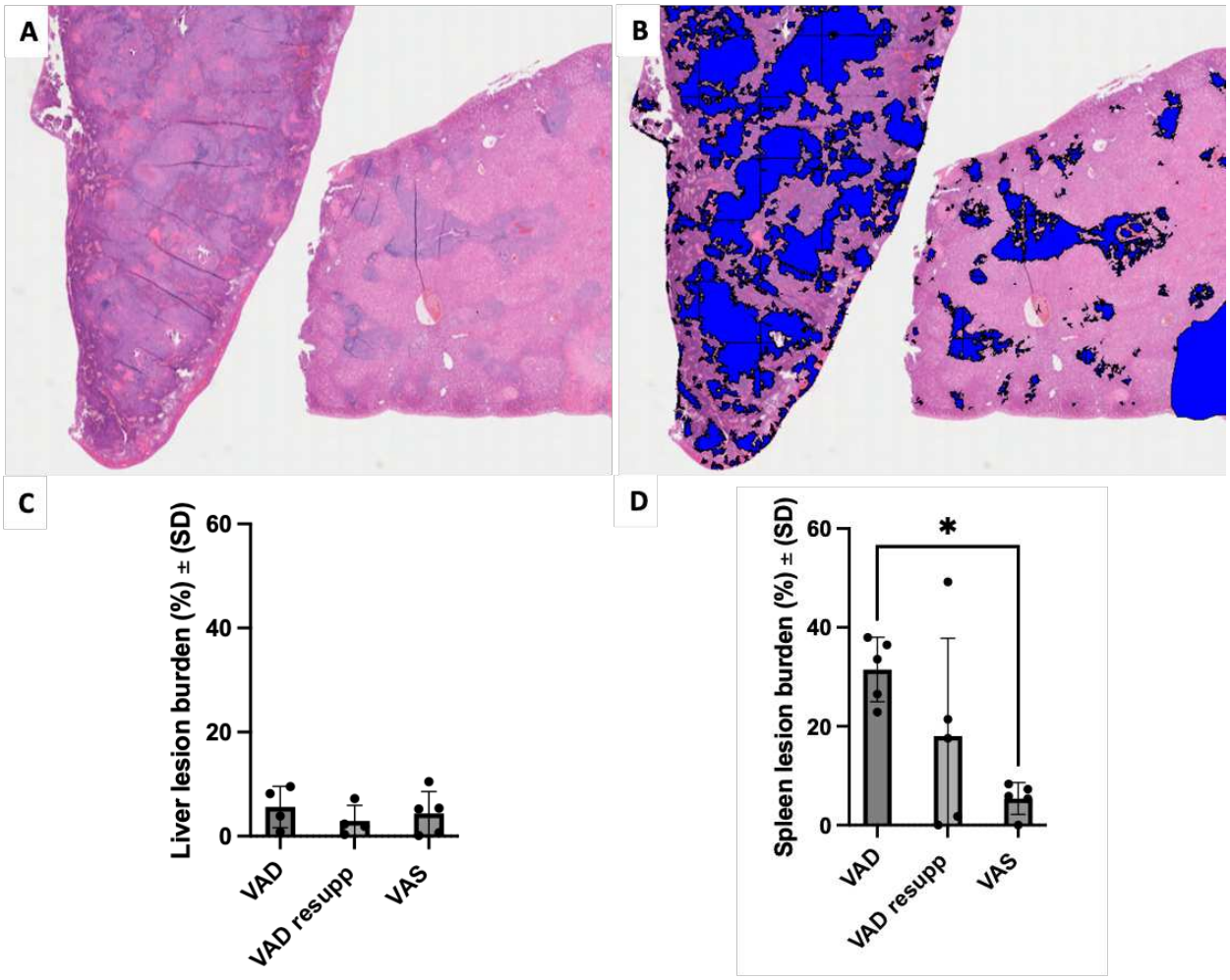

Figure 9. Vitamin A status affects splenic lesion burden. **Histologic quantification of liver and spleen from VAS, VAD, VAD resupplementation animals at 60 days post infection.** A-B) Representative samples of liver and spleen with lesion and correlating Visiopharm analysis. C) Percent lesion of liver based on lesion area vs whole tissue area. D) Percent lesion of spleen based on lesion area vs whole tissue area. *$P \leq 0.05$; utilizing a one-way ANOVA and Dunett correction test.

Lymphocytic and myeloid cellular population shift in relation to vitamin A status

To breakdown shifts of inflammatory cellular subsets flow cytometry was performed on CD45+ cell from infected tissues from sufficient, deficient and resupplemented animals on bronchiolar alveolar lavage cells and isolated granulomas. Bronchiolar lavage derived cells demonstrate significant shifts in lymphocytic and myeloid populations, with VAD animals having increased percentages of lymphocytes ($P \leq 0.03$) and decreased percentages of myeloid cells ($P \leq 0.03$) compared to VAS animals **(Fig. 10A)**. Further assessment of the lymphocyte T cell lineages reveals a dramatic shift in percentages of CD4+ and CD8+ T cells. VAD animals had a significantly higher population of CD8+ T cells, 33.97% CD8+ $\pm$ 5.025%, compared to VAS animals, 12.27% CD8+ $\pm$ 4% ($P \leq 0.01$). In juxtaposition VAD animals had decreased CD4 populations, 37.75% CD4+ $\pm$ 2.60%, compared to VAS animals, 57.72% CD4+ $\pm$ 19.62% ($P \leq 0.01$) **(Fig. 10B)**. These shifting populations gave VAD animals a CD4:CD8 ratio of 1.11 compared to VAS animals with a CD4:CD8 ratio of 4.7. Interesting resupplementation guinea pigs had a mixed phenotype of the two other groups in both myeloid and lymphocytic cellular populations and CD4+/CD8+ distributions.

Cells derived from granulomas lose significant changes of myeloid and lymphocytic cellular populations in the face of vitamin A status differences **(Fig. 10C)**; however, a significant shift of CD4+ and CD8+ is in line with bronchiolar alveolar lavage cells ($P \leq 0.02$) **(Fig. 10D)**. With granuloma derived VAD CD4:CD8 ratio at 1.88 and VAS CD4:CD8 ratio at 2.6. Gating strategy of flow cytometric analysis is provided in supplemental (Sup. fig .4). Remainder of data and breakdown of myeloid cellular populations in provided in the supplement (Sup. fig. 5).

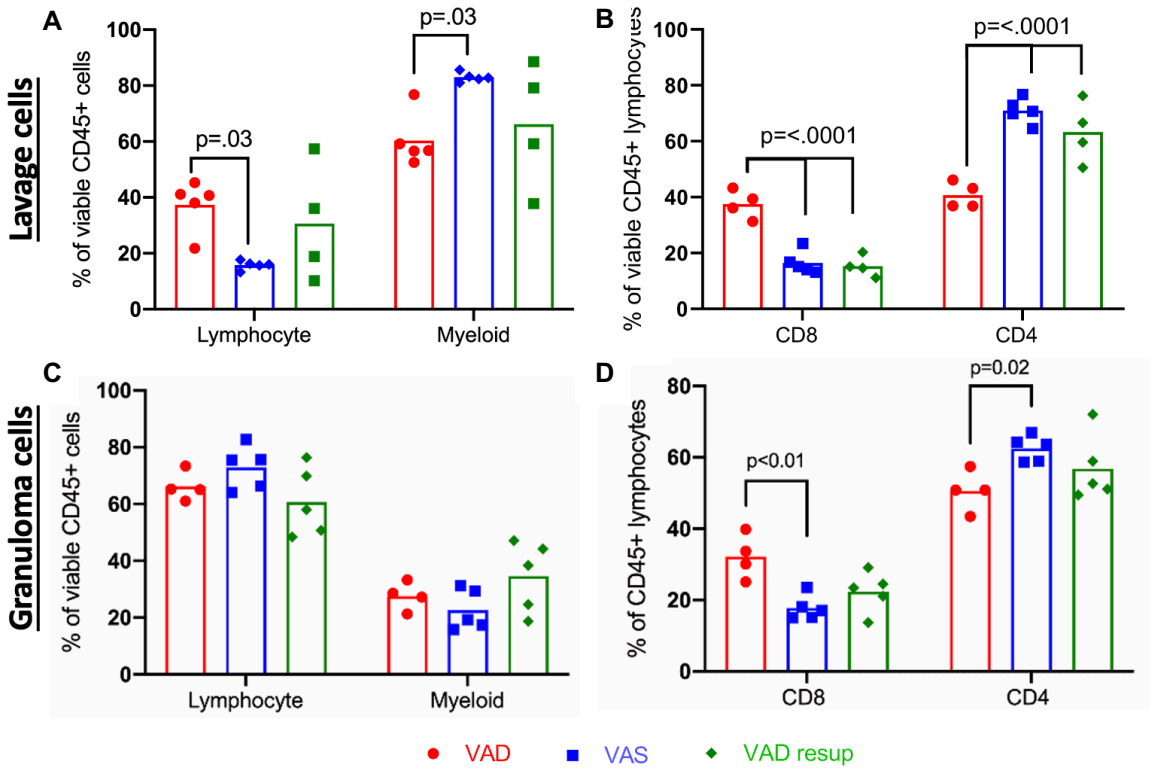

Figure 10. ***Vitamin A status effects inflammatory cell prevalence and composition.*** A-B) Flow cytometric analysis of bronchiolar alveolar derived cells. C-D) Flow cytometric analysis of cells derived from isolated and processed granulomatous lesions. A, C) Breakdown of CD45+ into myeloid and lymphocytic cellular population based on cellular size, forward scattered, and cellular complexity, side scatter. B, D) further differentiation of lymphocytic T cell populations utilizing CD8 and CD4 antibodies. Statistical analysis was performed via a two-way ANOVA using a Tukey's correction. Reproduced from Podell et al. 2022[22].

Vitamin A sufficient and vitamin A deficient animals have different genotypic profiles in both naïve and infected states

To examine how vitamin A status skews gene expression in regards to inflammatory pathways, lipid metabolism and vitamin A metabolism both infected and naïve lung homogenates from VAS, VAD and VAD resupp. animals were processed and submitted for RNA Nanostring expression quantification. In unsupervised heat map clustering of normalized gene expression, VAS and resupplemented animals cluster together and not with VAD animals in inflammatory pathways **(Fig. 11)**, as well as lipid mediator and vitamin A metabolic pathways **(Fig. 12)**.

Investigating fold change expression of individual genes, utilizing VAS animals as base line, demonstrated significant shift in several genes involved with lymphocytic cell proliferation and vitamin A metabolism for VAD animals. In naive animals there is clear and significant down regulation of vitamin A metabolism with lowered expression of DHRS3, RARB, RARG, RBP1 ($P \leq 0.05$ and $P \leq 0.01$), and an attempt to increase any available ATRA with marked down regulation of ATRA catabolic enzymes CYP26A1 and CYP26B1 ($P \leq 0.01$). Naive VAD animals had heightened inflammatory status compared to sufficient animals with increased expression of STAT3, CCR5, LCN2, CD1B4, CD1C2, CXCR2, CXCR1, CCR1 and A4B7 ($P \leq 0.05$ and $P \leq 0.01$). Additionally, T cell differentiation in deficient animals skewed towards Th17 T cells and follicular helper T cells with increased expression of STAT3 and BCL6 ($P \leq 0.05$ and $P \leq 0.01$) **(Fig. 13)**.

While naïve VAD guinea pigs had coordinated regulatory changes in both immune status and vitamin A metabolism infected VAD animals lost coordination and had dysregulated immune and metabolic responses. Infected VAD animals both enhanced, via DHRS9, and down regulated, via RARG, RXRG, RARB, ADH1C, vitamin A metabolism ($P \leq 0.05$ and $P \leq 0.01$). A similar dysregulated response was appreciated in immune status with contradicting expression of T cell inhibitory molecules, CTLA4 and KLRG1, and inflammatory interleukin receptors, IL-12 and IL-1 ($P \leq 0.05$) **(Fig 14A)**. In line with much of the previous data, VAD resupp. animals lacked any significant gene variation compared to VAS animals **(Fig. 14B)**. All Nanostring heatmaps, including day 30 post infection Nanostring evaluation and list of evaluated genes is in supplemental (Sup Fig 6, Sup table 2).

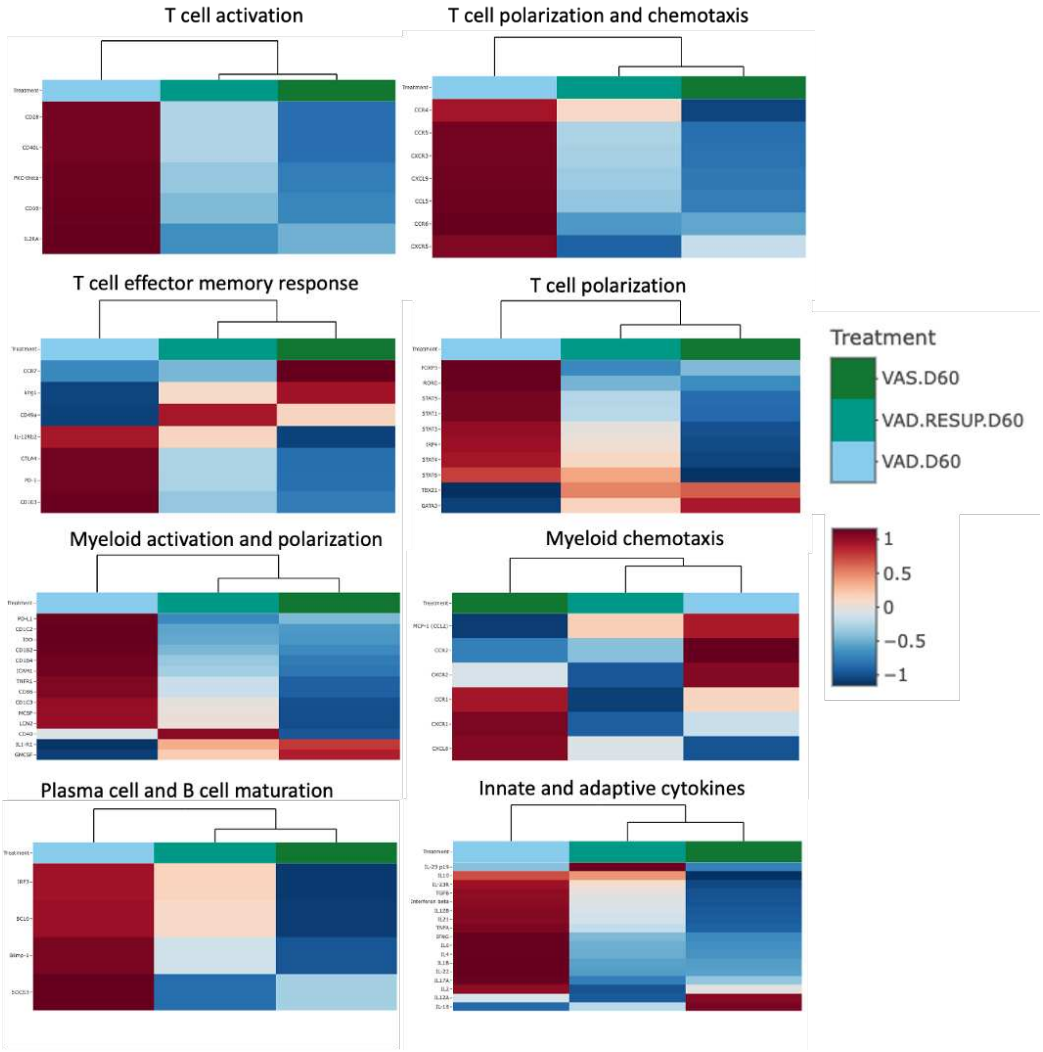

Figure 11. Day 60 post infection VAD animals cluster separately from VAS and VAD resupp.. Unsupervised clustered of gene expression of inflammatory pathways in relation to a variety of T cell, B cell and myeloid cellular processes and chemotaxis.

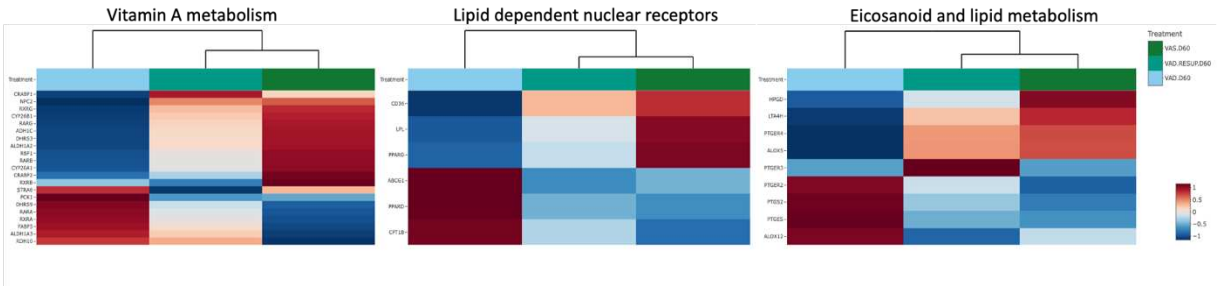

Figure 12. Day 60 post infection VAD animals cluster separately from VAS and VAD resupp. Unsupervised clustered of gene expression for a host of lipid and vitamin A metabolic pathways.

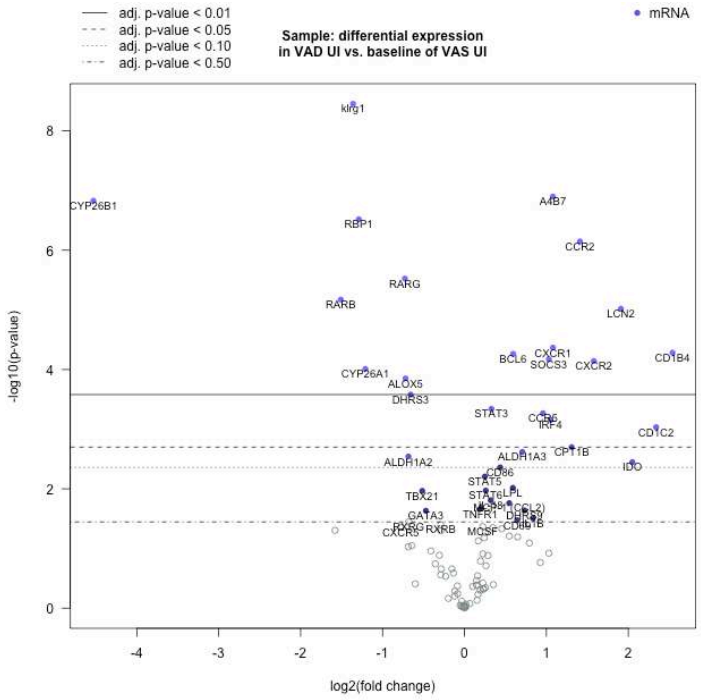

Figure 13. Volcano plot demonstrates differences between naive VAD and VAS animals in key pathways. VAD fold changes and significance compared to VAS baseline gene expression.

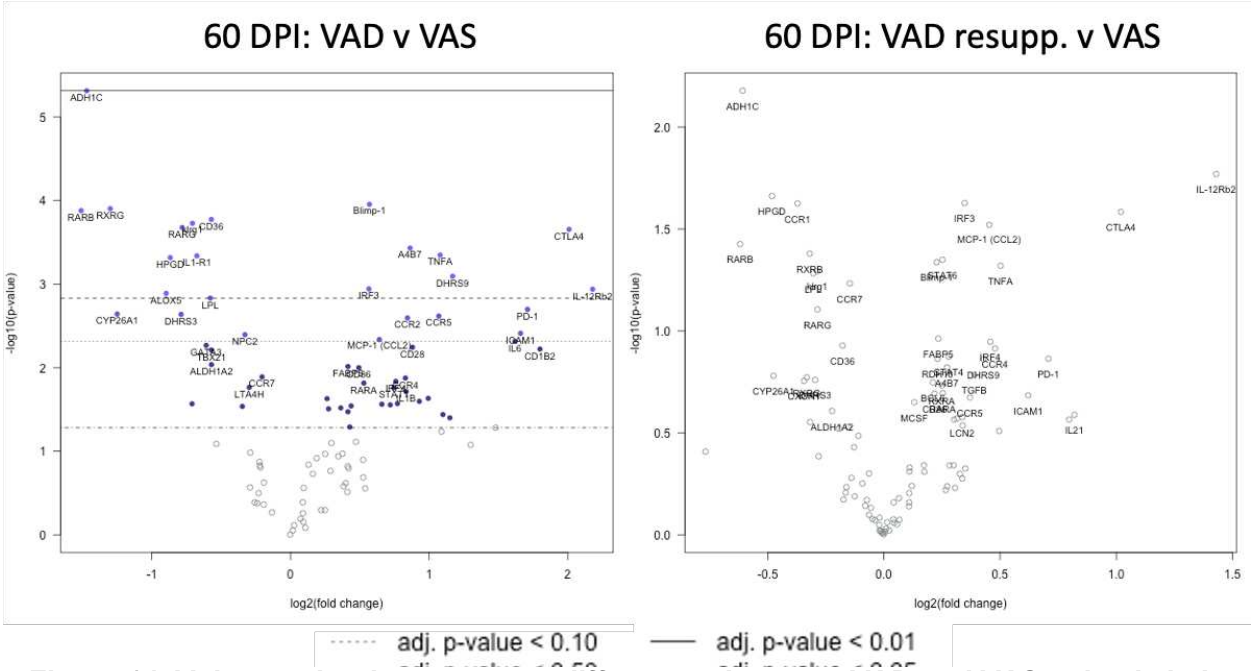

Figure 14. Volcano plot demonstrates differences between VAD and VAS animals in key pathways. VAD and VAD resupp. fold changes and significance compared to VAS baseline gene expression.

Bacterial burden in the lung is dependent on vitamin A status.

Bacterial burden was assessed via colony forming unit counts. CFU counts from the lung demonstrate a significantly higher bacterial burden in the lung in VAD animals compares to both VAS and VAD resupp. animals ($P \leq 0.05$) **(Fig. 15A)**. In contrast to the significant increase of VAD splenic lesion burden, no significant CFU changes were observed in splenic tissue between VAD and VAS animals. However, VAD resupp. does trend down in splenic CFU counts compared to both VAS and VAD animals **(Fig. 15B)**.

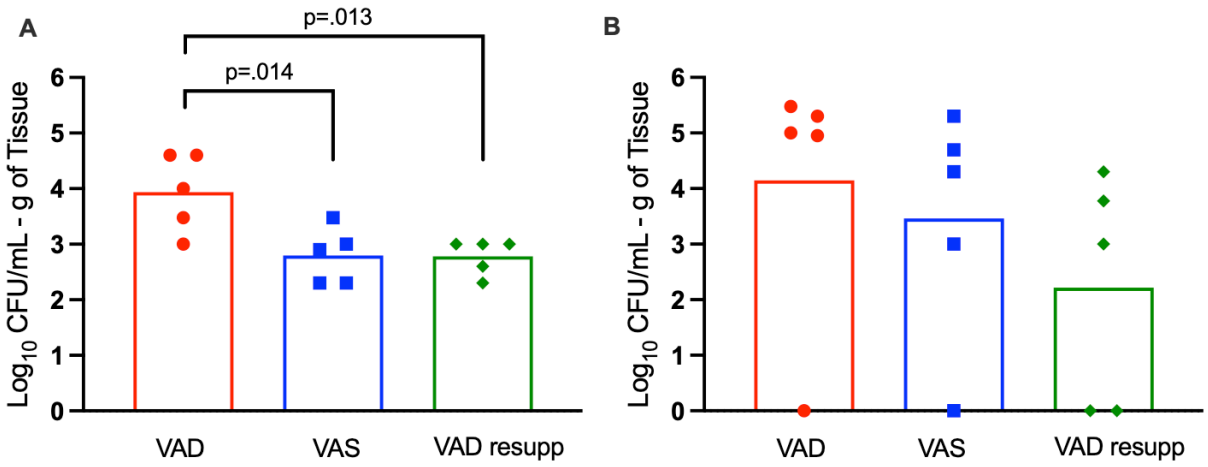

Figure 15. Bacterial burden in the lung is dependent on vitamin A status. Bacterial enumeration, via CFU count, of VAD, VAS and VAD resupp. guinea pigs 60 days post infection. A) Colony forming units count of infected lung homogenates. B) Colony forming units counts of infected splenic homogenates. Reproduced from Podell et al. 2022[22].

Discussion:

Vitamin A retinol deficiency leads to a host of disease manifestations centered around dysregulation of physiological homeostasis in a variety of cell types and organ systems[148,149]. Several studies have discerned the invaluable role vitamin A plays in the functionality of both innate and adaptive immune processes[13,150,151]. In 2017, Dr. Megan Murray, correlating micronutrient abnormalities to active and progressive Mtb infections discovered a remarkable relationship of subclinical vitamin A deficiency to clinical tuberculosis[6]. However, the pathophysiology of this correlation had yet to be elucidated in humans or transitional animal models. This chapter aimed to close this gap in knowledge by creating the first vitamin A deficient guinea model and examining differences in lesion morphology, lesion burden, bacterial burden and genotypical immunological profiling between both naïve and infected vitamin A sufficient and vitamin A deficient animals.

To accomplish this study guinea pigs were fed a diet devoid of retinyl palmitate, the dietary source of vitamin A. This diet, fed to neonatal animals, was able to prevent hepatic retinol storage and lower serum retinol levels to below the definition of subclinical vitamin A deficiency, 20 ug/dl[152]. The model required further refinement with initial animals demonstrating overt clinical effects of vitamin A deficiency with systemic epithelial metaplasia and hyperkeratosis. Further finesse, with weekly supplementation of 100 units of retinyl palmitate, allowed for achievement of a reliable subclinical vitamin A deficient animal model with translational ramifications to vitamin A deficiency in humans.

With a validated vitamin A deficient model in place, VAS, VAD and VAD re-supplementation animals were infected with Mtb. As expected, retinol serum level in VAD animals was relatively unaffected throughout the course of the infection, continuing a downward trend during the acute phase of infection, reaching the limit of detection by 30 days post infection. However, an unexpected finding was the precipitous drop in VAS animals from days 14 post infection to days 40 post infection. Previous studies have described a relative drop in serum retinol levels during the acute stages of innate immunity[153,154]; however, the physiology of this drop requires further investigation. Some theories on decreased serum levels include: the reduction of retinol movement via decreased retinol binding proteins as negative acute phase proteins are ramped up in the face of a systemic inflammatory response[153]; increased use of retinol metabolism by macrophages and dendritic cells at sites of inflammation, as seen in *in vitro* studies [155] ; overt loss of retinol and retinol binding protein through glomeruli filtration[156,157]. One study in vitamin A sufficient rats observed a significant down regulation of retinol binding protein and serum retinol levels with the induction of lipopolysaccharide induced inflammation and correlated the decrease to a reduction in hepatocellular retinol binding protein synthesis[23]. This study, in concert with a variety of observational human studies, established that serum plasma levels are not an accurate measure of vitamin A status during an inflammatory state[158–

[160]. This known phenomenon is something that we could be appreciating in this study; however, the delay of infection to onset of serum retinol loss warrants further mechanistic investigation.

To Further evaluate the loss of retinol of infected sufficient guinea pigs future studies utilizing isotope specific retinol are needed to trace distribution of these macromolecules to fully elicit how retinol is utilized in the face of an intracellular pathogen and corresponding inflammatory response[161]. Additionally, evaluation of urine retinol is needed in future studies to provide a complete picture of vitamin A metabolism and lost in the face of an Mtb infection.

As briefly mentioned, another clinical parameter for evaluating vitamin A status in human patients is quantifying retinol binding protein 4 (RBP4). RBP4 is primarily made within hepatocytes and stellate cells, the primary cells for retinol storage in the form of retinyl esters, and is only released from cells when bound to retinol (holo-RBP4) [162]. Holo-RBP4 levels thus can be utilized as an indirect methodology for assessing retinol concentration[163,164]. Evaluation of RBP4 via western blot analysis in this study further confirms the utility of RBP4 to assess vitamin A status in both serum and liver samples. Of note, kinetic assessment of serum RBP4 levels of infected VAS animals demonstrated a drop of overall protein concentration beginning at days 20 post infection and rebounding at days 40 post infection. This significant reduction closely aligns with decreased serum retinol levels in the same animals. Again, further studies are required to evaluate if the RBP4 is down regulated, sequestered in hepatocytes, lost in glomerular filtration or is delivering retinol to the site of active inflammation and then is excreted in the urine as apo-RBP. Terminal serum RBP4 protein concentrations further coincides with serum retinol levels with significant decreased protein concentration between VAS and VAD and variable drop of RBP4 protein between VAS naïve and infected animals.

Further confirming RBP4 physiologic release from hepatocytes only as a holo protein, evaluation of terminal liver RBP4 levels shows a significant increase in protein concentration in VAD animals compared to VAS. Collectively, serum retinol levels and RBP data demonstrates a

complete collapse of retinol and retinol-associated transport apparatuses in both naïve and infected VAD animals, while leaving intriguing questions regarding retinol metabolism in infected sufficient animals.

Looking past retinol and RBP serum status and examining tissue level differences, vitamin A status has minimal effect on overall lesion burden at the site of primary Mtb infection, the lung; however, there is an observable difference in lesion morphology between groups. VAS animals demonstrated classic primary casseous Mtb granulomas with well demarcated lesions defined by circumscribing fibrosis, outer pockets of lymphocytes, with inner foamy macrophages and centralized necrosis[165]. This morphology stands in stark contrast to the VAD animals that have poorly demarcated lesions lacking well organized layering of inflammatory cells, indicating a dysregulated inflammatory response to the intracellular bacteria. Leading into the larger debate of the role of the granuloma and its benefit to the host of the bacteria[166,167]; this change of lesion morphology and lack of coordinated inflammatory response may explain the reason for an increase in CFU burden in the lung and significant increase of lesion burden in distant visceral organs, such as the spleen.

To further examine vitamin A's role in the immunopathogenesis on Mtb infections, gene expression profiles between naïve and infected vitamin A groups were investigated. Examining naive VAD animals against the baseline of naive VAS animals, there is significant upregulation and down regulation of several genes correlating to specific cellular and immune pathways. Naïve VAD animals have an enhanced inflammatory state compared to VAS animals with heightened expression of variety of chemokines, and enhanced immune pathways with upregulated IRF4, a lymphocytic regulator, LCN2, a pleotropic mediator of a variety of inflammatory processes, and CD1b4, a lipid antigen binding complex[168,169]. Not only do VAD animals have generalized upregulation of inflammatory genes, but they also have increased propensity for T differentiation towards follicular helper T cells and expanded humoral immunity

via the synergistic upregulation of STAT3 and BCL6[170,171]. Follicular T cells are essential for B cell maturation and germinal center formation and Interestingly, have been shown to play a beneficial role in Mtb protection in mice[172]. Within naïve VAD animals there is a distinct down regulation of gene regulating vitamin A pathways correlating to a lack of systemic retinol or functional retinoic acid to induce upregulation of this subset of genes.

Gene expression of infected VAD animals demonstrated a generalized dysregulated response and contradictory changes in terms of both inflammatory and vitamin A pathways. The genes with the most pronounced upregulation are IL-12rb2 and and CTLA4. These genes have contradicting role with IL-12 receptors promoting T cell activation, particularly to Th1 lineages, while CTLA4 in combination with CD80 induces T cell anergy. Further indicating immune functional dysregulation is the upregulation of inflammatory promoters IRF3, TNFα with downregulation of inflammatory mediator IL-1-R1. Similar dysregulation of vitamin A pathways is appreciated with down regulation of many vitamin A metabolic genes but upregulation of a key metabolic gene DHRS9, responsible for converting retinol to retinoic acid.

Interestingly both naïve and infected VAD animals have enhanced expression of key regulators of lymphocyte differentiation and maturation, with BCL6 upregulated in naïve animals and BLIMP-1 up regulated in infected animals. The BCL6-BLIMP-1 axis has been extensively studied in several disease processes and general B cell and T cell maturation[173,174]. As previously discussed, BCL-6 enhances follicular T cells and proliferation of germinal B cells[175]. These cells, working in conjunction, lead to an enhanced humoral immunity and generalized immune regulation. In juxtaposition, BLIMP-1 enhances T cell differentiation in a variety of T helper cells, while downregulating follicular T cells[176]. Furthermore, BLIMP-1 has shown to be upregulated in exhausted CD4+ T cells leading to CD8+ T cell dysfunction[177]. The heightened expression of this essential gene axis may explain the large shifts in lymphocytes proliferation and CD4+ to CD8+ distributions from VAD to VAS animals as assessed via flow cytometry.

As stated, VAD animals have an expanded lymphocytic population and skewed CD4 to CD8 ratio compared VAS animals. Though there is no reference for a normal guinea pig CD4+/CD8+ ratio, a normal healthy ratio in humans 1.5 to 2.5[178]. A lower ratio can be indicative immune dysfunction including in humans: HIV, hematopoietic pathology, multiple sclerosis or evidence of immune depletion due to chemotherapy[179]. VAD bronchoalveolar lavage cells had a CD4+:CD8+ ratio of 1.11 compared to VAS ratio of 4.77. This marked cellular shift in VAD animal, in combination with the contradicting inflammatory gene profiles, speaks to the overt dysregulation of the immune response to an Mtb infection. Further, this skewed cellular ratio, and the importance of CD4 for driving granuloma formation, may help to explain the morphologic disparity between VAS and VAD animals.

This study not only aimed to examine the effect vitamin A deficiency has on tuberculosis disease progression but also looked to understand how the effects of that deficiency could be altered with the reintroduction of a vitamin A sufficient diet during an ongoing infection. Throughout almost all parameters and assays resupplemented animals were partially rescued from the observed detrimental effects of a vitamin A deficient state. In terms of retinol and RBP4 levels, VAD resupp. animals were able to resume movement and metabolism of any of the received dietary retinol with decreased liver RBP4 levels, partially recovering terminal serum RBP and retinol as well as a vitamin A metabolic gene profiling in line with VAS animals. Lung lesion morphology of VAD resupp. animal's perfectly blends the other two groups, with a mosaic of well delineated granulomas and poorly delineated disorganized granulomas. VAD resupp. animals align closely with VAS animals in terms of bacterial burden, inflammatory cell populations and all gene expression profiles. The partial rescue of VAD resupp. animals require more investigation to fully comprehend the effects of vitamin A supplementation during infection and whether increased supplementation or earlier dietary intervention can further sway animals away from deficient disease features to a more classic sufficient disease state.

Cumulatively, data from this study exhibits vitamin A status has a profound effect on the pathogenesis of tuberculosis in the guinea pig in terms of lesion morphology, T cell distributions, bacterial burden and genetic profiling of key inflammatory and retinoid regulators. Coinciding with Dr. Megan Murray's epidemiologic study linking vitamin A deficiency to clinically apparent Mtb, our deficient guinea pigs has progressive granulomatous lesions, and altered ability to respond to an Mtb infection. This study went further by establishing the ability to reverse detrimental effects of vitamin A deficiency via reintroduction of a sufficient diet during an active infection, which could have profound implications on human Mtb disease and treatment.

This study leaves many questions open for further investigation. Such as further understanding the pathophysiology of decreased serum retinol and RBP4 in sufficient animals during late innate immunity. Investigating the role vitamin A has on T cell functionality and CD4+ T cell proliferative abilities in the face of an Mtb infection; and exploring the cause and effect of the distinct morphologic differences between VAD and VAS granulomas.

As alluded to, vitamin A plays an essential role in a host of physiological processes throughout the body including immunologic functionality. This study, marrying previous human epidemiologic work, created a novel vitamin A deficient guinea pig model to evaluate intersecting pathophysiology of vitamin A deficiency and Mtb infections. This study found increased disease burden, altered lesion morphology, and dysregulated inflammatory responses corresponding to an increased lung bacterial infection. Though several questions remain unanswered, this study lays the foundation for understanding the role vitamin A has in intracellular pathogen such as Mtb. The need to understand comorbidities, such as this, is essential as we face mounting pressures with this deadly disease including collapse of surveillance systems, ineffective vaccines and ever-growing threat of multidrug resistant Mtb. By fully comprehending the interplay of vitamin A and Mtb we might not only be able to mitigate this

newly discovered comorbidity but may also be able to harness this essential micronutrient to diminish the prevalence of clinical active tuberculosis.

CHAPTER 2: Kinetic expression and functionality of CD-restricted lipid-based immunity at a tissue level in a *Mycobacterium tuberculosis* infection using a guinea pig model

Summary:

CD1 complexes are membranous antigen presenting glycoproteins that are homologous to MHC I complexes; however, CD1 complexes present lipid antigen rather than protein. Several studies have investigated CD1 complexes and the corresponding antigen-restricted immunity to specific lipid antigens of *Mycobacterium tuberculosis* (Mtb). However, understanding the role of CD1-restricted immunity in response to Mtb infection has been limited by availability of animal models naturally expressing a CD1 repertoire comparable to that of humans. Guinea pigs, in contrast to other rodent models, have a CD1 ortholog expression similar to humans. In these studies, we utilize the guinea pig to establish the kinetic protein and gene expression of CD1b orthologs, as well as Mtb lipid-antigen and CD1b-restricted activity at the tissue level over the course of Mtb infection. Our results indicate CD1b complex expression has transient upregulation during the effector phase of adaptive immunity that wanes with disease chronicity. In congruence with other studies, we show high CD1b3 expression on B cells, identifying CD1b3 as the predominant CD1 ortholog in pulmonary granuloma lesions. Cytotoxic activity of CD1b-restricted immunity closely paralleled the kinetic changes in CD1b expression in Mtb infected lung and spleen. Interestingly, ortholog-specific PCR revealed that each of the four CD1b orthologs in the guinea pig has a unique kinetic gene expression pattern, with two complexes being upregulated during the innate phase of immunity. This study demonstrates that CD1b expression is modulated by Mtb infection in lung and spleen, leading to establishment of CD1b-restricted immunity as a component of the antigen-specific response to Mtb infection.

Introduction:

CD1 lipid-restricted immunity represents a relatively novel branch of immunology that is driven by CD1 glycoprotein mediated expansion of CD1-restricted T cells and invariant natural killer T cells[105,180]. CD1 glycoproteins have homologous structuring to MHC I antigen-presenting molecules but bind and present a variety of lipid antigens[181, 32]. There are 5 known CD1 glycoproteins, CD1a-e, which are divided into two functional groups; group 1 composed of CD1a-c and group 2 composed of CD1d[35,182183]. Group 2 CD1 complexes have been found to be constitutively expressed on a variety of cell types and involved with a host of endogenous and exogenous lipids leading to the expansion of invariant natural killer T cells[184, 185]. In contrast, Group 1 CD1 complexes have inducible expression and are confined to professional antigen presenting cells, loading a variety of endogenous and exogenous lipids, such as those derived from *Mycobacterium tuberculosis* (Mtb), leading to an expansion of a variety of functionally nonpolymorphic CD1-restricted αβ and γδ T cells[117,186,187]. Due to their ability to encounter, load and present microbial lipids, group 1 CD1 complexes are relevant to the pathogenesis of several infectious diseases.

Owing to the lipid-rich composition of Mtb, multiple studies have investigated the potential role of CD1-restricted immunity in tuberculosis (TB). Several studies examining peripheral blood of Mtb-infected human subjects found increased expression of CD1 glycoproteins on myeloid cells and corresponding presence of CD1-restricted T cells[125,188,189]. Other studies have taken additional strides in isolation of Mtb-lipid specific T cells via detection with lipid loaded CD1 tetramers[190,191]. Though these studies lay a foundational understanding of CD1-restricted immunity during Mtb infection, there is still a multitude of fundamental gaps within the field including: whether CD1-restricted immunity contributes as a component of innate or adaptive branches of immunity, whether CD1 expression is modulated by Mtb infection *in*

vivo, and whether CD1 plays a functional role in disease pathogenesis and granuloma formation in the tissue response to infection[35,125,182].

One major limitation to further understanding of CD1 lipid-restricted immunity in response to Mtb is the lack of a translatable animal model with naturally occurring group I CD1 expression. The majority of rodent species naturally express only CD1d, group 2 CD1 complexes. However, guinea pigs have a similar CD1 complex repertoire to humans containing 4 orthologs of CD1b glycoproteins and 3 orthologs of CD1c from group 1, as well as CD1d[134, 192]. Previous studies have characterized this CD1 repertoire *in vivo* and *ex vivo* as well as in the face of administered lipids isolated from cultured Mtb, and BCG vaccination[134,116,193,]. However, there is limited understanding of how Mtb infection impacts CD1 expression and the development of CD1-restricted T cell immunity over the course of TB disease in infected tissue.

In this current study we utilized the guinea pig model of pulmonary TB and reagents specific to CD1b orthologs to kinetically measure CD1b-restricted immunity at innate, early adaptive, and late adaptive stages of TB within the lung and spleen. Overall, this work demonstrates that CD1 immunity actively responds to Mtb and indicates a possible larger functional role in the control of infection. Importantly, this study establishes the ability to assess CD1 immunity at the protein and molecular level within infected tissue utilizing a highly translatable model, which sets the stage for additional investigations and potential closure of fundamental knowledge gaps within the field of CD1-restricted immunity.

Material and Methods:

Animals:

Two separate animal studies were performed to kinetically monitor CD1b expression in blood and tissue over the course of Mtb infection. Female outbred Dunkin-Hartley guinea pigs

weighing 250-300 g were obtained from either Charles River Laboratories (Wilmington, MA) or Elm Hill Labs (Chelmsford, MA). In the first study, guinea pigs infected with Mtb were evaluated at 14-, 30- and 60-days post-infection (DPI) (n=6 per endpoint). In the second study, Mtb-infected guinea pigs evaluated at 14, 30 and 60 DPI (n=5 per endpoint) were compared to uninfected, naïve guinea pigs (n=3) at each necropsy endpoint to compare impact of infection over baseline CD1b expression. Tissues and cells from inbred strain 13 guinea pigs, a colony maintained at CSU, were utilized for assay development, including cytotoxicity, CD1 expression via flow cytometric analysis, and validation of antibodies for immunohistochemistry on fresh frozen tissue. All animals were pair housed and monitored via the Colorado State University (CSU) Lab Animal Resources staff and veterinarians. All animal studies were performed in accordance with protocols approved by the Institutional Animal Care and Use Committee at Colorado State University under protocol number 1401.

CD1-specific reagents:

104C1 guinea pig fibroblast cell lines transfected with CD1b1, CD1b2, CD1b3 and CD1b4 were previously described[194]. Specific CD1b ortholog-expressing cell lines were compared to a mock-transfectant containing only the empty pcDNA3.1 vector. The process for generation of synthetic lipid antigens, glucose monomycolate and mycolic acid has been previously described[195]. These lipid antigens were chosen as known CD1b ligands with demonstrated antigen-specific response in previous studies with antigen-specific IFNγ production or antigen-specific CD1b tetramer-based detection of cells in human peripheral blood[195,196,197]. Guinea pig-specific reagents and synthetic lipid antigens were provided by Dr. D. Branch Moody, Brigham and Women's Hospital, including pure synthetic mycolic acid and glucose monomycolate Mtb lipids, CD1 transfected 104C1 cells (CD1B1-4 and CD1C1-3), and anti-guinea CD1 mouse monoclonal antibodies with varying ortholog specificity (sup. Fig. 8 & table 3)[194].

Infection and euthanasia:

In the first study, a low-dose aerosol exposure of guinea pigs to Mtb was performed using the Madison chamber aerosol generation device (College of Engineering Shops, University of Wisconsin, Madison, WI) calibrated to deliver approximately 20-50 bacilli of the H37Rv strain of Mtb isolated during log-phase growth in Proskauer-Beck media. The second study used the Glas-Col aerosol chamber (Terre Haute, IN) to deliver a low-dose exposure of <50 bacilli of the Erdman strain of Mtb. On pre-determined endpoints, 14, 30 and 60 DPI, guinea pig groups were euthanized. Euthanasia was performed via an initial induction of an anesthetic state via intramuscular injection of 30 mg of ketamine and 8 mg of xylazine in combination, followed by an intraperitoneal injection of an overdose of 3 ml/animal of 390 mg/ml sodium pentobarbital.

Necropsy and tissue processing:

Once euthanized, animal tissues and cells were harvested which included airway-accessible macrophages and other leukocytes by bronchoalveolar lavage, PBMCs from anticoagulated peripheral blood, and cell suspensions derived from lung and splenic parenchyma, as previously reported[144,22]. In brief, the right cranial and caudal bronchi were clamped and lung lobes removed and processed for either RNA preservation in RNAlater solution (Thermofisher, Waltham, MA), OCT-embedding for fresh-frozen immunohistochemistry (Sakura, Torrance, CA), or for bacterial enumeration by colony forming units (CFU). Airway-accessible leukocytes were collected via post mortem bronchioalveolar lavage utilizing an 18-gauge catheter and flushing with 25 ml of HBSS containing 0.01 μM EDTA solution in five, 5 ml, intervals. Following bronchoalveolar lavage, the remaining lung was perfused with 5 μg/ml collagenase (Sigma-Aldrich, cat#: C9263) and incubated for 30 minutes in a 37°C water bath. The digested lung parenchyma and collected spleen were individually processed through 40 μm cell strainers.

Once strained, all samples were subjected to hypotonic solution for 20 to 45 seconds for lysis of erythrocytes. To increase overall cell viability for downstream assays, all tissue-derived cell suspensions were subjected to magnetic bead negative selection using biotinylated annexin V and streptavidin-conjugated magnetic nanobeads. To complete this protocol, cells were placed in 4 ml of 1X annexin binding buffer (Biolegend, cat#: 422201) with biotinylated annexin V (Biolegend, Cat # 640904) and incubated for 30 minutes. Following incubation, cells were centrifuged at 500 x g for 5 minutes, washed with additional binding buffer, centrifuged again and resuspended in 500 µl of binding buffer. Thirty µl of streptavidin nanobeads (Biolegend, cat#: 480016) were added and incubated for 20 minutes with intermittent vortexing. Following incubation additional binding buffer was added to bring solutions to a total of 4 ml. The cell suspension was placed on a magnetic rack for 10 minutes to allow for magnetic binding of nanobeads. Finally, unbound cells were collected with a serologic pipette. Collected cells were washed in Hank's balanced salt solution then viability and cell count assessed via a hemocytometer and trypan blue exclusion. Splenic and lung suspension cells were used for analysis of CD1b expression by flow cytometry and remaining cells plated in RPMI media containing 10% fetal bovine serum and an antimicrobial cocktail, then incubated overnight at 37°C with 5% CO_2 to allow for separation of adherent cells (histiocytic/dendritic in origin) and non-adherent cells (lymphocytes). PBMCs were collected via a right ventricular intracardiac blood draw directly following euthanasia, diluted 1:2 in HBSS and separated on a density gradient using Lympholyte mammal media (Cedarlane, cat#: CL5110) per manufacturer's instructions.

Intradermal *M. tuberculosis* antigen challenge:

Performed only in the second study and 48-hours prior to each euthanasia endpoint, both infected and naïve guinea pigs received an intradermal hypersensitivity challenge to either Mtb

lipid antigens, Mtb protein antigen in the form of PPD, or sterile PBS. Each guinea pig received seven intradermal injections: 1. Mycolic acid liposome, 2. Glucose monomycolate liposome, 3. Mycolic acid in PBS, 4. Glucose monomycolate in PBS, 5. Unloaded liposome, 6. Mtb purified protein derivative (PPD) (Tuberculin PPD Bovine, USDA Veterinary Services), or 7. Sterile PBS. Liposomes were made using distearoylphosphatidylcholine (DSPC) (Avanti lipids, cat#: 850365P) and cholesterol (Avanti lipids, cat#: 700100P) lipids with or without synthetic Mtb lipid (molar ratio 7:2:1, respectively) via a lipid extruder (Avanti Lipids, Alabaster, AL). For liposomal formulation, DSPC and cholesterol were weighed out to meet specific molar ratio and added to a pre-rinsed glass container. Lipids were dissolved in a solution of 10:1 chloroform and methanol, either with or without solubilized mycolic acid or glucose monomycolate. Once dissolved, the lipid solution was completely evaporated utilizing a nitrogen gas bath. Dried lipids were then suspended in PBS prewarmed to 68°C. The solution was then vortexed and incubated in a water bath at 68°C for 40 minutes, with vortexing every 10 minutes, to allow for liposome formation. During the incubation the liposome extruder apparatus (Avanti lipids, Alabaster, AL) was assembled to company specifications and warmed to 70°C. After incubation, the liposome solution was passed through the extruding system 7-8 times to allow for formation of a uniform unilamellar liposomes at approximately 150μm in diameter. Liposomal size was confirmed with a Nanosight instrument and capacity for macrophage phagocytosis confirmed using guinea pig bone marrow-derived macrophages in *in vitro* culture (sup. Fig 9). The free Mtb lipid solution was prepared with similar nitrogen drying methodology. PBS lipid suspensions were sonicated using a Misonix ultrasonic liquid processor at 80 A for 4 minutes on a 20-second-on, 20-second-off cycle. All lipid injection sites received 4 μg of lipid whether in liposomal formulation or free lipid in PBS. PPD was administered at 2 μg per site. Guinea pigs were ventrally shaved from the point of the caudal xiphoid to the cranial aspect of the pubis. Injection sites were labelled and administered via intradermal injection using an insulin syringe

at 50 µl of sample per site. All sites were measured at 24 hours and 48 hours after the initial injection using calipers to measure cranial to caudal and lateral diameters.

Kinetic CD1 expression:

CD1b expression was measured by flow cytometry on cell suspensions from lung and spleen, cells isolated from bronchoalveolar lavage, and PBMCs from each animal. Flow cytometry methods are previously described[144,22]. Briefly, 1.5 x 10^6 cells from each sample were blocked with 2.24 µg/ml of guinea pig and rabbit immunoglobulin (Jackson Immunoresearch, Cat#: 011-000-003 and 006-000-002) in FACS buffer (PBS containing 1% FBS and 0.01% sodium azide) or using Fc-receptor block (Innovex, Cat#: 50-486-808). Cells were labeled with an antibody panel targeting CD1 expression among professional antigen presenting cells. (sup. table 4). Viability of cells was assessed via Zombie Yellow amine-reactive permeability dye (BioLegend, Cat# 423103). Data were acquired using a spectral unmixing Cytek Aurora flow cytometer (Cytek, Fremont, CA) and analyzed via Flowjo software version 10.8 (Flowjo, Ashland, OR) using a minimum of 100,000 total events, based on the gating strategy described in supplemental Figure 10. The degree of surface CD1 expression was inferred by comparing the mean fluorescence intensity (MFI) values for lung and spleen cells from each infected guinea pig to naïve guinea pigs after applying the same gating strategy (sup. figure 11).

CD1 cytotoxicity:

Previous reports suggest cytotoxic activity as a major function of CD1-restricted T cell responses in peripheral blood and as induced by immunization with lipid antigens[198,199]. To measure the cytotoxic activity of CD1b-restricted immunity over the course of Mtb infection, CD1b fibroblast transfectants (CD1b1-b4 or mock-transfected) served as target cells and were

incubated with effector cells, composed of the non-adherent cells isolated from the lung or spleen of each animal. Detection of cytotoxicity was performed using a flow cytometric technique previously described based on assessing membrane permeability, and thus, viability of target cell populations[200]. In brief, $1x10^7$ CD1b1 and CD1b3 transfected cells were collected and incubated with 0.5 μM Cell Trace Violet (Thermofisher, C34557) for 15 minutes in unmodified RPMI media. The reaction was quenched with 10 ml of additional RPMI containing 10% FBS for 10 minutes and cells pelleted and washed twice. Cells were plated in a 96-well plate at $5x10^4$ per well. Free lipid solutions were prepared as previously described for the intradermal skin testing and resuspended in RPMI media. Specified wells were then loaded with 4 μg of either synthetic mycolic acid or glucose monomycolate Mtb lipid, or mock-loaded to use as unloaded controls for determination of lipid-antigen specific cytotoxicity. Cells and lipid were incubated overnight to allow for lipid cellular trafficking and lipid presentation in the context of CD1b. These target cells were then incubated with non-adherent inflammatory cells derived from the lung and spleen from either naïve or Mtb-infected guinea pigs for 4 hours at a target:effector ratio ranging from 1:0 to 1:8. Incubated cells were then stained for viability using Zombie Yellow dye, diluted at 1:500 in PBS dilution then added at 100μl per sample (BioLegend, Cat# 423103). A pilot study was performed to validate this methodology against the guinea pig fibroblast target cells and identify the best CD1b orthologs to utilize for the main experiment. From the pilot, CD1b1 and CD1b3 had the highest degree of cellular lysis (sup Fig. 12). Data were acquired using a Cytek Aurora spectral unmixing flow cytometer (Cytek, Fremont, CA). Data were analyzed via Flowjo software version 10.8 (Flowjo, Ashland, OR) using a minimum of 50,000 events following the gating strategy demonstrated in sup. Fig. 13 with fibroblasts identified based on size and presence of cell trace violet signal. Mock-transfected fibroblasts, containing the empty vector with no CD1b construct, or CD1b1 and CD1b3 transfected fibroblasts without added lipid antigen were used as negative controls to identify cytotoxicity associated with CD1 restriction and specific lipid antigens. Data were

normalized to background using the mean cellular death among CD1b1 and CD1b3 transfectants without addition of effector cells (1:0 target to effector ratio).

Kinetic expression of specific CD1b orthologs by qRT-PCR relative gene expression:

Kinetic relative gene expression of CD1b was measured with CD1b ortholog-specific primers (CD1b1-b4) designed *de novo*. All primer set sequences were created using Geneious software (Auckland, NZ) via a 4-sequence alignment and selecting for non-consensus primer sets, which were then synthesized by Integrated DNA Technologies (IDT) (Coralville, IA) (sup. table 5). Primer set specificity was evaluated via the use of synthetic gene segments from IDT for each CD1b sequence (sup. Fig. 14). Primers were demonstrated to be specific for each of the CD1b1-4 orthologs without cross-reactive detection, and expression of CD1b1-b4 was confirmed in each respective fibroblast transfectant (sup. Fig. 15). For RNA isolation, freshly isolated lung tissue at each endpoint of day 14, 30 or 60 post-infection was minced in RNALater (Sigma, cat#: R0901), incubated at 4°C for 24 hours, then frozen at -80°C until RNA extraction. Tissue was thawed at room temperature and approximately 50 mg of tissue homogenized in RLT buffer (Qiagen) containing β-mercaptoethanol using Lysing Matrix A tubes (VWR, cat# 75784-610) in a bead beater instrument at full speed for two cycles of 20 seconds (MP Biomedical, cat# C321001). Proteinase K was added to the homogenate, incubated at 55°C for 15 minutes, then RNA was extracted with the RNeasy mini kit (Qiagen, cat# 74106) per manufacturer's instructions. Nucleic acid was eluted from the column, digested with DNase-I for 30 minutes at 37°C, then purified again using the RNeasy mini kit. Sample concentration was measured using a Nanodrop spectrophotometer and quality analyzed on an Agilent TapeStation. Generation of cDNA was performed using the iScript cDNA synthesis kit (BioRad cat# 1708890), reverse transcribing 1 µg of RNA per reaction. 25 ng of cDNA template was added to an iScript Sybr Green master mix containing 1.5mM $MgCl_2$ and 0.1 µM of each forward

and reverse primer. Relative gene expression was measured by normalizing log_2-fold expression to reference genes HPRT and β-actin using the ΔΔCt method, as previously described[22,142].

Distribution of tissue CD1 expression by immunohistochemistry:

Lung, and spleen were isolated fresh at necropsy, embedded in OCT medium (Thermofisher, cat#: 23-730-571) and cryopreserved in a liquid nitrogen bath, then stored at -80°C until further use. OCT-embedded tissue was sectioned using a cryotome maintained at -16 to -18°C, and a 7 µm section adhered to charged glass slides. After sectioning, tissues were immediately placed in a 100% chilled methanol fixation for 45 minutes to fix the tissue and inactivate the Mtb organism. All DAB chromogenic and fluorescent immunohistochemistry protocols were completed on methanol fixed tissue sections utilizing a Leica Bond RXm automated slide stainer using previously validated protocols (sup. tables 6 & 7). Fluorescent multiplex IHC was achieved using Opal fluorochromes 570 and 690 (Akoya Biosciences, cat# 570- FP1488001KT, 690- FP1495001KT, 690- FP1497001KT) to detect CD1-ortholog specific expression and distribution across myeloid/histiocytic, based on morphology, and B cell subsets, based on Pax5 transcription factor expression (clone 24, CellMarque, cat# 312M). All tissues were blocked in 2.5% goat serum solution (Vector Labs, cat# S-1012-50) and primary antibodies diluted in 2.5% goat serum. Primary antibodies were detected using a goat anti-mouse HRP secondary (Vector Labs, cat# MP-7452-50) and incubated with DAB substrate for chromogenic IHC or Opal fluorochromes for fluorescent IHC protocols. Quantification of immunohistochemistry was performed using Visiopharm analytical software (Hoersholm, Denmark). In brief, a nuclei-detect application was developed to discern between DAPI stained nuclei and Pax5 positive nuclei as well as identifying all cells within tissue preparations. This application was further developed to

delineate nuclei based on membranous CD1 expression. The end outputs of the analysis were $Pax5^{-}$ $CD1^{-}$ cells, $Pax5^{-}$ $CD1^{+}$ cells, $Pax5^{+}$ $CD1^{-}$ cells, and $Pax5^{+}$ $CD1^{+}$ cells.

Quantification of tissue bacterial burden:

Lung bacterial burden was quantified as previously described[22]. In brief, tissue homogenate was plated on 7H11 agar quad plates in 5-fold serial dilutions. Plates were incubated for 8 weeks and counted. Colony-forming units were log_{10}-transformed and expressed as colony-forming units per gram of tissue.

Statistical analysis:

All analyses, with the exception of the cytotoxicity assay, were performed utilizing Prism version 9.4.1 (GraphPad, San Diego, CA). Data distribution was evaluated via a Shapiro-Wilks test. Based on distribution, a One-Way ANOVA test or Kruskal-Wallis test was performed to determine statistical significance for flow cytometric analysis, gene expression, and histologic quantifications. Statistical significance was set at $p \leq 0.05$. For the cytotoxicity assay, all analyses were performed using R Statistical Software (v4.2.1; R Core Team 2021). AUC was calculated based on the ratio of effector to target cells and normalized percent killing via the metrumrg R package (v5.57)[201]. A 2-factor ANOVA with Sidak's correction was used to determine the significance between groups or time with the rstatix R package (v0.7.0)[202]

Results:

Kinetic upregulation of CD1b expression within tissue during Mtb infection is largely restricted to small leukocyte populations:

Initially, we sought to evaluate the impact of Mtb infection on CD1b expression over the course of TB disease. Surface CD1b expression was evaluated across two independent *in vivo* infection studies in spleen and lung of Mtb-infected guinea pigs among viable CD45+ leukocytes. An increased frequency of CD1b+ cells were demonstrated among infected animals compared to time matched naïve controls via flow cytometric analysis **(Fig. 16A-D)**. Inflammatory cells derived from lung parenchyma had similar basal surface CD1b expression during the initial innate response at day 14 of infection, with 11.55% ± 6.3% CD1b+ among infected and 9.96% ± 6% among naïve controls. The frequency of CD1b-expressing cells in lung of infected animals was greatest at day 30 of infection, a point during infection when the effector adaptive response has peaked. At day 30 of infection, there was a mean 43.5% ± 10.7% CD1b+ cells in infected lung, compared to 10.0% ± 6% CD1b+ cells among naïve, uninfected guinea pigs. CD1b expression among infected guinea pigs at day 30 of infection was significantly greater than naïve time-matched guinea pigs and kinetically compared to infected guinea pigs at either day 14 or day 60 of infection ($p \leq 0.0001$). Frequency of CD1b expressing leukocytes decreased with infection chronicity in the late adaptive immune phase at day 60 of infection, 24.1% ± 6.3% CD1b+. Guinea pigs at day 60 of infection had a significantly greater frequency of CD1b+ leukocytes compared to animals at day 14 of infection ($P \leq 0.05$) but was not significantly greater than time matched naïve guinea pigs **(Fig. 16B)**. Splenic CD45+ leukocytes followed similar surface CD1b expression kinetics to lung CD45+ cells. The greatest frequency of CD1b+ positive cells in spleen was observed at day 30 of infection (37.8% ± 8.7% CD1b+) with significant upregulation compared to guinea pigs at day 14 of infection (16.5% ± 4.2% CD1b+), guinea pigs at day 60 of infection (20.3% ± 8% CD1+), and naïve time matched control guinea pigs ($p \leq 0.0001$). In contrast to lung CD45+ cells, splenic CD45+ cells had significantly increased CD1b expression at day 14 of infection compared to naïve controls ($p \leq 0.05$) **(Fig. 16B)**.

To further discriminate the CD45+ leukocyte populations expressing CD1b over the course of infection, cells were gated by forward and side scatter to differentiate small and large leukocyte populations, previously shown to capture lymphocyte and myeloid populations, respectively [144,203,22]. Large cell leukocytes from both the lung and spleen had low basal surface expression of CD1b with no significant kinetic upregulation over the course of Mtb infection or compared to time-matched naïve control guinea pigs **(Fig. 16C)**. In contrast, lung derived small cell leukocytes had marked upregulation at day 30 of infection (51.2% ± 17.4% CD1b+) with significant upregulation compared to naïve guinea pigs ($p \leq 0.001$) and exposed guinea pigs at Day 14 (17% ± 5.1% CD1b+), and day 60 post-infection (19.9% ± 5.2% CD1b+) ($p \leq 0.0001$). Similarly, CD1b expression peaked among splenic small cell leukocytes at day 30 post-infection (40.6% ± 19.7%) compared to time-matched naïve, uninfected control animals ($p \leq 0.01$) and guinea pigs at day 14 post-infection (22.8% ± 12% CD1b+) ($p \leq 0.05$) **(Fig. 16D)**.

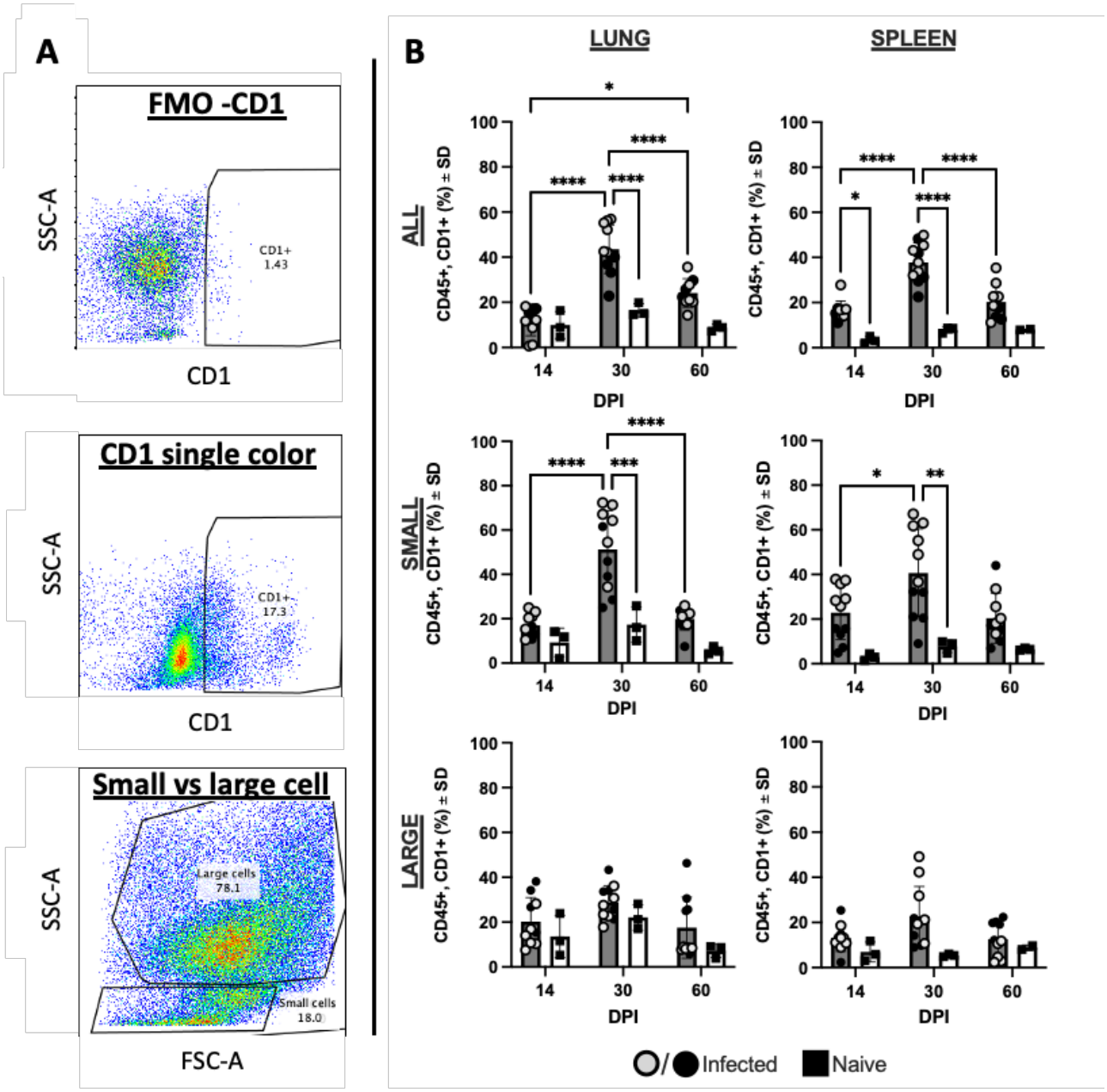

Figure 16. CD1b expression over the course of Mtb infection. Flow cytometric analysis of leukocytes at 14-, 30- and 60-days post infection (DPI). Cells were gated for live, CD45+ cells and evaluated for overall CD1 expression using the anti-CD1b monoclonal antibody, 1B12. Open and closed circles represent two separate experimental sets of identical study design. Naïve, time-matched controls were performed solely in one of two experiments. (A) Scatter plot gating of CD1 positive cells, demonstrating fluorescence-minus-one FMO gating control (top), gating of CD1b-expressing cells (middle), and gating strategy for isolating small vs large CD45+ leukocytes (bottom). (B-D) Proportion of cells expressing CD1b among lung- and spleen-derived cells. Graphs represent All CD45+ cells (B), delineated large leukocyte populations (C), and delineated small leukocyte populations (D). * P≤0.05, **P≤0.01, ***P≤0.001, and **** P≤0.0001; (B-D) Two-way ANOVA with Tukey post-hoc correction for multiple comparisons.

To evaluate the degree of CD1 modulation on individual CD1-positive antigen presenting cells, mean fluorescence intensity (MFI) was measured in Mtb-infected guinea pigs compared to naïve, uninfected animals at all three endpoints, 14, 30, and 60 days of infection. In correlation with the cellular breakdown by scatter parameters, MFI was examined in all CD45+ cells, large leukocytes, and small leukocytes (sup fig. 11). Increased surface expression of CD1b was observed primarily in lung-derived cells at day 30 of infection compared to naïve guinea pigs, the same endpoint when greater frequency of CD1b+ cells were observed ($p \leq 0.05$). No significant differences were observed at 14 DPI. These data suggest that increased expression of CD1b over the course of Mtb infection is the result of both increased cell frequency and upregulation of surface expression on cells capable of expressing CD1b.

Guinea pig CD1b orthologs have different spatial cellular expression profiles and kinetically specific gene expression patterns during the course of Mtb infection:

Having identified changes in CD1b expression among leukocytes responding to Mtb infection in tissue, we sought to evaluate the specific CD1b orthologs expressed such that antigen-specific CD1-restricted T cell immunity, as measured by cytotoxicity, could be evaluated in an ortholog-specific manner. Among monoclonal antibodies available to discriminate individual CD1b orthologs, the 1D12 clone is specific for CD1b1 and MsGp9 is specific for CD1b3 (sup. fig 8). Lung and spleen tissue from naïve guinea pigs were evaluated for expression of these specific orthologs by immunohistochemistry **(Fig 17A-F)**. Cell- and ortholog-specific expression patterns were evident across lung and spleen tissue. In lung, alveolar macrophages and interepithelial myeloid cells within the airways expressed CD1b1. In contrast, CD1b3 was expressed within the B cell regions of the splenic white pulp, corroborating with previous literature[194]. In disparity to CD1b3, CD1b1 within spleen is rare and limited predominantly to myeloid cells within the sinuses of the splenic red pulp.

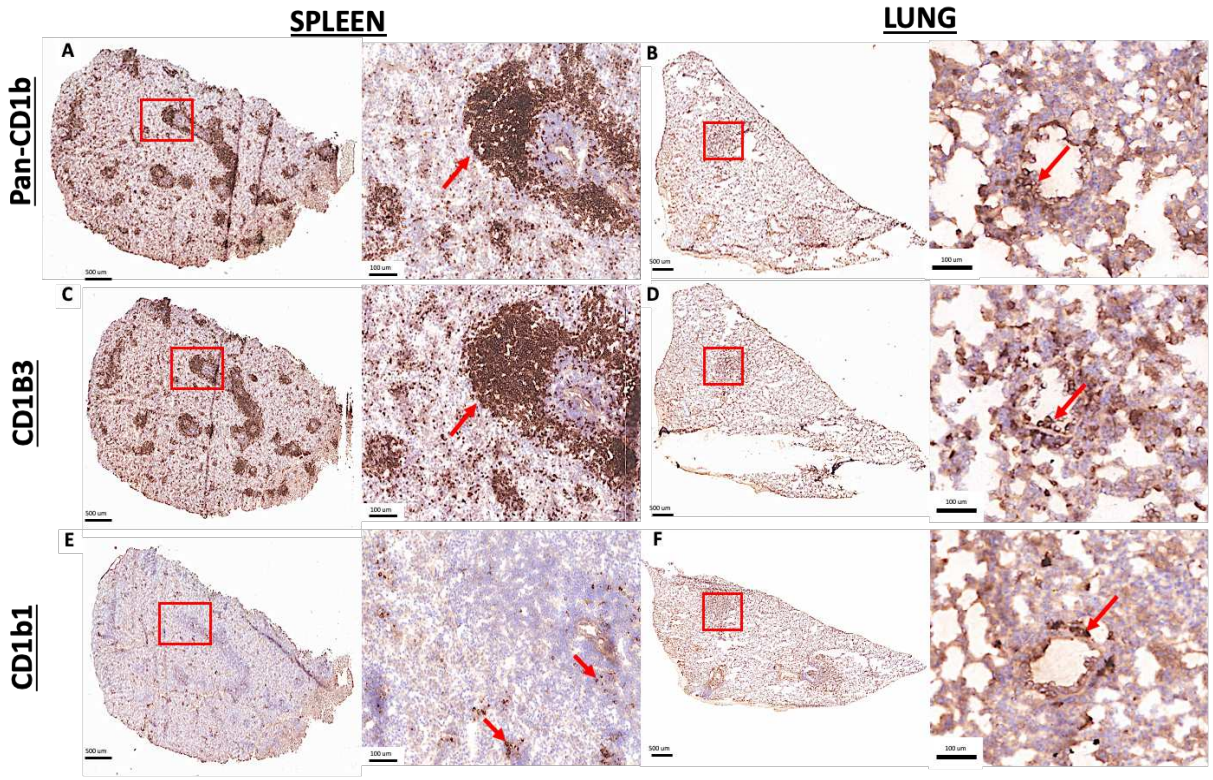

Figure 17. Tissue distribution of specific CD1b orthologs. Fresh-frozen naïve lung and spleen tissue cryosections were fixed in absolute methanol and labeled by immunohistochemistry using monoclonal antibodies against all CD1b orthologs, or specifically targeting CD1b1 and CD1b3. (A-B) Distribution of all CD1b orthologs in spleen and lung after labeling with pan anti-CD1b antibody, 6B5. (C-D) Distribution of the CD1b3 ortholog, specifically, in spleen and lung after labeling with the anti-CD1b3 monoclonal antibody, MsGP9. (E-F) Distribution of the CD1b1 ortholog, specifically, in spleen and lung after labeling with the anti-CD1b1 monoclonal antibody, 1D12. High magnification images are representative of the areas delineated by red boxes in each figure A-F.

The same chromogenic IHC approach and antibodies were utilized to evaluate specific ortholog spatial expression within lung granulomas. Serial sections of lung from an infected guinea pig at the day 30 endpoint were evaluated. IHC performed with the pan-CD1b antibody, 6B5, highlights a population expressing CD1b within the lymphocytic regions at the periphery of primary granulomas. Further delineating ortholog-specific expression, IHC with the CD1b3-specific MsGp9 clone demonstrated strong membranous immunolabeling among morphologically small cells consistent with lymphocytes **(Fig. 18A, B)**. In contrast, CD1b1

assessed by IHC with clone 1D12, showed weak membranous immunolabeling in the wall of the granuloma among the region of cell infiltrate also expressing CD1b3 **(Fig 18C)**. The clear differences across tissue and cellular distribution of CD1b1 and CD1b3 expression would suggest that tissue compartments and cellular populations may have specific regulation of CD1b orthologs in naïve tissue and during the course of Mtb infection

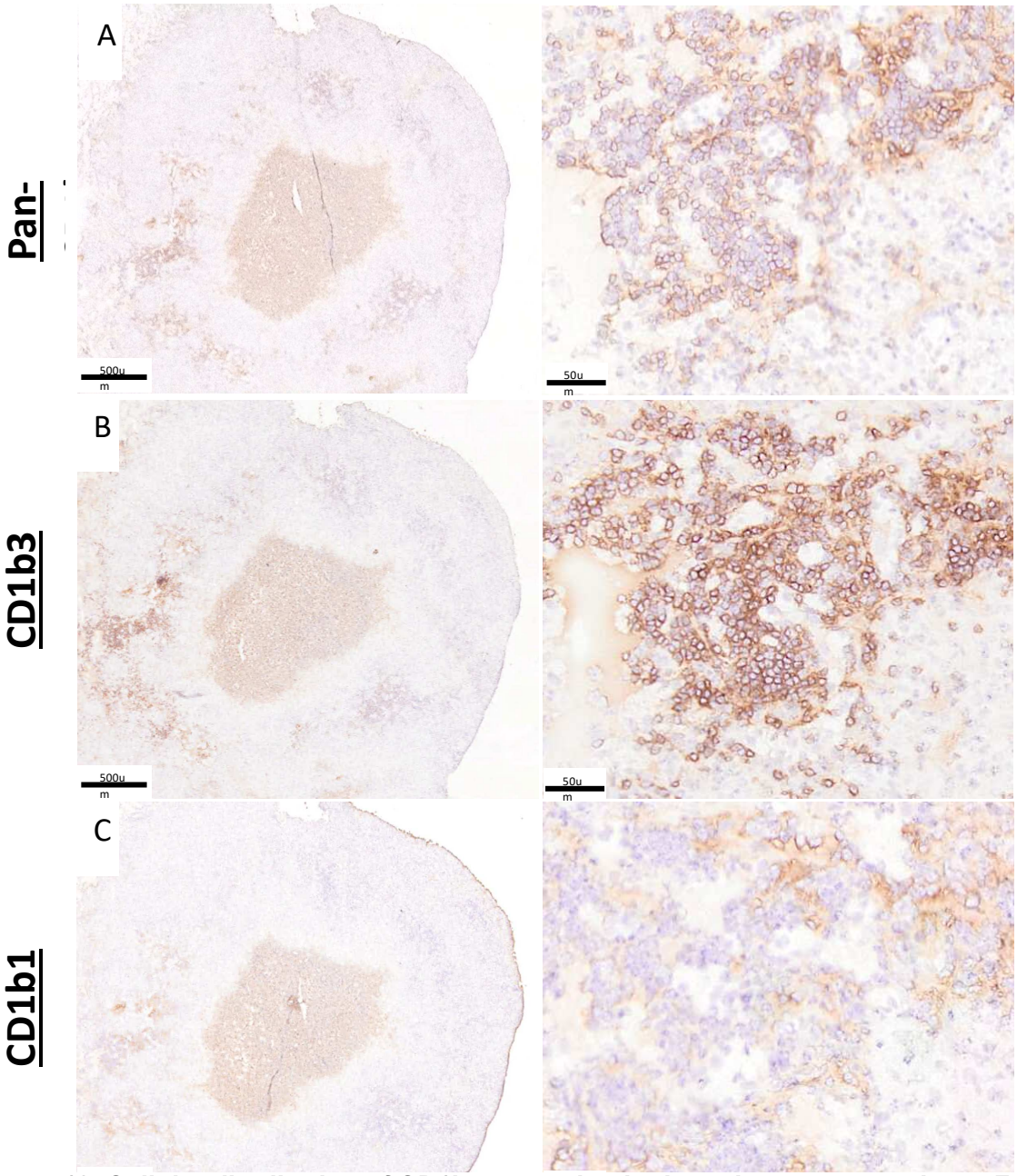

Figure 18. Cellular distribution of CD1b expression in the pulmonary granuloma. Fresh frozen serial sections of a lung granuloma from an Mtb-infected guinea pig at 30-days post-infection were fixed in absolute methanol and labeled by immunohistochemistry using monoclonal antibodies against all CD1b orthologs, or specifically targeting CD1b1 and CD1b3. (A) Distribution of all CD1b orthologs detected with pan anti-CD1b antibody, 6B5; (B) Distribution of the CD1b3 ortholog, specifically, with anti-CD1b3 antibody, MsGP9. (C) Distribution of the CD1b1 ortholog, specifically, with anti-CD1b1 antibody, 1D12. (D) Negative control omitting the primary anti-CD1b antibodies. High magnification images are representative of the areas delineated by red boxes in each figure A-C.

To determine how specific CD1b orthologs are regulated in the course of Mtb infection, we designed ortholog-specific primers targeting CD1b1-b4 and evaluated kinetic changes in relative gene expression in total RNA isolated from infected and naïve lung. Relative gene expression of specific CD1b orthologs (CD1b1-b4) performed on total lung cDNA demonstrated altered expression of CD1b orthologs in infected guinea pigs compared to total lung cDNA from naïve guinea pigs **(Fig. 19A-D)**. Interestingly, each ortholog had a unique expression pattern over the course of Mtb infection. CD1b1 **(Fig. 19A)** had low naïve tissue gene expression (4.78 ± 5.32) with a six-fold mean increase and peak in the early adaptive immune phase at day 30 (29.1 ± 20.08; $p \leq 0.05$). CD1b1 waned with chronicity of infection at day 60 (12.53 ± 11.49). CD1b2 **(Fig. 19B)** showed the greatest increase in relative expression during infection, beginning at day 14 and reaching a peak at day 30 with a 36-fold mean increase (147.3 ± 86.1; $p \leq 0.01$) compared to naïve controls. CD1b2 expression waned slightly with infection chronicity at day 60 (89.65 ± 99.8). CD1b3 **(Fig. 19C)** had low naïve expression, 1.85 ± 1.58, with a 14-fold mean increase at day 14 of infection (26.55 ± 15.4; $p \leq 0.05$) and a 28-fold mean increase at day 30 of infection (52.55 ± 30.1; $p \leq 0.01$). Expression of CD1b3 also waned slightly with infection chronicity at day 60 (30.95 ± 39.3). In contrast to the other orthologs, CD1b4 **(Fig. 19D)** had upregulated expression only during the innate phase of immunity at day 14 of infection with an 18-fold mean increase (73.9 ± 55.84; $p \leq 0.01$), then progressively waned over days 30 and 60 of infection.

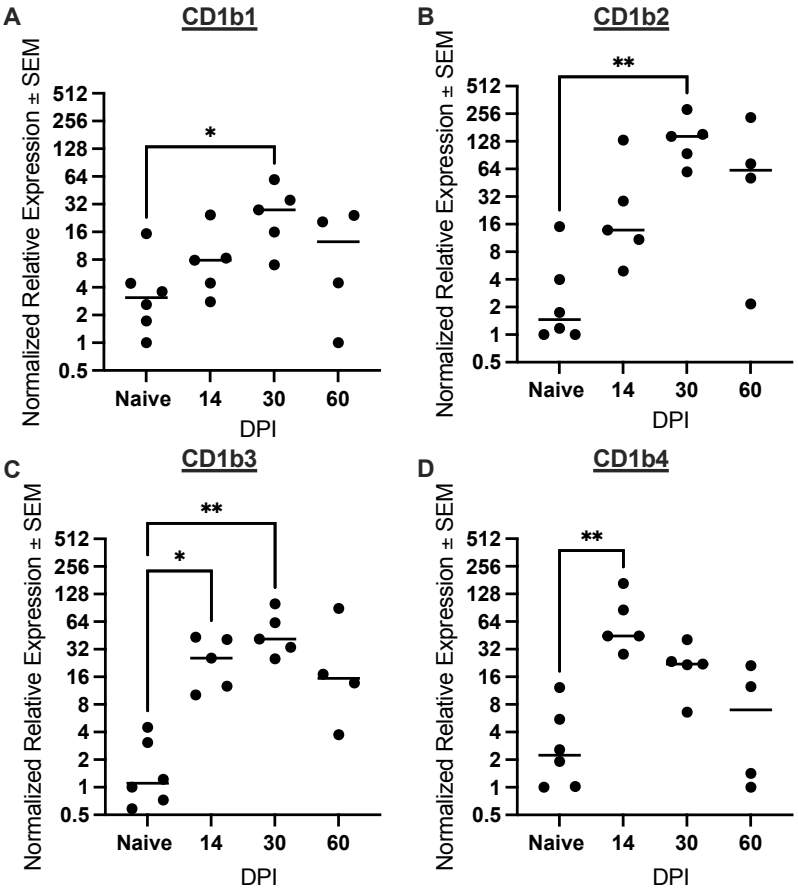

Figure 19. Kinetic gene expression of each CD1b ortholog over the course of Mtb infection. Ortholog specific primers were designed to amplify only CD1B1-4, respectively. Relative gene expression of each ortholog was measured by quantitative RT-PCR on total RNA isolated from lung samples of Mtb-infected and naïve guinea pigs at 14, 30, and 60 days post-infection (DPI). Expression across naïve and infection endpoints were normalized to the naïve control animal having the lowest expression of the CD1b1 ortholog, designated at a relative expression of 1. Ortholog-specific expression was assayed for (A) CD1b1, (B) CD1b2, (C) CD1B3, and (D) CD1b4. *P≤0.05; **P≤0.01; One-way ANOVA multiple comparison with a Dunnet correction.

CD1b expression within Mtb granulomas is primarily restricted to B cells along the periphery of pulmonary lesions.

With increased frequency of CD1b-expression on small CD45+ cells via flow cytometric analysis, and chromogenic IHC highlighting small cells morphologically consistent with lymphocytes, we further pursued CD1b expression via multiplex IHC to identify the cell phenotypes and locations of CD1b-expressing leukocytes within infected lung parenchyma.

Evaluation of multiplex immunohistochemistry showed the majority of CD1b expression is centered on B cells located along the periphery of Mtb granulomas **(Fig. 20A-D)**. Correlating with flow cytometric analyses, CD1b was kinetically regulated during the course of Mtb infections, with the highest number CD1b expressing cells appreciated in the effector phase of adaptive immunity, 30 days post-infection, with a mean 21,369 ± 9,829 CD1+ cells per animal among lung granulomas **(Fig. 20E-F)**. Interestingly, the frequency of CD1+ cells in TB granuloma lesions reflects a greater proportion of the initial cells recruited in the early response to Mtb infection, as evidenced by the increased proportion of CD1+ cells among all granuloma-associated infiltrate at day 14 of infection **(Fig. 20G-H)**. Because these cells are largely Pax5+ **(Fig. 20I)**, this represents a population of early responding B cells that may contribute to the establishment of lipid-restricted immunity. Collectively, evaluation of CD1b expression by IHC methods demonstrates that B cell populations dominate among CD1b-expressing cells in the granuloma, with a surprising paucity of CD1b expression among non-B cell leukocytes in the walls of TB granulomas.

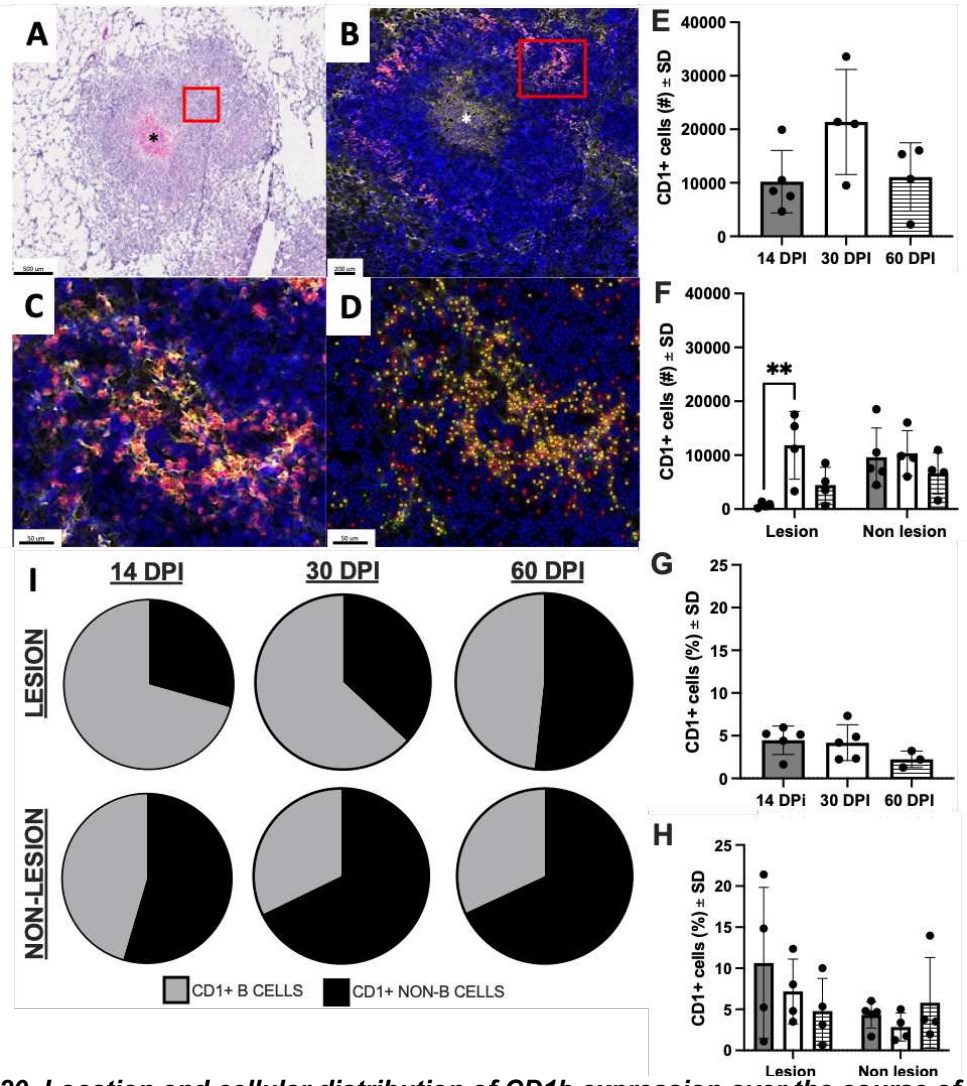

Figure 20. Location and cellular distribution of CD1b expression over the course of Mtb infection. Fresh frozen sections of lung and spleen at 14, 30, and 60 days post-infection (DPI) were fixed in absolute methanol and labeled with antibodies targeting all CD1b orthologs (6B5, Opal 520) or the B cell transcription factor, Pax5 (clone 24, Opal 690), using Opal fluorochrome immunohistochemistry and nuclear counterstain, DAPI. (A-D) Representative sections of a lung granuloma demonstrating: H&E stained image of the granuloma labeled by IHC (A); Multiplexed IHC detecting CD1b (yellow) and Pax5 (red) demonstrating the distribution of expression across the granuloma (B). Asterisk in sections represents the region of central necrosis; high magnification view of CD1+, Pax5+ region designated by the red boxes in panels A and B (C); and the same high magnification field of view overlayed with Visiopharm analysis annotation of CD1+ and Pax5+ B cells (yellow), CD1- and Pax5+ B cells (red), or CD1+ and Pax5- representing CD1-expressing cells other than B cells (green) (D). For Visiopharm analysis, all nuclei in the tissue were detected to designate individual cells, then each cell identified based on nuclear and membranous immunolabeling patterns. (E-F) Visiopharm-derived quantitative output of CD1+ cell numbers across the entire lung section (E) or separated into lesional and non-lesional regions of each lung section at 14, 30, and 60 days post infection (DPI) (F). (G-H) Proportion of CD1+ cells among all detected cells in whole lung (G) or separated into lesional and non-lesional regions of each lung section at 14, 30, and 60 days post infection (H). (I) Breakdown of CD1+ cell into B cells or non-b cells in both lesional and non-lesional parenchyma at 14, 30, and 60 days post infection Visual designation of CD1+ cell phenotypes as pie diagrams across lesional and non-lesional lung tissue at 14, 30 and 60 DPI. **P<0.01; one-way ANOVA with a tukey correction.

Mtb infection elicits lipid-antigen specific and CD1b-restricted cytotoxicity.

To examine the kinetic functional response of CD1b-restricted immunity to Mtb lipids, non-adherent effector cells isolated from spleen and lung parenchyma were incubated with CD1b1- and CD1b3-transfected fibroblast cell lines loaded with either mycolic acid or glucose monomycolate synthetic lipid antigens. Lung effector cells **(Fig. 21A)** failed to demonstrate significant antigen-specific cytotoxicity during innate immunity in any condition, though antigen-loaded samples trended toward increased cytotoxicity compared to unloaded controls. Maximal cytotoxic effect with lung-derived effector cells was observed during early adaptive immunity, 30 days post-infection, within all conditions except for CD1b3 transfectant target cells loaded with mycolic acid. Though all conditions demonstrated a higher level of cytotoxicity in antigen-loaded CD1b-expressing target cells, a significant increase in cellular cytotoxicity was only appreciated in glucose monomycolate-loaded CD1b3 target cells ($P \leq 0.01$) and mycolic acid-loaded CD1b1 target cells ($P \leq 0.05$). The greatest cytotoxic effect was appreciated comparing lipid loaded target cells to unloaded target controls from infected animals among CD1b1 and CD1b3 targets loaded with glucose monomycolate and CD1b1 targets loaded with mycolic acid. Where lipid antigen-specific and CD1-restricted responses were detected, there is a corresponding increase in antigen-specific cytotoxicity with increasing ratio of effector:target cells. Proportions of cytotoxicity, indicated as percent cell death, are exhaustively listed in supplemental table 4A-B. Comparing only infected samples kinetically over time, all conditions at day 30 post-infection, except for mycolic acid-loaded CD1b3 target cells, have significantly greater cytotoxic effect in lung than the same condition at days 14 or 60 post-infection ($P \leq 0.05$) (sup. fig. 16A).

Similar to the lung, spleen-derived effector cells **(Fig. 21B)** lacked cytotoxic function during innate immunity for all conditions, with no significant differences between antigen-loaded target

cells and unloaded controls. During early adaptive immunity, at day 30 of infection, the only antigen and CD1b ortholog demonstrating significant cytotoxic activity was seen in mycolic acid loaded CD1b3 target cells compared to unloaded controls ($P \leq 0.05$). In contrast to lung, maximal cytotoxic effect with spleen-derived effector cells was observed during chronic disease, at 60 days post-infection, with significant lipid antigen-specific cytotoxicity observed in all conditions, glucose monomycolate-loaded CD1b1 and CD1b3 ($P \leq 0.01$), mycolic acid-loaded CD1b1 ($P \leq 0.001$) and mycolic acid-loaded CD1b3 ($P \leq 0.0001$). Comparing only infected samples kinetically over time, day 30 and 60 endpoints were significantly higher than the day 14 innate endpoint. Additionally, in all conditions significantly greater cytotoxicity was appreciated at 60 days of infection compared to 30 days of infection (Sup. fig 9B). All comparisons and controls utilized in this spleen cytotoxicity assay are included in supplemental data (Sup. Fig. 17A-B and sup table 8A-B).

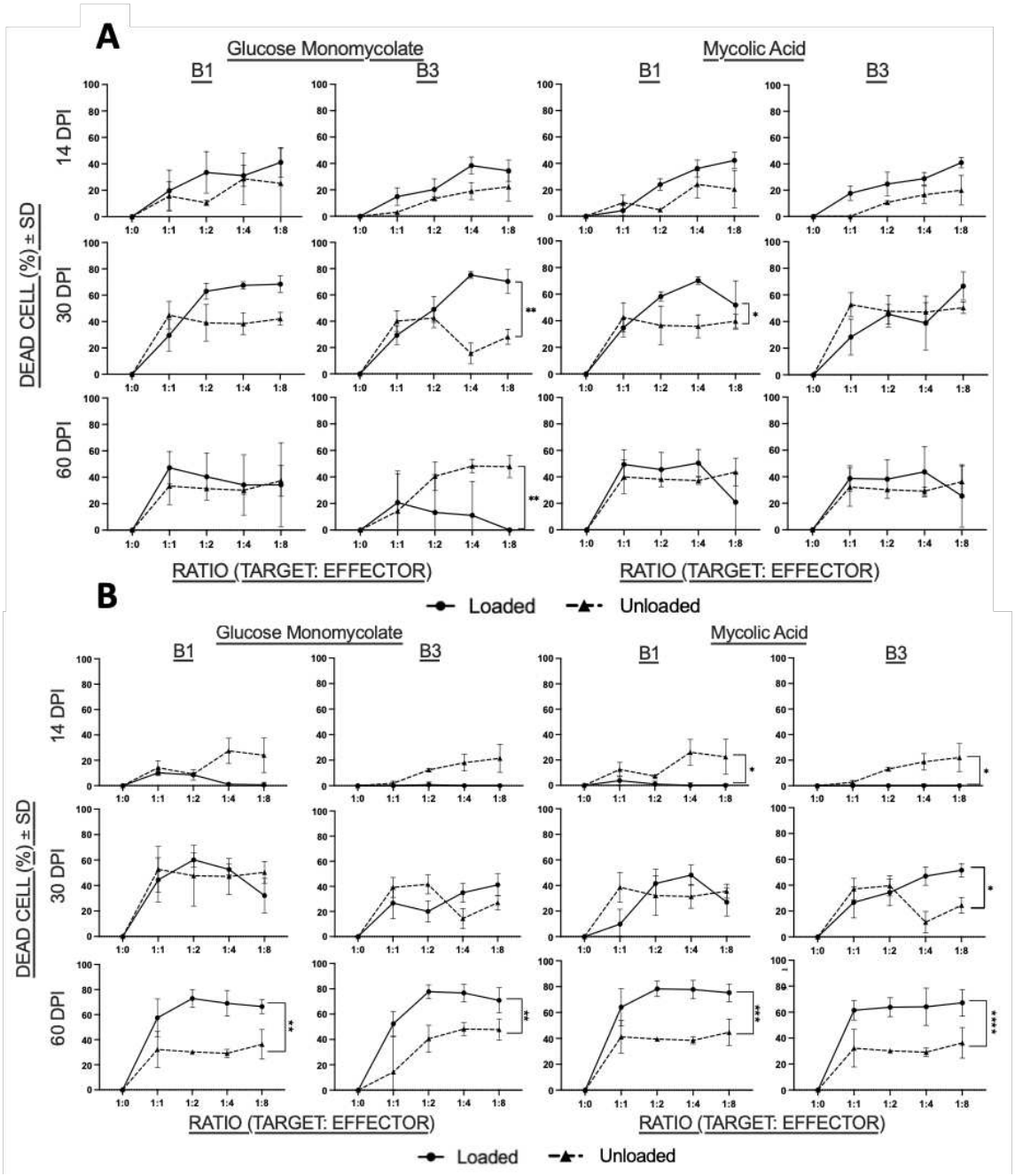

Figure 21. Lipid antigen-specific and CD1b-restricted cytotoxic activity among cells isolated from Mtb-infected lung and spleen. Guinea pig OT1 fibroblast cell line transfected with CD1b1 or CD1b3 were labeled with CellTrace Violet tracking dye then mock-loaded (unloaded) or loaded with synthetic glucose monomycolate or mycolic acid Mtb lipids to be used as target cells in this cytotoxicity assay. Target cell fibroblasts were incubated with non-adherent cells isolated from the lung or spleen of Mtb-infected or naïve guinea pigs at 14, 30 and 60 days post-infection (DPI) at ratios ranging from 1:0 to 1:8 target:effector cells. Fibroblasts in co-culture were identified by flow cytometric gating on CTV-labeled cells and viability assessed using permeability dye exclusion. Cytotoxicity is expressed as the proportion dead, permeable CTV-labeled target fibroblasts. A) Fibroblasts incubated with effector cells derived from the lung. B) Fibroblasts incubated with effector cells derived from spleen. All control measures and cytotoxicity comparisons are comprehensively shown in supplemental figure 9 & 10. * $P<0.05$, ** $P<0.01$, and *** $P<0.001$; two-way ANOVA with a Sidak's correction.

Guinea pig CD1b expression is not upregulated among peripheral blood mononuclear cells over the course of Mtb infection.

We assessed kinetic CD1 expression and CD1-restricted cytotoxic capacity among peripheral blood mononuclear cells (PBMCs) to determine how CD1-restricted immunity is manifested over the course of Mtb infection in peripherally accessible samples. PBMCs, collected via weekly antemortem blood draws and from our specified terminal endpoints, were analyzed for CD1b expression and CD1b-restricted cytotoxicity. CD1b expression failed to demonstrate significant upregulation in the PBMC populations across any of the specified collection points over the course of Mtb infection, or when compared to specified time-matched naïve guinea pigs **(Fig. 22A)**. Due to the requirement for high cell numbers, functional cytotoxicity assays were performed only on PBMCs collected at the specified termination endpoints. Regardless of the infection endpoint, CD1b ortholog-expressing target cell, or Mtb lipid antigen, no cytotoxic effect was demonstrated among PBMCs isolated from infected guinea pigs compared to PBMCs from naïve guinea pigs **(Fig. 22B).**

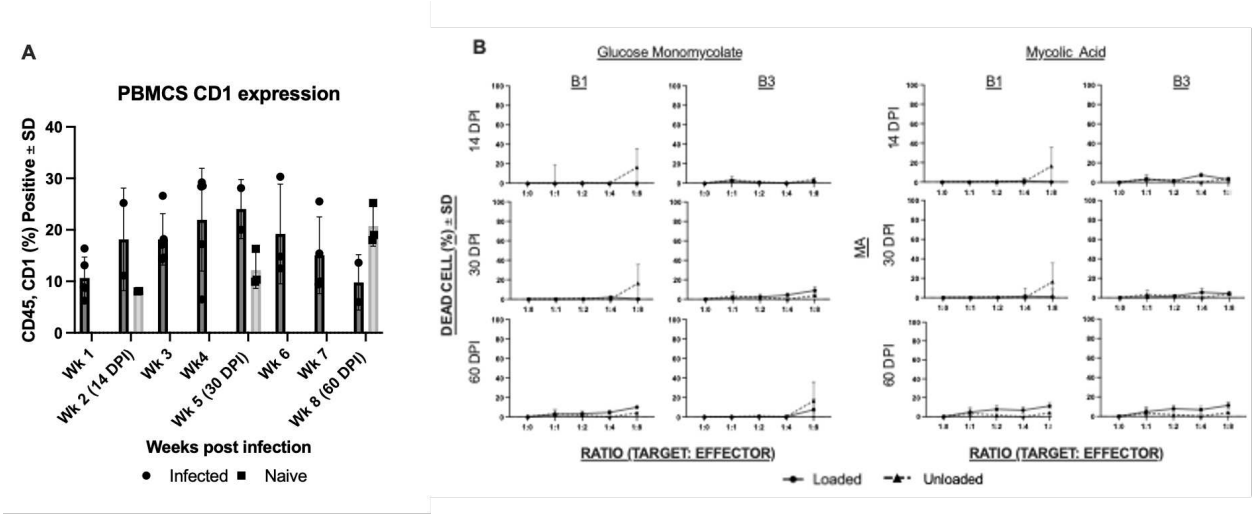

Figure 22. CD1b expression and cytotoxic activity in peripheral blood of naïve and Mtb-infected guiena pigs. (A) Flow cytometric analysis of PBMCs collected weekly after Mtb infection. Cells were gated for live, CD45+ cells and evaluated for overall CD1b expression using the anti-CD1b monoclonal antibody, 1B12. Naïve, time-matched controls were performed at specific termination endpoints of 14, 30, and 60 days post infection (DPI). (B) Guinea pig OT1 fibroblast cells transfected with CD1b1 or CD1b3 were labeled with CellTrace Violet tracking dye then mock-loaded (unloaded) or loaded with synthetic glucose monomycolate or mycolic acid Mtb lipids to be used as target cells in this cytotoxicity assay. Target cell fibroblasts were incubated with PBMCs derived from Mtb-infected and naïve guinea pigs at 14, 30 and 60 DPI at ratios ranging from 1:0 to 1:8 target:effector cells. Fibroblasts in co-culture were identified by flow cytometric gating on CTV-labeled cells and viability assessed using permeability dye exclusion.

Mtb lipids fail to elicit a delayed type-IV hypersensitivity via intradermal challenge.

To assess whether Mtb lipid antigens alone could elicit an immunologic recall response during Mtb infection, infected and naïve guinea pigs were injected with glucose monomycolate or mycolic acid lipid in either a PBS or liposomal formulation. Regardless of formulation administered, synthetic lipid antigens delivered at innate, early adaptive or late adaptive stages of immunity failed to elicit a delayed-type hypersensitivity response. In contrast, and as expected, Mtb purified protein derivative (PPD) was able to elicit a dermal response during early and late adaptive phases of immunity, at day 30 and day 60 of infection, with no antigen-specific response to PPD identified in the innate phase at day 14 of infection **(Fig. 23)**.

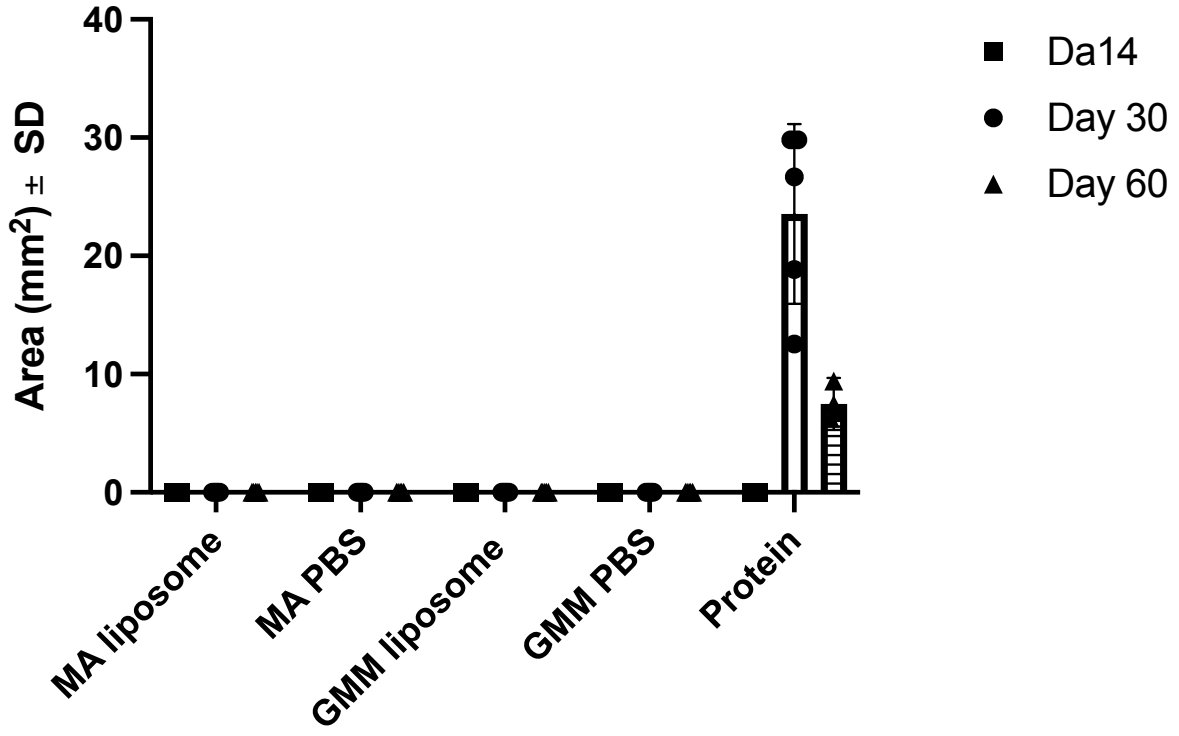

Figure 23. Intradermal Mtb antigen challenge. At 48-hours prior to specific endpoint termination, Mtb-infected and naïve guinea pigs were administered intradermal injections of glucose monomycolate, mycolic acid, purified protein derivative (PPD), or saline control, either free in liquid suspension or incorporated into liposomes. Reaction was not observed at any saline negative control injection site, or among any antigen preparation across the naïve guinea pigs (data not shown). Lipid antigens, regardless of formulation, yielded no observable skin induration or erythema in Mtb-infected guinea pigs.

Enumeration of tissue bacterial burden:

The burden of Mtb was assessed via culture of lung homogenates and the formation of colony forming units (CFU). CFU counts were consistent with validated and published low-dose aerosol exposure in the guinea pig model (supp. Fig. 18)[22]. In brief, mean CFU for day 14 of infection were 4.56 ± 0.304 per gram of tissue, day 30 post infection were 4.79 ± 0.451, and day 60 post infection were 4.76 ± 0.134 CFU per gram of tissue.

Discussion:

The role of lipid antigen-specific, CD1-restricted immunity in TB remains poorly understood. In previous human and animal studies, it was established that CD1 expression is modulated in myeloid cells derived *in vitro* from peripheral blood of Mtb-infected human subjects and in tissues from infection studies using CD1-transgenic mice[129,204–206]. This modulation has further been investigated utilizing lipid antigens purified from liquid Mtb culture or BCG vaccination to examine tissue CD1 expression in guinea pigs[207]. However, the presence and kinetically regulated pattern of CD1-restricted immunity over the course of Mtb infection remained unknown. This study aimed to demonstrate the presence and functional activity of CD1-restricted immunity in pulmonary and extrapulmonary Mtb infection using the guinea pig model.

Here we utilized the guinea pig model of TB to establish the presence of CD1 expression and CD1-restricted immunity in the tissue response to Mtb infection. In this study, we found that CD1 expression increased in leukocytes isolated from infected lung with kinetic changes over the innate and adaptive immune stages of infection. CD1-restricted cytotoxic activity was demonstrable in infected lung and spleen tissue, with kinetic responses tracking in parallel with changes in CD1 expression. Uniquely, we have identified that group I CD1 expression is primarily localized to B cells within granulomatous lesions of the spleen and lung, suggesting this cell population may contribute a previously unrecognized role to the development and maintenance of CD1-restricted immunity.

In this study, we found that CD1 expression increases over the course of Mtb infection, most evident during the establishment and effector phase of adaptive immunity at day 30 of infection. It was noted that the predominant lesion-associated CD1-expressing cell is the Pax5+ B cell. Although many Pax5+ B cells express CD1b, there is also a substantial population of Pax5+ B cells that are negative for CD1b. The difference in function between these cells and their contribution to ongoing granuloma-associated immune responses remains unexplored. We

also observed that there is a proportionally greater frequency of CD1+ and Pax5+ B cells in the early immune response at day 14 of infection. This early manifestation of CD1 expression might suggest an efficient and early presentation of lipid antigens and an unexpected role for B cells in the early response to Mtb infection.

Of note, there is a clear paucity of CD1b expression among non-B cell phenotypes within the granuloma, thus indicating that the vast majority of granuloma-associated macrophages do not express CD1b orthologs. The cause and consequence of this absent expression among lesion-associated macrophages remains unknown but could be explained by direct modulation by intracellular infection, a downregulation influenced by the surrounding inflammatory environment, or potentially that recruited inflammatory macrophages are not, under any given circumstance, expressing CD1b proteins. The downregulation of CD1 expression by intracellular Mtb infection has been previously demonstrated *in vitro* using human monocyte-derived macrophages[129,205,206]. An alternative explanation may be that cells expressing lipid antigens in the context of CD1b are efficiently eliminated from the response by cytotoxic activity of CD1-restricted T cells, thereby creating a relative absence of CD1-expression in the granuloma. Importantly, it should be noted that antibodies used in this study are specific for CD1b, thus, we cannot rule out a different cellular distribution expression profile of CD1c orthologs.

Other readouts of CD1-restricted T cell activation, such as antigen-stimulated IFNγ production measured by ELISpot, was not a feasible nor a robust measure in this model, despite the previous utility of this assay as a readout of lipid antigen-specific responses in human peripheral blood[125,208]. It is unclear whether this difference represents a compartmental difference in peripheral blood, used in human subjects, or a feature unique to the tissue response, as evaluated in this study. Regardless, it is notable that cytotoxicity was identified as a major readout of functional activity of CD1-restricted T cells, a feature that is also reported in isolated human CD1-restricted T cells[209]. The field would be further advanced by a better

understanding of the phenotype and activity of these cells, to determine whether cytotoxic activity provides a measurable contribution to TB immunity *in vivo*.

Due to limitations in cell yields from infected tissues, we prioritized the application of effector cells in multiple increasing ratios to target cells for select CD1 orthologs, over the use of all CD1b1-b4 transfectants as target cells. Thus, we made an informed decision to utilize CD1b1 and CD1b3 as targets based on their unique tissue distribution in lung and spleen in naïve animals, previously conducted cytotoxicity pilot studies, and previous literature[116]. We were unable to evaluate cytotoxicity against CD1b2 and CD1b4 in this current study. Because these orthologs have different kinetic transcriptional expression profiles as well as differences in magnitude of expression, as revealed by this study, it is possible that these orthologs may also contribute to induction of cytotoxic activity or other functional response in CD1-restricted T cell populations.

Interestingly, we observed that CD1b1 and CD1b3 have remarkably different cellular expression patterns in naïve tissues of interest. The presence of CD1b1 on alveolar macrophages in lung and macrophage-like cells in the splenic red pulp would suggest that CD1b1 is a myeloid-cell associated CD1b ortholog. In contrast, CD1b3 was highly expressed on B cells and identified within the B cell zone of the splenic white pulp, indicating that CD1b3 is a B cell-associated molecule expressed in both naïve and infected conditions. Further adding to the complexity, CD1b3 has a unique cell trafficking pattern compared to other guinea pig CD1b orthologs, lacking the key YXXZ tyrosine cytoplasmic tail motif for late endosomal trafficking. The absence of this cytoplasmic tail motif directs CD1b3 to the cell surface and superficial endosomes, an antithetical distribution to CD1b1, b2, and b4[33,45,194]. Collectively, these data suggest that CD1b orthologs may serve multiple distinct roles in the contribution to immunity against *M. tuberculosis* infection.

In these studies, we observed cytotoxic activity in an antigen-restricted manner. Synthetic lipid antigens, mycolic acid and glucose monomycolate, both served as effective antigen targets for the induction of cytotoxic activity, observed to a greater degree in antigen loaded CD1b1 or CD1b3 transfected fibroblast target cells compared to unloaded controls. The presence of cytotoxic activity against cells highlights a currently poorly understood immunological conundrum: CD1 functions to elicit CD1-restricted T cell responses, but the same molecule also serves as a target for cytotoxicity. This may relate to the MHC-I-like nature of the CD1 molecule, where expression in the absence of a co-stimulatory factor and/or functional cytokine milieu leads to cytotoxicity, while presence of co-stimulatory function may provide an antigen-specific activation signal. The molecule that serves as a co-stimulatory signal for CD1-restricted T cell activation has been shown as a mechanism for CD1- restricted double negative T cell proliferation but remains to be identified[210]. Altogether, this study provides evidence that CD1-restricted killing of target cells in active TB requires a lipid antigen in association with CD1.

In this study, there was no discriminate cytotoxic activity against either lipid antigen evaluated in the context of CD1b1 or CD1b3. However, it was noted that higher activity could be demonstrated against CD1b3 transfectant target cells in general, compared to CD1b1. These findings may suggest that orthologs not only demonstrate kinetic differences in expression but may also contribute different functional roles in the response to Mtb infection. It is possible that this functional activity is related to the tissue compartmental restriction of the CD1-restricted immune response observed in this study. We attempted to measure CD1-restricted activity in peripheral blood, from which limited to no cytotoxic activity was observed. We also conducted lipid antigen skin testing side-by-side with PPD antigen preparation, where no skin reactivity was observed to synthetic lipid antigens compared to PPD. This indicates that either insufficient antigens or non-reactive antigens were used, or that recall responses and recruitment to skin antigen is not a functional characteristic of CD1-restricted T cells.

CD1-restricted T cell activity has been shown to be differentially present in the circulation of patients with active compared to latent TB, and also contributes to the vaccine response to BCG in non-human primates[211,212]. Here we demonstrated that CD1 expression is inducible by *M. tuberculosis* infection, that this expression is associated with early phases of the initial adaptive immune response, and that this induction of CD1 expression is associated with a functional population of CD1-restricted antigen-specific cells. The use of synthetic lipid antigens in this study is a significant strength. Confidence that preparations are absent of contaminating protein antigens, which may be present in lipid antigens purified directly from the Mtb organism, eliminates the possibility that the antigen-restricted functional response observed in this study is the result of contaminating protein antigens over the lipids themselves. Despite these novel findings, this study carries some limitations. We cannot ensure that fibroblasts represent the most effective target population for effector cells or that these outcomes are reflective of what occurs *in vivo*. However, this remains one of the very few guinea pig cell lines available for use in research with this species. Additionally, a fibroblast line transfected with CD1d is not available for testing of cross-reactivity among our antibody reagents. Therefore, while we can confirm that antibodies used in this study do not bind CD1c, it remains a possibility that some CD1 expression observed is a result of detecting constitutive CD1d expression. However, this remains less of a concern given the demonstration of CD1b-restricted cytotoxicity as a functional readout from cells isolated from infected lung and spleen.

Having now established the presence of CD1-restricted immunity at the primary sites of Mtb infection achieved by low-dose aerosol exposure in the guinea pig model, it remains critical to better understand the contributions of this branch of immunity to TB disease outcome. It is still unknown whether CD1-restricted responses provide a benefit or detriment to the host, and how these antigen-presentation molecules contribute among the mix of a significantly larger

repertoire of protein-based antigens in the context of classical MHC class I or class II antigen presentation.

CHAPTER 3: Modulation of CD1-restricted immunity during a *Mycobacterium tuberculosis infection* in the guinea pig, and its effect on overall disease progression

Summary:

CD1 lipid-based immunity has been shown to present *Mycobacterium tuberculosis* (Mtb) lipid antigens in Mtb infected humans and animal models. However, fundamental questions remain as to the role CD1 lipid immunity plays in the pathogenesis of Tuberculosis (TB) in terms of lesion burden, local bacterial burden and ability of the Mtb bacillus to achieve systemic spread. Exploiting the guinea pigs' translatable characteristics for both Mtb infections and CD1 immunity, this study aimed to answer how altering CD1 lipid restricted immune functionality effects TB disease progression. To achieve this, this study modulated CD1 glycoprotein expression on antigen presenting cells in vivo utilizing ortholog specific CD1 morpholinos, for CD1 down regulation, and a murine growth factor FLT3-L, for CD1 upregulation. In pilot experiments using naïve guinea pigs, both compounds were able to cause decisive modulation of CD1, with up to a 100% upregulation of CD1 under FLT3-L stimulation and 50% knockdown of CD1 with morpholinos. In infected animals, FLT3-L failed to further enhance CD1 protein or gene expression and paradoxically lowers CD1-restricted T cell cytolytic functionality compared to controls. In contrast, morpholinos were able to knockdown CD1 protein expression and completely inhibit CD1-restricted T cell cytolytic ability. Interestingly, animals receiving both morpholino and FLT3-L were able to recover CD1 protein and gene expression and had better cytolytic ability then either the FLT3-L or morpholino treatment animals. Regardless of CD1 glycoprotein modulation, disease progression as assessed via lesion and bacterial burden, were relatively unchanged. This study provides the first model of CD1 immune modulation *in vivo*, and sets the stage for additional investigations to understand the relationship of CD1 immunity to Mtb infections and TB disease pathogenesis.

Introduction:

CD1 lipid-based immunity represents a relatively novel branch of immunology that is driven by CD1 glycoprotein mediated expansion of CD1-restricted T cell and invariant natural killer cells[105,180]. CD1 glycoproteins are antigen presenting structures with homologous structuring to MHCI but bind and present a variety of lipid antigens[181, 32]. There are 5 known CD1 glycoproteins, CD1a-e, which are divided into two functional groups; group 1 composed of CD1a-c and group 2 composed of CD1d[35,182,183]. Group 2 CD1 complexes have been found to be constitutively expressed on a variety of cell types and involved with a host of endogenous and exogenous lipids leading to the expansion of invariant natural killer cells[184, 185]. In contrast, Group 1 CD1 complexes have inducible expression and confined to professional antigen presenting cells, loading a variety of exogenous lipids, such at Mtb lipid, leading to an expansion of a variety of functionally nonpolymorphic CD1-restricted $\alpha\beta$ and $\gamma\delta$ T cells[117,186,187]. Due to their ability to encounter, load and present microbial lipids group 1 CD1 complexes have become a large focus of study for the pathogenesis of several infectious diseases including the lipophilic bacterium *Mycobacterium tuberculosis* (Mtb). The guinea pig, in contrast to other rodent models, have been found to have an analogous CD1 repertoire to humans, with the addition of having 4 CD1b orthologs and 3 CD1c orthologs. This in combination with their translational Mtb pathology makes them an ideal model for both CD1 and Mtb research.

Several studies have investigated CD1 in relation to Mtb infections in humans, and animal models. Several studies have noted the expansion of CD1-restricted T cells in infected individuals *vs* naïve counterparts[110,213,214]. Other studies utilizing guinea pig and transgenic mouse models, have investigated the utility of lipid derived vaccines for lowering TB lesion burden[207,215].However, no study has directly correlated CD1 glycoprotein expression, and thus lipide antigen presentation or overall functionality of this niche branch of immunity, to TB disease progression. This leaves fundamental questions remaining including if a stimulated CD1

immune system benefits the host for limiting disease progression or the bacteria for enabling disease progression and systemic spread. This study looked to answer these questions by modulating CD1b glycoprotein expression in the guinea pig.

CD1 glycoprotein modulation for this study was based on two compounds, morpholinos for downregulation, and FLT3-L for upregulation. Morpholinos are custom synthetic anti-sense RNA segments that irreversibly bind to specified mRNA sequences to block protein translation. Our lab has had previous success with these innovative compounds working with diabetic Mtb infected guinea pigs. Via the NIH GenBank CD1b1-4 annotation morpholinos were created to block CD1b1, CD1b2 and CD1b3. However, due to the annotation and location of the start codon a CD1b4 morpholino could not be created. Human FLT3-L was selected as a CD1 upregulating growth factor based on previous guinea pig CD1 studies performed by Procelli laboratory, and our labs experience with this differentiating guinea pig bone marrow cells into high CD1 expressing dendritic cells[33].

An on-going deliberation within the field of CD1 immunology is the role of this immune system in innate or adaptive immunity. Previous work in our lab demonstrated peak CD1 glycoprotein expression, and CD1-restricted T cells functionality in the early adaptive immune phase, day 30 post infection in the guinea pig. This expression and functionality appears to wane within the late adaptive immune phase, day 60 post infection. To evaluate the effects of CD1 modulation on infection, this study started dosing one set of animals before aerosol infection of Mtb and continued dosing these animals until day 30 post infection when animals were terminated. Dosing for a second set of animals was started during the early adaptive phase of infection, until day 26 post infection, and continued until animal termination at 60 days post infection. This design allowed assessment of whether CD1 can be altered before and/or during infection and whether we can stimulate direct change at a later time point where CD1 immunity naturally wanes in the guinea pig.

The ability to alter CD1 immunology will enable us to answer a plethora of questions for Mtb infections and other disease processes. This *in vivo* modulation could be utilized to assess the true contributions that CD1 immunity has with diseases both within the infectious, autoimmune and neoplastic processes. This first of its kind model could lay the ground work for comprehensive lipid-based vaccination studies that would have large scale implications on *Mycobacterium tuberculosis* infections in human populations.

Methods:

Animals:

A small pilot study was performed with naïve guinea pigs which were divided into 3 treatment groups 1) saline control, 2) FLT3-L and 3) morpholino (n=3). The main study utilized 48 mixed gendered Dunkin-Hartley guinea pigs (male n=24, female n=24) weighing between 250-300 g were obtained from Elm Hill Labs (Chelmsford, MA). Guinea pigs were divided into 4 treatment groups (n=12) 1) saline control treatment, 2) FLT3-L treatment, 3) morpholino treatment, and 4) FLT3-L and morpholino combination treatment groups. Treatment group animals were further divided into specific timepoint of dosing and termination (n= 6 per group per set). One set of treatment animals started treatments 6 days before infection and were terminated at 30 days post infection. The second set of treatment animals started dosing at 26 days post infection and were terminated at 60 days post infection. All animals were pair housed and monitored via the Colorado State University (CSU) Laboratory Animal Resources staff and veterinarians under the Institutional Animal Care and Use Committee protocol (#1401).

Morpholino compound development and ex-vivo validation:

Morpholino (Gene tools, OR) anti-sense synthetic RNA strands were utilized for down regulation of CD1b complexes within guinea pigs in invivo and exvivo experiments. CD1b1-2 and CD1b3 morpholino anti-sense synthetic RNA strands were developed using the annotated mRNA sequences from NIH gene bank (sup. table 9). Acquired morpholino segments were reconstituted at 0.5 mM in sterile water and stored long term at room temperature. Ex-vivo validation of compounds was performed utilizing CD1 specific transfected fibroblasts and bone marrow derived dendritic cells (BMDCs). Guinea pig BMDCs were formed with previously validated laboratory protocols. In short, $1X10^8$ Bone marrow stem cells, collected from naïve guinea pigs, were incubated in 10 ml complete RPMI media (10% FBS, 1% penstrep antibiotics and 1% anti- anti) for 7 days. To stimulate dendritic cell differentiation cells were stimulated with 20ng/ml FLT3-L on day 1 and 3 of the incubation. BMDCs or fibroblast combinations were incubated with morpholino compounds using 10 ul of resuspended morpholino for 4 hours in serum free OptiMEM media. Cells were than washed twice with PBS and replated with complete RPMI. Cells were evaluated for CD1 complex knockdown via CD1 specific flow cytometry using an Aurora spectral flow cytometer (Cytek, Fremont, CA) and analyzed via Flow Jo v10.8.

FLT3-L ex-vivo validation:

Human FLT3-L (Geminibio, cat# 300-807P), a pleotropic growth factor for any cells expressing FLT3 receptors, was utilized for CD1 expression upregulation. Intraperitoneal dosing of FLT3-L of 10ul/dose was previously established for dosing of guinea pig CD1 upregulation[33]. Lyophilized FLT3-L was resuspended in 0.1% BSA PBS solution at 0.1mg/ml and stored at -80C for long term storage. Validation of FLT3-L was performed in a series of ex-vivo experiments on differentiated bone marrow derived macrophages with evaluation of CD1

expression by flow cytometry. Bone marrow derived macrophages were differentiated in a similar protocol to the BMDCs with the exception of using macrophage colony stimulating factor (Geminibio, cat# 300-332P) instead of FLT3-L. An additional ex-vivo study was performed to examine the effects of FLT3-L modulation on BMDCs during an infection with a virulent auxotrophic strain Mtb expressing mCherry. In this study $2x10^6$ BMDCs were infected with mCherry Mtb at a multiplicity of infection of 1:1 and 5:1 and compared to uninfected controls. These conditions were further divided into FLT3-L treated and not FLT3-L treated groups. Cells were incubated in complete RPMI media for 24 hours and analyzed via flow cytometric analysis for CD1 expression or spun at 500 X g on to charged slides and stained with CD1b-reactive monoclonal antibodies.

Intrapulmonary administration and dosing of morpholino and FLT3-L:

Both FLT3-L and morpholino compounds were delivered via a Buxco aerosol inhalation tower (DSI, St. Paul MN). This innovative nebulizing inhalation apparatus allows for dictating and monitoring of aerosol parameters such as particle size, aerosolized particle concentration, breathing rate of individual animals, humidity and the ability to assess overall accumulated inhaled aerosol. A small pilot study utilizing CellTrace to label intrapulmonary cells (ThermoFisher, cat#: C34557) was utilized to validate particle size and overall distribution of particles both within the bronchoalveolar macrophages and within individualized lung lobules. For the main study, guinea pigs were loaded into individualized aerosol chambers, 6 guinea pigs at time in accordance with specific treatment groups. Guinea pig were restrained utilizing a neck collar with their nose positioned in a secure rubber gasket to ensure minimal waste of nebulized airflow. Compounds were loaded to the nebulizing unit, 600ul of FLT3-L per specified groups, 100ul per animal, and 360ul morpholino per specified groups, 60ul per animal (sup.

table 10). All nebulized volumes were equalized, utilizing sterile PBS, to bring all groups to 1.3ml of solution per exposure. The entire volume of the solution was nebulized to ensure adequate exposure to compounds. The in-vivo pilot study was dosed following similar parameters to the main study with the exception of 3 animals being dosed per run with a total of 300ul of total volume being administered per compound. To ensure animal comfort relative humidity of between 30-70% was maintained at animal inhalation ports. All exposure times ran between 10 and 20 minutes with the variation due to relative humidity in the exposure room and trying to remain our targeted port humidity. Regardless, animals were exposed to uniform total dose compounds.

Dosing of animal models:

For all experimental animal models dosing of compounds was performed every 3 days, in accordance within *ex-vivo* findings. Animals in the pilot study received a total of four doses and then were terminated. For the main infection study, dosing for treatment groups for the day 30 post treatment group started 4 days pre infection. One additional dose was administered 1-day pre infection. Dosing continued every three days utilizing the buxco inhalation tower with the final dosing on day 29 post infection. Dosing for the day 60 post infection animals began on day 26 post infection and continued every 3 days until days 59 post infection. In total all groups in the main study, regardless of timepoint, received 12 doses of compound or saline. To ensure no off-target effects of morpholino all saline animals received a negative control morpholino at every other dosing, for a total of 6 doses. Guinea pigs were terminated at specified time points, followed by a necropsy and tissue collection.

Infection and euthanasia:

A low-dose aerosol exposure of guinea pigs to *M. tuberculosis* was performed using the Glascol aerosol chamber (Terre Haute, IN) to deliver a low-dose exposure of <50 bacilli of the Erdman strain of *M. tuberculosis*. On pre-determined endpoints, days 30 and 60 post-infection, guinea pig treatment groups were euthanized. Euthanasia was performed via an initial induction of an anesthetic state via IM injection of 30 mg of ketamine and 8 mg of xylazine in combination, followed by an IP injection of an overdose of 3ml/kg of sodium pentobarbital. Guinea pigs in validating pilot studies were euthanized via the same methodology as used for the main experimental study.

Necropsy and tissue processing:

Once euthanized, animal tissues and cells were harvested which included alveolar macrophages by bronchoalveolar lavage, PBMCs from anticoagulated peripheral blood, and cell suspensions derived from lung parenchyma, as previously reported[144,22]. In brief, two lung lobes were clamped off and removed and processed for PCR via RNALater solution (Thermofisher, cat #: AM7020), OCT-embedded fresh-frozen immunohistochemistry (Sakura, cat#: 4583), fixed in 4% paraformaldehyde, or for bacterial enumeration by colony forming units (CFU). Alveolar macrophages were collected via post mortem bronchoalveolar lavage utilizing an 18-gauge catheter and flushing with 25 ml of HBSS containing 0.01 μM EDTA solution in 5 ml intervals. Following bronchoalveolar lavage, the remaining lung was perfused with 5 ml of collagenase at 5μg/ml (Sigma-Aldrich, Cat#: C9263) and incubated for 30 minutes in a 37°C water bath. The digested lung parenchyma was processed through 40 μm cell strainers. Once strained, all samples were subjected to erythrocyte lysis solution for 20 to 45 seconds. To increase overall cell viability for downstream assays, lung-derived cell suspensions were subjected to an

annexin V magnetic bead separation protocol. To complete this protocol, cells were placed in 4 ml of 1X annexin binding buffer (Biolegend, cat#: 422201) containing 50 µl of biotinylated annexin V (Biolegend, cat # 640904) and incubated at room temperature for 20 minutes. Following incubation, cells were centrifuged at 500 x g for 5 minutes, washed with additional binding buffer, then centrifuged and resuspended in 500 µl of binding buffer. Thirty µl of streptavidin-conjugated nanobeads (Biolegend, cat#: 480015) were added and incubated for 20 minutes with intermittent tube inversion. Following incubation, additional binding buffer was added up to 4 ml total volume. The cellular solution was put on a magnetic rack for a minimum of 5 minutes to allow for nanobeads to bind to the side of the tube. Finally, unbound cells were collected with a serologic pipette. Collected cells were washed in HBSS then viability and cell count were assessed via a hemocytometer with trypan blue exclusion. Lung inflammatory cells were then plated in RPMI media containing 10% fetal bovine serum and an antimicrobial cocktail, then incubated overnight at 37°C with 5% CO_2 to allow for separation of adherent cells (histiocytic/dendritic in origin) and non-adherent cells (lymphocytes). PBMCs were collected via a left ventricular intracardiac blood draw directly following euthanasia, diluted 1:2 in HBSS and separated on a density gradient using Lympholyte mammal (Cedarlane, cat#: CL5110) per manufacturer's instructions. In brief, up to 6ml of obtained blood was diluted 1:1 in HBSS solution. The diluted blood was added to a 15ml conical tube containing 3mls of Lympholyte at a 45° angle as to maintain separation of blood and the Lympholyte. Samples were than centrifuged at 800 x g for 20 minutes with no decelerating brake. Lastly the separated, PBMCs, were collected from the interface and washed.

CD1 expression:

CD1 expression was measured by flow cytometry on cells isolated from bronchoalveolar lavage cells and cells derived from the lung parenchyma. Flow cytometry methods are previously

described [144,22]. Briefly, $5x10^5$ cells from each sample were blocked utilizing Fc-receptor block (Innovex, Cat#: 50-486-808). Cells were labeled with an antibody panel (supp. Table 12). Viability of cells was assessed via Zombie Yellow amine-reactive dye (BioLegend, Cat# 423103). Data acquisition was performed using a spectral unmixing Cytek Aurora flow cytometer (Cytek, Fremont, CA). Data were analyzed via Flowjo software version 10.8 (Flowjo, Ashland, OR) using a minimum of 50,000 total viable events. A table of utilized antibodies is located in the supplement (sup. table 11)

CD1 cytotoxicity:

Previous reports suggest cytotoxic activity is a major function of CD1-restricted T cell responses in peripheral blood and as induced by immunization with lipid antigens[198,199]. To measure the cytotoxic functionality of CD1-restricted immunity over the course of Mtb infection, CD1b fibroblast transfectants (target cells) from all conditions and time points were incubated with non-adherent inflammatory cells from the lung (effector cells). Detection of cytotoxic effect was performed using a flow cytometric technique previously described based on assessing target-cell viability using target cell labeling and permeability dye penetration[200]. In brief, $1x10^7$ CD1b1 and CD1b3 transfected cells were collected and incubated with 0.5uM Cell Trace Violet (Thermofisher, C34557) for 15 minutes in unmodified RPMI media. The reaction was quenched with 10ml of additional complete RPMI containing 10% FBS for 10 minutes and cells pelleted and washed twice. Cells were plated on a 96-well plate at $5x10^4$ per well.

Preparation of Mtb synthetic lipid antigens included taking dissolved mycolic acid and glucose monomycolate lipids in a 10:1 mixture of choroform: methanol at 0.5mg/ml and evaporating the solution utilizing a sterile nitrogen gas bath. Once evaporated the dried lipids were resuspended

in complete RPMI back to the concentration of 0.5mg/ml. Lipids were completely dissolved via sonication using a Misonix-2400 sonicator in a 4-minute sonication at an amplitude of 80 delivered in pulses of 20 seconds each. Specified wells were then loaded with 4ug of either of synthetic MA or GMM Mtb lipid, or mock-loaded to use as unloaded controls for determination of lipid-antigen specific cytotoxicity. Cells and lipid were incubated overnight to allow for lipid cellular trafficking and presentation in the context of CD1b. These target cells were then incubated with non-adherent inflammatory cells derived from the lung for 4 hours at a target:effector ratio ranging from 1:0 to 1:8. Incubated cells were then stained for viability using Zombie Yellow dye (BioLegend, cat# 423103). Data acquisition was performed utilizing a Cytek Aurora spectral unmixing flow cytometer (Cytek, Fremont, CA). Data were analyzed via FlowJo software version 10.8 (Flowjo, Ashland, OR) using a minimum of 50,000 events with gating for fibroblasts based on size and presence of CellTrace violet signal. Mock-transfected fibroblasts, containing the empty vector with no CD1b construct, and CD1b1 and CD1b3 transfectants without added lipid antigen (unloaded control) were used as negative controls to differentiate antigen-restricted cytotoxicity from non-CD1 restricted factors. Data was normalized to background using the average cellular death among CD1b1 and CD1b3 transfectants without additional of effector cells (1:0 target to effector ratio).

Gene expression of specific CD1b orthologs by qRT-PCR relative gene expression:

Kinetic genetic expression of CD1b was measured by utilizing *de novo* CD1b isoform specific primers (CD1b1-b4) (Supp. Table 13). All primer sequences were created using Geneious software (Auckland, NZ) via a 4-sequence alignment and selecting for non-consensus primer sets, which were then synthesized by Integrated DNA Technologies (IDT) (Coralville, IA). Primer set specificity was evaluated via the use of synthetic gene segments, capturing the first 500 base pairs of each CD1b ortholog sequence. Primers were demonstrated to be specific for each

of the CD1b1-4 isoforms without cross-reactive detection, with amplification of CD1 specific transfected fibroblasts and sequencing of amplicon products aligning back to specific isoform sequences. For RNA isolation, freshly isolated lung tissue at each endpoint of day 30 or 60 post-infection was minced in RNALater (Sigma, Cat#: R0901), incubated at 4°C for 24 hours, then frozen at -80°C until RNA extraction. Tissue was thawed at room temp and ~50 mg of tissue homogenized using Lysing Matrix A tubes in a bead beater instrument (MP Biomedical, C321001). Proteinase K was added to the homogenate, incubated at 55°C for 15 minutes, then RNA was extracted with the RNeasy mini kit (Qiagen cat. 74106) per manufacturer's instructions. Nucleic acid was eluted from the column, digested with DNase-I for 30 minutes at 37°C, then purified again using the RNeasy mini kit. Sample concentration and 260/280 ratios were measured using a Nanodrop spectrophotometer. Generation of cDNA was performed using the iScript cDNA synthesis kit (BioRad cat# 1708890), reverse transcribing 1 µg of total RNA per reaction. 25 ng of cDNA template was added to an iScript Sybr Green master mix containing 1.5mM $MgCl_2$ and 0.1 µM of each forward and reverse primer. Relative gene expression was measured by normalizing log_2-fold expression to reference genes HPRT and beta-actin using the ΔΔCt method, as previously described[22]. Primer sequence are provided in the supplement (sup. table 14).

Brightfield histology lesion quantification:

Lung, liver, lymph node and spleen were fixed in 4% paraformaldehyde for 48-72 hours. Trimmed specimens were routinely processed, sectioned at 5 microns, collected on charged slides, and stained with hematoxylin and eosin (HE) for evaluation by brightfield microscopy. All slides were digitized via a Vectra Polaris scanning scope (Akoya Biosciences, Marlborough, MA). Lesion quantification was performed via artificial intelligence Visiopharm

analytical software (Hoersholm, Denmark). For the lung, application development involved first isolating lesions and airway spaces from normal tissue. A second application delineated airways and associated tissues from true lesion. A final application was utilized to differentiate lesion morphology including: macrophages, lymphocytes, necrosis and mineralization. For the liver and spleen, one application was developed to delineate lesion from normal parenchyma. Lesion quantification was calculated by ratio of area of lesion to area of total tissue and lesion parameters by a ratio of lesion parameter area to total lesion area.

Distribution of tissue CD1 expression by quantitative immunohistochemistry:

Lung parenchyma was isolated fresh at necropsy, embedded in OCT medium (Sakura, cat#: 4583), and cryopreserved in a liquid nitrogen bath, then stored at -80°C until further use. OCT-embedded tissue was sectioned using a cryotome maintained at -16 to -18°C, and a 7µm section adhered to charged glass slides. After sectioning, tissues were immediately placed in a 100% chilled methanol fixation for 45 minutes to fix the tissue and inactivate the Mtb organism. All 3.3'-diaminobenzidine (DAB) chromogenic and fluorescent immunohistochemistry protocols were completed on methanol fixed tissue sections utilizing a Leica Bond RXm automated slide stainer and previously validated protocols (Sup. table 5). Fluorescent multiplex IHC was achieved using Opal fluorochromes 570 and 690 (Akoya Biosciences, 520- FP14887001KT, 690- FP1497001KT) to detect CD1-isoform specific expression and distribution across myeloid/histiocytic and B cell subsets using antibodies described in sup. table 14. All tissues were blocked in 2.5% goat serum solution (Vector Labs, cat#: S-1012-50) and primary antibodies diluted in 2.5% goat serum. Primary antibodies were detected using a goat anti-mouse HRP-conjugated secondary antibody (Vector Labs, Cat#: MP-7452-50) and incubated with DAB substrate for chromogenic IHC or Opal fluorochromes for fluorescent IHC protocols. Quantification of immunohistochemistry was performed using Visiopharm analytical software

(Hoersholm, Denmark). An application was first developed to identify cellular nuclei based on DAPI staining. Nuclei labeling was then changed to B cell+ nuclei based on nuclear staining of Pax-5. A final application was utilized to change all nuclei, B cell and non-B cell, labelling to CD1+ labels based on membranous staining with the CD1 monoclonal antibody. Counts of non-B cell CD1-, B cell CD1-, Non-B cell CD1+ and B cell CD1+ nuclei were quantified for raw numbers and further calculations.

Quantification of tissue bacterial burden:

Lung, lymph node, spleen and liver bacterial burden was quantified as previously described. In brief, tissue homogenate was plated on 7H11 agar quad plates in 5-fold serial dilution and colonies counted after 8 weeks of incubation. Colony-forming units were $\log_{10}$-transformed and expressed as colony-forming units per gram of tissue.

Statistical analysis:

All analyses, with the exception of cytotoxicity assay, were performed utilizing prism version 9.4.1 (GraphPad, San Diego, CA). Data distribution was evaluated via a Shapiro Wilks test. Based on distribution One-Way ANOVA tests or Kruskal-Wallis test was performed to determine statistical significance for flow cytometric analysis, gene expression, and histologic quantifications. Statistical significance was set at $p \leq 0.05$. For the cytotoxicity assay, all analyses were performed using R Statistical Software (v4.2.1; R Core Team 2021). AUC was calculated based on the ratio of effector to target cells and normalized percent killing via the metrumrg R package (v5.57; Bergsman et. al 2013). A 2-factor ANOVA with Sidak's correction was used to determine the significance between groups or time with rstatix R package (v0.7.0; Kassambara 2021).

Results:

FLT3-L and morpholino compounds modulates CD1 expression both *in vitro* and *in vivo* in naïve guinea pigs.

To ensure that FLT3-L and morpholino compounds could modulate CD1 expression several invitro experiments and exposure studies in naïve guinea pigs were performed. Invitro studies utilized guinea pig bone marrow derived dendritic cells (BMDCs), bone marrow derived macrophages (BMDMs), transfected CD1 fibroblasts and/or bronchoalveolar lavage cells (BAL cells). Administration of CD1b1-2 and CD1b3 morpholino compounds on transfectant CD1b1, CD1b2 and CD1b3 fibroblasts knocked down CD1 expression, with a maximal knockdown of greater than 50% in CD1 protein expression compared to negative control conditions (sup. fig. 19). In contrast, FLT3-L treatment of BMDMs and BAL cells stimulated upregulation of CD1 expression compared with non-FLT3-L controls with a twofold increase in overall expression (sup. fig 20). Both cell types lost enhanced CD1 expression, returning to basal CD1 expression, by day 3 post FLT3-L stimulation. Finally, a small ex-vivo infection, utilizing mCherry expressing Mtb, was performed to demonstrate the acute effects of an intracellular Mtb infection on CD1 expression and how FLT3-L stimulation alters such expression. Flow cytometric analysis of mCherry positive cells validates previous studies demonstrating that infection with Mtb leads to down regulation of CD1[129,205,206]. However, mCherry infected cells treated with FLT3-L were able to maintain consistently high levels of CD1 regardless of multiplicity of infection of the bacteria (sup. fig 21). This study was key to demonstrating that FLT3-L has the ability to modulate CD1 in the face of an active intracellular infection.

After validation of FLT3-L and morpholino CD1 modulatory efficacy in *invitro* a pilot study, with saline control, FLT3-L and morpholino treatment conditions, was performed to

assess compound ability to modulate CD1 expression *in vivo* via intrapulmonary administration. Intrapulmonary administration was achieved via a Buxco inhalation tower, allowing for control of several parameters of exposure treatments (sup. fig. 22). Two guinea pigs were utilized to ensure proper alveolar placement of particles via inhalation exposure to CellTrace Violet fluorescent dye and assessment of cellular fluorescence in individual lung lobes (sup. fig. 23).

For the naïve FLT3-L and morpholino *in vivo* efficacy study, flow cytometric analysis of BAL cells established the ability of FLT3-L to significantly increase overall expression of CD1 in CD45+ cells ($p \leq 0.05$). Since naïve lung derived CD45+ cells have low basilar expression of CD1, BAL cells from all conditions were stimulated ex-vivo with FLT3-L to reveal morpholino effect. Under this ex-vivo CD1 stimulation, the morpholino group had significantly lower CD1 expression than both saline control and FLT3-L conditions ($p \leq 0.05$) **(Fig. 24).** Similar findings were concordant with CD1b ortholog specific gene expression of homogenized lung, with FTL3-L treated guinea pigs having significantly increased gene expression compared to saline control and morpholino treated guinea pigs ($p \leq 0.0001$ and $p \leq 0.05$) for all CD1b orthologs **(Fig. 25)**. Lastly, the effect of compound modulation is appreciated in cytologic analysis of BAL cells and spatially via immunohistochemical analysis of sectioned fresh frozen lung tissue, with FLT3-L animals having significantly greater CD1 positive cells in lung tissue sections ($p \leq 0.001$) **(Figs. 26-27)**. This *in vivo* proof-of-principle provided clear evidence that under normal conditions intrapulmonary administered FLT3-L provides upregulation of all CD1b orthologs; while morpholino compounds are able to prevent CD1 upregulation in *ex-vivo* FLT3-L stimulated conditions.

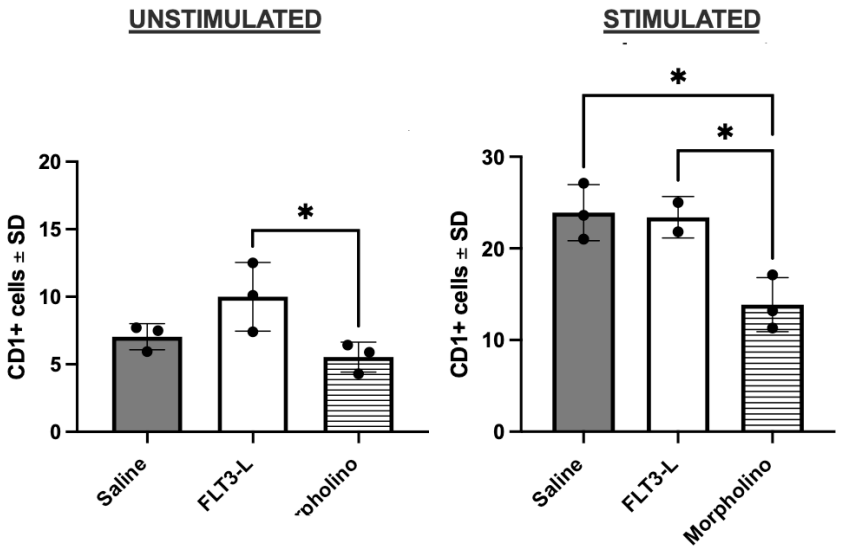

Figure 24. Naïve guinea pig FLT3 and morpholino CD1 modulation. Bronchioalveolar derived cells were taken from guinea pigs treated with either saline, FLT3-L and morpholino compounds for 4 exposures. Unstimulated cells were taken directed from terminated guinea pigs and analyzed via flow cytometry for CD1. Stimulated cells were taken from guinea pigs and stimulated with 20ng/ml FLT3-L in complete RPMI for 18 hours and evaluated for enhanced CD1 expression. * $P \leq 0.05$; one-way ANOVA with Tukeys correction.

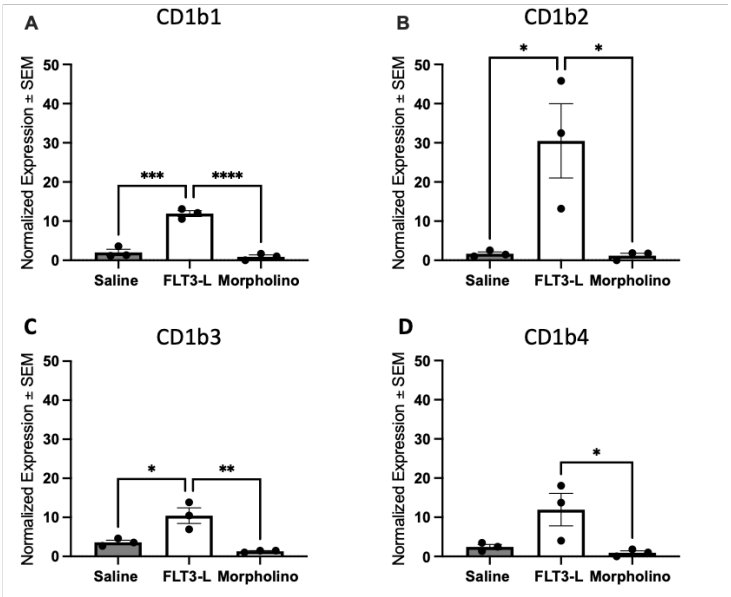

Figure 25. Gene expression of naïve guinea pigs with FLT3-L and morpholino exposure. Ortholog specific real time PCR gene expression of all three treatment groups in naïve guinea pigs. A) CD1b1, B) CD1b2, C) CD1b3, D) CD1b4. *P≤0.05, **P≤0.01, ***P≤0.001, ****P≤0.0001; one-way ANOVA with Tukeys correction

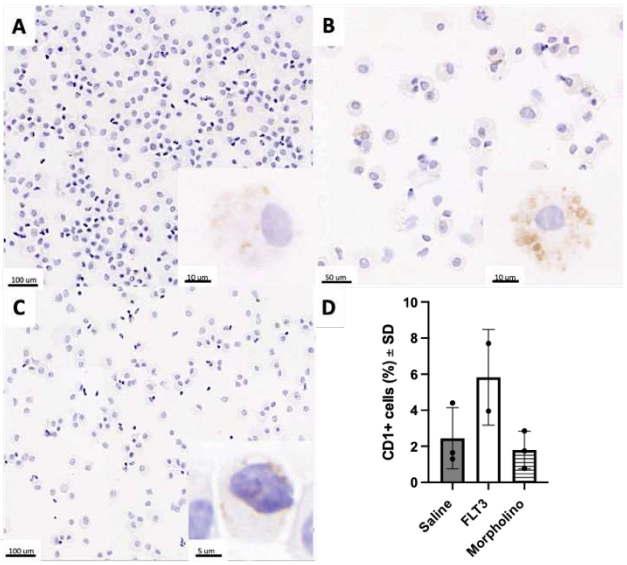

Figure 26. Immunocytochemistry of Bronchioalveolar cells. 1X10^6 cells were centrifuged against a positively charged slide and then chromogenic immunocytochemistry was performed utilizing a pan CD1b antibody (6B5). A-D) cytologic images of cells with CD1 stain A) saline group, B) FLT3-L group and C) morpholino group. Insets are higher magnifications of CD1 positive cells demonstrating endosomal and cell membrane localization. D) Quantitative assessment of CD1 positivity of CD1 spins from all treatment groups.

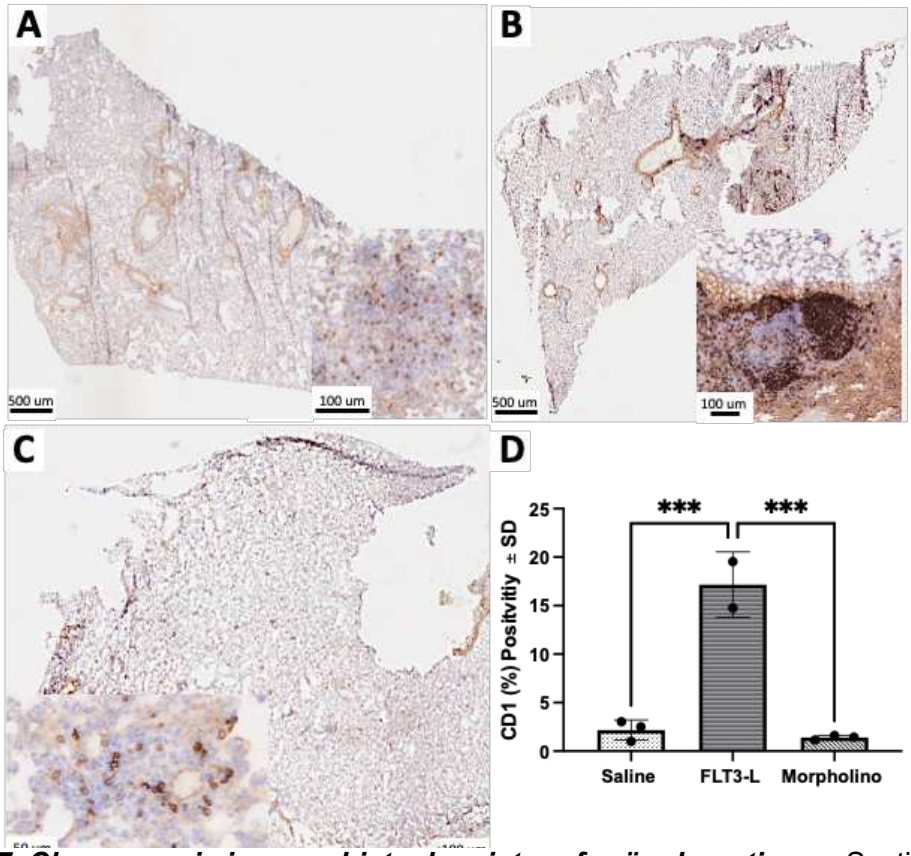

Figure 27. Chromogenic immunohistochemistry of naïve lung tissue. Sections of fresh frozen lung tissue are stained with a pan CD1b antibody (6B5). A) representative saline control lung section, B) representative of FLT3-L treatment lung sections, and C) representative morpholino treatment lung section. Inserts are higher magnification of representative sections. D) quantification of CD1 expression of all treatment groups via visiopharm software ($p< 0.001$).

Morpholinos are able to knockdown CD1 complex expression at days 30 post infection but not day 60 post infection within homogenized lung tissue and bronchioalveolar lavage cells.

To evaluate the ability of morpholino and FLT3-L compounds to modulate CD1 complex expression on CD45+ leukocytes during Mtb infection we utilized flow cytometric analysis. Saline treatment groups, both at day 30 and 60 post infection, have similar CD1 expression profiles to previously performed CD1 kinetic work in the face of Mtb infections, day 30: 29.23% ± 5.28% CD1b and day 60: 16.84 ± 4.4% CD1b (**Fig. 28** and sup.fig 24). In concordance with

previous studies, there is a significant difference between day 30 and day 60 post infection in saline control guinea pigs ($p \leq 0.001$) **(Fig. 28A)**. Similar findings are appreciated from BAL derived saline control group ($p \leq 0.001$) **(Fig. 28B)**. The FLT3-L and combination treatment groups have similar CD1 expression to the saline control at both days 30 and 60 post infection among lung derived cells and BAL. Lung parenchyma derived cells from the morpholino treatment group have significantly decreased expression of CD1 expression at day 30 compared to all groups (saline and FLT3 groups: $P \leq 0.0001$, Combination group: $P \leq 0.001$). Similar knockdown was appreciated within morpholino treatment group BAL cells ($p \leq 0.001$) with the exception of no significant reduction when compared to the combination treatment group. However, the morpholino treatment group loses all significant knockdown effect at day 60 post infection in both the lung and BAL derived cells. Interestingly, the combination treatment group within the lung at day 30 was able to recover comparable CD1 expression to both the saline control and FLT3-L treatment animals, but loses that recovery of expression in day 60 post infection compared to FLT3 guinea pigs ($p \leq 0.05$). BAL derived cells from the combination treatment group does not significantly recover CD1b expression regardless of the time point. Correlating with our *in vitro* infection pilot, lung derived cells from FLT3-L animals don't have significant reduction in CD1 expression from day 30 to day 60 post infection. Gating for flow analysis was performed using previously validated methodology in our lab (sup. fig. 25).

Noting the differences in CD1 positive cells between treatment groups. We further evaluated these CD1 positive cells for the degree of surface CD1 glycoprotein expression, based on mean fluorescent intensity (MFI). MFIs are significantly lowered within the morpholino treatment group compared to other groups from both BAL and lung derived cells within the day 30 post infection group ($p \leq 0.0001$) **(Fig. 28C-D)**. The difference in MFI is diminished at day 60 post infection animals in both BAL and lung parenchyma derived cells **(Fig. 28E-F)**.

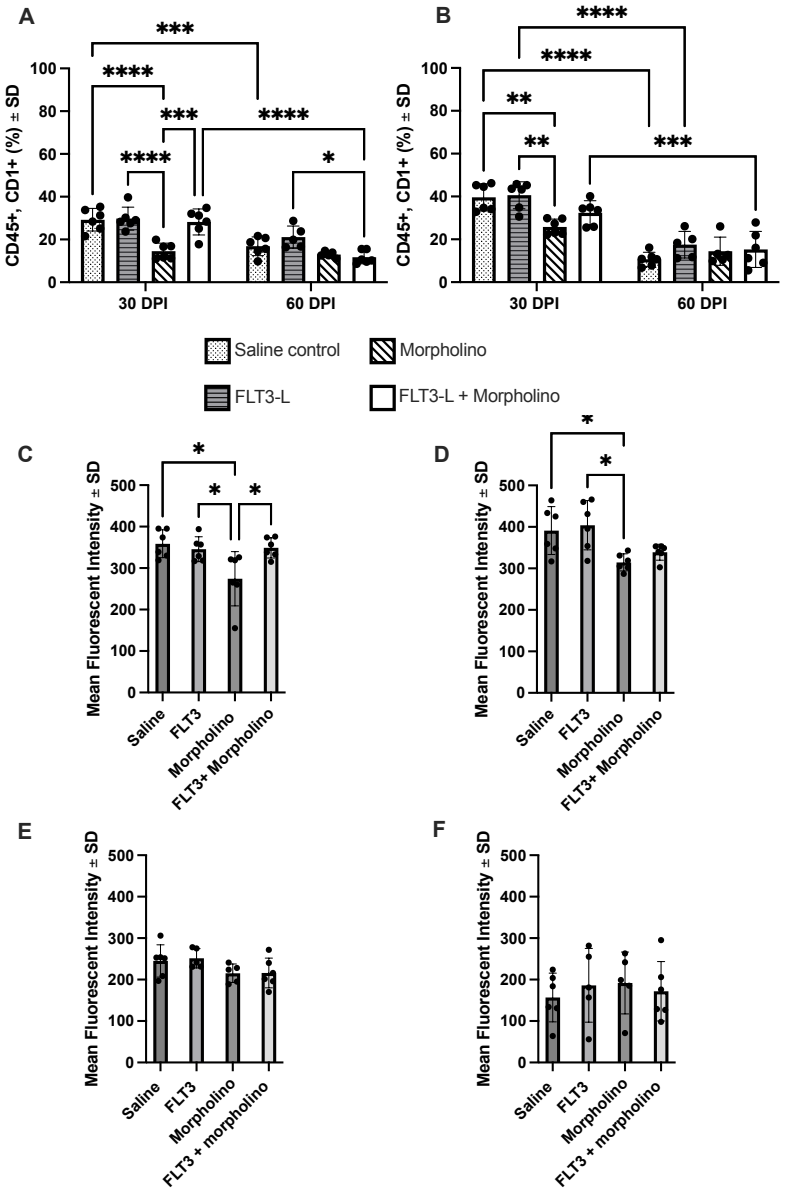

Figure 28. CD1 complex expression during Mtb infection. Flow cytometric analysis of antigen presenting cells at 30- and 60-days post infection (DPI) for all treatment groups. Cells were gated for, live, CD45 + cells and evaluated for overall CD1 expression via 1B12 CD1 antibody. Both homogenized lung cells (A) and bronchioalveolar (BAL) cells (B) were evaluated. Mean fluorescent intensity (MFI) was evaluated for CD1+ cells from both lung and BAL cells at days 30 and 60: C) CD1+ lung MFI at 30 DPI, D) BAL cells MFI from 30 DPI, E) Lung MFI from 60 DPI, and F) BAL MFI from 60 DPI. Statistical significance: * P<0.05, **P<0.01, ***P<0.001, and **** P<0.0001; two-way ANOVA with Tukeys correction.

Morpholino treatment group changes the B cell population at day 30 post infection, but does not significantly influence B cell CD1 expression.

Utilizing a guinea pig B cell marker, we evaluated the effect of treatments on B cell populations and CD1b expression on that B cell population. The morpholino treatment group has significantly decreased B cells within homogenized lung parenchyma ($p \leq 0.05$) and trends down with BAL cells **(Fig. 29A-B)**. The day 60 morpholino treatment does not influence B cell populations. In contrast the combination treatment group recovers B cell numbers, which is more in line with the saline control and FLT3-L treatment groups in the lung tissue at day 30 post infection. This variation in B cell population is reciprocated in breakdown of CD1 expression between B cells and non-B cells. Though not significantly, B cell CD1 expression trends down in morpholino and combination treatment groups in lung parenchyma **(Fig. 29C, D)**. Interestingly, the FLT3-L and combination group BAL cells at day 60 does have significant upregulation of CD1 in B cells compared to non-B cells (FLT3-L $p \leq 0.05$ and combination $p \leq 0.001$) **(Fig. 29F)**.

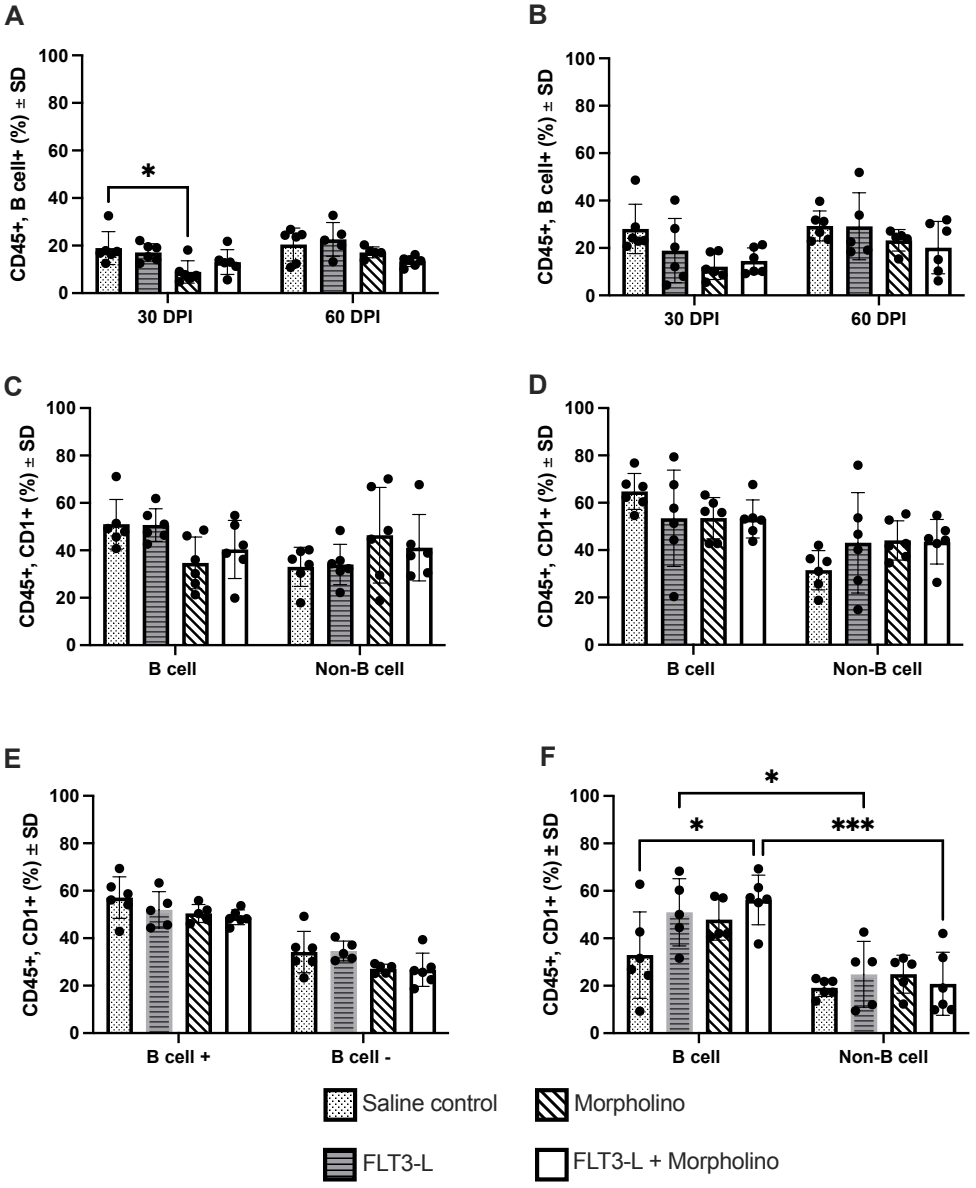

Figure 29. B cell population distribution and B cell vs non B cell CD1 positivity. Flow cytometric analysis of B cells at 30- and 60-days post infection (DPI) for all treatment groups. Cells were gated for, live, CD45 + cells and B cell frequency was assessed via a commercial guinea pig B cell antibody from homogenized lung (A) and Bronchioalveolar (BAL) cells (B). CD1+ distribution among B cells and non-B cells in both cellular population C) Lung at 30 days post infection, D) BAL cells at 30 days post infection, E) Lung at 60 days post infection, and F) BAL cells at 60 days post infection. * P<0.05, ***P<0.001; two-way ANOVA with Tukeys correction.

Treatments cause modulation of CD1b1 orthologs at day 30 but not day 60 of infection.

To further evaluate FLT3-L and morpholino compounds CD1 modulation CD1b ortholog specific primers were utilized to assess CD1b gene expression from RNA extracted from lung tissue (sup. fig. 26 & 27) . CD1b1 gene expression trends up with morpholino guinea pigs and is significantly upregulated with combination guinea pigs ($p \leq 0.05$) when compared to both the saline and FLT3-L groups. The increased expression of the combination group may be explained due to the stimulating effect of FLT3-L while the morpholino blocks formation of CD1 proteins translation, thus inhibiting negative feedback loops. This differential expression is lost at day 60 post infection time point **(Fig. 30A).** CD1b3 also exhibits differential gene expression at day 30 with the saline control group having significant up regulation compared to FLT3-L ($p \leq 0.001$) and combination ($p \leq 0.05$) guinea pigs. Interestingly, CD1b3 in both the morpholino and combination treatment groups trend up compared to FLT3-L. This expression differentiation may correlate to the unique expression of the CD1b3 ortholog, which is more or less constitutively expressed on B cells regardless of infection status. Chronic FLT3 stimulation of this already highly expressed ortholog may have induced strong negative feedback. This theory would add credence to why differences between the saline group and combination animals is less significant and why the morpholino group has no significant difference. Any significant differentiation of CD1b3 ortholog expression between groups is lost within the day 60 time point **(Fig. 30C)**. No significant modulation of orthologs CD1b2 **(Fig. 30B)** or CD1b4 **(Fig. 30D)** are appreciated at either day 30 or day 60 post infection time points; however, Combination and morpholino treatment groups expression of CD1b4 trends up compared to saline and FLT3-L animals.

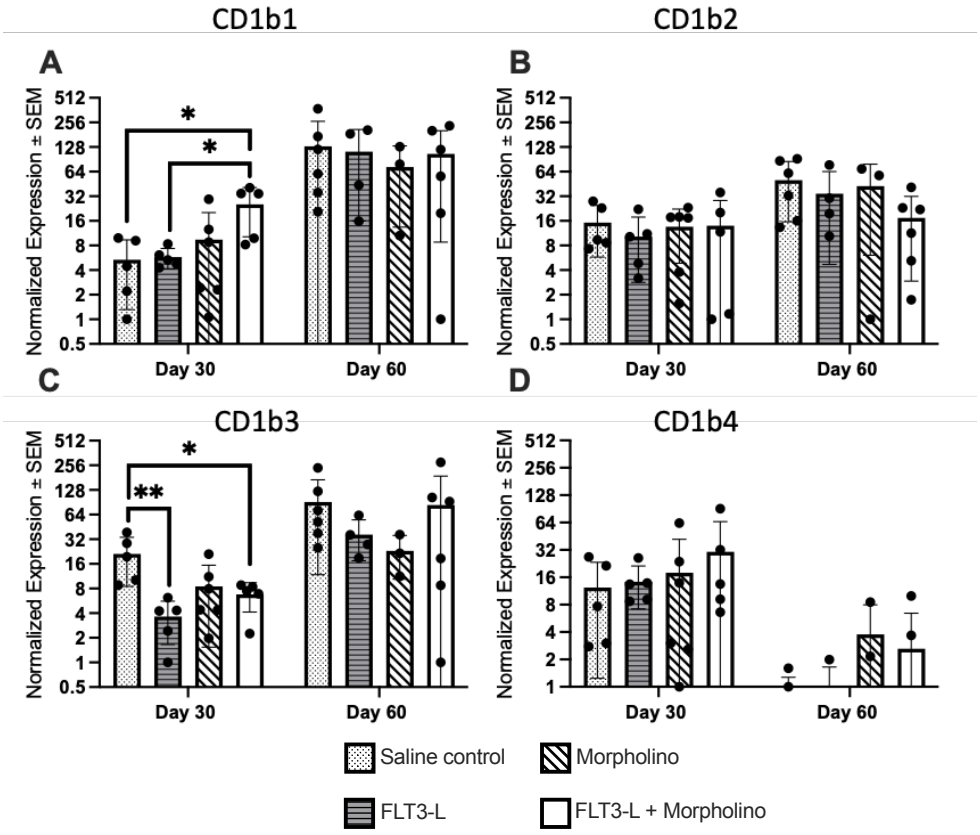

Figure 30. Isoform specific CD1 kinetic gene expression. Isoform specific primers for CD1B1-4 were utilized for real time PCR on lung samples from all treatment groups of infected guinea pigs. Expression was normalized to the lowest expression of each ortholog. A-D) Ortholog specific expression on day 30 and 60 post infection, CD1b1 (A), CD1b2 (B), CD1b3 (C), CD1b4 (D). E-H) Statistical significance was analyzed via a one-way ANOVA is as follows: ***≤ 0.05, **≤ 0.01.

Treatment groups have no difference on lesion burden within lung, liver or spleen at either time point.

Collected lung was analyzed via Visiopharm quantitative histology software to evaluate the area of overall lesion burden, area of lymphocyte infiltration, area of necrosis representing chronic lesions and areas of mineralization indicating lesions undergoing resolution. Representative image of a saline control lung and Visiopharm annotation is shown (**Fig. 31A-B).** Analysis reveals no intertreatment group variability in any of the measured parameters either at days 30 or days 60 post infection **(Fig. 31C-F)**. Of unknown implication, there is a significant decrease in

lymphocytic infiltration from the saline control and FLT3-L treatment from the day 30 to day 60 post infection time points($p \leq 0.01$).

Due to the complexity of the spleen and liver tissue architecture, only overall lesion burden area was assessed and quantified. Representative sections of liver and splenic parenchyma from day 60 animals are shown **(Fig. 32A-B)**. As with the lung, there is no significant intertreatment group variability at either day 30 and day 60 post infection. Interestingly, Only the FLT3-L treatment group in the liver has significantly increased lesion burden when comparing day 30 to day 60 time points **(Fig. 32C-D)**.

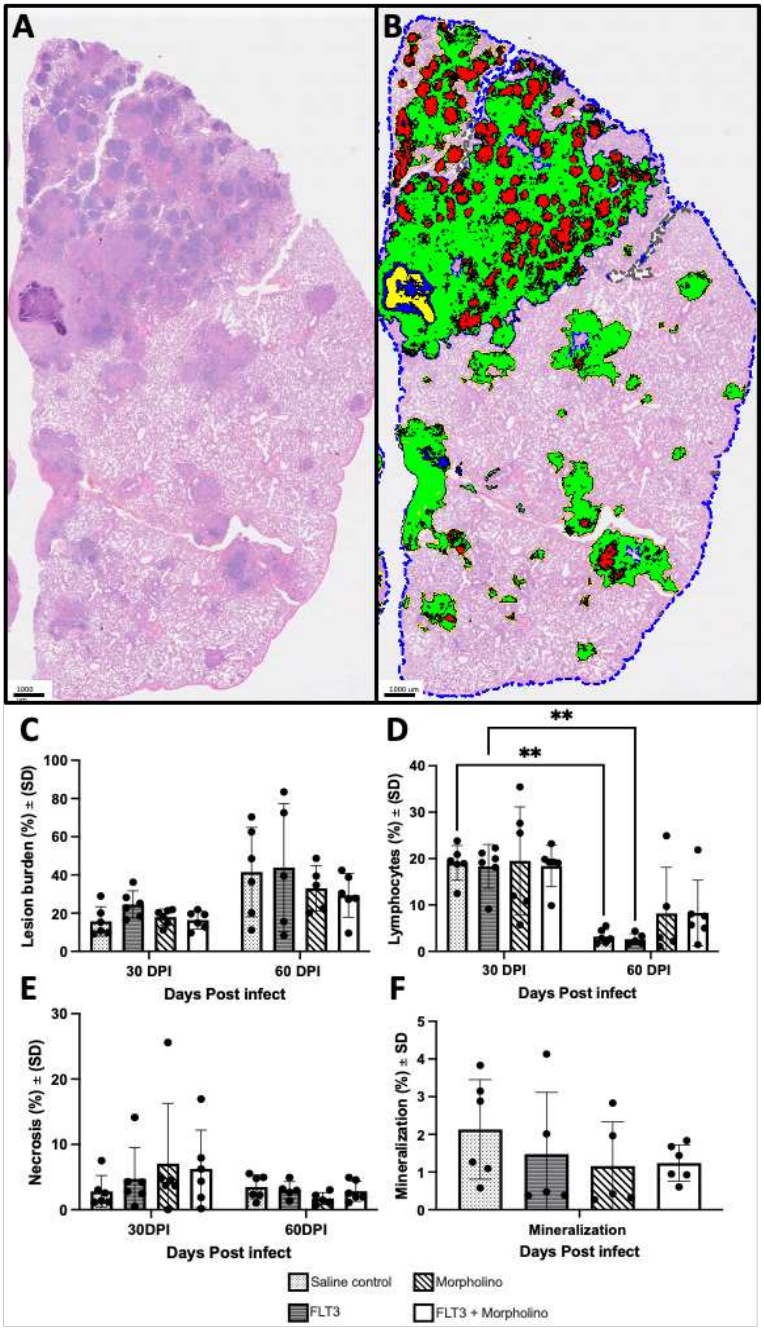

Figure 31. Lung H&E lesion quantification and classification. H&E sections of infected lung tissue from days 30 and 60 post infection from all treatment groups. All sections were analyzed utilizing Visiopharm quantitative software. A) A representative section of lesion from the animal model at day 60 post infection. B) Breakdown of lesions into histiocytic inflammation (green), lymphocytic (red), necrosis (blue), and mineralization (yellow). C-F) Quantitative assessment of lesions and lesion breakdown via area assessment, Lesions percentage to whole lung (C), percent lymphocytes within lesions (D), percent necrosis within lesions (E), and Percent mineralization within lesions (F). Statistical significance was analyzed via a two-way ANOVA is as follows: ** $\leq$ 0.01.

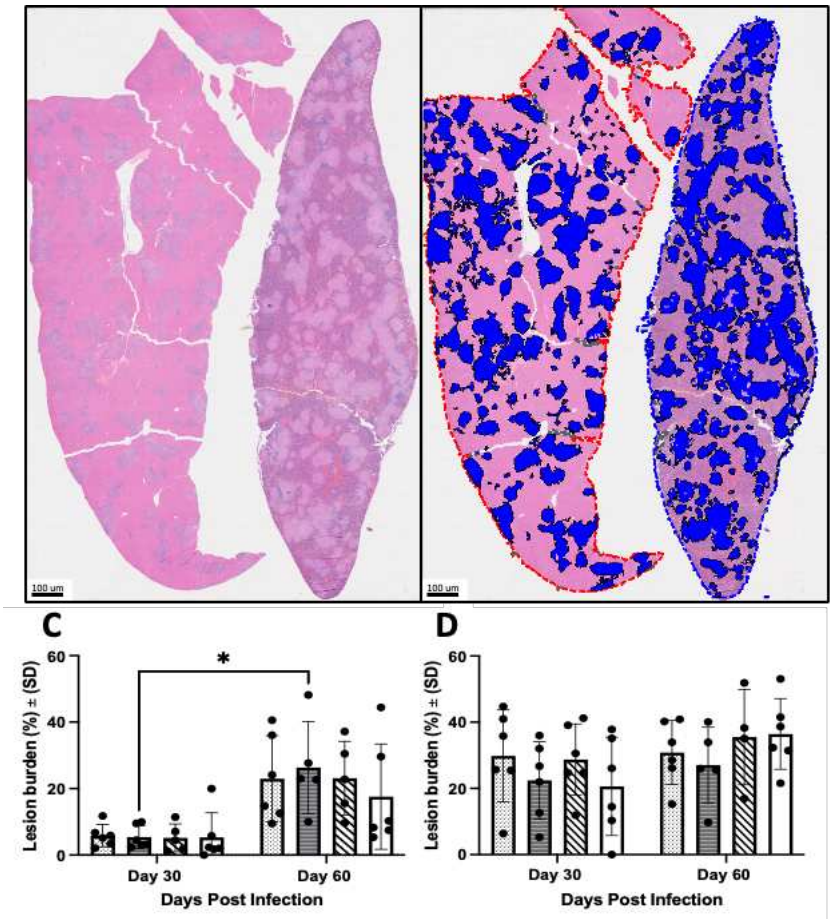

Figure 32. Liver and spleen H&E lesion quantification. H&E sections of infected liver and spleen tissue from days 30 and 60 post infection from all treatment groups. All sections were analyzed utilizing Visiopharm quantitative software. A) a representative sections spleen and liver with lesion from a guinea pig at day 60 post infection. B) The same representative sections demonstrating quantification of lesion (blue is lesion). C-D) Lesion percent as compared to area of normal tissue in the liver (C) and spleen (D). Statistical significance was analyzed via a one-way ANOVA is as follows: * $P \leq 0.05$.

Treatments affects lung CD1 and B cell prevalence in lesional and lesion-free lung tissue.

To further assess CD1 expression multiplex immunohistochemistry was performed on fresh frozen lung sections with monoclonal CD1 and B cell antibodies. Though no significant difference could be established, trends of overall CD1 expression closely aligns with previously discussed CD1 flow cytometric data. At day 30, CD1 expression among FLT3 animals trends upward, while morpholino animal's trend downward and are in line the saline treatment group.

Corresponding to other data, combination animals have higher overall CD1 positivity compared to saline and morpholino groups. There is a loss of this distinct expression patterns at 60 days post infection, with the combination trending high with overall expression at that time point **(Fig. 33E)**.

Tissue based immunohistochemistry allowed for evaluation of CD1 expression in both lesion and normal lung parenchymal compartments. This breakdown allowed for visual evaluation of where the compound is having its maximally modulatory effect. At 30 days post infection, FLT3-L, while increasing expression in both compartments, seems to have maximal effect within the granulomatous compartment. The morpholino treatment group, in contrast to FLT3-L, equally down regulates CD1 regardless of tissue compart. Surprisingly, the combination treatment animals demonstrated increased CD1 expression compared to the morpholino group, which in contrast to the FLT3-L group, also effects both compartments. As demonstrated throughout all previously discussed data sets, there is loss of CD1 modulation in either tissue compartment regardless of treatment groups **(Fig. 33F-G)**.

Multiplexing of CD1 and B cell antibodies allowed for investigation of a breakdown of which cells are presenting CD1 and in which tissue compartment. Saline animals have similar breakdown of CD1 expression in terms of cell type and compartment as previously described in our previous CD1 experiments (sup fig. 28). In contrast to the flow cytometric measures, CD1 expression in both FLT3-L and morpholino groups has expanded CD1+ B cell populations in both lesion and normal tissue compartments. However, the combination group, has expanded B cell CD1 B cell expression in the granuloma, which is more in line with the saline group in

normal parenchyma. Interestingly, data from 60 days post infection demonstrates that all treatments groups still have increased CD1+ B cells compared to the saline group **(Fig. 33H).**

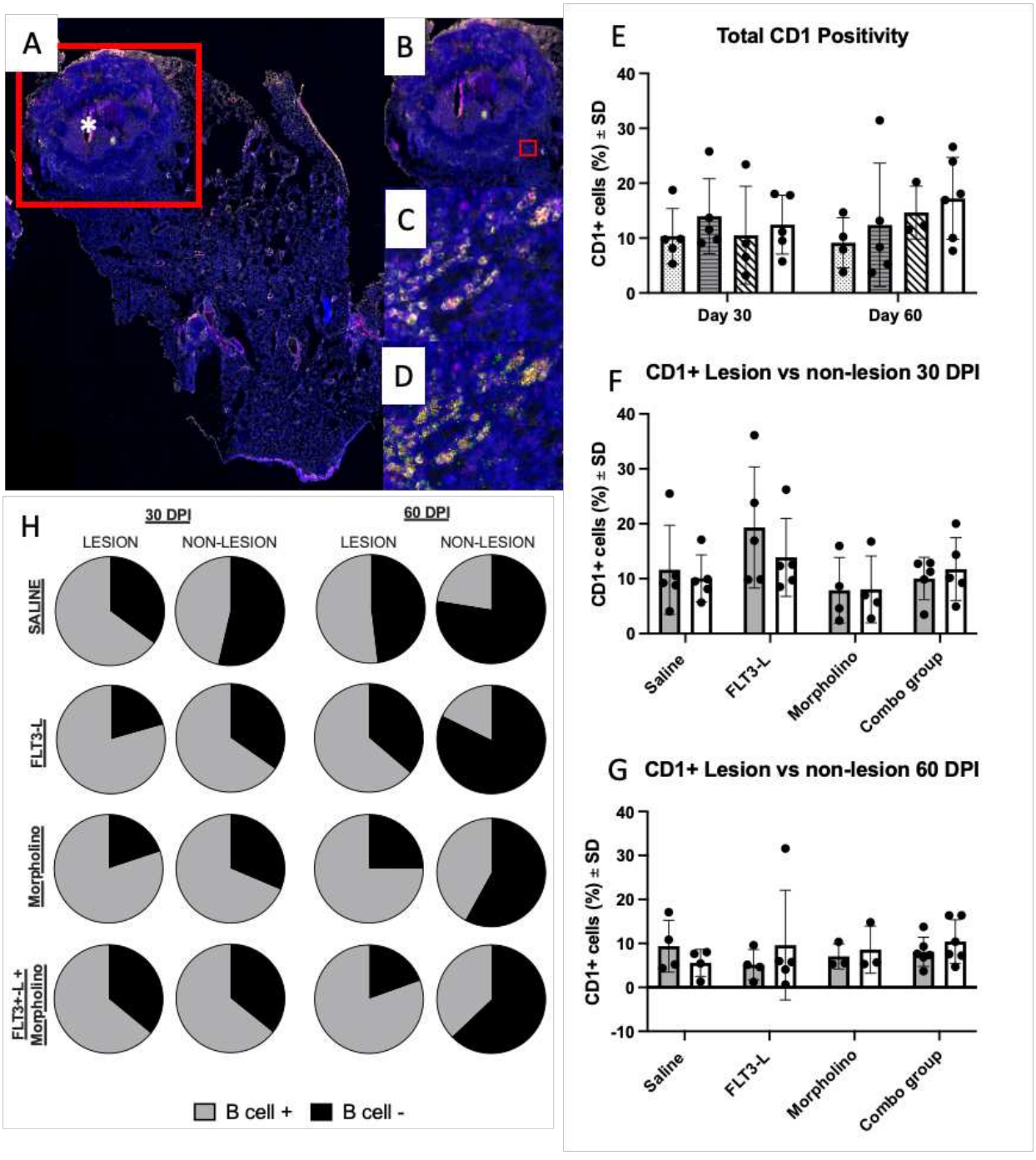

Figure 33. Multiplex immunohistochemistry and visiopharm analysis. Fresh frozen sections of lung from days 30 and 60 post infection and all four treatment groups were stained with 6B5 (Opal 520), PAX5 (clone 24, Opal 570), and DAPI utilizing opal multiplex (Akoya) technology. A-D) Representative sections of a lung granuloma demonstrating: fresh frozen low magnification HE section (A) to low magnification serial sectioned multiplex IHC section (B) to higher magnification of CD1+, Pax5+ region (B) and the high magnification section with overlayed visiopharm analysis software (D). Asterisk in sections represent a region of necrosis, the red box indicates the region of higher magnification in C-D. For Visiopharm analysis, all nuclei in the tissue were detected and then labeled based on nuclear and membranous staining of the associated cells. Labels include: B cell- red (pax5+, CD1-), CD1+ B cells- yellow (PAX5+, CD1+), CD1+ other cells- green (CD1+, PAX5-), and negative cells- blue (CD1-, PAX5-). E-H) Visiopharm derived quantitative percentages of all cells and B-cell specific CD1 expression at 14, 30 and 60 DPI of Mtb infected guinea pigs. E) Total CD1 membranous positivity of entire analyzed tissues from all treatment groups on days 30 and 60 post infection. F) Breakdown of CD1 membranous positivity of all treatment groups between granulomatous and normal parenchyma from day 30 post infection. G) Breakdown of CD1 membranous positivity of all treatment groups between granulomatous and normal parenchyma from day 60 post infection. H) Breakdown of CD1 positivity between B cells and non-B cells of all treatment groups examining lesion vs non-lesion from days 30 and 60 post infection.

Treatments significantly impact lung derived CD1-restricted T cell cytotoxic activity.

Previous literature has proven that CD1-restricted T cells have a cytolytic activity towards CD1 lipid antigen presenting cells[116,198,216]. Our lab has previously established the ability to assess the functionality of tissue derived CD1-restricted T cells via a flow cytometric cytotoxicity assay (sup. fig. 29). Non-adherent effector cells isolated from lung parenchyma were incubated with CD1b1 and CD1b3 transfectant fibroblasts cell lines loaded with either mycolic acid (MA) or glucose monomycolate (GMM) synthetic lipid antigens. Gating strategy is provided in the supplement data (sup. fig. 12). Lung effector cells from morpholino guinea pigs lack any cytotoxic effect compared to the normalized control condition, and frequently have lower cytotoxic effect than the antigen unloaded control conditions. The lack of cytotoxic effect for the morpholino treatment group is maintained regardless of the CD1b ortholog, Mtb lipid antigen or infection time point, with significant decrease compared to saline control targeting CD1b1 fibroblasts cells loaded with either Mtb lipid antigen ($p \leq 0.05$) **(Fig. 34)**. Interestingly, the treatment group with the second lowest cytolytic ability is the FLT3-L guinea pigs. FLT3-L effector cells had increased cytolytic ability compared to both unloaded controls and the

morpholino treatment group but trended lower than both saline control and combination treatment groups at 30 days post infection; with maximal cytolysis demonstrated in the GMM CD1b3 condition at 1:4 ratio 14.4% cell death ± 26.5%. At day 60 post infection FLT3-L effector cells frequently aligns with degree of cytotoxicity of both saline control and combination treatment groups, with maximal day 60 post infection of cytolysis again appreciated at the GMM CD1b3 condition at 1:8 ratio 24.5% cell death ± 26.9%. As mentioned, Saline controls and combination treatment group have the highest degree of cytolysis of any treatment groups with the highest degree of mean cytolysis appreciated with the GMM CD1b3 transfectant fibroblasts at 30 days post infection, Saline: 37.2% cell death ± 17.2% and combination: 37.1% cell death ± 8.9%. This finding may correlate with the noted ortholog specific gene expression, where saline control and combination treatment guinea pigs have increased gene expression compared to the FLT3-L treatment group. Correlating with the previous CD1 kinetic data, all treatment groups wane in their degree of functional cytolysis at 60 days post infection. However, the combined treatment group effector cells in the GMM CD1b3 fibroblast condition increased overall cytolytic ability compared to the day 30 time point, 1:8 42.7% cell death ± 29.5%. This may indicate a synergistic effect of FLT3-L and morpholino compounds that was able to continue CD1-restricted T cell stimulation and enhance the functionality of CD1-GMM-restricted T cells, also referred to GEM T cells, past that what is normally appreciated in previous studies and the saline control animals[114,115].

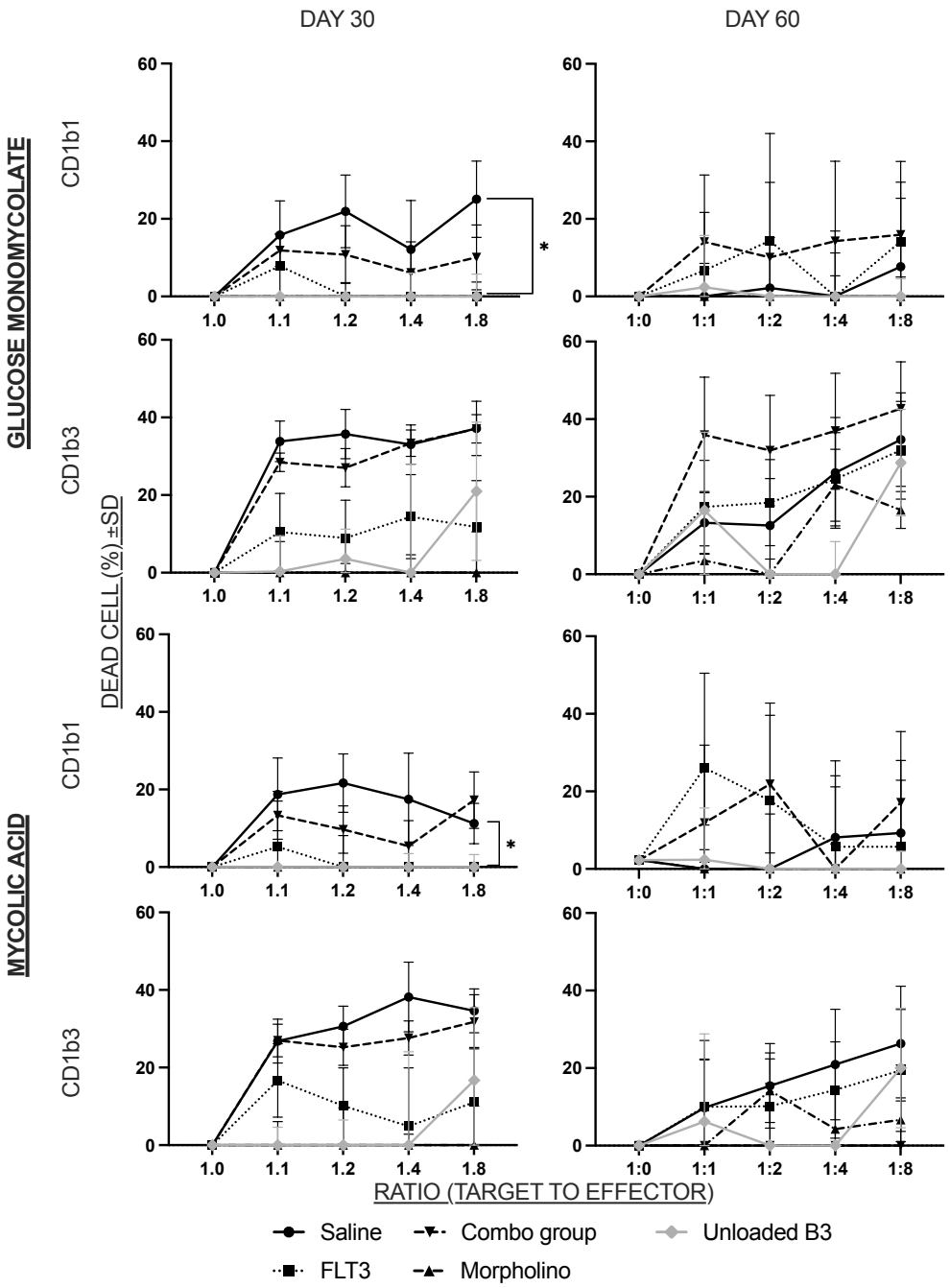

Figure 34. Lipid specific cytotoxicity assay with splenic effector cells. Cell trace violet labelled CD1 transfected fibroblasts CD1b1 or CD1b3 (target cells) were loaded with either synthetic glucose monomycolate or mycolic acid Mtb lipid. Fibroblasts were then incubated with inflammatory cells from the lung derived from Mtb infected and naïve guinea pigs at 30 and 60 DPI at ratio ranging from 1:0 to 1:8 target to effector cells. Fibroblast viability was assessed via flow cytometric analysis. Effector cells from all treatment groups were assessed as well as loaded with targets cells that were not incubated with Mtb lipids (unloaded control). Significance is calculated based on area under the curve ($p < 0.05$).

Treatment groups have limited effect on tissue bacterial burden:

The local and systemic burden of Mtb were assessed via culture of lung, spleen, liver, and hilar lymph node homogenates and the formation of colony forming units (CFU) **(Fig. 35)**. All treatment group CFU counts demonstrated bacteria counts which are consistent with the labs validated and published low-dose aerosol guinea pig models[22,142]. Interestingly, and possibly correlating with cytotoxicity data, CFU burden in the combination treatment group trends down compared all other treatments in all cultured organs, averaging 4.78 CFU/ml in all organs, and is significantly lower than the lung CFU burden from the morpholino treatment, 5.179 ± 0.33 CFU/ml, ($p \leq 0.05$), at 30 days post infection **(Fig. 35A)**. Additionally, at the same time point, the morpholino treatment animals CFU burden trends up in lung, liver and splenic tissue, averaging 5.236 CFU/ml, compared to all other treatments and saline controls. Less variation in CFU burden is appreciated 60 days post infection, with only the FLT3-L treated guinea pigs exhibiting significantly upregulated burden in the liver compared to the morpholino guinea pigs ($P \leq 0.05$) **(Fig. 35F)**. No other clear trend can be appreciated among the day 60 CFU data.

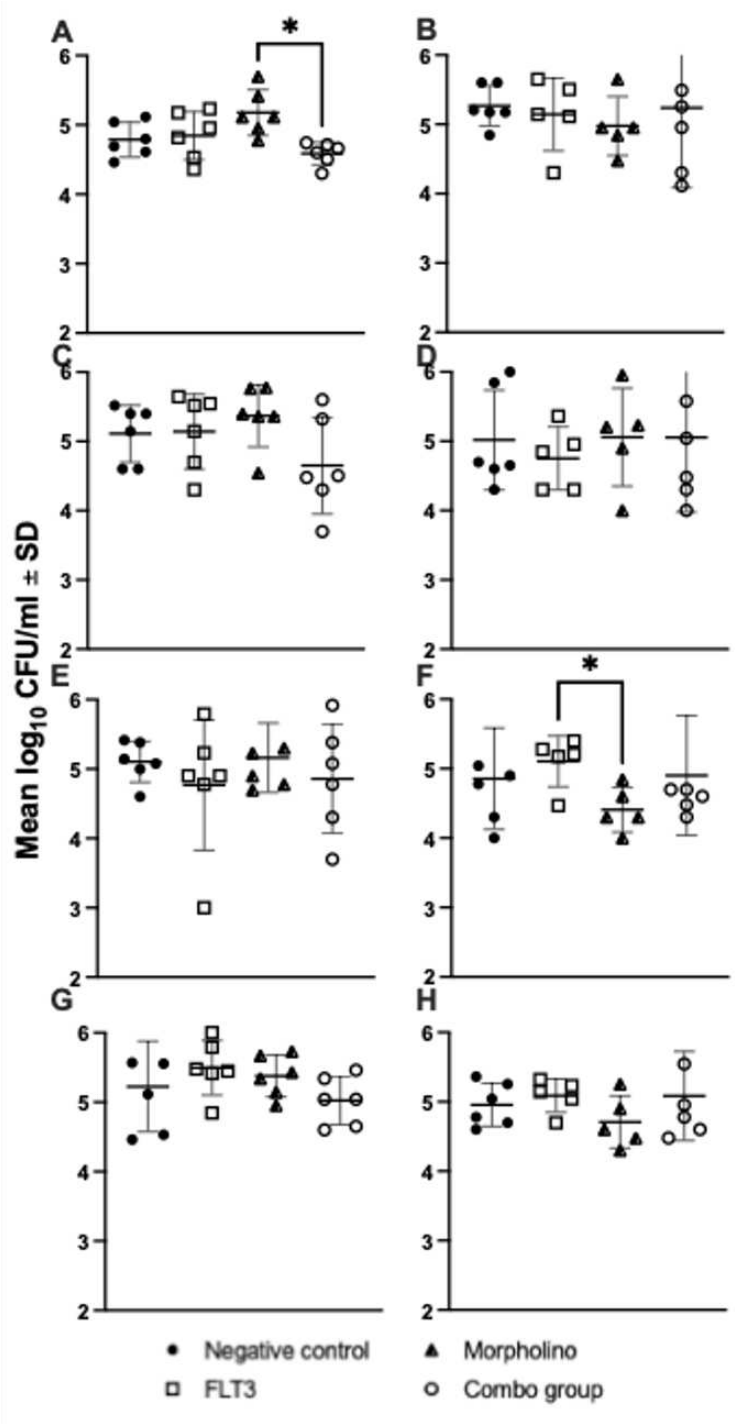

Figure 35. Mycobacterium tuberculosis colony forming units assessment. A-H) Tissue homogenates from lung day 30 (A) and 60 (E) post infection, spleen day 30 (C) and 60 (D) post infection, liver day 30 (E) and 60 (F) post infection, or lymph node day 30 (G) and 60 (H) post infection were plated to the 1 in 10^6 dilutions. Colony forming units were counted for 8 weeks and log transformed to provide colony forming units per ml of tissue. * $p<0.05$.

Discussion:

The role of CD1-restricted immunity in directing the pathogenesis, lesion development and disease progression of TB is currently unknown. From the literature, many human and animal studies have established CD1 glycoproteins are not only able to present Mtb specific lipids but are also modulated as a result of infection[128,130]. Other studies investigated how Mtb lipid vaccinations effect overall disease progression of Mtb infections, demonstrating decreased lesion burden[217–219]. However, these studies do not directly correlate disease progression with CD1 immune status in terms of CD1 glycoprotein expression or CD1-restricted T cell functionality. This study aimed take a step back and evaluate how modulating CD1b glycoprotein in the face of an Mtb infection effects not only CD1-restricted T cells functionality but also assess how this modulation can affect overall disease progression in guinea pigs.

Successful modulation of CD1 glycoproteins was established utilizing both morpholino and FLT3-L in a series of invitro and *in vivo* pilot studies. These studies demonstrate that in naïve conditions FLT3-L drives decisive and profound upregulation of CD1 glycoproteins in both cell culture and when administered via an intrapulmonary route when examining both protein and gene expression. In correlation to our naïve studies, one invitro infection study demonstrated the ability of FLT3-L to maintain CD1 expression in the face of increasing bacteria burden compared to non-FLT3-L conditions. The findings of decreased CD1 expression with Mycobacterial intracellular infection in untreated cells correlates well several previous studies observing similar finding in human and transgenic mouse models[220221]. Due to the low basilar level of CD1 in the lung in naïve tissue proof of concept for successful blocking of CD1 via morpholino was more challenging. However, a combination of knocking down of CD1 specific transfectant fibroblasts and ability of intrapulmonary treated morpholino cells to inhibit ex-vivo FLT3-L stimulation demonstrated the ability of these compounds to have a minimum efficacy of a 20% CD1 knockdown compared to controls. Cumulatively, these pilots are the first to

demonstrate how exogenous compounds can modulate CD1, in a phenotypical and genotypical fashion, within cell culture and in *in vivo* lung environments.

Applying the results of the pilot studies, we utilized CD1 morpholinos and FLT3-L to modulate CD1 expression in guinea pigs during an active Mtb infection. Similar effects of the CD1 morpholino compound compared to the pilot were appreciated, causing CD1 expression knockdown compared to all other groups from both homogenized lung tissue and BAL cells at the early adaptive immune, 30 days post infection. The larger revelations were found with the FLT3-L and FlT3-L+ morpholino combination treatment groups. In contrast to the naïve pilots, FLT3-L guinea pigs closely mirrored CD1 expression of saline control groups at day 30 post infection. It could be that the highly complex inflammatory environment is releasing a host of endogenous paracrine or autocrine drivers of CD1 stimulation causing FLT3-L to have negligible stimulatory effect. The most direct evidence of FLT3-L effecting CD1 expression was observed in the combination treatment group, which recovered partial CD1 expression compared to morpholino treated guinea pigs. This recovery was unexpected as we utilized FLT3-L in the previous naïve studies to demonstrate efficacy of morpholino knockdown. This could indicate that within the tissue inflammatory environment the morpholino knockdown could be overcome with abundant CD1 mRNA transcription. Another possibility is that *in vivo* FLT3-L could be a major stimulator of CD1b4, the ortholog that our current morpholinos cannot target but our CD1 antibodies readily detect without discrimination. Of unknown significant, and warranting further investigation, is the ability for the morpholino compound to significantly shift B cells populations in the lung at day 30 post infection. B cells are a major expressor of CD1b3, it could be possible that a shift in the express of CD1b3 negative impacted B cell recruitment and proliferation within the lung parenchyma. Although not significant, morpholino and combination animals do shift CD1 expression distribution of CD+ B cell vs non-B cells.

To further dissect individual ortholog specific changes due to modulatory compounds during Mtb infection ortholog specific PCR primers were validated and utilized in RT-PRC amplification experiments. Gene expression of CD1b orthologs reflects findings found in flow cytometric findings. Morpholino animals trend slightly higher in all orthologs at day 30 than FLT3-L, and higher than saline conditions in CD1b1 and CD1b4. This heightened expression is a common paradoxical effect in morpholino experiments as the compound blocks protein translation thus leading the cellular feedback system to call for increased mRNA expression in an attempt to compensate. This same theory would explain FLT3-L guinea pig gene expression, that is either congruent or lower than the saline control animals. We may be observing that slight increases in CD1 protein expression, as seen in MFI data, leads to negative feedback on gene expression of CD1 orthologs. Further validating this is the combination treatment group, which has significant upregulation of gene expression compared to all groups in CD1b1 and trends up in the CD1b3 and CD1b4 orthologs. With morpholino inhibiting protein synthesis and FLT3-L increasing overall stimulation for CD1mRNA translation there seems to be an abundance of mRNA transcription, which reflecting on the flow CD1 expression data, leads to partially overcoming of the morpholino effect. Interestingly, under Mtb infection conditions CD1b2 is recalcitrant to exogenous modulation standing in contrast to naïve and invitro studies. Another finding of unknown significance is the upregulation of CD1b3 in the saline guinea pigs compared to others groups. CD1b3 is unique compared to other CD1b orthologs, in that it is almost constitutively expressed on B cells[45,54,134]. Perhaps its expression pattern and presenting cell type led to aberrant changes from FLT3-L and morpholino compounds during infection. Further studies investigating FLT3-L and morpholino effect on B cells is needed to understand the impact they may be having on this key immune cell population.

One of the primary functions of CD1-restricted T cells is lysing cells presenting exogenous lipid antigens[217,222]. This ability was assessed in this study utilizing lung derived inflammatory cells. Most significantly this assay demonstrated morpholino guinea pigs' complete inability to cause cellular lysis of Mtb lipid presenting transfectant fibroblasts regardless of the antigen, ortholog or time point of the study. However, the most unexpected results again came from the FLT3-L and combination conditions. It was initially speculated that FLT3-L animals would have highly sensitive or expanded CD1-restricted T cells populations leading to increased cellular cytotoxic effect. Contrary to this thought, FLT3-L had only minimal increased cytotoxic to our unloaded lipid controls and were lower in efficacy than both saline controls and combination treatment guinea pigs. This indicates that FLT3-L either through direct CD1 or off target effects is inhibiting CD1 glycoprotein functionality possibly by altering CD1 glycoprotein cellular trafficking or the proteins' ability to load, bind or present Mtb lipids. Although FLT3-L is a known stimulator of CD1 it has never been examined how this increased protein expression and broad growth factor effects the ability to CD1 to transverse intracellular endosomes, which is critical for CD1 antigen presentation. Interestingly, the combination group is able to perform better than FLT3-L animals with CD1b1 ortholog fibroblasts and is able to align or perform better than saline control with CD1b3 fibroblasts. It may be no coincidence that the combination treatment group has the highest gene expression in CD1b1 ortholog when examining the RT-PCR. Perhaps the combination group allowed the CD1b1 ortholog to become the dominate ortholog on antigen presenting cells, and that FLT3-L only stimulation led the expression of multiple orthologs lowering the ability of CD1b1 to properly load and present Mtb lipid antigens to cause CD1b1 specific T cell proliferation. The ability of the combination animals to regain normal to enhanced cytotoxic ability to saline animals with CD1b3 fibroblasts may again point to the unique characteristics of CD1b3. The profound negative effect FLT3-L has on gene expression may directly affect overall constitutive expression of CD1b3 and thus dampen overall functionality. The blocking effects of morpholino lowering the protein expression with the

addition of FLT3-L stimulation seems to bring functionality back, thus may be normalizing CD1b3 expression. The fact that combination treatment group regains cytolytic functionality compared to FLT3-L animals helps to rule out some off target effects of FTL3-L like impeding generalized T cells proliferation and activity. Additional studies investigating the effect of FTL3-L on CD1b3 and correlating that to functionality are required to further deconvolute these surprising findings.

This study was designed to assess the effects of exogenous CD1 compounds with a set of animals starting dosing before infection and another set starting dosing after the initial infection, at the point of adaptive immunity. Throughout all of our cellular and genetic data all intra-time point significance was found with animals that started dosing before the infection and terminated 30 days post infection. In fact, it seems the effects of both compounds were relatively diminished in the animals where treatment was started at day 26 post infection and continued to day 60. Previous studies in our lab have shown that CD1 expression and functionality significantly wanes in the chronic adaptive immunity phase of an Mtb infection, day 60 post infection in the guinea pig. This may indicate that these compounds are unable to alter CD1 expression in chronic infections. Alternatively, the formation of a maturing granuloma, and the corresponding fibrosis, may have inhibited overall efficacy of compound delivery to target antigen presenting cells lowering modulatory ability. Lastly, this may indicate the decreased ability of these exogenous compounds to modulate CD1 in a complex adaptive inflammatory environment, like a granuloma, regardless of the ability of reaching target cells. A pitfall of this study was the inability to have sets of guinea pigs where treatment commenced prior and during infection at each termination time point, days 30 and 60. Additional studies are needed to further complete this investigatory work, including adding an innate time point, day 14 post infection, to fully encapsulate the abilities of these compounds and overt effect on TB disease pathogenesis.

Although significant changes in CD1 expression, and effector cell functionality were observed in this study the overall disease status was relatively unchanged in terms of lesion or bacterial burden and ability of the bacteria to spread systemically. This may be explained by the studies focus of the CD1b isoform. Reagents for investigating and monitoring CD1b in the guinea pig are relatively abundant compared that of CD1c or CD1d. It is possible that these other isoforms play a larger role in Mtb pathogenesis than previously thought. Alternatively, CD1b4, CD1c and CD1d expression may have increased to compensate for the protein knockdown of CD1b1-3 via morpholino administration. Even with these possibilities, morpholino compounds did have a partial effect on day 30 CFU counts, trending up in the lung, spleen and liver. We also need to further explore the non-CD1 effects of adding a broad-spectrum growth factor, FLT3-L, has on the overall inflammatory environment. One reason for having a combined treatment group was to assess for non-CD1 FLT3-L effects, not realizing the ability of FLT3-L to overcome CD1 morpholino knockdown and thus confounding our results. Additional investigations are needed including examining overall effects of FLT3-L through broad genetic assessment such as a Nanostring immunologically based panel.

Several studies have investigated how Mtb influences CD1 immunity and if Mtb lipid antigen stimulation can be utilized for prophylactic treatment for TB. However, no study has examined whether CD1 immunity is beneficial to the host or Mtb for lesion formation and bacterial burden. This study aimed to answer that question by modulating CD1 glycoprotein expression at the cellular level and directly correlating that modulation back to Mtb disease status. Although this study noted few changes to disease progression in any treatment group, we show the ability to effect CD1 glycoprotein expression and CD1-restricted effector functionality. We also discovered unexpected variables and findings that potentially confounded our ability to draw direct correlations of our experimental changes to disease progression. Further refinement of this model and expansion of time point assessments are needed to further

compare CD1 immune status to TB disease burden. However, this study provides the first tools to actively skew CD1 immunity *in vivo*, which lays the foundation for insightful work with CD1 immunity in relation to TB and a host of disease processes, including eventually harnessing CD1 immunity to change disease pathogeneses and prognoses via antigen lipid vaccination schemes.

FUTURE DIRECTIONS

Throughout all aims, this dissertation laid the investigatory groundwork for examining a relatively novel comorbidity, vitamin A deficiency, and a niche branch of immunology, CD1 lipid-based immunity; However, much work remains to be done in these arenas of Mtb research. By continuing the work of this dissertation, it is this Author's hope that we can transform vitamin A from a comorbidity to a useful a useful tool in Mtb treatment regimens and utilize the unique properties of CD1 glycoproteins for an efficacious prophylactic Mtb vaccination scheme.

In Aim 1, we created a translatable vitamin A deficient animal model and examined the effect that deficiency had on the pathogenesis of Mtb infections; however, many questions remain to be investigated. One intriguing, and unexpected finding coming from this aim was the loss of serum retinol and serum retinol binding protein 4 (RPB4) in vitamin A sufficient guinea pigs during a Mtb infection. Several studies have demonstrated a similar decline of serum retinol in human during acute infections due to negative acute proteins effecting on RPB4; however, Additional work is needed in the guinea pig model to further assess this process[223,224]. To fully assess whether retinol is sequestered in the liver or is actively being utilized at the point infection, the lung, heavy isotope tracing could be performed. Heavy isotope tracing works by labelling retinol with either a stable heavy or radioactive isotope. This methodology has been frequently been utilized to assess vitamin A status in human by comparing the ratio of heavy isotopes, tracer, compared to unlabeled vitamin A, tracee[225,226]. Additional mathematical equations can be utilized to compartmentalize heavy isotope vitamin A into visceral organs[226,227]. These methodologies could be utilized to understand where and how vitamin A is stored and transported in the face of a Mtb infection.

An additional intriguing finding was the collapse of normal CD4:CD8 T cell ratios and the dysregulated immune gene profile. To further investigate these findings further ex-vivo studies could be performed to evaluate possible T cell dysfunction. Assays include T cell activation assays, such as an Elispot IFN-y assay or cytotoxicity assay, or a cellular proliferation assay. Lastly, further investigation of T cell helper population shifts and macrophage subtyping could provide key insights into the degree of tuberculosis disease progression and atypical lesion morphology in vitamin A deficient guinea pigs.

In aim 2, we established the kinetic expression of CD1b glycoproteins at a tissue level in a guinea pig model in the face of a Mtb infection. Although this study comprehensively details CD1b expression additional work is needed to assess CD1c, another essential group 1 CD1 glycoprotein. This work would require additional reagent validation including development of more diverse CD1c monoclonal antibodies. This aim went further by correlating CD1 glycoprotein expression to functionality of CD1-restricted T cells. However, due to cell number restrictions only 2 of the 4 orthologs of CD1b, CD1b1 and CD1b3, transfectant fibroblasts were utilized. To complete this work this author would like run this functional assay utilizing CD1b2 and CD1b4 as well as CD1c orthologs.

The linchpin of CD1 immunology relies on CD1-restricted T cells; however, relatively little is known about this unique cellular population compared to CD1 glycoproteins. Human based studies have progressed this T cell research with antigen specific CD1 glycoprotein tetramers to attach to CD1-restricted T cells for further evaluation and cell sorting. Similar tetramers have been made for the guinea pig CD1 repertoire via the NIH tetramer core. The author of this dissertation attempted to utilize these tetramers to isolate CD1-restricted T cells, but was unsuccessful developing consistent results. Further work and validation of these essential tools is needed to investigate tissue derived CD1-restricted T cells.

In aim 3, We applied the knowledge gained from aim 2 to assess how modulating CD1 glycoprotein expression effects Mtb disease progression in a guinea pig model. This aim established the ability to modulate CD1 proteins in-vivo but failed to correlate this modulation to a change in disease progression. One large question stemming from this initial study centered around the ability of CD1b4, CD1cs or CD1d to compensate for the down regulation of CD1b1-3. To answer this question and potential pitfall additional morpholinos need be synthesized to block all CD1 glycoproteins. For this to occur proper gene annotation of all CD1c and CD1d guinea pig orthologs is needed.

Another limitation of the study was the study design itself. Due to financial limitation, dosing groups were limited to one group getting treatments from the start of infection to day 30 post infection and other dosing group getting treatment at day 30 which continued to day 60 post infection. In future studies I would have three dosing groups that all start before the infection time point and then are terminated at 14-, 30- and 60-days post infection. This continuation in dosing would allow for a more thorough comparison of how consistent CD1 modulation effects disease outcomes during innate immunity, day 14 post infection, early adaptative immunity, day 30 post infection, and late adaptative immunity, day 60 post infection.

The future directions laid out here are just a small subset of possible directions this initial work could go in. The overarching goal of this dissertation, for this author, was to investigate novel aspects of Mtb immunology as the Mtb community faces a host of future challenges such as a lack of funding, recently increasing infection rates, and increasing incidence of multidrug resistant bacteria. It is the author's hope that this work lays the foundation for future and groundbreaking studies that have broad and translation impact for humans with Mtb infections and clinical tuberculosis.

CONCLUSION

As discussed throughout this work, *Mycobacterium tuberculosis*, the causative agent of tuberculosis, is one of the leading causes of death for infectious diseases worldwide causing 1.7 billion people as of 2018 and killing 1.6 million people in 2021[1,2]. Unfortunately, like many other infectious diseases there are a multitude of challenges facing this disease including the rise of comorbidities, such as diabetes, the rise of multidrug resistant strains of Mtb, and the collapse of normal surveillance and treatment apparatuses due to the Sars-cov-2 global pandemic. Further compounding these issues are antiqued vaccines regimens and a lack of new effective anti-microbials. With these pressing challenges there is a drive within the Mtb research community to think outside the box to identify and mitigate TB comorbidities, develop innovate prophylactic treatments, and to investigate niche host immunity to decrease pervalence of clinically active disease. This dissertation aimed to aid in this overarching effort by laying the initial ground for understanding the pathophysiology of vitamin A deficiency in relation to Mtb infections, a newly discovered comorbidity, and investigating the unique branch of lipid-based host immunity in relation to lipophilic *Mycobacterium tuberculosis*.

In aim one, this dissertation examined vitamin A deficiency in a Mtb guinea pig model. This vitamin A deficient guinea pig model, the first of its kind, allowed assessment of how vitamin A deficiency effects disease progression in terms of lesion formation, bacterial burden and altered gene profiles. Through this innovate model this dissertation was able to establish a marked shift in granuloma morphology, a collapse of normal lymphocytic and myeloid populations and demonstrate dysregulated inflammatory gene profiles. Colectively, this data demonstrated a clear alteration in disease pathogenesis from deficient, and sufficient animals. Additionally, this dissertation illustrated the ability to reserve detrimental effects of vitamin A deficiency through the reestablishment of a sufficient diet during the course of an active infection. There are still more investigations to be done to further elicit the ultimate pathogenesis

of this comorbidity; however, this work set the foundation for looking at vitamin A utilizing this innovative model, particularly examining if vitamin A supplementation could aid in enhancing existing vaccination and antibiotic regimens.

Aim two of this dissertation examined a relatively new branch of immunology based on lipid presentation via CD1 glycoproteins. Several previous investigatory studies have been performed to examine the role of CD1 lipid-based immunology has in relation to Mtb infections; however, studies have thus far had limited ability to assess this branch of immunology within infected tissues. Again, utilizing the guinea pig, this dissertation established the kinetic expression of CD1 within the lung and spleen through the course of an infection. This work then correlated that expression back to lytic functionality of CD1-restricted T cells. This work established that CD1 kinetic expression is ortholog specific with maximal expression and lytic functionality observed during the early adaptive immunity. Overall, this work is the first study to show CD1 glycoprotein expression throughout an Mtb infection, and could be instrumental for future studies looking to harness this branch of immunology to mitigate TB disease status.

Aim three of this dissertation built upon aim two to assess how CD1 immunity effects Mtb infections and TB disease progression. This aim was completed utilizing a pleotropic growth factor, FLT3-L, for upregulation of CD1b glycoproteins and anti-sense synthetic RNA, morpholino, for downregulation of CD1b glycoproteins. This first of its kind modulating experiment demonstrated the efficacy of these compounds to effect CD1 expression in-vivo in the face of Mtb infection. This shift in CD1 glycoprotein expression directly correlated back to the cytotoxic functionality of CD1-restricted T cells. However, the modulation of these CD1b glycoproteins failed to significantly alter disease progression in terms of lesion morphology, lesion burden or bacterial burden. This lack of disease shift may be due to the only partial ability to knockdown CD1b protein expression and current inability to inhibit CD1c and CD1d

orthologs. This study establishes the ability to alter CD1 expression *in vivo* allowing for additional investigations of CD1 immunity in relation to Mtb infection pathogenesis.

Cumulatively, the aims of this dissertation built the foundation for investigating two unique, and relative unknown, aspects of TB pathogenesis and host immunology. The findings within chapter 1 have launched a host of different investigations examining the ability of this essential micronutrient to not only prevent clinical TB but to also serve as an immunologic boost to enhance the efficacy of a variety of Mtb treatment regimens. Chapters 2 and 3 reexamined CD1 immunity and the utility of the guinea pig for lipid immunologic work. Though much work has yet to be done in this niche branch of immunology, these chapters lay the ground work and provide the new tools for future studies into potential efficacious and translatable lipid-based vaccination schemes. Tuberculosis, caused by *Mycobacterium tuberculosis*, is a disease with global ramifications that requires innovative research to meet the new challenges on the horizon. This dissertation looked to meet those challenges by contributing new knowledge to two developing fields of immunologic research while also laying out the tools for future groundbreaking work.

REFERENCES

1. Global Health - Newsroom - Tuberculosis. https://www.cdc.gov/globalhealth/newsroom/topics/tb/index.html.

2. World Health Organization. Annual Report of Tuberculosis. *Annu. Glob. TB Rep. WHO* 1–68 (2022).

3. Tuberculosis deaths and disease increase during the COVID-19 pandemic. https://www.who.int/news/item/27-10-2022-tuberculosis-deaths-and-disease-increase-during-the-covid-19-pandemic.

4. Ragonnet, R., Trauer, J. M., Denholm, J. T., Marais, B. J. & McBryde, E. S. High rates of multidrug-resistant and rifampicin-resistant tuberculosis among re-treatment cases: Where do they come from? *BMC Infect. Dis.* **17**, 1–10 (2017).

5. Pawlowski, A., Jansson, M., Sköld, M., Rottenberg, M. E. & Källenius, G. Tuberculosis and HIV Co-Infection. *PLOS Pathog.* **8**, e1002464 (2012).

6. Aibana, O. *et al.* Clinical Infectious Diseases Impact of Vitamin A and Carotenoids on the Risk of Tuberculosis Progression. doi:10.1093/cid/cix476.

7. Stevens, G. A. *et al.* Trends and mortality effects of vitamin A deficiency in children in 138 low-income and middle-income countries between 1991 and 2013: a pooled analysis of population-based surveys. *Lancet Glob. Heal.* **3**, e528–e536 (2015).

8. Reboul, E. Absorption of Vitamin A and Carotenoids by the Enterocyte: Focus on Transport Proteins. *Nutr. 2013, Vol. 5, Pages 3563-3581* **5**, 3563–3581 (2013).

9. Haaker, M. W., Vaandrager, A. B. & Helms, J. B. Retinoids in health and disease: A role for hepatic stellate cells in affecting retinoid levels. *Biochim. Biophys. Acta - Mol. Cell Biol. Lipids* **1865**, 158674 (2020).

10. Christou, G. A., Tselepis, A. D. & Kiortsis, D. N. The metabolic role of retinol binding protein 4: An update. *Horm. Metab. Res.* **44**, 6–14 (2012).

11. Blomhoff, R. & Blomhoff, H. K. Overview of retinoid metabolism and function. *J. Neurobiol.* **66**, 606–630 (2006).

12. Roszer, T., Menéndez-Gutiérrez, M. P., Cedenilla, M. & Ricote, M. Retinoid X receptors in macrophage biology. *Trends Endocrinol. Metab.* **24**, 460–468 (2013).

13. Huang, Z., Liu, Y., Qi, G., Brand, D. & Zheng, S. G. Role of Vitamin A in the Immune System. *J. Clin. Med. 2018, Vol. 7, Page 258* **7**, 258 (2018).

14. Kang, B. Y. *et al.* Retinoid-mediated inhibition of interleukin-12 production in mouse macrophages suppresses Th1 cytokine profile in CD4+ T cells. *Br. J. Pharmacol.* **130**, 581–586 (2000).

15. Ross, A. C. Vitamin A and retinoic acid in T cell–related immunity. *Am. J. Clin. Nutr.* **96**, 1166S-1172S (2012).

16. Hall, J. A. *et al.* Essential Role for Retinoic Acid in the Promotion of CD4+ T Cell Effector Responses via Retinoic Acid Receptor Alpha. *Immunity* **34**, 435–447 (2011).

17. Lo, H. M., Wang, S. W., Chen, C. L., Wu, P. H. & Wu, W. Bin. Effects of all-trans retinoic acid, retinol, and β-carotene on murine macrophage activity. *Food Funct.* **5**, 140–148 (2013).

18. Geissmann, F. *et al.* Retinoids Regulate Survival and Antigen Presentation by Immature Dendritic Cells. *J. Exp. Med.* **198**, 623–634 (2003).

19. Wang, W., Nakashima, K. ichi, Hirai, T. & Inoue, M. Anti-inflammatory effects of naturally occurring retinoid X receptor agonists isolated from Sophora tonkinensis Gagnep. via retinoid X receptor/liver X receptor heterodimers. *J. Nat. Med.* **73**, 419–430 (2019).

20. Moraes-Vieira, P. M. *et al.* Retinol binding protein 4 primes the NLRP3 inflammasome by signaling through Toll-like receptors 2 and 4. *Proc. Natl. Acad. Sci. U. S. A.* **117**, 31309–31318 (2020).

21. Sozzani, S. Dendritic cell trafficking: More than just chemokines. *Cytokine Growth Factor Rev.* **16**, 581–592 (2005).

22. Podell, B. K. *et al.* The Impact of Vitamin A Deficiency on Tuberculosis Progression. *Clin. Infect. Dis.* (2022) doi:10.1093/CID/CIAC326.

23. Rosales, F. J., Ritter, S. J., Zolfaghari, R., Smith, J. E. & Catharine Ross, A. Effects of acute inflammation on plasma retinol, retinol-binding protein, and its mRNA in the liver and kidneys of vitamin A-sufficient rats. *J. Lipid Res.* **37**, 962–971 (1996).

24. Anand, P., Kaul, D., Immunology, M. S.-J. of M. & 2008, undefined. Synergistic action of vitamin D and retinoic acid restricts invasion of macrophages by pathogenic mycobacteria. *academia.edu*.

25. Mourik, B. C. *et al.* Immunotherapy added to antibiotic treatment reduces relapse of disease in a mouse model of tuberculosis. *atsjournals.org* **56**, 233–241 (2017).

26. Ali, W., Ahmad, I., Srivastava, V., … R. P.-J. of natural & 2014, undefined. Serum zinc levels and its association with vitamin A levels among tuberculosis patients. *ncbi.nlm.nih.gov*.

27. Beckman, E. M. *et al.* Recognition of a lipid antigen by GDI-restricted αβ+ T cells. *Nature* (1994) doi:10.1038/372691a0.

28. Zeng, Z. H. *et al.* Crystal structure of mouse CD1: An MHC-like fold with a large hydrophobic binding groove. *Science (80-.).* **277**, 339–345 (1997).

29. Blumberg, R. S., Gerdes, D., Chott, A., Porcelli, S. A. & Balk, S. P. Structure and function of the CD1 family of MHC-like cell surface proteins. *Immunol. Rev.* **147**, 5–29 (1995).

30. The CD1 system: Antigen-presenting molecules for T cell recognition of lipids and clycolipids - ProQuest. https://www.proquest.com/openview/ab5acf80bc29b404469c3f0d18b5dad3/1?pq-origsite=gscholar&cbl=47332.

31. Van Rhijn, I. *et al.* A conserved human T cell population targets mycobacterial antigens presented by CD1b. *Nat. Immunol.* (2013) doi:10.1038/ni.2630.

32. Brossay, L. & Kronenberg, M. Highly conserved antigen-presenting function of CD1d molecules. *Immunogenetics* vol. 50 146–151 (1999).

33. Dascher, C. C. *et al.* Conservation of CD1 Intracellular Trafficking Patterns Between Mammalian Species. *J. Immunol.* (2002) doi:10.4049/jimmunol.169.12.6951.

34. Godfrey, D. I., Uldrich, A. P., Mccluskey, J., Rossjohn, J. & Moody, D. B. The burgeoning family of unconventional T cells. *Nature Immunology* vol. 16 1114–1123 (2015).

35. Pereira, C. S. & Macedo, M. F. CD1-restricted T cells at the crossroad of innate and adaptive immunity. *Journal of Immunology Research* (2016) doi:10.1155/2016/2876275.

36. Barral, D. C. & Brenner, M. B. CD1 antigen presentation: how it works. *Nat. Rev. Immunol. 2007 712* **7**, 929–941 (2007).

37. Martin, L. H., Calabi, F., Lefebvre, F. A., Bilsland, C. A. & Milstein, C. Structure and expression of the human thymocyte antigens CD1a, CD1b, and CD1c. *Proc. Natl. Acad. Sci.* **84**, 9189–9193 (1987).

38. Wollenberg, A., Kraft, S., Hanau, D. & Bieber, T. Immunomorphological and Ultrastructural Characterization of Langerhans Cells and a Novel, Inflammatory Dendritic Epidermal Cell (IDEC) Population in Lesional Skin of Atopic Eczema. *J. Invest. Dermatol.* **106**, 446–453 (1996).

39. Olivier, M., Foret, B., Le Vern, Y., Kerboeuf, D. & Guilloteau, L. A. Plasticity of Migrating CD1b+ and CD1b- Lymph Dendritic Cells in the Promotion of Th1, Th2 and Th17 in Response to Salmonella and Helminth Secretions. *PLoS One* **8**, e79537 (2013).

40. Sugita, M., Van Der Wel, N., Rogers, R. A., Peters, P. J. & Brenner, M. B. CD1c molecules broadly survey the endocytic system. *Proc. Natl. Acad. Sci.* **97**, 8445–8450 (2000).

41. Wu, D. *et al.* Bacterial glycolipids and analogs as antigens for CD1d-restricted NKT cells. *Proc. Natl. Acad. Sci. U. S. A.* **102**, 1351–1356 (2005).

42. Rothchild, A. C., Jayaraman, P., Nunes-Alves, C. & Behar, S. M. iNKT Cell Production of GM-CSF Controls Mycobacterium tuberculosis. *PLOS Pathog.* **10**, e1003805 (2014).

43. Sköld, M. & Behar, S. M. The role of group 1 and group 2 CD1-restricted T cells in microbial immunity. *Microbes Infect.* **7**, 544–551 (2005).

44. Dascher, C. C. & Brenner, M. B. Evolutionary constraints on CD1 structure: insights from comparative genomic analysis. *Trends Immunol.* **24**, 412–418 (2003).

45. Reinink, P. & Van Rhijn, I. Mammalian CD1 and MR1 genes. *Immunogenetics* **68**, 515–523 (2016).

46. Dutronc, Y. & Porcelli, S. A. The CD1 family and T cell recognition of lipid antigens. *Tissue Antigens* **60**, 337–353 (2002).

47. Moody, D. B., Zajonc, D. M. & Wilson, I. A. Anatomy of CD1–lipid antigen complexes. *Nat. Rev. Immunol. 2005 55* **5**, 387–399 (2005).

48. Moody, D. B. The Surprising Diversity of Lipid Antigens for CD1-Restricted T Cells. *Adv. Immunol.* **89**, 87–139 (2006).

49. Lawton, A. P. & Kronenberg, M. The Third Way: Progress on pathways of antigen processing and presentation by CD1. *Immunol. Cell Biol.* **82**, 295–306 (2004).

50. Sugita, M. *et al.* Separate Pathways for Antigen Presentation by CD1 Molecules. *Immunity* **11**, 743–752 (1999).

51. Zhou, D. *et al.* Editing of CD1d-Bound Lipid Antigens by Endosomal Lipid Transfer Proteins. *Science (80-.).* **303**, 523–527 (2004).

52. Sugita, M., Cernadas, M. & Brenner, M. B. New insights into pathways for CD1-mediated antigen presentation. *Curr. Opin. Immunol.* **16**, 90–95 (2004).

53. Moody, D. B. & Porcelli, S. A. CD1 Trafficking: Invariant Chain Gives a New Twist to the Tale. *Immunity* **15**, 861–865 (2001).

54. Dascher, C. C. *et al.* Conservation of a CD1 Multigene Family in the Guinea Pig. *J. Immunol.* **163**, 5478–5488 (1999).

55. Hiromatsu, K. *et al.* Characterization of guinea-pig group 1 CD1 proteins. *Immunology* **106**, 159–172 (2002).

56. Gumperz, J. E. The Ins and Outs of CD1 Molecules: Bringing Lipids Under Immunological Surveillance. *Traffic* **7**, 2–13 (2006).

57. Moody, D. B. & Porcelli, S. A. Intracellular pathways of CD1 antigen presentation. *Nat. Rev. Immunol. 2003 31* **3**, 11–22 (2003).

58. Le Nours, J., Shahine, A. & Gras, S. Molecular features of lipid-based antigen presentation by group 1 CD1 molecules. *Semin. Cell Dev. Biol.* **84**, 48–57 (2018).

59. Gadola, S. D. *et al.* Structure of human CD1b with bound ligands at 2.3 Å, a maze for alkyl chains. *Nat. Immunol. 2002 38* **3**, 721–726 (2002).

60. Batuwangala, T. *et al.* The Crystal Structure of Human CD1b with a Bound Bacterial Glycolipid. *J. Immunol.* **172**, 2382–2388 (2004).

61. Shahine, A. The intricacies of self-lipid antigen presentation by CD1b. *Mol. Immunol.* **104**, 27–36 (2018).

62. Van Rhijn, I., Ly, D. & Moody, D. B. CD1a, CD1b, and CD1c in immunity against mycobacteria. *Adv. Exp. Med. Biol.* **783**, 181–197 (2013).

63. Scharf, L. *et al.* The 2.5 Å Structure of CD1c in Complex with a Mycobacterial Lipid Reveals an Open Groove Ideally Suited for Diverse Antigen Presentation. *Immunity* **33**, 853–862 (2010).

64. de Jong, A. *et al.* CD1c Presentation of Synthetic Glycolipid Antigens with Foreign Alkyl Branching Motifs. *Chem. Biol.* **14**, 1232–1242 (2007).

65. Koch, M. *et al.* The crystal structure of human CD1d with and without α-galactosylceramide. *Nat. Immunol. 2005 68* **6**, 819–826 (2005).

66. Wang, J. *et al.* Lipid binding orientation within CD1d affects recognition of Borrelia burgorferi antigens by NKT cells. *Proc. Natl. Acad. Sci. U. S. A.* **107**, (2010).

67. Looringh van Beeck, F. A. *et al.* Functional CD1d and/or NKT cell invariant chain transcript in horse, pig, African elephant and guinea pig, but not in ruminants. *Mol. Immunol.* **46**, 1424–1431 (2009).

68. Zeissig, S. *et al.* Primary deficiency of microsomal triglyceride transfer protein in human abetalipoproteinemia is associated with loss of CD1 function. *J. Clin. Invest.* **120**, (2010).

69. Dougan, S. K. *et al.* Microsomal triglyceride transfer protein lipidation and control of CD1d on antigen-presenting cells. *J. Exp. Med.* **202**, (2005).

70. Sugita, M., Barral, D. C. & Brenner, M. B. Pathways of CD1 and lipid antigen delivery, trafficking, processing, loading, and presentation. *Curr. Top. Microbiol. Immunol.* **314**, 143–164 (2007).

71. Dascher, C. C. *et al.* Conservation of CD1 Intracellular Trafficking Patterns Between Mammalian Species. *J. Immunol.* **169**, 6951–6958 (2002).

72. Melián, A., Beckman, E. M., Porcelli, S. A. & Brenner, M. B. Antigen presentation by CD1 and MHC-encoded class I-like molecules. *Curr. Opin. Immunol.* **8**, 82–88 (1996).

73. De Libero, G. & Mori, L. How the immune system detects lipid antigens. *Prog. Lipid Res.* **49**, 120–127 (2010).

74. Moody, D. B. *et al.* Lipid length controls antigen entry into endosomal and nonendosomal pathways for CD1b presentation. *Nat. Immunol. 2002 35* **3**, 435–442 (2002).

75. Moody, D. B. & Cotton, R. N. Four pathways of CD1 antigen presentation to T cells. *Curr. Opin. Immunol.* **46**, 127–133 (2017).

76. Ly, D. & Moody, D. B. The CD1 size problem: Lipid antigens, ligands, and scaffolds. *Cell. Mol. Life Sci.* **71**, 3069–3079 (2014).

77. Sugita, M., Peters, P. J. & Brenner, M. B. Pathways for Lipid Antigen Presentation by CD1 Molecules: Nowhere for Intracellular Pathogens to Hide. *Traffic* **1**, 295–300 (2000).

78. Briken, V., Moody, D. B. & Porcelli, S. A. Diversification of CD1 proteins: sampling the lipid content of different cellular compartments. *Semin. Immunol.* **12**, 517–525 (2000).

79. Relloso, M. *et al.* pH-Dependent Interdomain Tethers of CD1b Regulate Its Antigen Capture. *Immunity* **28**, 774–786 (2008).

80. Teyton, L. Role of lipid transfer proteins in loading CD1 antigen-presenting molecules. *J. Lipid Res.* **59**, 1367–1373 (2018).

81. Van der Wel, N. N. *et al.* CD1 and major histocompatibility complex II molecules follow a different course during dendritic cell maturation. *Mol. Biol. Cell* **14**, 3378–3388 (2003).

82. Cao, X. *et al.* CD1 Molecules Efficiently Present Antigen in Immature Dendritic Cells and Traffic Independently of MHC Class II During Dendritic Cell Maturation. *J. Immunol.* **169**, 4770–4777 (2002).

83. Peña-Cruz, V., Ito, S., Dascher, C. C., Brenner, M. B. & Sugita, M. Epidermal Langerhans Cells Efficiently Mediate CD1a-Dependent Presentation of Microbial Lipid Antigens to T Cells. *J. Invest. Dermatol.* **121**, 517–521 (2003).

84. Van Kaer, L., Wu, L. & Joyce, S. Mechanisms and Consequences of Antigen Presentation by CD1. *Trends Immunol.* **37**, 738–754 (2016).

85. Zajonc, D. M., Elsliger, M. A., Teyton, L. & Wilson, I. A. Crystal structure of CD1a in complex with a sulfatide self antigen at a resolution of 2.15 Å. *Nat. Immunol.* **4**, (2003).

86. Cipriani, B. *et al.* Upregulation of Group 1 CD1 Antigen Presenting Molecules in Guinea Pigs with Experimental Autoimmune Encephalomyelitis: An Immunohistochemical Study. *Brain Pathol.* **13**,

1–9 (2003).

87. Adams, E. J. Diverse antigen presentation by the Group 1 CD1 molecule, CD1c. *Mol. Immunol.* **55**, 182–185 (2013).

88. Briken, V., Jackman, R. M., Watts, G. F. M., Rogers, R. A. & Porcelli, S. A. Human Cd1b and Cd1c Isoforms Survey Different Intracellular Compartments for the Presentation of Microbial Lipid Antigens. *J. Exp. Med.* **192**, 281–288 (2000).

89. Sugita, M. *et al.* Failure of Trafficking and Antigen Presentation by CD1 in AP-3-Deficient Cells. *Immunity* **16**, 697–706 (2002).

90. Speak, A. O., Cerundolo, V. & Platt, F. M. CD1d presentation of glycolipids. *Immunol. Cell Biol.* **86**, 588–597 (2008).

91. Shin, J. H. & Park, S. H. The effect of intracellular trafficking of CD1d on the formation of TCR repertoire of NKT cells. *BMB Rep.* **47**, 241 (2014).

92. Lawton, A. P. *et al.* The Mouse CD1d Cytoplasmic Tail Mediates CD1d Trafficking and Antigen Presentation by Adaptor Protein 3-Dependent and -Independent Mechanisms. *J. Immunol.* **174**, 3179–3186 (2005).

93. Angénieux, C. *et al.* Characterization of CD1e, a third type of CD1 molecule expressed in dendritic cells. *J. Biol. Chem.* **275**, 37757–37764 (2000).

94. Angénieux, C. *et al.* The Cellular Pathway of CD1e in Immature and Maturing Dendritic Cells. *Traffic* **6**, 286–302 (2005).

95. Garcia-Alles, L. F. *et al.* Crystal structure of human CD1e reveals a groove suited for lipid-exchange processes. *Proc. Natl. Acad. Sci. U. S. A.* **108**, 13230–13235 (2011).

96. Facciotti, F. *et al.* Fine tuning by human CD1e of lipid-specific immune responses. *Proc. Natl. Acad. Sci. U. S. A.* **108**, 14228–14233 (2011).

97. Moody, D. B. *et al.* Structural requirements for glycolipid antigen recognition by CD1b- restricted T cells. *Science (80-.).* **278**, 283–286 (1997).

98. Moody, D. B. & Cotton, R. N. Four pathways of CD1 antigen presentation to T cells. *Current Opinion in Immunology* vol. 46 127–133 (2017).

99. Kawano, T. *et al.* CD1d-restricted and TCR-mediated activation of V(α)14 NKT cells by glycosylceramides. *Science (80-.).* **278**, 1626–1629 (1997).

100. De Jong, A. *et al.* CD1a-autoreactive T cells recognize natural skin oils that function as headless antigens. *Nat. Immunol. 2013 152* **15**, 177–185 (2013).

101. Birkinshaw, R. W. *et al.* αβ T cell antigen receptor recognition of CD1a presenting self lipid ligands. *Nat. Immunol. 2015 163* **16**, 258–266 (2015).

102. Mansour, S. *et al.* Cholesteryl esters stabilize human CD1c conformations. *Proc. Natl. Acad. Sci. U. S. A.* **113**, E1266–E1275 (2016).

103. Ly, D. *et al.* CD1c tetramers detect ex vivo T cell responses to processed phosphomycoketide antigens. *J. Exp. Med.* **210**, 729–741 (2013).

104. Roy, S. *et al.* Molecular Analysis of Lipid-Reactive Vδ1 γδ T Cells Identified by CD1c Tetramers. *J. Immunol.* **196**, 1933–1942 (2016).

105. Porcelli, S. *et al.* Recognition of cluster of differentiation 1 antigens by human CD4-CD8- cytolytic T lymphocyte. *Nature* **341**, 447–450 (1989).

106. Siddiqui, S., Visvabharathy, L. & Wang, C. R. Role of group 1 CD1-restricted T cells in infectious disease. *Frontiers in Immunology* (2015) doi:10.3389/fimmu.2015.00337.

107. Behar, S. M. & Porcelli, S. A. CD1-restricted T cells in host defense to infectious diseases. *Current Topics in Microbiology and Immunology* vol. 314 (2007).

108. Kasmar, A. G. *et al.* Cutting Edge: CD1a Tetramers and Dextramers Identify Human Lipopeptide–Specific T Cells Ex Vivo. *J. Immunol.* (2013) doi:10.4049/jimmunol.1301660.

109. Kasmar, A. G. *et al.* CD1b tetramers bind αβ T cell receptors to identify a mycobacterial glycolipid-reactive T cell repertoire in humans. *J. Exp. Med.* **208**, 1741–1747 (2011).

110. Adams, E. J. Lipid presentation by human CD1 molecules and the diverse T cell populations that respond to them. *Current Opinion in Immunology* vol. 26 (2014).

111. De Lalla, C. *et al.* High-frequency and adaptive-like dynamics of human CD1 self-reactive T cells. *Eur. J. Immunol.* **41**, (2011).

112. Pigozzi, B., Bordignon, M., Fortina, A. B., Michelotto, G. & Alaibac, M. Expression of the CD1a molecule in B- and T-lymphoproliferative skin conditions. *Oncol. Rep.* **15**, (2006).

113. Colonna, M. Skin function for human CD1a-reactive T cells. *Nature Immunology* vol. 11 (2010).

114. Chancellor, A. *et al.* CD1b-restricted GEM T cell responses are modulated by Mycobacterium tuberculosis mycolic acid meromycolate chains. *Proc. Natl. Acad. Sci. U. S. A.* **114**, E10956–E10964 (2017).

115. Rascle, A. *et al.* A 'GEM' of a cell. *Nat. Immunol. 2013 147* **14**, 694–695 (2013).

116. Hiromatsu, K. *et al.* Induction of CD1-Restricted Immune Responses in Guinea Pigs by Immunization with Mycobacterial Lipid Antigens. *J. Immunol.* (2002) doi:10.4049/jimmunol.169.1.330.

117. Cohen, N. R., Garg, S. & Brenner, M. B. Chapter 1 Antigen Presentation by CD1. Lipids, T Cells, and NKT Cells in Microbial Immunity. *Advances in Immunology* (2009) doi:10.1016/S0065-2776(09)01201-2.

118. Bienemann, K. *et al.* iNKT cell frequency in peripheral blood of caucasian children and adolescent: The absolute iNKT cell count is stable from birth to adulthood. *Scand. J. Immunol.* **74**, (2011).

119. Yu, K. K. Q. *et al.* Conservation of molecular and cellular phenotypes of invariant NKT cells between humans and non-human primates. *Immunogenetics* **71**, (2019).

120. Chandra, S. & Kronenberg, M. Activation and Function of iNKT and MAIT Cells. *Adv. Immunol.* **127**, 145–201 (2015).

121. Matsuda, J. L., Mallevaey, T., Scott-Browne, J. & Gapin, L. CD1d-restricted iNKT cells, the 'Swiss-Army knife' of the immune system. *Curr. Opin. Immunol.* **20**, 358–368 (2008).

122. Macho-Fernandez, E. & Brigl, M. The extended family of CD1d-restricted NKT cells: Sifting through a mixed bag of TCRs, antigens, and functions. *Frontiers in Immunology* vol. 6 (2015).

123. Josepha DeLay1. Postmortem findings in Ontario racehorses, 2003–2015. *J. Vet. Diagnostic Investig.* **29**, 457–464 (2017).

124. Felio, K. *et al.* CD1-restricted adaptive immune responses to Mycobacteria in human group 1 CD1 transgenic mice. *J. Exp. Med.* **206**, 2497–2509 (2009).

125. Ulrichs, T., Branch Moody, D., Grant, E., Kaufmann, S. H. E. & Porcelli, S. A. T-Cell Responses to CD1-Presented Lipid Antigens in Humans with Mycobacterium tuberculosis Infection Downloaded from. *Infect. Immun.* **71**, 3076–3087 (2003).

126. Van Rhijn, I. & Moody, D. B. CD1 and mycobacterial lipids activate human T cells. *Immunol. Rev.* **264**, 138–153 (2015).

127. Schaible, U. E. & Kaufmann, S. H. E. CD1 and CD1-restricted T cells in infections with intracellular bacteria. *Trends in Microbiology* vol. 8 (2000).

128. Gagliardi, M. C. *et al.* Cell wall-associated alpha-glucan is instrumental for Mycobacterium tuberculosis to block CD1 molecule expression and disable the function of dendritic cell derived from infected monocyte. *Cell. Microbiol.* (2007) doi:10.1111/j.1462-5822.2007.00940.x.

129. Stenger, S., Niazi, K. R. & Modlin, R. L. Down-regulation of CD1 on antigen-presenting cells by infection with Mycobacterium tuberculosis. *J. Immunol.* **161**, (1998).

130. Gagliardi, M. C. *et al.* Mycobacteria exploit p38 signaling to affect CD1 expression and lipid antigen presentation by human dendritic cells. *Infect. Immun.* (2009) doi:10.1128/IAI.00607-09.

131. Layre, E. *et al.* Mycolic Acids Constitute a Scaffold for Mycobacterial Lipid Antigens Stimulating CD1-Restricted T Cells. *Chem. Biol.* **16**, 82–92 (2009).

132. Gilleron, M. *et al.* Diacylated Sulfoglycolipids Are Novel Mycobacterial Antigens Stimulating CD1-restricted T Cells during Infection with Mycobacterium tuberculosis. *J. Exp. Med.* **199**, (2004).

133. Ulrichs, T., Moody, D. B., Grant, E., Kaufmann, S. H. E. & Porcelli, S. A. T-cell responses to CD1-presented lipid antigens in humans with Mycobacterium tuberculosis infection. *Infect. Immun.* (2003) doi:10.1128/IAI.71.6.3076-3087.2003.

134. Hiromatsu, K. *et al.* Characterization of guinea-pig group 1 CD1 proteins. *Immunology* (2002) doi:10.1046/j.1365-2567.2002.01422.x.

135. Dascher, C. C. *et al.* Immunization with a mycobacterial lipid vaccine improves pulmonary pathology in the guinea pig model of tuberculosis. *International Immunology* (2003) doi:10.1093/intimm/dxg091.

136. Tuberculosis remains one of the deadliest infectious diseases worldwide, warns new report. https://www.ecdc.europa.eu/en/news-events/tuberculosis-remains-one-deadliest-infectious-diseases-worldwide-warns-new-report.

137. Huang, Z., Liu, Y., Qi, G., Brand, D. & Zheng, S. G. Role of Vitamin A in the Immune System. *J. Clin. Med.* **7**, (2018).

138. Smith, S. M., Levy, N. S. & Hayes, C. E. Impaired Immunity in Vitamin A-Deficient Mice. *J. Nutr.*

117, 857–865 (1987).

139. Darnton-Hill, I. Public Health Aspects in the Prevention and Control of Vitamin Deficiencies. *Curr. Dev. Nutr.* **3**, (2019).

140. World Health Organization. Global prevalence of vitamin A deficiency in populations at risk 1995-2005 : WHO global database on vitamin A deficiency. *WHO Iris* 55 (2009).

141. Stevens, G. A. *et al.* Trends and mortality effects of vitamin A deficiency in children in 138 low-income and middle-income countries between 1991 and 2013: A pooled analysis of population-based surveys. *Lancet Glob. Heal.* **3**, e528–e536 (2015).

142. Podell, B. K. *et al.* Non-Diabetic Hyperglycemia Exacerbates Disease Severity in Mycobacterium tuberculosis Infected Guinea Pigs. *PLoS One* (2012) doi:10.1371/journal.pone.0046824.

143. Ackart, D. F. *et al.* Expression of antimicrobial drug tolerance by attached communities of Mycobacterium tuberculosis. *Pathog. Dis.* **70**, 359–369 (2014).

144. Frenkel, J. D. H. *et al.* Metformin enhances protection in guinea pigs chronically infected with Mycobacterium tuberculosis. *Sci. Reports 2020 101* **10**, 1–11 (2020).

145. shiny: Web Application Framework for R version 1.7.4 from CRAN. https://rdrr.io/cran/shiny/.

146. Podell, B. K. *et al.* A model of type 2 diabetes in the guinea pig using sequential diet-induced glucose intolerance and streptozotocin treatment. *Dis. Model. Mech.* **10**, 151–162 (2017).

147. Ryan, G. J. *et al.* Multiple M. tuberculosis Phenotypes in Mouse and Guinea Pig Lung Tissue Revealed by a Dual-Staining Approach. *PLoS One* **5**, e11108 (2010).

148. Sommer, A. Vitamin A Deficiency and Clinical Disease: An Historical Overview. *J. Nutr.* **138**, 1835–1839 (2008).

149. West, K. P. & Darnton-Hill, I. Vitamin A Deficiency. *Nutr. Heal. Dev. Ctries.* 377–433 (2008) doi:10.1007/978-1-59745-464-3_13.

150. Ahmad, S. M., Haskell, M. J., Raqib, R. & Stephensen, C. B. Markers of Innate Immune Function Are Associated with Vitamin A Stores in Men. *J. Nutr.* **139**, 377–385 (2009).

151. Manicassamy, S. & Pulendran, B. Retinoic acid-dependent regulation of immune responses by dendritic cells and macrophages. *Semin. Immunol.* **21**, 22–27 (2009).

152. Nestel, P., Melara, A., Rosado, J. & Mora, J. O. Vitamin A deficiency and anemia among children 12-71 months old in Honduras. *Rev Panam Salud Publica;6(1),jul. 1999* **6**, 1999 (1999).

153. Thurnham, D. I., McCabe, G. P., Northrop-Clewes, C. A. & Nestel, P. Effects of subclinical infection on plasma retinol concentrations and assessment of prevalence of vitamin A deficiency: meta-analysis. *Lancet* **362**, 2052–2058 (2003).

154. Filteau, S. M. *et al.* Influence of morbidity on serum retinol of children in a community-based study in northern Ghana. *Am. J. Clin. Nutr.* **58**, 192–197 (1993).

155. Anand, P. K., Kaul, D. & Sharma, M. Synergistic action of vitamin D and retinoic acid restricts invasion of macrophages by pathogenic mycobacteria. *J Microbiol Immunol Infect* **41**, 17–25 (2008).

156. Alvarez, J. O., Salazar-Lindo, E., Kohatsu, J., Miranda, P. & Stephensen, C. B. Urinary excretion of retinol in children with acute diarrhea. *Am. J. Clin. Nutr.* **61**, 1273–1276 (1995).

157. Mitra, A. K. *et al.* Urinary retinol excretion and kidney function in children with shigellosis. *Am. J. Clin. Nutr.* **68**, 1095–1103 (1998).

158. Stephensen, C. B. & Gildengorin, G. Serum retinol, the acute phase response, and the apparent misclassification of vitamin A status in the third National Health and Nutrition Examination Survey. *Am. J. Clin. Nutr.* **72**, 1170–1178 (2000).

159. Inflammation-induced changes in the nutritional biomarkers s... : Current Opinion in Clinical Nutrition & Metabolic Care. https://journals.lww.com/co-clinicalnutrition/Abstract/2001/11000/Inflammation_induced_changes_in_the_nutritional.2.aspx.

160. Bang, Y. J. *et al.* Serum amyloid a delivers retinol to intestinal myeloid cells to promote adaptive immunity. *Science (80-.).* **373**, (2021).

161. Burri, B. J. & Clifford, A. J. Carotenoid and retinoid metabolism: insights from isotope studies. *Arch. Biochem. Biophys.* **430**, 110–119 (2004).

162. Steinhoff, J. S., Lass, A. & Schupp, M. Biological Functions of RBP4 and Its Relevance for Human Diseases. *Front. Physiol.* **12**, 294 (2021).

163. Mahmood, K. *et al.* Serum Retinol Binding Protein as an Indicator of Vitamin A Status in Cirrhotic Patients with Night Blindness. *Saudi J. Gastroenterol.* **14**, 7 (2008).

164. De Pee, S. & Dary, O. Biochemical Indicators of Vitamin A Deficiency: Serum Retinol and Serum Retinol Binding Protein. *J. Nutr.* **132**, 2895S-2901S (2002).

165. Cronan, M. R. In the Thick of It: Formation of the Tuberculous Granuloma and Its Effects on Host and Therapeutic Responses. *Front. Immunol.* **13**, 878 (2022).

166. Silva Miranda, M., Breiman, A., Allain, S., Deknuydt, F. & Altare, F. The tuberculous granuloma: An unsuccessful host defence mechanism providing a safety shelter for the bacteria? *Clin. Dev. Immunol.* **2012**, (2012).

167. Palmer, M. V. Emerging Understanding of Tuberculosis and the Granuloma by Comparative Analysis in Humans, Cattle, Zebrafish, and Nonhuman Primates. *Veterinary Pathology* vol. 55 8–10 (2018).

168. Moschen, A. R., Adolph, T. E., Gerner, R. R., Wieser, V. & Tilg, H. Lipocalin-2: A Master Mediator of Intestinal and Metabolic Inflammation. *Trends Endocrinol. Metab.* **28**, 388–397 (2017).

169. Huber, M. & Lohoff, M. IRF4 at the crossroads of effector T-cell fate decision. *Eur. J. Immunol.* **44**, 1886–1895 (2014).

170. Kaminskiy, Y. & Melenhorst, J. J. STAT3 Role in T-Cell Memory Formation. *International Journal of Molecular Sciences* vol. 23 (2022).

171. Huang, C. X. & Melnick, A. Mechanisms of action of BCL6 during germinal center B cell development. *Sci. China Life Sci.* **58**, 1226–1232 (2015).

172. Slight, S. R. *et al.* CXCR5+ T helper cells mediate protective immunity against tuberculosis. *J. Clin.*

Invest. **123**, 712–726 (2013).

173. Crotty, S., Johnston, R. J. & Schoenberger, S. P. Effectors and memories: Bcl-6 and Blimp-1 in T and B lymphocyte differentiation. *Nat. Immunol. 2010 112* **11**, 114–120 (2010).

174. Ciucci, T. *et al.* Dependence on Bcl6 and Blimp1 drive distinct differentiation of murine memory and follicular helper CD4+ T cells. *J. Exp. Med.* **219**, (2021).

175. Nurieva, R. I. *et al.* Bcl6 mediates the development of T follicular helper cells. *Science (80-.).* **325**, 1001–1005 (2009).

176. Fu, S. H., Yeh, L. T., Chu, C. C., Yen, B. L. J. & Sytwu, H. K. New insights into Blimp-1 in T lymphocytes: a divergent regulator of cell destiny and effector function. *J. Biomed. Sci. 2017 241* **24**, 1–17 (2017).

177. Hwang, S. J., Cobb, D. A., Bhadra, R., Youngblood, B. & Khan, I. A. Blimp-1–mediated CD4 T cell exhaustion causes CD8 T cell dysfunction during chronic toxoplasmosis. *J. Exp. Med.* **213**, 1799–1818 (2016).

178. McBride, J. A. & Striker, R. Imbalance in the game of T cells: What can the CD4/CD8 T-cell ratio tell us about HIV and health? *PLOS Pathog.* **13**, e1006624 (2017).

179. CD4-CD8 Ratio - Health Encyclopedia - University of Rochester Medical Center. https://www.urmc.rochester.edu/encyclopedia/content.aspx?contenttypeid=167&contentid=cd4_cd8_ratio.

180. Beckman, E. M. *et al.* Recognition of a lipid antigen by GDI-restricted αβ+ T cells. *Nature* **372**, 691–694 (1994).

181. Brigl, M. & Brenner, M. B. CD1: Antigen Presentation and T Cell Function. *Annu. Rev. Immunol.* **22**, 817–890 (2004).

182. Dougan, S. K., Kaser, A. & Blumberg, R. S. CD1 expression on antigen-presenting cells. *Current Topics in Microbiology and Immunology* (2007) doi:10.1007/978-3-540-69511-0-5.

183. Chancellor, A., Gadola, S. D. & Mansour, S. The versatility of the CD1 lipid antigen presentation pathway. *Immunology* **154**, 196–203 (2018).

184. Rossjohn, J., Pellicci, D. G., Patel, O., Gapin, L. & Godfrey, D. I. Recognition of CD1d-restricted antigens by natural killer T cells. *Nat. Rev. Immunol. 2012 1212* **12**, 845–857 (2012).

185. Brossay, L. *et al.* CD1d-mediated Recognition of an α-Galactosylceramide by Natural Killer T Cells Is Highly Conserved through Mammalian Evolution. *J. Exp. Med.* **188**, 1521–1528 (1998).

186. Moody, D. B. *et al.* Cd1b-Mediated T Cell Recognition of a Glycolipid Antigen Generated from Mycobacterial Lipid and Host Carbohydrate during Infection. *J. Exp. Med.* **192**, 965–976 (2000).

187. Reijneveld, J. F. *et al.* Human γδ T cells recognize CD1b by two distinct mechanisms. *Proc. Natl. Acad. Sci. U. S. A.* **117**, 22944–22952 (2020).

188. Montamat-Sicotte, D. J. *et al.* A mycolic acid-specific CD1-restricted T cell population contributes to acute and memory immune responses in human tuberculosis infection. *J. Clin. Invest.* **121**, 2493–2503 (2011).

189. Van Rhijn, I. & Moody, D. B. CD1 and mycobacterial lipids activate human T cells. *Immunol. Rev.*

264, 138–153 (2015).

190. James, C. A. *et al.* CD1b Tetramers Identify T Cells that Recognize Natural and Synthetic Diacylated Sulfoglycolipids from Mycobacterium tuberculosis. *Cell Chem. Biol.* (2018) doi:10.1016/j.chembiol.2018.01.006.

191. Ly, D. *et al.* CD1c tetramers detect ex vivo T cell responses to processed phosphomycoketide antigens. *J. Exp. Med.* **210**, 729–741 (2013).

192. Moody, D. B. & Suliman, S. CD1: From Molecules to Diseases. *F1000Research* (2017) doi:10.12688/f1000research.12178.1.

193. Dascher, C. C. Immunization with a mycobacterial lipid vaccine improves pulmonary pathology in the guinea pig model of tuberculosis. *Int. Immunol.* **15**, 915–925 (2003).

194. Hiromatsu, K. *et al.* Characterization of guinea-pig group 1 CD1 proteins. *Immunology* **106**, 159–172 (2002).

195. Tahiri, N. *et al.* Total Synthesis of a Mycolic Acid from Mycobacterium tuberculosis. *Angew. Chem. Int. Ed. Engl.* **59**, 7555–7560 (2020).

196. Kasmar, A. G. *et al.* CD1b tetramers bind αβ T cell receptors to identify a mycobacterial glycolipidreactive T cell repertoire in humans. *J. Exp. Med.* (2011) doi:10.1084/jem.20110665.

197. Lopez, K. *et al.* CD1b Tetramers Broadly Detect T Cells That Correlate With Mycobacterial Exposure but Not Tuberculosis Disease State. *Front. Immunol.* (2020) doi:10.3389/fimmu.2020.00199.

198. Lee, D. J., Abeyratne, A., Carson, D. A. & Corr, M. Induction of an Antigen-specific, CD1-restricted Cytotoxic T Lymphocyte Response In vivo. *J. Exp. Med.* **187**, 433–438 (1998).

199. Campos-Martín, Y., Gómez del Moral, M., Gozalbo-López, B., Suela, J. & Martínez-Naves, E. Expression of human CD1d molecules protects target cells from NK cell-mediated cytolysis. *J. Immunol.* **172**, 7297–7305 (2004).

200. Wu, X., Zhang, Y., Li, Y. & Schmidt-Wolf, I. G. H. Improvements in Flow Cytometry-Based Cytotoxicity Assay. *Cytom. Part A* **99**, 680–688 (2021).

201. Bergsma, T. T. *et al.* Facilitating pharmacometric workflow with the metrumrg package for R. *Comput. Methods Programs Biomed.* **109**, 77–85 (2013).

202. Kassambara, A. rstatix:Pipe-Friendly Framework for Basic Statistical Tests. R package version 0.7.0. *https://CRAN.R-project.org/package=rstatix* (2021).

203. Orme, I. M. & Ordway, D. J. Mouse and Guinea Pig Models of Tuberculosis. *Microbiol. Spectr.* **4**, (2016).

204. Felio, K. *et al.* CD1-restricted adaptive immune responses to Mycobacteria in human group 1 CD1 transgenic mice. *J. Exp. Med.* (2009) doi:10.1084/jem.20090898.

205. Giuliani, A. *et al.* Influence of Mycobacterium bovis bacillus Calmette Guérin on in vitro induction of CD1 molecules in human adherent mononuclear cells. *Infect. Immun.* **69**, 7461–7470 (2001).

206. Roura-Mir, C. *et al.* Mycobacterium tuberculosis Regulates CD1 Antigen Presentation Pathways through TLR-2. *J. Immunol.* **175**, 1758–1766 (2005).

207. Brenner, S. A. P. *et al.* with Mycobacterial Lipid Antigens Responses in Guinea Pigs by Immunization Induction of CD1-Restricted Immune. *J Immunol Ref.* **169**, 330–339 (2002).

208. Kawashima, T. *et al.* Cutting Edge: Major CD8 T Cell Response to Live Bacillus Calmette-Guérin Is Mediated by CD1 Molecules. *J. Immunol.* **170**, 5345–5348 (2003).

209. Hamaoka, T., Shimizu, J., Suda, T. & Fujiwara, H. Induction of tumor-specific in vivo protective immunity by immunization with tumor antigen-pulsed antigen-presenting cells. *Princess Takamatsu Symp.* **19**, 265–275 (1988).

210. Behar, S. M., Porcelli, S. A., Beckman, E. M. & Brenner, M. B. A pathway of costimulation that prevents anergy in CD28− T Cells: B7-independent costimulation of CD1-restricted T cells. *J. Exp. Med.* **182**, (1995).

211. Ulrichs, T., Moody, D. B., Grant, E., Kaufmann, S. H. E. & Porcelli, S. A. T-cell responses to CD1-presented lipid antigens in humans with Mycobacterium tuberculosis infection. *Infect. Immun.* **71**, 3076–3087 (2003).

212. Park, S. H. & Bendelac, A. CD1-restricted T-cell responses and microbial infection. *Nature* vol. 406 (2000).

213. Lopez, K. *et al.* CD1b Tetramers Broadly Detect T Cells That Correlate With Mycobacterial Exposure but Not Tuberculosis Disease State. *Front. Immunol.* **11**, 199 (2020).

214. Siddiqui, S., Visvabharathy, L. & Wang, C. R. Role of group 1 CD1-restricted T cells in infectious disease. *Frontiers in Immunology* vol. 6 1 (2015).

215. Zhao, J. *et al.* Mycolic acid-specific T cells protect against Mycobacterium tuberculosis infection in a humanized transgenic mouse model. *Elife* **4**, (2015).

216. Spada, F. M. *et al.* Self-Recognition of Cd1 by γ/δ T CellsImplications for Innate Immunity. *J. Exp. Med.* **191**, 937–948 (2000).

217. Shang, S. *et al.* Induction of Mycobacterium Tuberculosis Lipid-Specific T Cell Responses by Pulmonary Delivery of Mycolic Acid-Loaded Polymeric Micellar Nanocarriers. *Front. Immunol.* **9**, 2709 (2018).

218. Morgun, E. *et al.* Mycolic acid nanoparticle vaccination leads to antigen persistence and unique differentiation of mycobacterial lipid antigen-specific T cells. *J. Immunol.* **208**, 181.13-181.13 (2022).

219. Dascher, C. C. Immunization with a mycobacterial lipid vaccine improves pulmonary pathology in the guinea pig model of tuberculosis. *Int. Immunol.* **15**, 915–925 (2003).

220. Amprey, J. L., Späth, G. F. & Porcelli, S. A. Inhibition of CD1 Expression in Human Dendritic Cells during Intracellular Infection with Leishmania donovani. *Infect. Immun.* **72**, 589–592 (2004).

221. Balboa, L. *et al.* Mycobacterium tuberculosis impairs dendritic cell response by altering CD1b, DC-SIGN and MR profile. *Immunol. Cell Biol.* **88**, 716–726 (2010).

222. Dutronc, Y. & Porcelli, S. A. The CD1 family and T cell recognition of lipid antigens. *Tissue Antigens* **60**, 337–353 (2002).

223. Derebe, M. G. *et al.* Serum amyloid A is a retinol binding protein that transports retinol during

bacterial infection. **3**, 3206 (2014).

224. Hibberd, M. The effects of micronutrient deficiencies on bacterial species from the human gut microbiota. *Sci. Transl. Med.* **9**, eaal4069 (2017).

225. Green, M. H. *et al.* A retinol isotope dilution equation predicts both group and individual total body vitamin A stores in adults based on data from an early postdosing blood sample. *J. Nutr.* **146**, (2016).

226. Gannon, B. M., Valentine, A. R., Davis, C. R., Howe, J. A. & Tanumihardjo, S. A. Duration of retinol isotope dilution studies with compartmental modeling affects model complexity, kinetic parameters, and calculated Vitamin A stores in US women. *J. Nutr.* **148**, (2018).

227. Bationo, J. F. *et al.* Liver retinol estimated by 13C-retinol isotope dilution at 7 versus 14 days in Burkinabe schoolchildren. *Exp. Biol. Med.* **244**, (2019).

228. Mori, L. & De Libero, G. Presentation of lipid antigens to T cells. *Immunol. Lett.* **117**, 1–8 (2008).

229. Mori, L. & De Libero, G. T cells specific for lipid antigens. *Immunol. Res.* **53**, 191–199 (2012).

Supplemental material for chapter 1:

Supplemental Table S1. Antibodies in guinea pig immune cell phenotyping by flow cytometry

Antibody Target	Species Specificity	Antibody Clone	Antibody Conjugate	Supplier
CD45 (total)	Guinea pig	IH-1	PE-Cy7	Bio-Rad
CD4	Guinea pig	CT7	FITC	Bio-Rad
CD8	Guinea pig	CT6	PerCP-Cy5	Bio-Rad
CD11	Guinea pig; pig; human	MIL4	PE	Bio-Rad
B cell	Guinea pig	MsGp10	DyLight-405	Bio-Rad
MHC-II	Human; cross-reactive in guinea pig	IVA-12	APC	ATCC; IVA12 hybridoma
CD80	Mouse	16-10A1	APC-fire750	BioLegend

Derived from Podell et al. 2022[22]

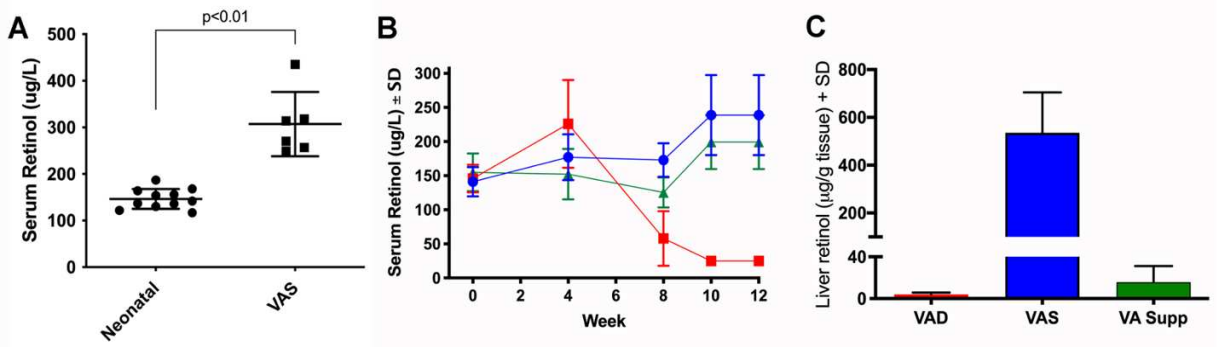

Supplementary figure S1. Establishing the guinea pig model of dietary vitamin A deficiency. Serum and liver retinol concentrations are shown from neonatal guinea pigs prior to dietary intervention and during the course of vitamin A deficiency model development. Neonatal guinea pigs (age 7-11 days) were used to develop the guinea pig model of vitamin A deficiency in order to minimize the hepatic stores of retinol and allow for timely induction of vitamin A deficiency. (A) Low serum retinol concentrations were present in neonatal guinea pigs (age 9-12 days) prior to dietary intervention as compared to guinea pigs at 12 weeks of age fed the vitamin A sufficient diet (VAS), indicating that a physiologic vitamin A deficiency exists in neonatal guinea pigs, similar to human neonates [7]. (B) Serum retinol concentration subsequently increased in guinea pigs receiving vitamin A sufficient diet (blue) over the course of 6-8 weeks while complete vitamin A deficiency (<50 ug/mL) was achieved in all guinea pigs receiving deficient diet (VAD) within 4-8 weeks. Guinea pigs consuming vitamin A deficient diet were monitored for a total of 12 weeks under conditions of complete deficiency or with low-dose supplementation in the form of oral retinyl palmitate in corn oil (100 IU/day, 5 days/week). (C) Liver retinol concentrations were qua,ntified after 12 weeks on respective diets. Replete liver storage was present in VAS guinea pigs but depleted in VAD guinea pigs, which despite higher serum retinol was not overcome by daily low-dose supplementation. *Derived from Podell et al. 2022*[22]

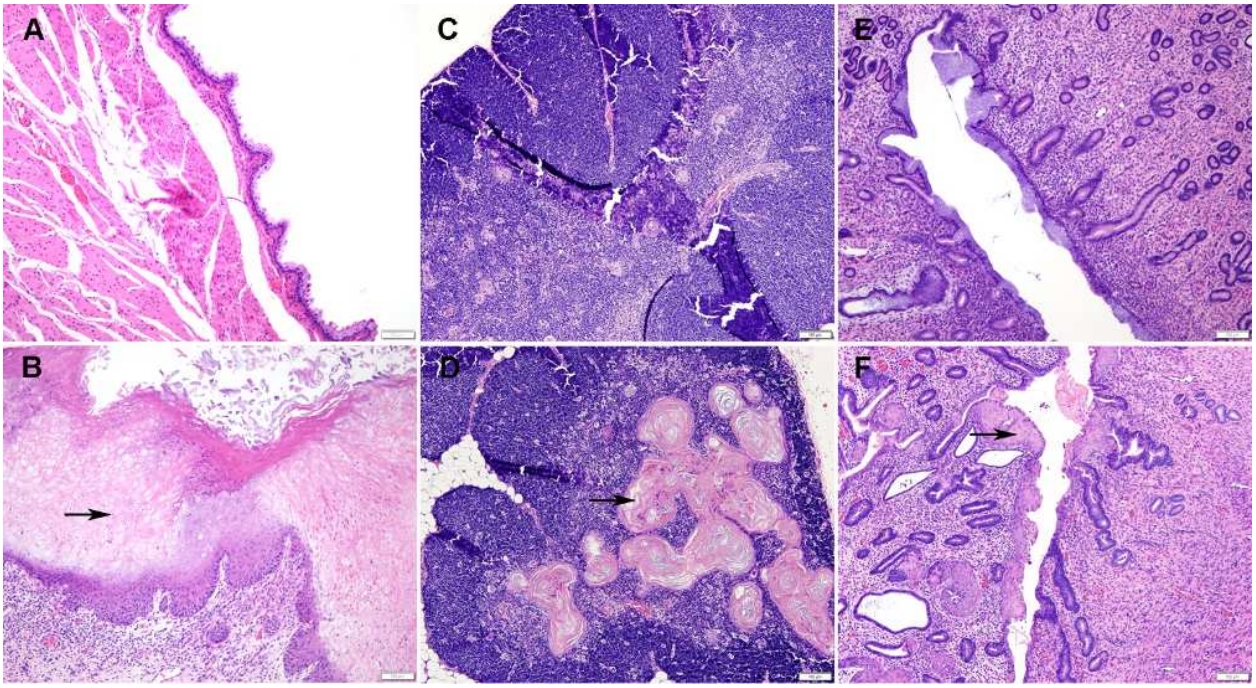

Supplementary figure S2. Histopathologic sequelae of complete vitamin A deficiency in the guinea pig model. *H&E stained tissue sections of organs most affected by vitamin A deficiency (VAD) induced metaplasia, compared to normal morphology of sufficient (VAS) guinea pigs.* Weight loss was noted after 12 weeks among completely vitamin A deficient guinea pigs along with an accumulation of yellow mucoid discharge around the vulva, changes that were not observed when guinea pigs received completely sufficient diet or minimal weekly supplementation (data not shown). Histopathology of organs with epithelial surfaces revealed severe squamous metaplasia as the primary sequelae of vitamin A deficiency with a predisposition in the guinea pig for organs of the urogenital tract. This pathology was mitigated in optimized model conditions through minimal oral supplementation of 100 IU retinyl palmitate per week. Epithelial metaplasia was not present in the airways of the lung (data not shown). Urinary Bladder; Normal urinary bladder mucosal surface of a VAS guinea pig (A). Urinary bladder of a VAD guinea pig without retinyl palmitate supplementation (B) has circumferential replacement of uroepithelium with keratinizing squamous epithelium and marked hyperkeratosis (arrow). Inflammation and edema are present in the subepithelial connective tissue. Thymus; Normal thymus of a VAS guinea pig (C). Affected thymus of a VAD guinea (D) with marked expansion of Hassall's corpuscles by accumulation of lamellar keratin (arrow). Uterus; Normal uterine endometrium of VAS guinea pig (E). Endometrium of a VAD guinea pig (F) has segmental replacement of epithelium with keratinizing squamous epithelium (arrow) and glandular loss throughout the stratum compactum. Bar = 100µm. *Derived from Podell et al. 2022*[22]

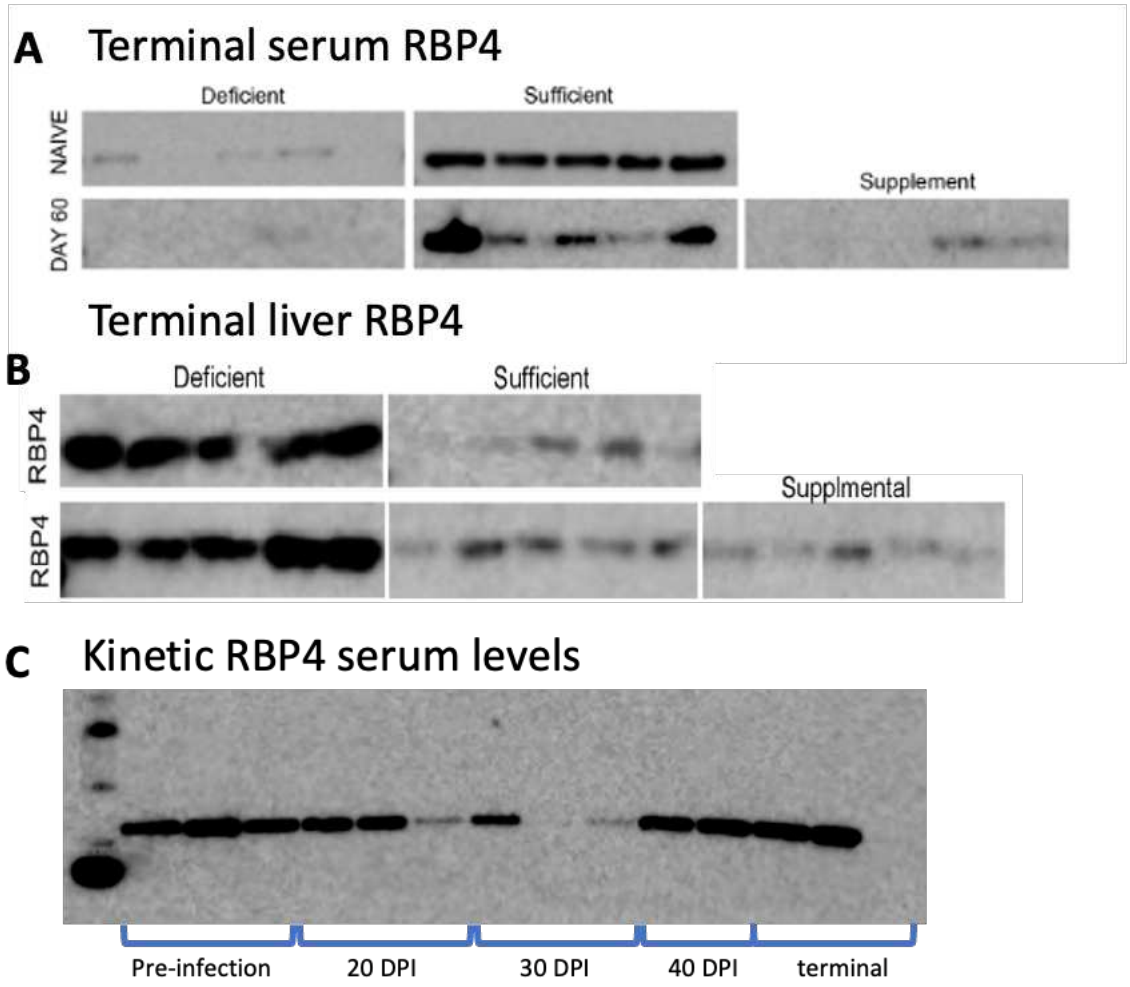

Supplementary figure S3. Western blot bands of RBP4 from vitamin A sufficient and deficient animals Mtb infected animals. A) RBP4 protein bands from terminal serum collection. B) RBP4 protein bands from collected, and homogenized, liver. C) RBP4 protein bands from antemortem blood draws of VAS infected animals.

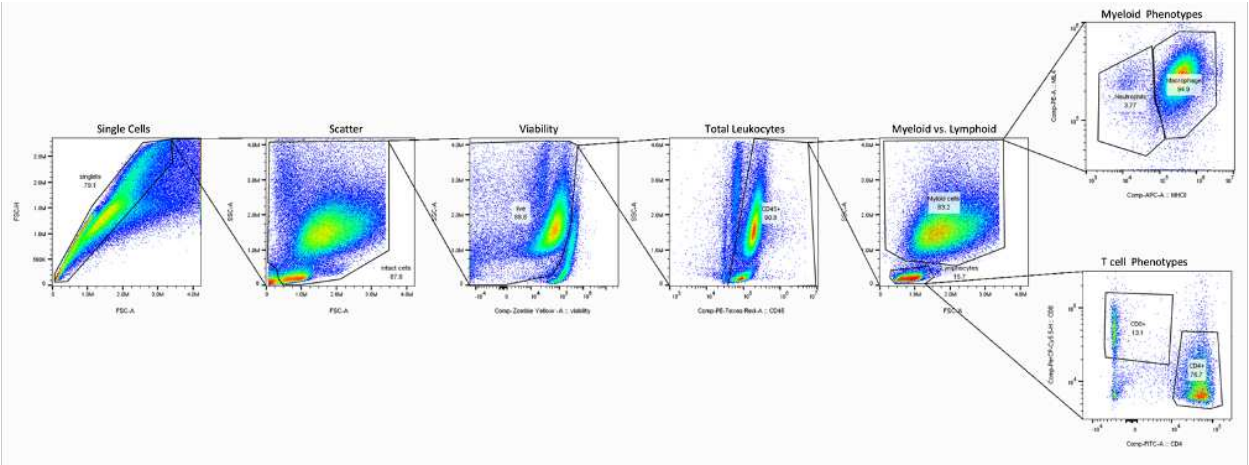

Supplementary figure S4. Gating strategy for flow cytometry phenotyping of cells isolated by bronchoalveolar lavage or from dissociated lung granulomas. The gating strategy for phenotyping of lung immune phenotypes isolated from guinea pigs is shown. Initial singlet gating was performed followed by forward and side scatter gating to eliminate cellular debris. Total leukocytes were gated among the population of viable cells based on expression of CD45. Additional forward and side scatter gating was used among CD45+ leukocytes to discriminate myeloid and lymphocyte cell populations, from which neutrophil and macrophage cells or CD4 and CD8 T cells were identified, respectively. Neutrophils are defined as high scatter MIL4/CD11+, MHC-II-. Macrophages are defined as high scatter MHCII+ CD11b+. CD4 or CD8 T cells are defined by respective targeting of each surface molecule among lymphocyte scatter gating, after dump gating of B cells.

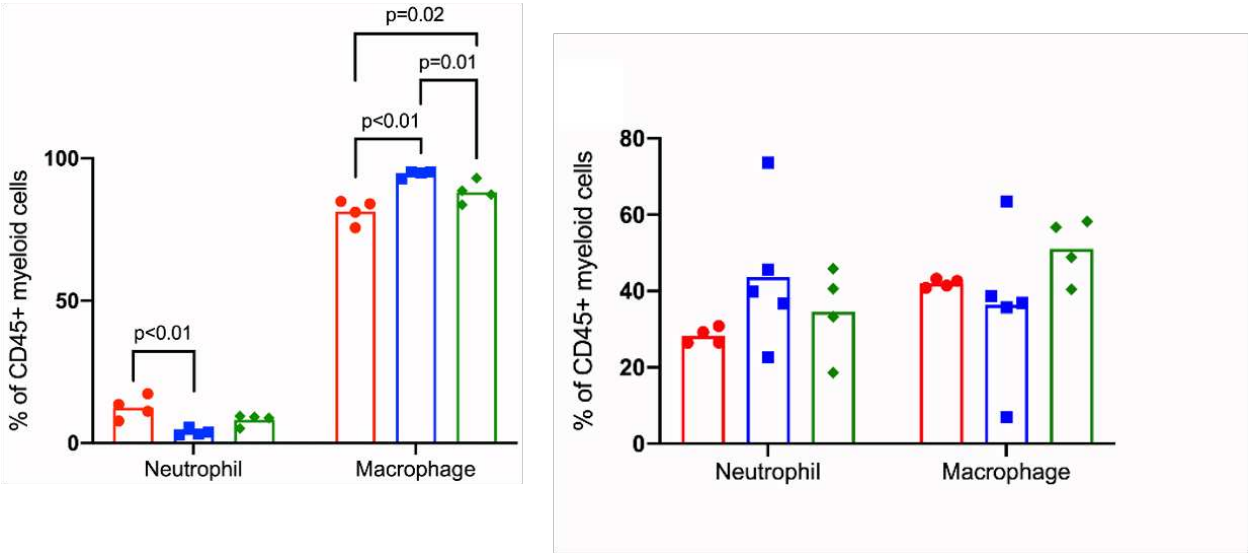

Supplementary figure S5. Myeloid leukocyte phenotypes in bronchoalveolar lavage and isolated granulomas of guinea pigs at day 60 of infection. Phenotypes of bronchoalveolar lavage-isolated and isolated granuloma myeloid cell populations determined by flow cytometry

in vitamin A deficient (VAD), sufficient (VAS), or deficient guinea pigs re-supplemented with vitamin A at 30 days after infection (VAD resupp

Table S2. List of genes evaluated via nanostring analysis and correlated animals' samples with quantitative gene expression

Probe Name	Accession #	Class Name	Species Nam	Annotation	VAD1.00.LG	VAD1.01.LG	VAD1.02.LG	VAD1.03.LG	VAD1.04.LG	VAD1.05.LG	VAD1.06.LG	VAD1.07.LG	VAD1.08.LG	VAD1.09.LG	VAD2.10.LG	VAD2.11.LG	VAD2.00.LG	VAD2.01.LG	VAD2.02.LG
A4B1	XM_0131512	Endogenous	Cp		10332	9359	13178	10462	11852	10245	10454	11629	11378	9921	6058	3286	11964	15189	12453
A4B7	XM_0034760	Endogenous	Cp		765	684	751	624	819	2409	1086	1218	2175	1603	1050	806	1291	2632	2146
ABCG1	XM_0034639	Endogenous	Cp		48	55	56	56	67	102	60	103	70	72	50	41	91	113	108
ADH1C	XM_0034680	Endogenous	Cp		239	449	471	476	356	281	289	269	319	465	97	117	545	865	550
ALDH1A2	XM_0034620	Endogenous	Cp		1446	1483	1616	2184	1893	787	1213	1140	1389	1198	460	344	2522	2585	2399
ALDH1A3	XM_0131585	Endogenous	Cp		2384	2431	4591	2922	3710	5697	5492	4953	5803	5789	2495	2066	3330	3776	2762
ALOX12	XM_0034662	Endogenous	Cp		31	30	48	20	28	71	26	38	53	62	25	13	39	36	34
ALOX5	XM_0034660	Endogenous	Cp		826	613	764	677	565	484	401	403	416	562	184	182	626	992	822
BCL6	XM_0131602	Endogenous	Cp		374	453	574	444	441	943	573	575	708	937	472	309	729	944	836
Blimp-1	XM_0034660	Endogenous	Cp		833	998	703	786	823	747	878	1094	970	796	416	212	994	806	736
CCL5	NM_0011729	Endogenous	Cp		11042	3806	9865	6756	8813	4810	3101	4447	9698	12795	1682	1126	8600	11431	10821
CCR1	XM_0050068	Endogenous	Cp		294	292	348	229	307	477	247	176	190	773	196	249	474	727	668
CCR2	XM_0131603	Endogenous	Cp		238	262	227	191	186	1205	285	448	709	626	362	376	556	838	812
CCR4	NM_0011734	Endogenous	Cp		73	85	102	102	85	96	113	110	177	51	54	21	63	169	98
CCR5	XM_0050068	Endogenous	Cp		270	339	303	342	273	1361	293	559	631	504	401	320	644	1213	1024
CCR6	XM_0034663	Endogenous	Cp		126	162	221	200	210	242	255	244	302	134	137	59	187	281	187
CCR7	XM_0034669	Endogenous	Cp		907	882	1096	888	1110	1331	1071	1160	1145	1189	556	351	1252	1243	1265
CCR9	XM_0235603	Endogenous	Cp		30	20	21	18	34	32	22	29	32	19	29	15	24	36	27
CD103	XM_0131522	Endogenous	Cp		49	87	77	85	108	55	54	59	77	42	63	24	69	240	108
CD1B2	NM_0011728	Endogenous	Cp		4	14	4	10	4	11	8	18	26	13	6	6	7	20	16
CD1B4	NM_0011728	Endogenous	Cp		31	25	60	90	97	147	429	491	487	109	95	46	49	48	20
CD1C2	NM_0011728	Endogenous	Cp		22	18	36	65	68	72	263	316	250	52	67	21	40	25	23
CD1C3	NM_0011728	Endogenous	Cp		25	22	39	58	55	57	173	180	184	24	29	9	23	34	28
CD28	XM_0131572	Endogenous	Cp		150	185	208	150	234	169	200	219	312	87	171	72	236	641	343
CD36	XM_0034698	Endogenous	Cp		1974	2514	2662	2976	2682	4088	2797	2933	2735	3914	2784	1312	2789	4356	3135
CD40	XM_0131503	Endogenous	Cp		144	151	180	20	119	148	79	136	94	194	76	18	139	302	205
CD40L	XM_0034647	Endogenous	Cp		42	41	77	41	64	36	48	73	112	23	33	18	85	234	140
CD49a	XM_0034702	Endogenous	Cp		5051	4982	6771	4530	6040	3526	5030	5519	5524	4130	2139	1182	5498	7500	6171
CD49d	XM_0034785	Endogenous	Cp		1013	1085	1072	951	1037	2393	831	1399	1466	1213	760	670	1733	3786	2506
CD69	XM_0034705	Endogenous	Cp		41	44	48	30	63	138	53	61	50	69	40	36	52	132	79
CD86	XM_0131518	Endogenous	Cp		1235	1188	1111	1175	977	2759	1050	1512	1631	1605	1218	640	1584	2525	1979
CPT1B	XM_0034615	Endogenous	Cp		20	26	29	22	26	91	29	23	39	101	32	34	45	56	45
CRABP1	XM_0034635	Endogenous	Cp		131	163	238	189	189	77	159	105	217	72	43	19	218	245	147
CRABP2	XM_0034756	Endogenous	Cp		449	253	681	519	419	362	246	283	386	651	172	185	801	922	622
CTLA4	XM_0034741	Endogenous	Cp		10	15	23	14	12	27	17	19	18	15	23	12	11	24	21
CXCL8	NM_0011733	Endogenous	Cp		475	480	450	258	343	663	472	202	483	757	398	267	460	852	874
CXCL9	XM_0034776	Endogenous	Cp		60	90	167	113	115	72	59	134	101	29	137	58	150	888	277
CXCR1	NM_0011734	Endogenous	Cp		368	295	374	313	361	792	640	462	830	1141	383	356	514	711	985
CXCR2	NM_0011728	Endogenous	Cp		76	72	87	57	85	232	140	77	286	417	86	153	154	200	245
CXCR3	XM_0131536	Endogenous	Cp		48	35	56	38	57	74	44	68	85	25	55	28	119	361	192
CXCR5	XM_0235662	Endogenous	Cp		38	41	30	16	43	14	21	35	29	21	16	9	22	66	29
CYP26A1	XM_0034623	Endogenous	Cp		394	301	377	420	505	145	194	210	153	235	97	68	575	330	530
CYP26B1	XM_0235647	Endogenous	Cp		334	374	746	326	407	27	39	20	25	23	24	6	361	1103	682
DHRS3	XM_0131539	Endogenous	Cp		2168	2112	2639	2175	2490	1423	1513	1513	1801	1625	966	532	2886	3098	2662
DHRS9	XM_0131426	Endogenous	Cp		38	78	67	68	70	172	122	82	94	98	200	48	52	110	100
FABP5	XM_0235616	Endogenous	Cp		6012	5061	5455	4989	4075	7258	6077	5108	4627	3194	4545	1505	4543	7180	7699
FOXP3	XM_0235618	Endogenous	Cp		74	75	73	87	81	93	94	106	86	48	64	21	75	98	70
GATA3	XM_0034734	Endogenous	Cp		1365	1245	1450	1274	1555	662	1202	1261	1272	863	372	240	1377	1405	1587
GMCSF	XM_0034645	Endogenous	Cp		50	75	58	43	53	55	66	57	57	47	36	26	59	79	60
HPGD	NM_0011729	Endogenous	Cp		20230	17660	23661	17470	25765	31254	25700	25160	26971	28346	8469	7044	25592	16036	24230
ICAM1	XM_0034608	Endogenous	Cp		154	140	142	154	161	179	168	240	196	161	151	74	177	215	224
IDO	XM_0034646	Endogenous	Cp		252	1513	329	263	203	10718	166	1381	652	820	2229	1936	5385	10702	5475
IFNG	NM_0011728	Endogenous	Cp		14	30	20	16	22	17	10	11	16	8	17	3	57	146	67
IL-12Rb2	XM_0235612	Endogenous	Cp		35	13	48	20	33	60	18	56	63	54	36	20	58	120	101
IL-18	XM_0131553	Endogenous	Cp		779	842	883	936	1064	1338	1308	1188	1060	1161	664	279	857	1112	1124
IL-22	XM_0034759	Endogenous	Cp		41	26	41	30	44	42	37	36	39	35	25	5	46	78	59
IL-23 p19	NM_0011729	Endogenous	Cp		9	10	8	4	8	6	7	5	11	10	3	6	13	14	15
IL-23R	XM_0131426	Endogenous	Cp		24	19	32	27	21	22	13	13	53	22	33	18	42	142	79
IL1-R1	XM_0034717	Endogenous	Cp		4013	3643	4564	4193	4308	5775	4286	3646	3571	4667	2861	1593	4800	5703	5403
IL10	NM_0012604	Endogenous	Cp		11	12	3	4	16	56	3	15	12	9	8	8	13	20	24
IL12A	NM_0011728	Endogenous	Cp		27	30	35	21	38	36	24	29	31	35	15	6	19	37	42
IL12B	NM_0011729	Endogenous	Cp		6	14	11	5	9	8	7	11	6	13	16	5	7	20	9
IL17A	NM_0012787	Endogenous	Cp		4	4	5	7	9	11	6	8	7	3	9	6	12	16	13
IL1B	NM_0011729	Endogenous	Cp		105	128	128	113	100	410	165	253	185	102	193	43	205	225	246
IL2	NM_0011728	Endogenous	Cp		9	8	11	10	10	10	17	21	16	14	7	7	9	29	12
IL21	XM_0034770	Endogenous	Cp		7	7	5	6	6	5	4	4	4	8	5	2	7	26	9
IL2RA	XM_0131563	Endogenous	Cp		55	80	86	65	68	88	79	94	108	61	48	23	66	129	85
IL4	NM_0012572	Endogenous	Cp		7	6	8	6	7	9	13	10	11	8	7	2	8	16	5
IL6	XM_0131523	Endogenous	Cp		10	29	11	16	20	78	28	17	28	17	50	14	28	100	40
IRF3	XM_0034655	Endogenous	Cp		709	753	998	702	898	812	799	944	759	772	592	367	962	1394	1252
IRF4	XM_0131450	Endogenous	Cp		113	144	166	150	222	239	371	481	401	216	158	62	183	381	214
Interferon be	XM_0235660	Endogenous	Cp		10	5	9	3	6	3	5	6	6	5	9	8	6	8	3
LCN2	XM_0050040	Endogenous	Cp		256	183	268	140	184	1191	346	151	629	1819	568	310	255	604	771
LPL	NM_0011729	Endogenous	Cp		10044	9903	10709	8189	11202	29834	11250	8664	10846	23294	7911	4766	11439	12634	10568
LTA4H	NM_0011729	Endogenous	Cp		2353	2004	2506	2206	2377	2474	2366	2549	2832	2267	1299	857	2450	3250	2868
MCP-1 (CCL	NM_0011729	Endogenous	Cp		2903	3040	3032	2744	2573	4796	3625	6141	4758	3262	3166	665	3669	4556	6004
MCSF	XM_0034792	Endogenous	Cp		1217	1716	1496	1244	1449	1922	1537	2015	2053	1528	1102	731	2445	2745	2418
NPC2	XM_0050048	Endogenous	Cp		12615	12317	15588	14038	13202	18699	12331	14027	13142	15013	8854	5634	12738	18882	16170
PCK1	XM_0034636	Endogenous	Cp		79	77	102	69	77	101	97	89	119	79	51	28	81	122	115
PD-1	XM_0034745	Endogenous	Cp		11	12	9	11	10	22	11	14	26	7	16	7	19	36	32
PD-L1	XM_0034722	Endogenous	Cp		123	186	157	124	147	254	133	248	269	126	140	67	353	600	385
PKC-theta	XM_0034734	Endogenous	Cp		592	441	832	521	714	642	958	828	846	519	398	215	727	1165	851
PPARD	XM_0034739	Endogenous	Cp		732	647	877	753	799	999	787	788	852	703	570	251	766	1034	1030
PPARG	XM_0131444	Endogenous	Cp		255	241	258	237	248	254	232	262	203	252	180	79	233	272	322
PTGER2	XM_0034717	Endogenous	Cp		103	114	165	110	170	229	75	120	157	222	85	55	165	265	180
PTGER3	XM_0034790	Endogenous	Cp		239	136	232	237	181	122	158	181	248	222	70	57	214	505	292
PTGER4	NM_0011730	Endogenous	Cp		906	848	937	730	922	1275	743	835	1175	1066	733	302	971	1485	1069
PTGES	XM_0034709	Endogenous	Cp		23	26	23	19	15	43	18	19	27	22	15	6	21	37	29
PTGS2	NM_0011730	Endogenous	Cp		132	229	178	180	218	172	184	231	131	121	70	32	236	230	222
RARA	XM_0034669	Endogenous	Cp		575	529	681	596	683	790	695	731	791	758	440	241	686	868	881
RARB	NM_0011727	Endogenous	Cp		185	194	256	213	220	49	114	107	96	51	34	11	203	229	207
RARG	XM_0050064	Endogenous	Cp		1058	1008	1165	1002	1119	636	629	641	855	731	318	233	1139	1312	1366
RBP1	XM_0050067	Endogenous	Cp		1212	1007	1494	1096	978	594	470	542	584	376	238	124	1026	1513	1197
RDH10	XM_0235616	Endogenous	Cp		970	1061	1290	1065	1284	1337	1188	1192	1079	1345	781	433	1156	1498	1417
RORC	XM_0131431	Endogenous	Cp		290	331	338	356	442	386	340	436	352	572	340	221	398	601	335
RXRA	XM_0131559	Endogenous	Cp		350	398	469	393	401	507	456	545	533	535	279	164	432	589	525
RXRB	XM_0050054	Endogenous	Cp		172	181	217	180	210	160	172	157	185	180	93	68	203	239	229
RXRG	XM_0034686	Endogenous	Cp		346	320	452	364	410	82	390	254	324	184	34	60	323	283	239
SOCS3	XM_0131471	Endogenous	Cp		607	1095	658	668	849	3095	1295	1068	1744	1732	1867	684	2053	2241	2641
STAT1	XM_0034787	Endogenous	Cp		2322	3879	2824	2637	2660	3361	2251	4871	3399	1512	2208	1129	7253	9809	6499
STAT3	XM_0050024	Endogenous	Cp		2099	2246	2760	2000	2283	3796	2581	2849	3199	3035	2004	1095	2951	4071	3806
STAT4	XM_0131426	Endogenous	Cp		104	82	115	99	130	72	90	125	113	62	47	18	171	353	229
STAT5	XM_0131496	Endogenous	Cp		1855	1854	2468	1843	2214	2848	2260	2237	2885	2872	1514	1045	2472	3176	2807
STAT6	XM_0034761	Endogenous	Cp		3510	3605	4442	3469	4031	5887	4322	4075	4807	5610	3019	1912	4136	5214	4747
STRA6	XM_0131417	Endogenous	Cp		24	20	18	17	12	17	22	18	20	15	10	5	27	25	26
TBX21	XM_0131494	Endogenous	Cp		1495	700	1641	871	1330	662	518	847	1096	1336	257	201	1313	2223	1933
TGFB	NM_0011730	Endogenous	Cp		743	626	823	710	784	1081	677	827	878	964	586	333	817	1186	1078
TNFA	NM_0011730	Endogenous	Cp		69	77	43	72	53	104	101	124	85	75	56	20	87	147	120
TNFR1	XM_0235621	Endogenous	Cp		1975	1870	2381	1895	2032	3164	2010	2175	2566	2718	1389	814	2375	3190	3055
klrg1	XM_0131530	Endogenous	Cp		850	536	1125	685	921	239	276	297	336	552	162	96	976	1491	1054
ACTB	NM_0011729	Housekeeping	Cp		113976	92082	126779	96348	105230	127842	101506	108134	124115	105884	68943	37884	114365	169636	142534
GAPDH	NM_0011729	Housekeeping	Cp		4791	4084	5071	4501	4513	8845	4337	5146	5914	5187	3875	2289	4493	8507	6258
HPRT	XM_0034626	Housekeeping	Cp		1059	950	1195	1159	1162	1728	1215	1152	1182	1185	820	452	1103	1659	1553
SDHA	XM_0034621	Housekeeping	Cp		2639	2370	2989	2652	2880	2538	2321	2488	2641	2565	1196	776	2654	3558	2686
TBP	XM_0050022	Housekeeping	Cp		847	719	995	860	831	871	824	819	898	912	441	268	840	1159	930
NEG_A	ERCC_00096	Negative	CUS		9	9	11	4	7	9	9	11	11	13	7	9	16	18	14
NEG_B	ERCC_00041	Negative	CUS		3	6	7	6	7	3	7	4	5	4	5	5	9	9	9
NEG_C	ERCC_00019	Negative	CUS		2	1	2	2	2	9	3	3	2	2	5	7	3	5	4
NEG_D	ERCC_00076	Negative	CUS		2	4	6	4	9	2	4	1	2	7	3	2	3	4	9
NEG_E	ERCC_00098	Negative	CUS		7	11	7	14	11	13	15	21	8	10	12	8	16	11	18
NEG_F	ERCC_00126	Negative	CUS		8	20	20	13	19	30	15	16	14	15	25	20	20	31	21
NEG_G	ERCC_00144	Negative	CUS		5	1	4	2	5	1	5	1	4	2	3	1	2	6	5
NEG_H	ERCC_00154	Negative	CUS		3	2	4	1	3	4	1	1	3	6	2	1	3	5	5
POS_A	ERCC_00117	Positive	CUS		49795	40814	47580	47314	54349	48240	50273	51777	51516	49430	47685	53160	58191	63591	58210
POS_B	ERCC_00112	Positive	CUS		16293	13655	15954	16084	17845	16156	16178	16750	17419	16362	15911	17639	19329	21233	19731
POS_C	ERCC_00002	Positive	CUS		4621	3826	4493	4345	4920	4652	4544	4584	4596	4476	4472	4753	5282	5924	5433
POS_D	ERCC_00092	Positive	CUS		1130	920	1091	1039	1247	1125	1160	1153	1201	1095	1073	1170	1346	1450	1328
POS_E	ERCC_00035	Positive	CUS		200	149	179	196	207	217	218	198	219	226	189	206	226	267	203
POS_F	ERCC_00034	Positive	CUS		63	53	49	54	85	69	74	74	68	62	74	77	76	104	72

Probe Name	VAD2.03.LG	VAD2.04.LG	VAD2.05.LG	VAD2.06.LG	VAD2.07.LG	VAD2.08.LG	VAD2.09.LG	VAD3.06.LG	VAD3.07.LG	VAD2.00.LN	VAD2.01.LN	VAD2.02.LN	VAD2.03.LN	VAD2.04.LN	VAD2.05.LN	VAD2.06.LN	VAD2.07.LN	VAD2.08.LN
A4B1	10996	10607	10950	11441	10844	13076	10355	21520	8786	3709	3547	4571	3396	5418	5346	5418	2599	5232
A4B7	1300	2375	2656	1286	2046	2013	1790	5622	2668	7515	5833	7401	4234	6752	7844	10822	5318	6969
ABCG1	48	69	95	64	81	111	77	184	98	61	54	80	77	91	87	111	53	70
ADH1C	189	234	510	260	430	334	421	741	270	10	22	63	27	5	7	232	27	26
ALDH1A2	2450	1891	1197	1891	2074	1757	1530	3828	998	211	198	159	103	132	89	193	46	114
ALDH1A3	2860	2436	2515	3666	2811	3672	3033	4511	1875	125	142	266	88	547	178	362	64	211
ALOX12	23	48	24	40	41	43	21	46	39	20	19	20	12	21	19	56	20	21
ALOX5	732	704	679	586	603	821	642	1772	516	10	16	16	26	19	8	20	9	18
BCL6	606	689	716	598	633	716	521	1376	504	590	373	473	279	484	420	595	327	537
Blimp-1	633	912	1190	707	968	854	766	2213	943	1383	1030	1592	827	1718	1949	1902	467	1623
CCL5	7490	12730	13526	5226	13493	9403	9179	39754	11633	36421	26539	38554	39771	33019	63538	17889	10886	40271
CCR1	513	738	534	268	459	546	403	1520	621	408	407	560	805	792	607	634	366	664
CCR2	459	699	888	459	686	704	585	2243	664	833	691	958	656	998	1115	783	698	1105
CCR4	79	146	126	63	132	107	58	298	220	105	96	101	76	120	89	241	141	114
CCR5	577	1307	1181	596	935	913	754	3146	1246	1838	1715	2287	1323	2307	2501	1814	977	2316
CCR6	170	223	303	139	306	244	186	573	364	1909	1467	1464	698	1192	1153	2298	1538	1080
CCR7	1021	1009	1057	1091	1041	1123	925	2044	811	666	541	626	482	756	768	809	364	698
CCR9	38	29	31	28	23	20	24	41	19	53	21	42	22	36	31	66	44	41
CD103	74	229	234	36	114	70	115	251	194	341	308	399	118	354	411	710	229	474
CD1B2	12	64	26	16	24	17	21	123	31	18	3	16	6	19	9	24	12	18
CD1B4	47	34	94	50	129	139	108	27	52	20	5	13	7	9	12	29	19	21
CD1C2	26	7	64	45	67	84	88	15	21	11	7	12	3	10	7	28	11	14
CD1C3	24	12	44	31	53	71	57	9	18	3	3	1	5	6	3	28	12	3
CD28	232	730	857	185	481	339	328	1635	852	4975	3300	3616	2099	3177	5501	6615	1809	4076
CD36	2750	2680	2419	2450	2242	3207	2054	4940	2319	52	52	49	23	125	40	116	52	35
CD40	177	170	264	152	143	54	176	341	121	429	341	485	319	443	356	580	315	252
CD40L	76	224	164	88	123	108	92	582	227	355	249	329	257	375	345	643	213	380
CD49a	5199	4406	5099	5105	4765	6001	4451	10180	3479	991	911	1023	741	1189	1487	1132	437	804
CD49d	1789	3295	3267	1467	2409	2235	1874	7108	2665	6984	5270	5509	2783	5816	5718	7134	3195	5307
CD69	73	136	179	55	99	64	91	378	187	1867	1656	1145	1401	2924	3308	5453	1434	4199
CD86	1559	2375	2470	1398	2141	1998	1573	6061	3032	1551	1589	2140	2768	2548	2340	1805	1459	2457
CPT1B	39	31	37	27	22	39	22	42	18	36	27	36	15	50	27	73	27	28
CRABP1	84	221	136	298	157	246	259	399	116	7	22	36	26	24	6	129	31	3
CRABP2	308	630	585	347	371	529	349	687	177	82	118	85	45	184	51	187	72	71
CTLA4	21	34	72	13	23	24	20	53	47	471	153	248	173	190	633	446	92	320
CXCL8	1079	1935	1712	297	1591	571	718	2362	778	1423	2015	2785	1293	6812	2254	3158	1920	3765
CXCL9	118	2386	4170	106	1076	205	642	6874	4137	4504	2625	3724	4322	4859	8486	4184	1049	3333
CXCR1	526	474	475	404	775	721	529	1188	453	100	59	154	40	159	85	189	81	125
CXCR2	120	153	131	134	213	204	127	285	99	56	36	59	35	50	49	65	43	50
CXCR3	108	422	344	119	243	164	175	943	333	1092	981	1261	919	947	1566	1250	536	1011
CXCR5	37	34	45	30	32	27	44	119	47	1178	921	855	662	916	794	1604	1398	879
CYP26A1	431	270	246	320	281	260	222	513	60	68	49	78	43	59	63	92	61	79
CYP26B1	486	555	100	20	28	53	44	1067	30	93	110	223	90	320	45	47	32	62
DHRS3	2328	1996	1734	1925	1777	2284	1905	4465	1089	121	128	132	122	224	98	168	92	107
DHRS9	67	184	162	118	166	171	46	255	110	211	174	191	68	274	79	338	99	132
FABP5	4687	6516	6800	4874	5354	5711	4269	20552	7396	1753	1759	2608	2127	3513	2217	1998	880	3758
FOXP3	78	98	107	71	106	102	57	155	134	346	289	330	133	289	236	525	251	388
GATA3	1260	915	1053	1363	1047	1653	994	1809	630	220	170	196	104	178	176	272	103	199
GMCSF	46	55	82	53	50	63	50	100	45	31	35	33	30	39	49	49	26	39
HPGD	19924	13856	16503	23244	16976	22767	16239	25114	9064	19	24	21	15	26	22	17	21	28
ICAM1	196	214	249	140	165	176	166	750	254	407	466	644	781	960	688	462	318	586
IDO	2970	13610	18237	2794	8090	3121	5816	36933	11441	15996	13999	19535	15333	23404	26436	16486	7877	19247
IFNG	44	420	551	28	200	65	80	1166	378	5871	5139	5294	6977	7411	15365	7287	2255	10114
IL-12Rb2	58	113	123	50	88	97	69	594	134	457	334	552	393	474	618	957	167	542
IL-18	811	1040	916	889	1062	1098	946	1865	1105	513	556	572	277	833	497	683	464	708
IL-22	40	121	88	40	82	57	50	177	35	1022	1486	1611	1333	1628	2392	1144	624	2102
IL-23 p19	12	9	14	2	12	15	6	14	9	34	44	63	98	93	67	63	34	78
IL-23R	77	161	148	69	97	96	74	327	95	421	465	631	318	492	877	992	216	656
IL1-R1	3597	4644	4020	3726	3857	4719	3357	7824	2658	730	766	946	581	1372	626	1576	586	770
IL10	10	27	18	11	12	13	12	41	12	50	42	95	30	47	143	73	17	101
IL12A	34	34	27	20	29	25	31	68	25	46	30	42	39	55	98	53	19	46
IL12B	16	13	10	14	15	6	3	18	10	28	51	41	45	47	37	50	22	66
IL17A	8	17	14	6	16	7	8	21	5	72	73	86	56	125	66	114	64	148
IL1B	339	563	462	89	557	177	181	719	308	652	1168	1544	720	2538	987	1437	903	1998
IL2	5	16	11	5	16	13	8	14	10	12	24	13	10	6	11	26	7	16
IL21	9	61	112	3	26	6	16	126	44	488	196	255	147	238	800	415	88	231
IL2RA	75	175	228	49	131	62	81	255	141	1415	1103	1119	768	1048	1910	1480	554	1372
IL4	14	3	14	16	11	7	8	14	9	12	4	9	8	7	6	19	5	9
IL6	31	135	204	30	209	21	28	232	94	884	749	713	365	1762	1108	2078	622	759
IRF3	929	1113	1069	918	838	1119	817	1985	672	1162	963	1394	665	1742	1090	2138	807	1514
IRF4	183	328	559	127	257	272	284	548	532	2626	1691	1784	1210	2086	2177	4467	1206	2529
Interferon be	11	5	8	1	7	9	5	8	9	9	2	5	2	5	8	159	73	3
LCN2	428	461	430	293	478	441	292	1194	274	149	284	192	82	283	67	521	91	167
LPL	15119	8008	7763	11728	9008	10050	10125	13013	4355	279	339	264	171	451	123	525	330	292
LTA4H	2102	2623	2985	2318	2605	2832	2329	6083	2592	1360	1120	1308	827	1357	1355	1403	825	1247
MCP-1 (CCL	5791	5514	6562	3536	6013	3280	3610	20547	7348	3299	4661	5718	5278	7932	6243	5877	2907	4850
MCSF	1920	2162	2449	1830	1978	2417	1896	5060	1839	1953	1515	2133	1706	3419	2093	2783	1348	2031
NPC2	11621	14964	14599	12804	13761	15854	12732	32114	14716	2348	2587	3142	6263	4351	4171	3268	2403	4897
PCK1	65	115	139	92	73	110	80	204	69	124	80	100	70	90	98	133	68	85
PD-1	25	59	72	14	35	18	28	100	56	330	191	258	198	197	409	297	139	203
PD-L1	244	1329	1290	219	768	239	358	2512	990	3808	3329	3735	2925	4513	4991	5312	1711	3151
PKC-theta	514	854	1116	737	880	832	772	1482	681	2579	1851	2151	1075	1905	2302	3368	969	2395
PPARD	743	862	983	720	766	906	715	2256	842	522	413	558	456	860	451	689	299	636
PPARG	260	254	258	232	238	283	180	439	256	33	15	28	27	29	21	42	28	24
PTGER2	172	274	259	113	263	215	165	473	221	350	317	466	321	382	481	470	190	462
PTGER3	211	199	220	194	245	253	171	441	151	81	67	36	14	43	34	130	35	42
PTGER4	981	1237	1290	781	1231	1082	966	1964	964	2114	1685	1629	1215	2091	2084	3023	1873	2389
PTGES	23	62	81	21	37	34	33	84	26	123	125	234	121	294	220	209	91	268
PTGS2	234	269	343	182	244	289	182	671	164	600	470	622	739	1160	1194	1053	345	813
RARA	627	571	698	563	696	831	660	1730	620	245	200	260	189	328	219	344	178	276
RARB	149	161	121	127	127	161	136	201	42	30	21	47	21	36	20	117	50	26
RARG	929	819	929	753	786	978	711	1680	530	248	148	240	137	239	155	321	117	221
RBP1	879	1254	1116	737	963	931	870	3043	868	1005	1209	1242	890	1789	1286	1189	803	1108
RDH10	1118	1135	1140	1123	1011	1359	970	2167	866	780	699	872	531	944	713	1376	411	798
RORC	355	329	388	306	215	460	287	752	258	446	281	591	150	381	347	511	153	339
RXRA	456	427	534	377	450	486	386	1312	490	86	98	128	113	219	137	147	82	155
RXRB	178	186	206	170	150	220	194	341	120	148	96	102	97	157	144	174	86	115
RXRG	176	174	263	331	194	279	206	205	99	4	2	3	2	1	2	27	17	3
SOCS3	1350	1904	1744	1083	1626	2261	1480	3923	1194	3379	2717	3149	2483	4535	4271	5755	3433	5766
STAT1	4149	11712	12723	4994	8557	5574	5999	32813	11840	14418	11401	12333	8386	14888	12245	16454	7826	12569
STAT3	2862	3117	3510	2799	2852	3331	2835	7723	2753	2418	1825	2191	1622	2422	2235	2978	1528	2517
STAT4	143	251	283	140	188	228	150	645	222	628	449	558	269	507	647	903	192	596
STAT5	2355	2340	2916	2146	2142	2855	2337	5092	1959	3091	2278	2916	1680	2669	3304	4219	1815	3123
STAT6	3615	3742	4292	3472	3759	4644	3116	10137	3529	2528	1809	2589	1504	2868	2283	2905	1528	2692
STRA6	16	15	26	15	15	17	10	35	17	46	32	44	28	42	41	43	36	47
TBX21	1358	1443	1590	1066	1767	1496	1455	2964	1173	2029	1504	2134	1393	1890	2517	2338	789	2212
TGFB	912	1000	957	680	973	998	807	2674	1072	1306	1063	1390	1348	1388	1446	1464	977	1579
TNFA	128	216	226	80	192	120	166	633	289	562	475	760	829	903	995	804	316	982
TNFR1	2204	2421	2521	2121	2313	2728	2340	6388	2074	823	759	1033	1061	1315	1107	1222	742	1052
klrg1	817	911	837	602	999	836	587	1340	524	785	1141	1007	529	1067	1208	822	347	1066
ACTB	101124	137282	149605	113997	133060	146618	119628	331874	135356	129025	116156	127371	91251	117819	136882	130538	91449	142799
GAPDH	4806	7910	9010	4966	6401	6030	6026	19093	7069	5521	5193	5742	4870	6618	6724	6520	3446	6082
HPRT	1178	1411	1660	1042	1267	1412	1171	2771	1378	951	821	1000	608	1021	855	1150	456	863
SDHA	2006	2455	2597	2394	2392	2961	2352	4971	2013	1220	1021	1072	699	1198	1241	1360	731	1035
TBP	823	855	904	840	828	881	730	1694	708	734	537	663	404	654	585	806	385	606
NEG_A	10	6	12	9	10	12	6	10	9	9	8	5	5	5	6	8	11	7
NEG_B	6	3	5	4	4	11	4	7	1	3	1	4	4	2	5	1	3	1
NEG_C	2	1	7	3	7	3	1	1	6	2	1	5	1	1	2	4	4	1
NEG_D	5	4	3	5	3	6	5	7	3	1	3	2	3	4	5	2	1	6
NEG_E	8	19	9	19	12	11	12	9	7	13	7	11	8	13	13	18	9	9
NEG_F	17	20	25	12	25	24	6	23	12	23	13	11	12	19	14	13	10	14
NEG_G	2	3	1	1	4	3	4	1	4	1	7	1	2	4	5	9	2	2
NEG_H	4	11	4	2	3	8	3	3	5	4	5	4	4	6	1	6	3	5
POS_A	49959	54914	53785	48305	49546	50145	47684	48985	42098	43149	41600	41264	43142	43684	39303	43750	36283	34617
POS_B	16664	18453	17674	15873	16494	16873	15445	14426	13453	13942	14048	13388	14145	14447	12924	14333	12833	12148
POS_C	4500	5215	4982	4350	4518	4688	4253	3975	3771	4008	3773	3725	3883	3961	3534	3938	3475	3225
POS_D	1108	1316	1218	1068	1155	1141	1059	1022	929	984	967	926	981	1054	907	998	861	814
POS_E	175	230	215	192	193	233	187	176	150	177	177	155	175	180	185	168	118	135
POS_F	68	93	81	74	68	68	61	66	52	51	45	62	58	78	48	65	53	41

Probe Name	VAD2.09.LN	VAD2.12.LG	VAD3.08.LG	VAD3.01.LG	VAD3.02.LG	VAD3.03.LG	VAD3.04.LG	VAD3.05.LG	VAD3.09.LG	VAD3.10.LG	VAD3.11.LG	VAD3.12.LG	VAD3.13.LG	VAD3.14.LG	VAD3.15.LG
A4B1	4687	6722	7506	10901	9566	9231	7168	5010	12661	10308	7220	7947	9789	7577	8790
A4B7	6079	1382	888	1951	3535	2380	1859	1444	1643	1156	1473	1289	1460	855	1261
ABCG1	62	75	23	34	115	74	59	52	46	55	49	39	63	47	69
ADH1C	13	174	163	122	173	169	130	89	444	255	336	227	511	336	559
ALDH1A2	79	1218	525	1388	1124	963	618	416	1815	1789	1196	1365	1541	1197	1438
ALDH1A3	162	2352	2259	2350	1732	2262	1828	1898	3505	2846	2330	1924	2708	2306	2065
ALOX12	8	29	13	28	40	34	19	51	42	34	26	27	37	28	30
ALOX5	13	315	381	535	563	403	278	97	1000	768	542	687	737	595	765
BCL6	427	413	344	511	628	574	311	383	630	478	394	434	414	339	397
Blimp-1	1385	592	448	823	1107	869	943	469	788	795	576	505	713	530	658
CCL5	26402	3362	10240	15017	23571	11665	10245	11176	18520	11596	10888	10619	11655	15365	11521
CCR1	863	172	237	557	661	390	320	285	387	438	574	552	602	429	468
CCR2	704	319	305	610	1372	825	467	536	478	357	494	447	376	342	480
CCR4	87	81	69	146	198	205	184	32	132	127	84	96	88	74	93
CCR5	1749	454	623	1097	1833	1306	837	997	712	428	818	604	655	326	667
CCR6	1560	202	108	333	369	327	299	91	270	203	245	180	256	150	238
CCR7	577	681	493	702	907	707	568	389	879	874	794	721	965	627	798
CCR9	30	13	16	36	28	22	20	23	45	22	21	17	23	25	25
CD103	320	164	32	193	112	135	141	40	103	54	67	89	94	41	61
CD1B2	16	15	33	77	145	118	35	30	18	19	55	12	22	14	28
CD1B4	13	166	4	20	60	55	33	13	23	58	10	15	14	29	20
CD1C2	15	95	3	10	34	67	31	14	30	43	12	15	10	24	10
CD1C3	3	50	4	8	17	37	14	5	16	42	6	11	6	16	7
CD28	3506	226	326	664	950	735	763	272	386	312	463	293	558	207	391
CD36	74	1765	1287	1210	2394	1550	1032	917	2311	2570	1707	2284	2885	1765	2148
CD40	444	109	92	157	164	96	94	15	122	143	113	89	205	31	41
CD40L	272	47	134	208	321	188	177	129	237	95	180	121	183	77	217
CD49a	768	2729	2678	3933	3967	3163	2822	1427	5560	5192	2695	3323	4553	3180	4640
CD49d	4863	741	1178	2263	3019	2044	1586	1176	1891	1493	1781	1775	2051	1040	1813
CD69	3524	62	40	92	192	114	138	53	74	103	88	86	130	53	102
CD86	2312	1194	1042	1855	3685	2095	1622	1165	1738	1417	1499	1611	1716	1010	1591
CPT1B	20	19	9	16	17	14	18	18	25	21	13	12	30	11	14
CRABP1	8	165	79	158	88	105	80	25	175	100	94	73	99	131	135
CRABP2	60	191	235	332	276	259	147	136	444	327	220	266	372	512	301
CTLA4	306	24	18	43	41	41	43	22	16	14	14	14	21	12	13
CXCL8	2895	537	237	442	658	548	549	198	428	711	638	495	756	358	640
CXCL9	5129	1419	751	1213	5473	2700	1592	1361	721	609	1690	805	1472	440	1237
CXCR1	146	338	274	331	438	660	309	403	766	418	486	629	568	507	488
CXCR2	58	72	65	85	99	180	93	140	198	116	86	148	166	103	95
CXCR3	874	93	223	352	467	357	249	152	190	104	257	175	237	116	155
CXCR5	1203	16	34	129	62	37	42	40	48	48	55	65	60	34	39
CYP26A1	56	98	133	149	112	116	84	60	244	336	259	182	337	253	218
CYP26B1	59	10	360	305	26	33	19	8	508	265	469	603	735	536	323
DHRS3	99	939	1269	1707	1316	1136	922	495	2379	2108	1694	1958	2329	1930	1852
DHRS9	125	114	51	165	195	126	83	71	88	79	97	75	38	31	53
FABP5	2260	4206	5217	9129	10030	7949	5804	3803	7697	7140	5578	6404	4800	4903	5972
FOXP3	282	71	26	93	53	71	116	26	100	57	47	74	70	63	70
GATA3	139	686	541	756	729	549	585	290	1236	1281	758	869	1103	843	995
GMCSF	39	38	11	28	44	22	22	8	40	39	31	31	46	29	31
HPGD	19	12184	6376	6612	8825	8118	8128	3785	11006	17215	14038	9734	20121	11038	13785
ICAM1	711	132	494	736	437	602	400	771	416	155	267	199	138	248	246
IDO	15356	3604	4645	8359	17526	10770	5095	9466	2399	1564	8422	5242	4644	1665	5251
IFNG	5172	125	133	298	467	387	260	327	88	82	348	114	181	57	174
IL-12Rb2	383	60	180	136	231	240	100	357	169	52	79	34	73	47	79
IL-18	667	623	266	509	1070	641	596	284	818	904	568	761	816	601	772
IL-22	1299	61	26	53	70	47	31	51	38	38	55	37	50	30	24
IL-23 p19	105	10	12	6	12	7	1	8	12	10	5	10	5	3	10
IL-23R	487	93	49	38	206	119	35	35	50	39	55	33	75	23	103
IL1-R1	713	2698	1178	1624	2940	2137	1395	884	3426	4347	2190	2404	3816	2544	3468
IL10	73	19	11	12	17	9	12	8	9	14	6	8	7	6	11
IL12A	32	16	22	28	40	19	23	14	34	28	40	21	24	27	26
IL12B	61	11	5	11	19	9	14	9	11	10	4	9	7	2	4
IL17A	87	8	5	13	13	14	10	4	9	7	11	5	10	5	7
IL1B	1244	181	119	379	398	235	291	200	111	150	234	117	180	91	291
IL2	8	13	12	12	22	9	12	8	12	8	9	10	15	10	12
IL21	243	31	19	48	62	39	42	15	10	20	29	8	34	4	19
IL2RA	1009	123	66	120	134	126	84	52	64	68	97	69	96	64	93
IL4	5	7	5	9	11	4	8	7	4	6	2	5	10	6	6
IL6	780	77	27	124	87	100	103	88	26	22	70	34	35	18	46
IRF3	1258	635	379	705	800	799	647	485	968	737	393	442	696	379	627
IRF4	2690	259	199	304	429	415	386	100	270	234	235	202	219	137	186
Interferon be	7	1	3	2	7	10	2	6	5	3	1	2	4	2	10
LCN2	86	260	189	293	302	433	278	393	474	274	215	323	272	168	226
LPL	335	6776	3020	4386	4669	4279	3282	2580	7111	7787	5535	5431	8562	5244	5797
LTA4H	1132	1777	961	1555	3262	1632	1215	694	2170	2230	1953	1856	2414	1607	2048
MCP-1 (CCL	4391	3581	2667	5627	7843	5364	5252	2652	4351	4421	4381	3313	4486	2358	3001
MCSF	1933	1180	1020	1730	2215	1833	1189	1218	2217	1662	1278	1446	1779	1140	1589
NPC2	5004	8967	5848	8802	17429	9511	6941	4124	13853	14796	10660	11727	12802	10501	11104
PCK1	78	57	50	70	109	69	54	37	61	80	63	53	98	55	61
PD-1	283	43	31	80	44	67	73	28	28	15	37	20	25	13	21
PD-L1	3673	402	169	518	1099	543	529	293	256	270	606	381	535	181	549
PKC-theta	1730	608	300	482	976	616	607	278	766	624	456	451	730	401	610
PPARD	510	524	506	911	1078	790	590	444	871	755	671	698	857	639	699
PPARG	17	149	116	135	317	180	180	75	242	241	165	188	265	185	215
PTGER2	300	66	117	192	299	174	112	81	192	185	166	179	153	135	188
PTGER3	33	167	110	179	209	159	103	89	320	233	87	179	231	170	161
PTGER4	2059	614	272	595	1110	617	415	222	825	1004	557	737	956	505	735
PTGES	316	28	44	49	49	66	40	38	37	19	39	24	30	20	33
PTGS2	909	141	80	149	222	163	169	102	115	156	121	124	116	100	197
RARA	234	407	483	739	799	697	661	586	1057	585	414	497	585	555	592
RARB	25	58	49	70	63	45	34	23	130	143	85	121	141	121	135
RARG	165	365	387	541	565	432	315	274	1063	813	582	715	935	765	780
RBP1	968	325	669	1792	716	838	605	423	1691	865	1154	1107	832	881	1334
RDH10	769	769	658	973	995	1000	701	604	1441	1081	641	708	957	652	896
RORC	274	308	155	267	399	291	241	149	400	254	224	174	323	220	305
RXRA	116	300	419	580	571	545	462	381	706	420	371	382	475	407	385
RXRB	103	123	63	132	146	131	94	74	186	181	127	114	202	158	154
RXRG	1	154	72	64	76	71	57	18	140	170	90	147	166	111	134
SOCS3	4033	1385	349	800	1385	848	611	721	646	1037	945	948	691	742	910
STAT1	10791	4135	6561	11989	15505	11793	7639	5967	6979	4299	9221	5811	6366	3607	7005
STAT3	2095	1869	1636	2499	3090	2692	1859	1685	3235	2576	2289	2319	2666	1955	2394
STAT4	434	59	131	171	296	207	178	118	227	150	144	117	243	91	182
STAT5	2372	1689	1086	1628	2522	1792	1293	1159	2277	1765	1421	1517	2072	1460	1681
STAT6	2070	2793	2646	3310	4510	3742	2631	2370	4780	3656	2523	2826	3578	2519	3016
STRA6	34	8	5	14	17	11	12	5	15	10	15	8	12	10	16
TBX21	1566	347	457	715	1537	515	555	382	1492	1522	762	905	1488	1085	1122
TGFB	1269	465	1140	1586	1299	1156	820	909	1210	738	906	849	694	658	778
TNFA	839	105	153	274	362	297	210	169	187	98	154	117	126	116	140
TNFR1	1018	1301	1188	2170	2562	1952	1564	1144	2660	2212	1699	2026	2051	1712	2028
klrg1	758	142	305	429	669	356	322	210	845	770	491	546	978	560	700
ACTB	95643	81968	55754	97722	162777	101709	72622	54003	115885	119048	93100	94011	108573	83589	97794
GAPDH	4904	4018	5285	10173	9116	7397	6384	6170	7534	5334	5777	4800	4607	4536	4742
HPRT	843	839	475	769	1624	955	793	497	1048	1207	760	908	1370	664	1245
SDHA	963	1470	1000	1672	2514	1623	1281	715	2786	2467	1755	1941	2660	1887	2039
TBP	495	517	323	500	757	556	410	231	824	812	566	495	795	589	670
NEG_A	9	8	3	5	14	6	4	7	10	9	14	7	4	9	6
NEG_B	2	2	4	6	8	7	6	2	2	5	5	4	2	3	5
NEG_C	4	2	5	3	6	7	4	1	5	4	3	5	4	3	3
NEG_D	2	2	1	4	4	2	5	3	3	2	7	3	4	3	3
NEG_E	12	11	5	15	11	11	11	11	9	13	10	18	10	7	16
NEG_F	13	9	15	20	17	25	8	11	14	12	14	12	7	17	14
NEG_G	3	2	3	2	2	3	2	2	6	1	4	1	4	2	7
NEG_H	3	3	1	5	6	3	2	4	3	3	3	4	1	2	1
POS_A	33957	38194	43552	57298	51644	55842	34859	51310	60638	46398	45550	40684	27094	46339	40584
POS_B	11122	12444	14080	18123	16723	18046	9904	15881	18943	15275	14541	13312	7670	14522	12839
POS_C	2925	3464	3821	5222	4604	4903	2871	4385	5109	4213	4121	3538	2252	4025	3596
POS_D	798	933	962	1256	1202	1275	831	1042	1359	1071	994	907	630	1052	901
POS_E	137	138	173	227	196	208	118	194	245	194	195	146	85	158	167
POS_F	54	64	72	90	62	61	50	78	82	57	63	57	33	61	43

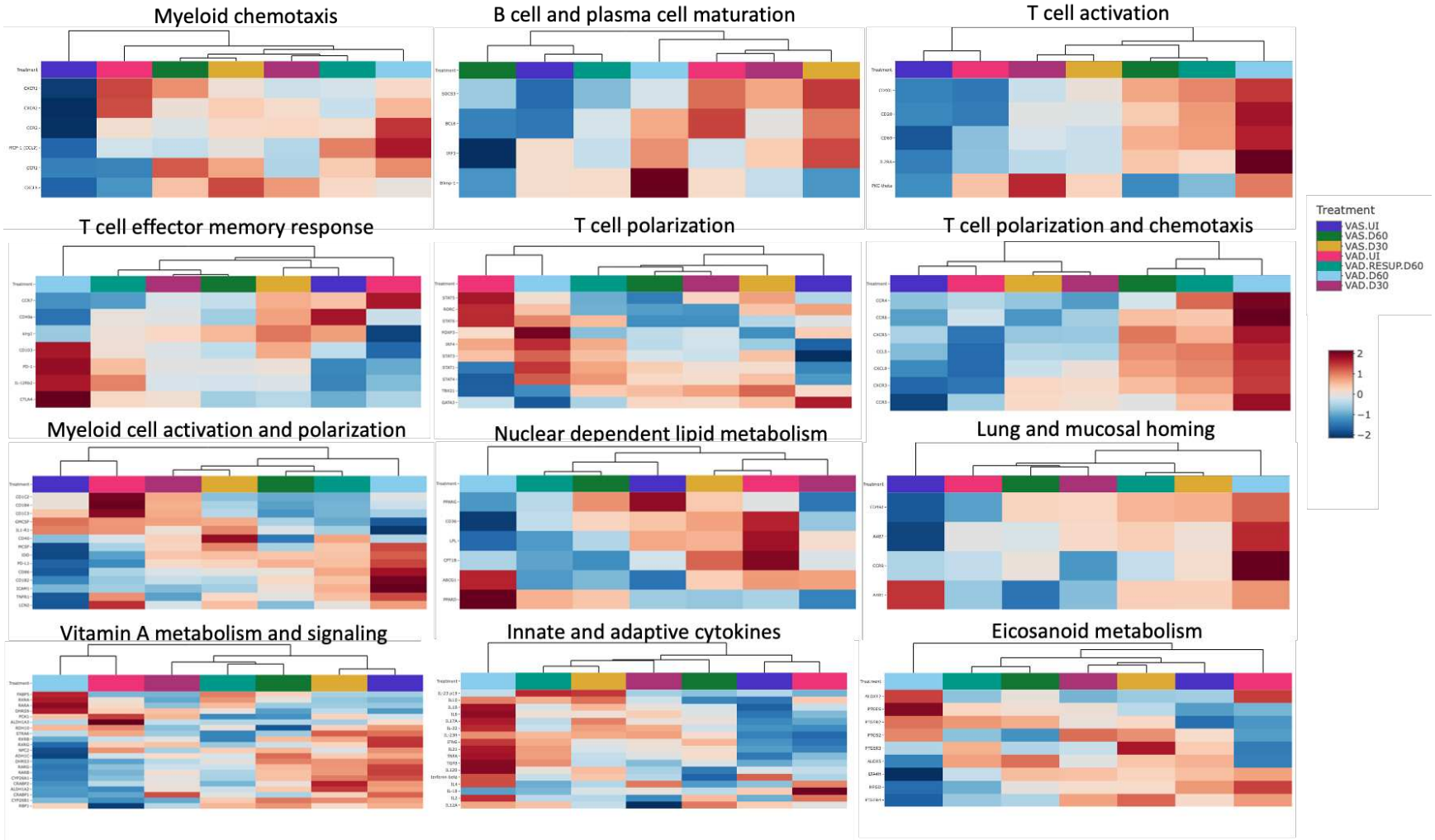

Supplementary figure S6. Unsupervised cluster of all vitamin A sufficient, vitamin A deficient and vitamin A deficient resupplementation groups.

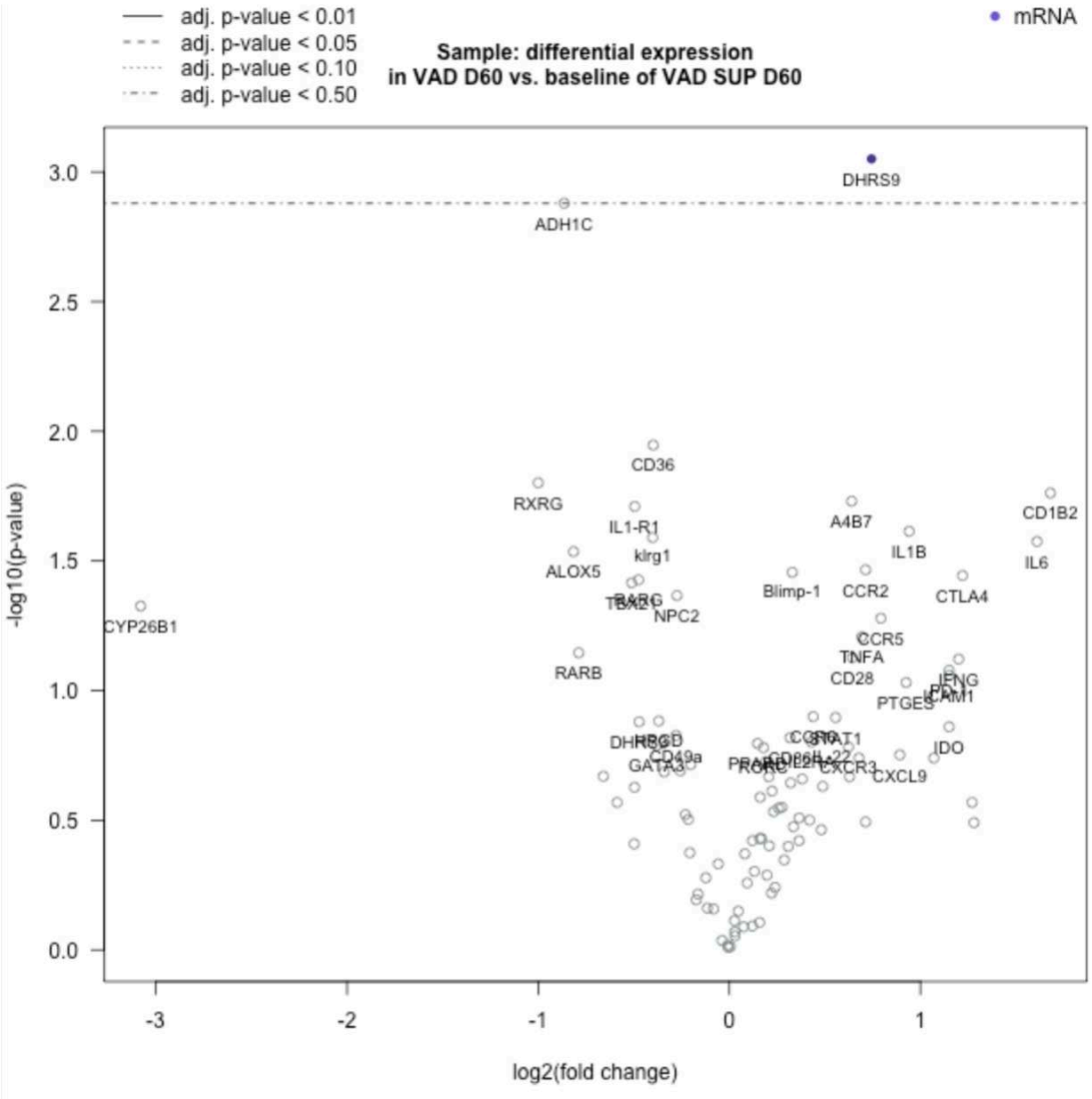

Supplementary figure S7. Volcano plot with gene expression fold changes of VAD compared to VAD resupplement animals

Supplemental work material for chapter 2:

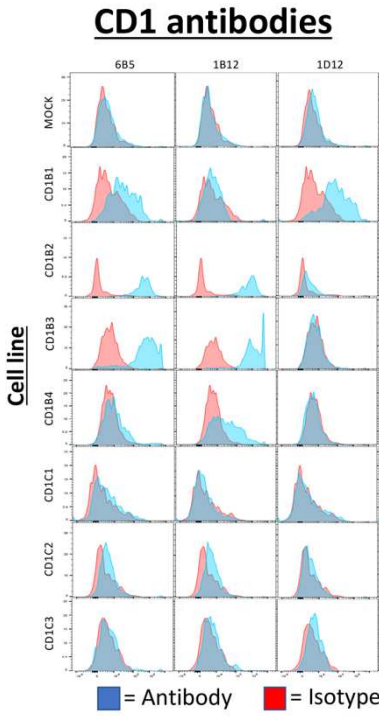

Supplement Figure S8. CD1 ortholog specificity of monoclonal antibodies. 104C1-transfected fibroblasts transfected with specific CD1b and CD1c orthologs were labeled with each anti-CD1 antibody to determine ortholog specificity. The non-specific P3 antibody clone was used as an isotype control.

Table S3: Collaborator provided antibodies to cross reactivity of specific CD1 isoforms

CD1 antibody	CD1 isoforms detection
P3	Negative isotype control
1B12	CD1B2, CD1B3, CD1B4
1D12	CD1B1
6B5	CD1B1, CD1B2, CD1B3, CD1B4
BCD	CD1B2, CD1B3, CD1B4, CD1C3
MsGP3	CD1b3

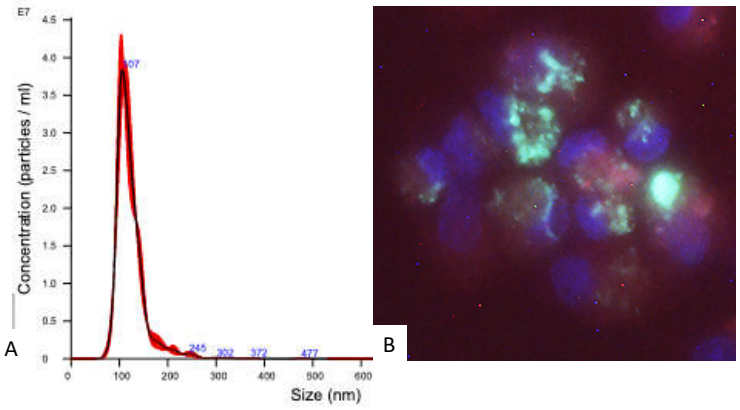

Supplemental figure S9. Liposome size and cellular uptake. A) Particle size analysis of liposomes formulated using the Avanti extrusion process. Particle size was analyzed using a Nanosight, instrument. B) Fluorescent microscopy of CellVue labelled liposomes (green) incubated with bone marrow derived macrophages (dapi labelled) and lysotracker dye (red) to define acidified compartments.

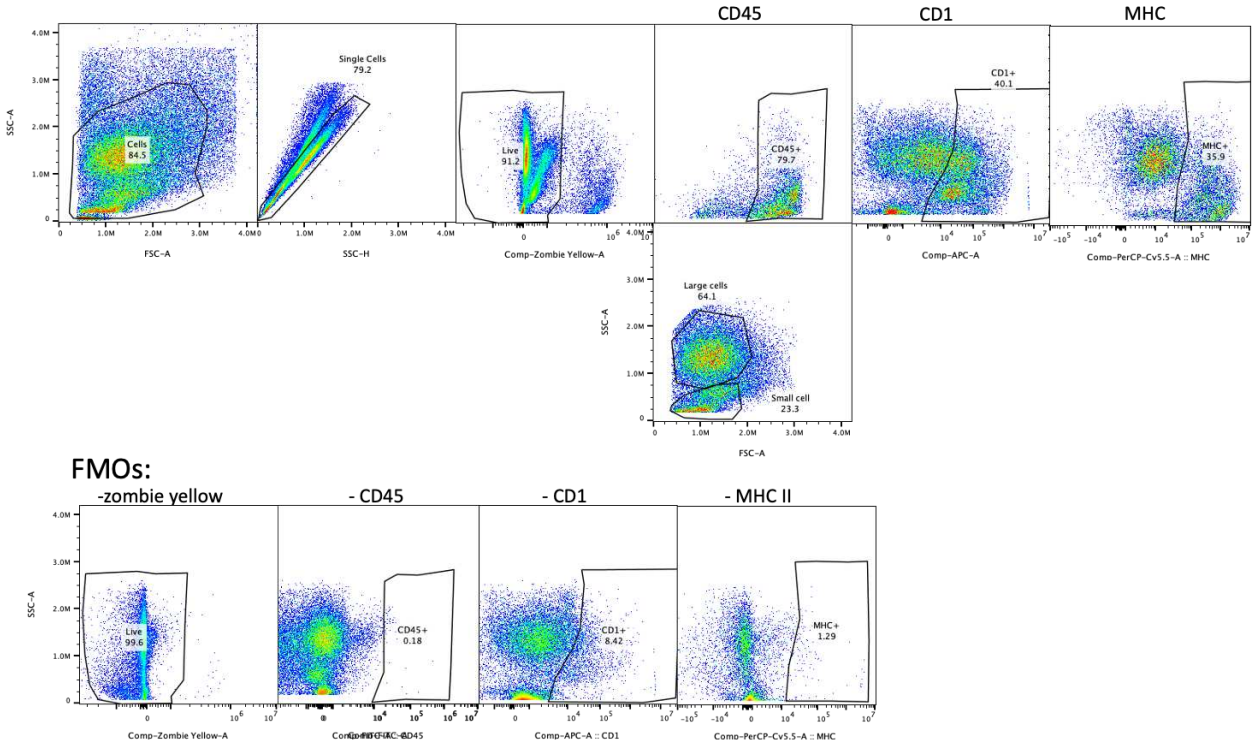

Supplemental Figure S10. CD1 expression gating strategy. Initial gating on scatter parameters and single cells identifies the cell population of interest. This population is gated on viable cells only by excluding those that accumulated Zombie Yellow permeability dye. Leukocytes are the identified by CD45, evaluated in total or by large and small leukocyte scatter gating for cells expressing CD1 and/or MHC II.

Table S4. Antibody and associated fluorophores utilized in flow cytometric assessments

Antibody	Fluorophore	Clone
CD45	FITC or PE	IH-1
MHC-II	PE-cy5.5	IVA12
CD11	PE	MIL4
CD1	PE-Texas red or APC	1B12

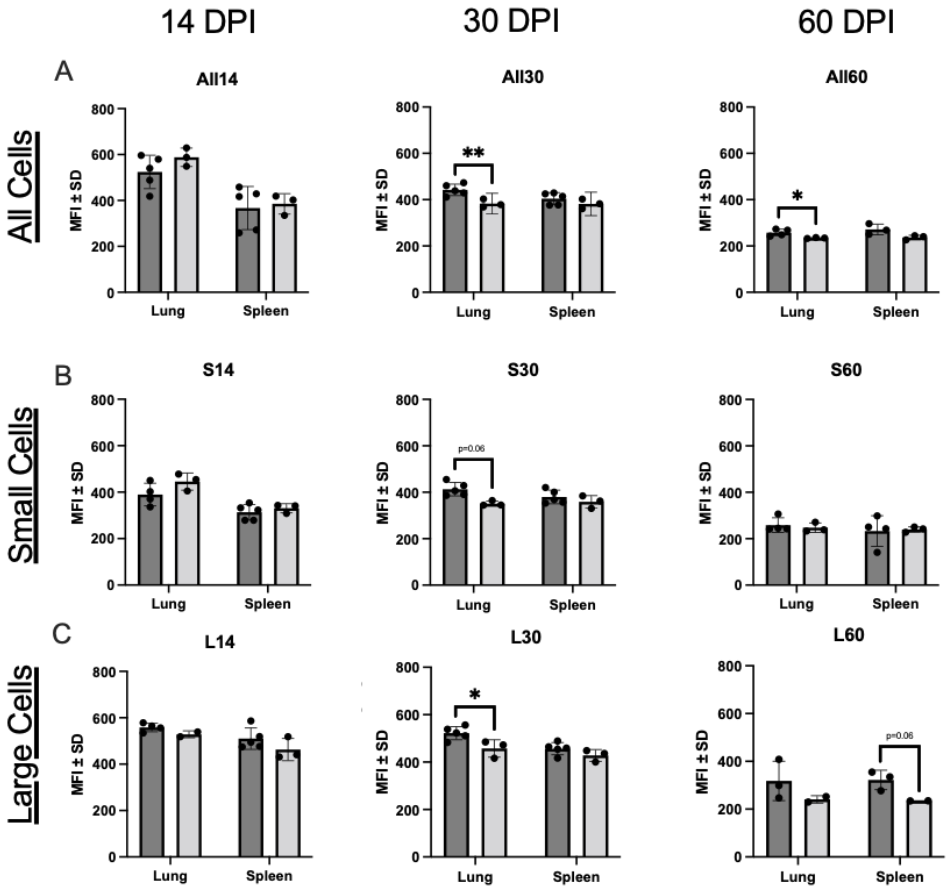

Supplemental Figure S11. Kinetic median fluorescence intensity of naïve and infected animals. Mean fluorescence Intensity (MFI) from 14, 30 and 60 DPI of CD1-expressing cells as gated in 1 B-D; (A) MFI of all CD45+ cells derived from lung and spleen (B) CD45+ large cells, (C) CD45+ small cells. Two-Way ANOVA multiple comparison with a tukey correction, (E-G) a non-parametric Kruskal-Wallis test with a Dunn correction.

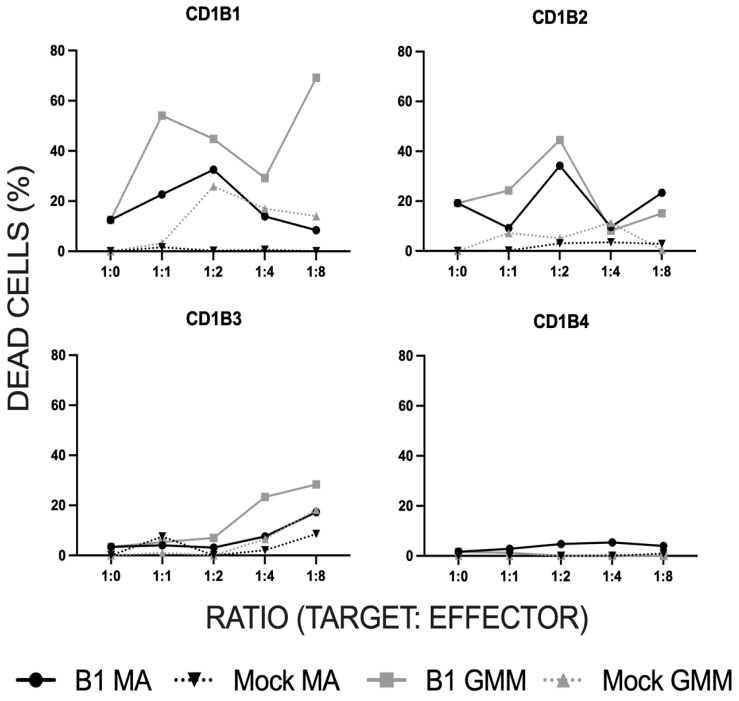

Supplemental Figure S12. Cytotoxicity pilot study. All CD1b ortholog transfectants (target cells) were incubated with cells isolated from infected lung. Cells were incubated in increasing ratio of Target to Effector cells (1:0 to 1:8) for four hours. Target cells were loaded with glucose monomycolate or mycolic acid Mtb lipids or mock loaded as a control for lipid antigen specificity. Mock transfected fibroblasts were used as a control for CD1-restricted activity (data not shown).

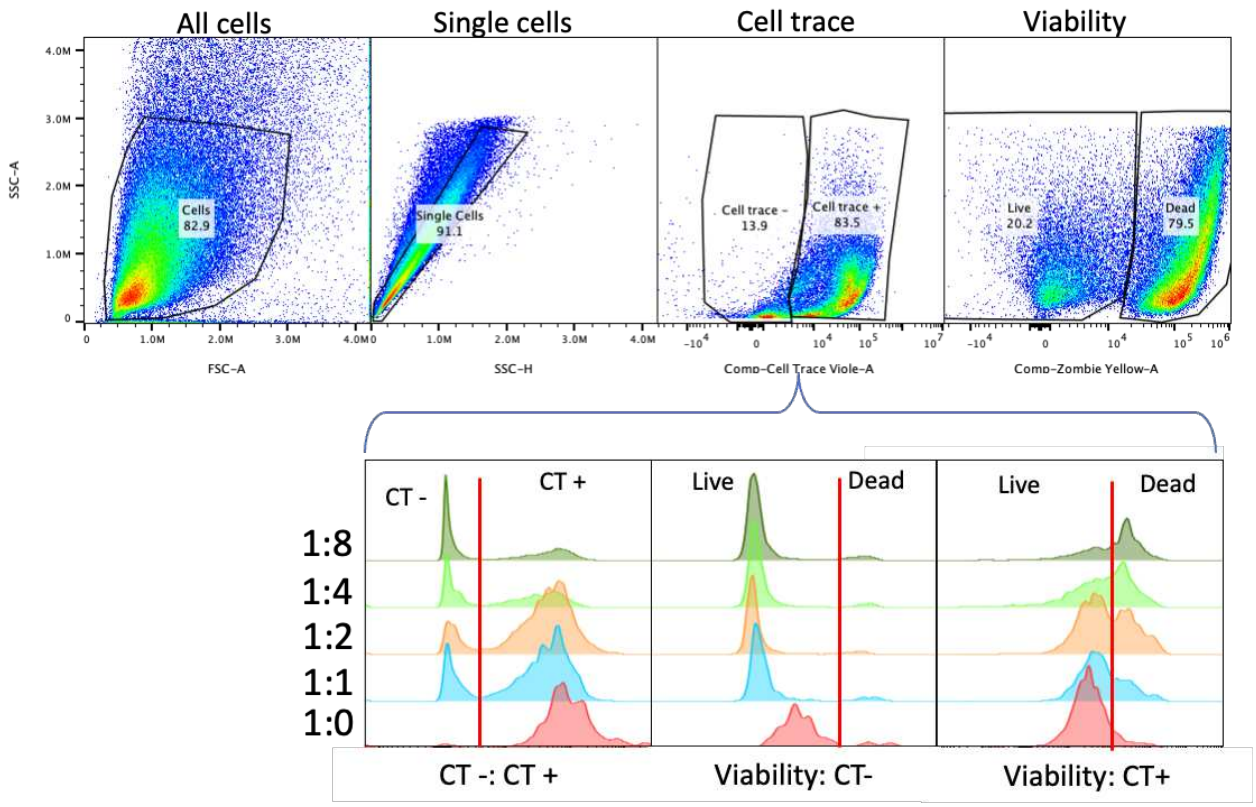

Supplemental Figure S13. CD1 cytotoxicity gating strategy. A) Initial gating identifies the cell population of interest and single cells. Single color CellTrace Violet is used to identify guinea pig fibroblast transfectants. CellTrace Violet positive cells represent the target cells for the cytotoxicity assay and are assessed for overall viability in all samples. B) Histogram demonstrate the changing ratio of CellTrace Violet positive cells (target cells) to CellTrace Violet negative cells (effector cells) within different target to effector cell samples. The other two histograms demonstrate a representative sample of viability with cell trace negative cells (effector cells) (C) and cell trace positive cells (target cells) (D) in differing ratio conditions.

Table S5. Denovo CD1 ortholog specific Primer sequences

CD1b Isoform	Sequence
CD1b1 forward	ACA GTG GCC AAC TTC TGT CC
CD1b1 Reverse	ATA GTG CCT GTG TCG CTG TC
CD1b2 Forward	GAG TTG CAT TCT GGA GGA GC
CD1b2 Reverse	CCC AGC TTC TAG GAC ACT CA
CD1b3 Forward	ACA AAA GCC CAC GTG AAT GC
CD1b3 Reserve	GTC CAG TCC TCC AAA GGC TC
CD1b4 Forward	GGC TGG TTG GGA GAT ATG GA
CD1b4 Reserve	TTC TGG GCT TCT CTG ACG AA

CD1B1 Gene block: (PCR product: 129)

```
  1 atgctgctcg tggcactggc attgcttgca tttctcttcc ctgctggtga cactcagaat
 61 gccttacagt ggccaacttc tgtccatggc atccaaatct catccttttt caaccatacc
121 atggcacaaa gtcgatgctc aggctggttg tcccgcagat ctccaggaaa tatggagctt
181 ggtagctttg acagcgacac aggcactatc atatttaaga aaccctggtc taaagcaaac
241 ttcagcaatg aagaggtttt ggagttggag gagctatttc aagtctacat gttgggattc
301 atcagagaag tacaggaacg tatgagcgat ttccagatgg aatatccctt tgagatccag
361 ggcattgcag gctgtgaact gatttctgga ggaaccattg atttcttcct gagaggagct
421 ttagagggac tagatttctt gagtattaag aattctacat gttggcctgc cccagaaggt
481 ggcaccaagg caaaaaaatt
```

CD1B2 Gene block: (PCR product: 225)

```
  1 attttggaaa tggaggagtt atttcgactc tacttcttag gatttgttaa agaagtccag
 61 gaacttgtca gtgatttcca gctggaatat ccttttgaga tccagggcat tgcaggctgt
121 gagttgcatt ctggaggagc cattgtaagc ttcttgatgg gagctataga aggactgcat
181 ttcatgagca tcaataatta ttcatgtttg tcccgcagat ctccacctgc cccagaaggt
241 ggtaccaggg cacagaaatt ctgtgcacta atcttacagt acaaaggaat ttgtgatatt
301 gtggaaaatc tcctcacaaa agtttgcccc agatatctga tgagtgtcct agaagctggg
361 aaggcagctc tgcagaagca cgtgaagcct gaggcctggc tatcccaggg acccagcccc
421 gagcctggct atctgcagct ggtgtgccac gtctctggct tctacccaaa gcctgtgtgg
481 gtgatgtgga tgagaggtga
```

CD1B3 Gene block: (PCR product: 171)

```
  1 tgggtgaaat atcaactctc aggctggttg ggagatttgc agattcatgg catggacagt
 61 gattcaggca ctgccatatt cctgaagccc tggtctaagg gcaacttcag caatgaagaa
121 atgtctgaag tggtggagct atttcgggtc tatatcgttg cattcattcg agaaacaaaa
181 gcccacgtga atgccttgca gatggaatac tcccgcagat ctccaccttt tgagatccag
241 ggcattgcag gctgtgagct gcattctgga ggtgccattg taagcttttt gcaaggagcc
301 tttggaggac tggactttgt gagtttcaag aattcttctt gtgttcctgc cccagaaggt
361 ggcagcaggg cacagacagt gtgcaaacta cttgctccat atcatgatat cttctacact
421 gtggagaagc tgctgtatga aacctgtcct caatatctct tgggtgtcct tcaagcagga
481 aaggcagatc tacacaggca
```

CD1B4 Gene block: (PCR product: 125)

```
  1 atgctgctcc tggccctggc attttttttc ccagctggtg acactcagaa cgttttgccg
 61 gggaaaattt ctttctatgg catccaaatc tcaacgtttt tcaaccatac cgtggtagag
121 aatcgaggat caggctggtt gggagatatg gagattagca gctgggacag tgaaaaagaa
181 actatcatat ttcggaaacc ctggtctaaa tcccgcagat ctccaggcaa cttcagcaat
241 gacgagattt tggaggtgga agagatattt caagtctact tctttggatt cgtcagagaa
301 gcccagaaac atatgagtga tttccaggtg gaataccct ttgagattca ggtcatctca
361 ggctgtgagg tgaactctca cagatccttt gattacttca tgagggtagc agtaaaggga
421 ttggatctcc tgagcatcaa gaatcattca tgttggcctg ccccagaagg tgtttctaga
481 gcacaggaaa tctggacatt
```

Segment gene Rv0733 in Mycobacterium tuberculosis H37Rv:

Tcccgcagatctcca

Supplemental figure S14. CD1b ortholog-specific gBlock sequences: 500 basepair GeneBlock sequences were synthesized to match each specific region of cDNA for CD1b1, b2, b3 and b4, then used for development and specificity confirmation of the primer sequences listed in Supplemental Table 3. Yellow highlighted regions represent the annealing sites for each forward and reverse primer set. Purple highlighted regions represent an inserted region of the Mtb Rv0733 gene, used to distinguish GeneBlock DNA from tissue-derived cDNA PCR product, in the event of contamination.

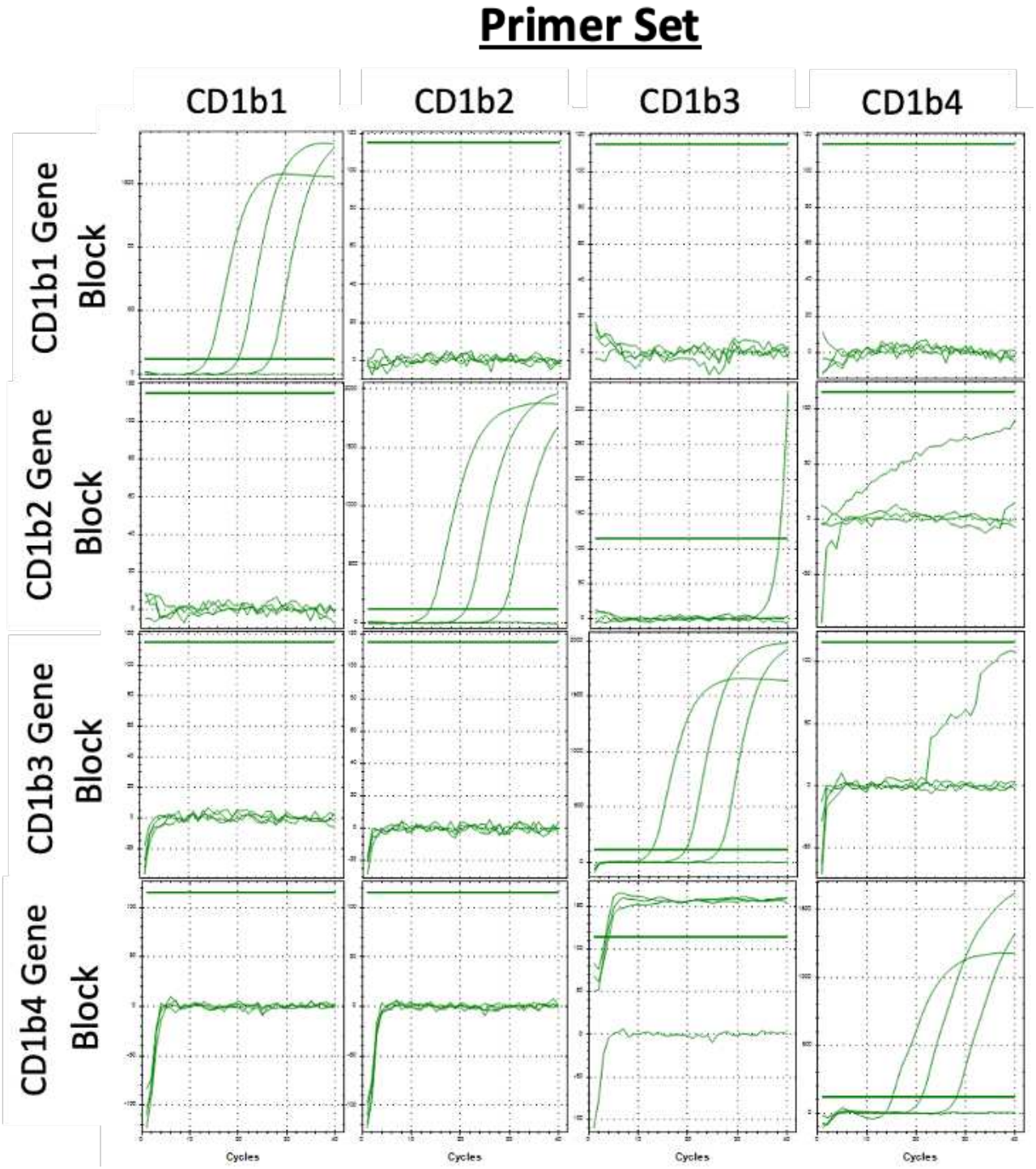

Supplemental figure S15. Confirmation of CD1b ortholog primer specificity. CD1b ortholog-specific primer pairs designated in Supplemental Table 3 were assessed for specificity against each targeted CD1b ortholog using gBlock synthetic sequences shown in Supplemental Figure 6. A checkerboard approach was used to confirm the specificity of each primer pair by qPCR.

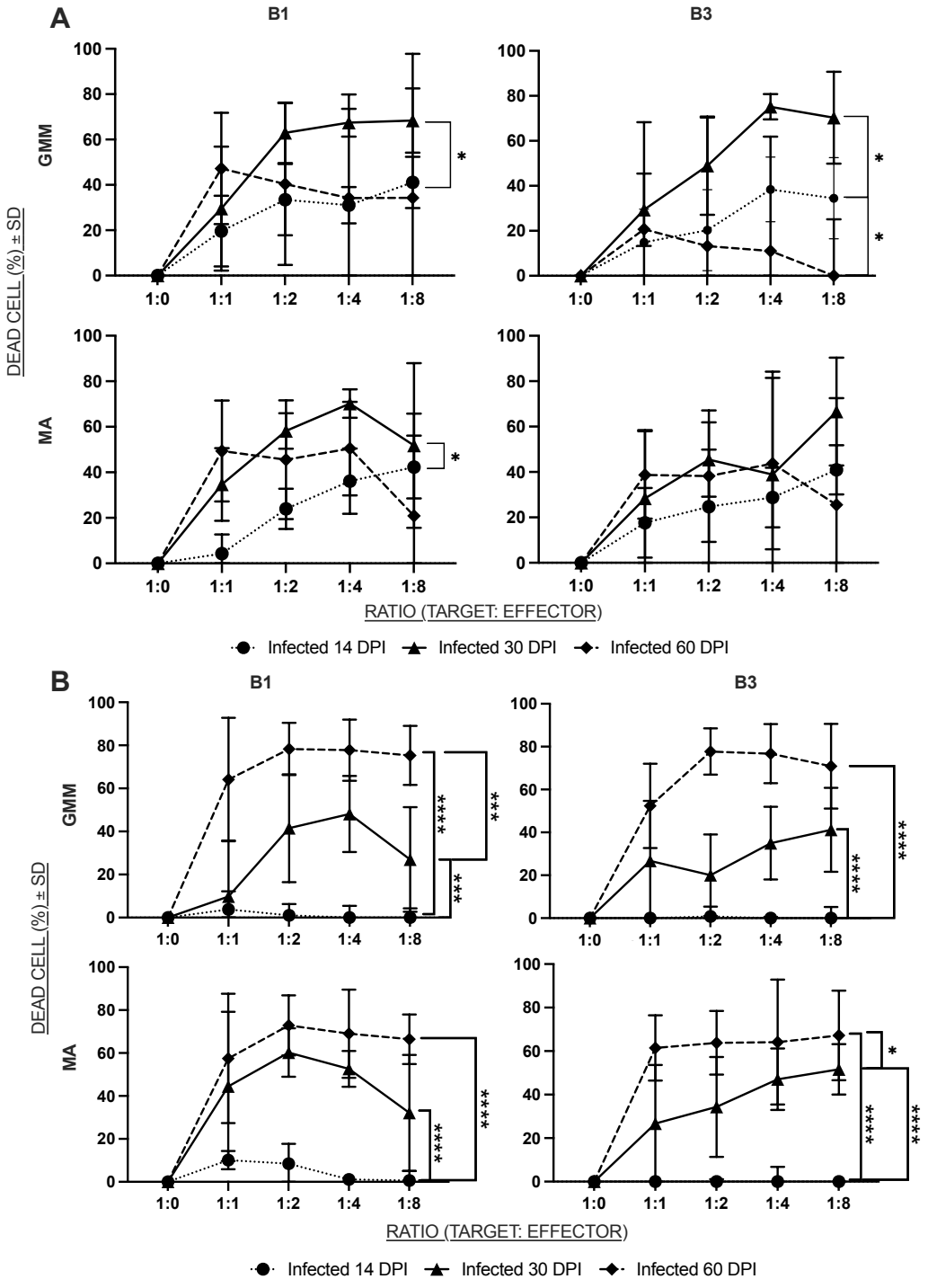

Supplemental figure S16. Kinetic evaluation of lipid antigen-specific and CD1-restricted cytotoxicity over the course of Mtb infection in the guinea pig. A-B) lung-derived (A) and spleen-derived (B) effector cells from Mtb-infected guinea pig were mixed at multiple increasing ratios with lipid-loaded CD1b-transfected fibroblasts (target cells). Cytotoxicity assessed as described in Materials and Methods. * $p \leq 0.05$, *** $p \leq 0.001$ and **** $p \leq 0.0001$; two-way ANOVA with a Sidak's correction

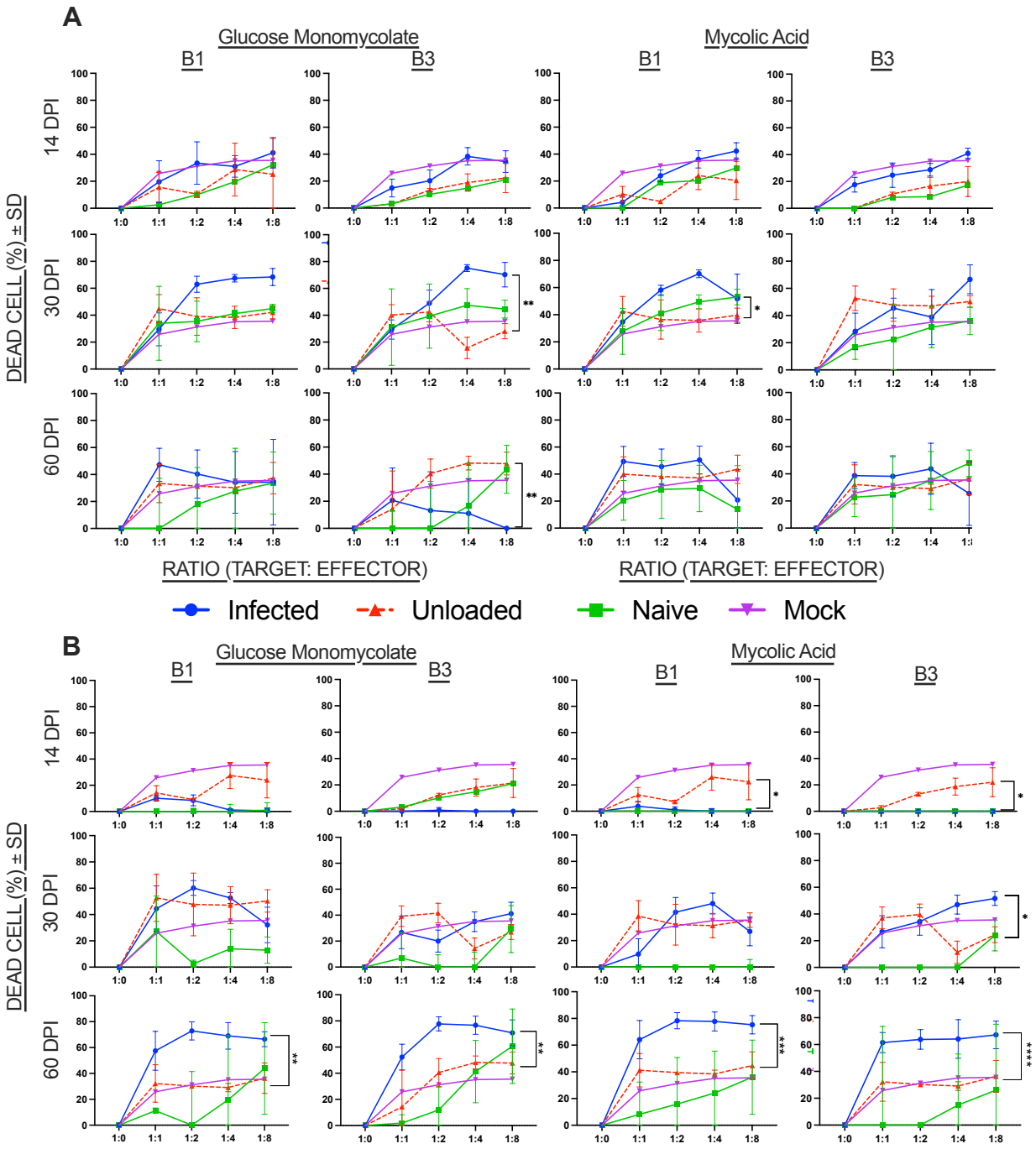

Supplemental Figure S17. Lipid-antigen specific and CD1-restricted cytotoxicity assay comparing all experimental and control conditions: Cytotoxic activity of lung- (A) and spleen-derived (B) cells examining lipid antigens, glucose monomycolate and mycolic acid, against transfected fibroblasts CD1b1, CD1b3 and mock control as target cells. All conditions are shown including lipid loaded conditions, unloaded conditions, mock-transfectant control conditions. * $p \leq 0.05$, ** $p \leq 0.01$, *** $p \leq 0.001$ and **** $p \leq 0.0001$; two-way ANOVA with a Sidak's correction

Table S6. Mean and standard deviation of all variables and timepoints from the cytotoxicity data. A) Data derived from lung effector cells; B) Data derived from splenic effector cells

A

			LUNG																	
			14 Infection		14 naïve		14 unloaded		30 Infection		30 naïve		30 unloaded		60 Infection		60 naïve		60 unloaded	
Cell line	Antigen	Ratio	Mean	SD	Mean	SD	Mean	SD	Mean	SD	Mean	SD	Mean	SD	Mean	SD	Mean	SD	Mean	SD
CD1b1	GMM	1:0	0	0	0	0	0	0	0	0	0	0	0	0	0	0	0	0	0	0
		1:1	19.6091	15.609	2.61428	0	15.6415	10.8508	29.5253	27.3185	33.9747	27.4434	44.8667	20.922	47.2212	24.5478	-0.8689	38.1028	33.3454	24.6189
		1:2	33.477	15.725	10.0462	0	10.5816	2.06358	62.9838	13.3288	35.4045	14.9911	39.0317	27.7796	40.3783	35.7001	17.8856	27.2916	31.3812	1.06273
		1:4	31.014	8.00707	19.6841	0	28.6795	19.5309	67.4247	6.14221	41.208	2.62528	38.4009	16.4952	34.1691	45.6812	27.6008	31.8421	30.2408	6.30168
		1:8	41.1017	11.2994	32.3205	0	25.2286	26.6007	68.3835	14.1934	44.9929	3.03054	42.1227	9.8963	34.2958	63.4917	33.5988	22.9877	37.3371	23.2202
	MA	1:0	0	0	0	0	0	0	0	0	0	0	0	0	0	0	0	0	0	0
		1:1	4.27804	8.45292	0.31573	0	10.2557	11.5435	34.6992	15.9543	27.7941	16.9481	42.5595	21.7976	49.3536	22.1657	20.6084	25.4687	40	22.161
		1:2	23.9551	8.86982	18.7716	0	4.87273	2.19533	58.2012	7.78459	41.2451	12.8633	36.4803	28.9422	45.5323	26.0878	28.7452	37.2446	38.2319	0.95663
		1:4	36.1109	14.3598	20.3665	0	24.126	20.7779	70.2151	6.28291	49.4822	5.16878	35.8231	17.1855	50.4373	20.5301	29.3536	29.7492	37.2053	5.67254
		1:8	42.3084	13.7973	29.7084	0	20.4548	28.299	51.7605	36.171	53.0311	5.75403	39.7006	10.3104	20.8365	44.9574	13.9163	56.0058	43.5932	20.9019
CD1b3	GMM	1:0	0	0	0	0	0	0	0	0	0	0	0	0	0	0	0	0	0	0
		1:1	14.8826	14.7226	3.222	0	3.01546	3.19805	29.3697	16.0666	31.175	28.4643	40.1072	15.6162	20.7473	47.5213	-6.4034	19.4447	14.3315	56.1001
		1:2	20.288	17.9707	10.1853	0	13.3424	2.47635	48.9516	21.8007	39.3237	23.8825	42.4891	14.9334	13.2069	57.1602	-0.015	34.706	40.5047	21.351
		1:4	38.4161	14.3949	14.7882	0	18.9484	12.8025	75.1528	5.64237	47.4723	12.3106	15.6298	15.8254	11.0076	50.8378	16.7415	31.275	48.1853	10.1086
		1:8	34.4978	18.0274	21.0433	0	22.315	21.7697	70.2636	20.4112	44.589	6.62536	28.1036	11.3552	-33.292	58.4304	43.6565	17.7321	47.8309	16.7413
	MA	1:0	0	0	0	0	0	0	0	0	0	0	0	0	0	0	0	0	0	0
		1:1	17.6042	12.3381	-3.3291	0	0.10507	3.29402	28.3595	30.0948	16.9091	9.11756	30.5192	18.1162	38.6993	19.2794	22.7731	14.2257	18.3033	53.4992
		1:2	24.6792	20.2925	8.21944	0	10.7419	2.55067	45.4916	16.388	22.4355	26.0591	33.2824	17.324	38.1922	28.9648	24.7263	28.7522	43.263	20.3611
		1:4	28.7637	10.5547	8.70569	0	16.5162	13.1867	38.8598	45.3376	31.4039	14.9169	2.12333	18.3588	43.7138	37.754	35.0934	21.4244	50.5876	9.6399
		1:8	40.9687	8.7084	17.2152	0	19.9838	22.423	66.6376	23.7506	36.0578	10.0773	16.5939	13.173	25.5715	46.9922	47.8643	9.7258	50.2495	15.9651

B

			SPLEEN																	
			14 Infection		14 naïve		14 unloaded		30 Infection		30 naïve		30 unloaded		60 Infection		60 naïve		60 unloaded	
Cell line	Antigen	Ratio	Mean	SD	Mean	SD	Mean	SD	Mean	SD	Mean	SD	Mean	SD	Mean	SD	Mean	SD	Mean	SD
CD1b1	GMM	1:0	0	0	0	0	0	0	0	0	0	0	0	0	0	0	0	0	0	0
		1:1	10.1111	4.23109	-1.7379	2.95077	14.1698	11.0401	44.4526	34.7147	27.2067	26.8844	52.7049	17.9476	57.4925	30.1171	11.2495	2.00382	32.2456	25.0251
		1:2	8.47243	9.19487	-0.6102	4.37608	9.02157	2.09959	60.2267	11.2807	2.61754	2.6493	47.6994	23.8303	72.8854	13.9946	-6.6552	48.0918	30.249	1.08027
		1:4	1.16583	2.6049	-0.0545	7.75059	27.4352	19.8717	52.6508	8.33768	13.9381	14.8312	47.1583	14.1501	69.021	20.5294	19.6222	49.5491	29.0897	6.40566
		1:8	0.62323	4.44546	1.03508	8.05877	23.9241	27.0647	32.1283	26.9835	12.9857	10.0021	50.351	8.48937	66.4448	11.5296	43.8386	35.3402	36.3031	23.6033
	MA	1:0	0	0	0	0	0	0	0	0	0	0	0	0	0	0	0	0	0	0
		1:1	3.80496	8.42981	-1.9233	4.23183	12.5333	11.2506	9.80049	25.9947	-32.48	2.78924	38.6025	23.2992	64.1284	28.6907	8.21626	24.1403	41.2197	21.7105
		1:2	1.00025	5.31788	-2.3952	2.10414	7.28697	2.13962	41.5249	25.042	-23.98	3.88512	32.1045	30.936	78.3206	12.1364	15.8897	34.8375	39.4875	0.93719
		1:4	-0.6652	6.09879	-3.6554	3.32108	26.0516	20.2506	48.1283	17.6593	-16.426	6.75607	31.402	18.3694	77.7618	14.1947	24.0847	31.4883	38.4818	5.55723
		1:8	-1.1827	5.49473	-2.4784	4.38885	22.4736	27.5808	26.9974	24.306	-3.1253	8.8547	35.5467	11.0207	75.3033	13.7005	36.0047	27.7754	44.7398	20.477
CD1b3	GMM	1:0	0	0	0	0	0	0	0	0	0	0	0	0	0	0	0	0	0	0
		1:1	-3.3093	5.7438	3.222	0	1.91963	3.23418	26.7302	27.99	6.98118	19.7248	39.2069	15.851	52.3801	19.6502	1.8456	6.41719	14.3315	56.1001
		1:2	0.79172	4.59898	10.1853	0	12.3632	2.50433	20.0115	19.0056	-1.0779	10.568	41.6246	15.1579	77.7262	10.7754	11.9289	17.4887	40.5047	21.351
		1:4	-6.045	6.7116	14.7882	0	18.0326	12.9471	34.9759	16.9582	-1.2052	12.72	14.3616	16.0633	76.7218	13.7983	41.3122	23.8284	48.1853	10.1086
		1:8	-3.7987	8.97203	21.0433	0	21.4372	22.0157	41.2365	19.5929	29.3345	18.1321	27.0229	11.5259	70.8727	19.7625	60.691	28.4716	47.8309	16.7413
	MA	1:0	0	0	0	0	0	0	0	0	0	0	0	0	0	0	0	0	0	0
		1:1	-4.6703	5.15971	-6.2615	8.12079	2.70707	3.20822	26.6981	26.8977	-16.402	7.03884	37.0823	16.405	61.4476	15.0213	-6.517	80.0977	-18.686	77.7215
		1:2	-4.3695	5.53536	-5.93	4.30318	13.0668	2.48423	34.3628	22.9591	-11.56	7.45675	39.5845	15.6876	63.8213	14.6239	-43.842	41.9407	17.5748	29.5798
		1:4	-3.1571	9.95977	-5.0598	6.08641	18.6907	12.8432	47.0582	14.1404	-7.6395	8.63019	11.3686	16.6247	64.1487	28.7207	14.9828	37.9799	28.2156	14.0045
		1:8	-8.7668	5.59275	-3.1832	0.08372	22.068	21.8389	51.6149	11.5587	23.9237	11.576	24.4724	11.9287	67.1773	20.5797	26.0056	49.0862	27.7245	23.1935

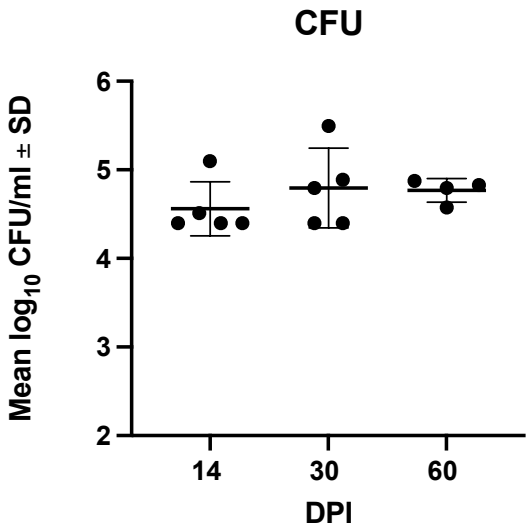

Supplemental Figure S18. Mtb burden in lung at all experimental endpoints. CFU burdens derived from lung tissue at days 14, 30 and 60 post-infection. CFUs were obtained and calculated via established lab protocols and are consistent with a standard low-dose aerosol guinea pig exposure.

Table S7. Chromogenic IHC protocol

CD1 Chromogenic Protocol:

Step number	Process	Time (mins)
1	Peroxide block	10
2-8	Bond wash solution	-
9	Block (2.5% goat serum)	10
10	Primary antibody	30
11-13	Bond wash solution	-
14	Post primary HRP antibody	10
15-25	Bond wash solution	-
26	Deionized water	-
27	Polymer (Leica)	10
28-31	Bond wash solution	-
32	Deionized water	-
33	Mixed DAB refine (Leica)	0
34	Mixed DAB refine (Leica)	10
35-40	Deionized water	-
41	Bond DAB enhancer (Leica)	5
42-44	Deionized water	-
45	Hematoxylin	5
46	Deionized water	-
47	Bond wash solution	-
48	Hematoxylin DAKO A	2
49-52	Deionized water	-

+ all volumes are dispensed at 150ul per step, all steps performed at room temp

Table S8. Multiplex fluorescence IHC protocol

IHC CD1 Opal Multiplex:

Step number	Process	Time (mins)
1		
2	Kit water (Leica)	0
3-4	Bond wash solution	-
5	H202	25
6-8	Bond wash solution	-
9	Block (2.5% goat serum)	5
10	Primary antibody	30
11-13	Bond wash solution	-
14	Secondary HRP antibody	10
15-19	Bond wash solution	-
20	Opal Fluorophore 1 (Akoya)	0
21	Opal Fluorophore 1 (Akoya)	10
22-25	Bond wash solution	-
26	Bond ER 1 solution (Leica)	0
27	Bond ER 1 solution (Leica)	0*
28	Bond ER 1 solution (Leica)	20*
29	Bond ER 1 solution (Leica)	0
30-35	Bond wash solution	-
36	H202	10
37-39	Bond wash solution	-
40	Block (2.5% goat serum)	5
41	2nd primary antibody	30
42-44	Bond wash solution	-
45	Secondary HRP antibody	10
46-50	Bond wash solution	-
51	Opal Fluorophore 2 (Akoya)	0
52	Opal Fluorophore 2 (Akoya)	10
53-59	Bond wash solution	-
60	DAPI	11
61-65	Bond wash solution	-

+ all volumes are dispensed at 150ul per step

*denotes 95C temperature incubation, all other steps are completed at room temp

Supplemental material for chapter 3:

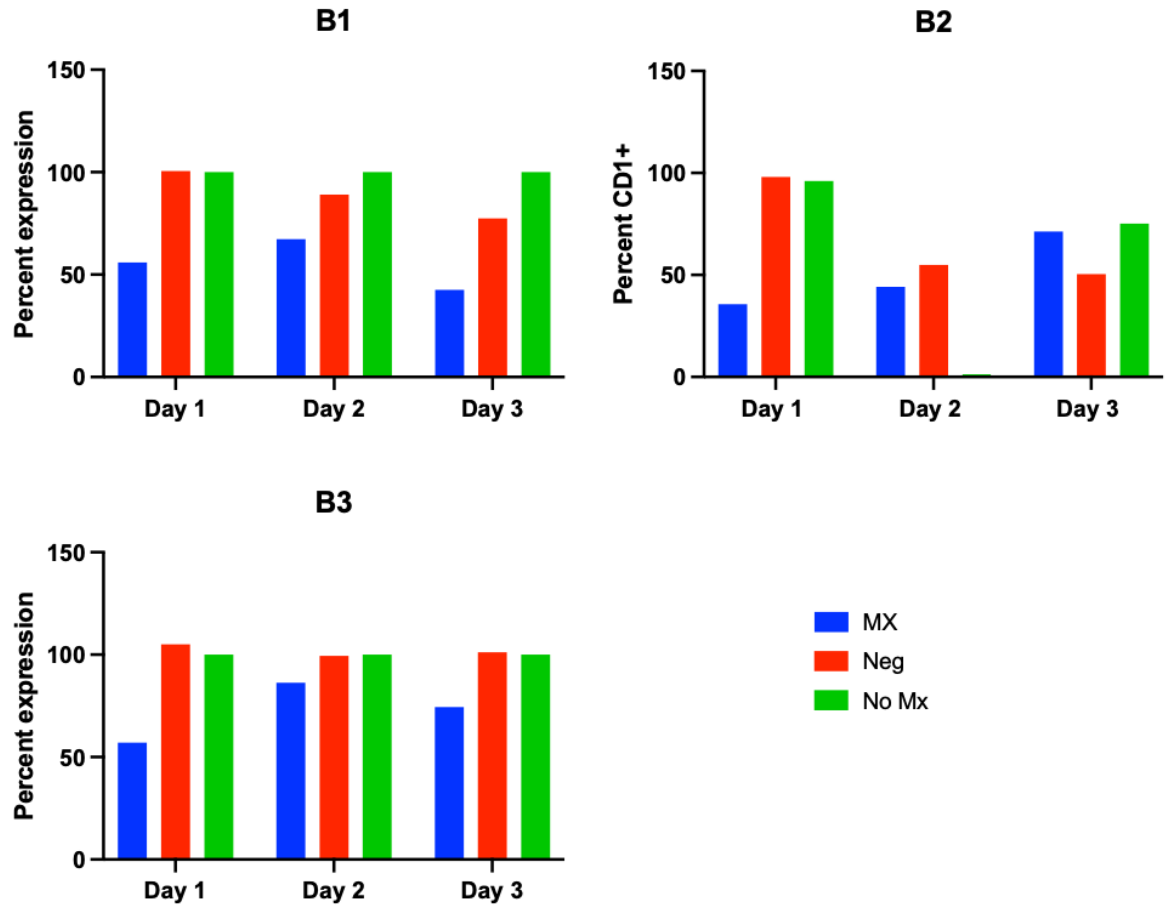

Supplemental Figure S19. Morpholino knockdown of CD1b transfectant fibroblasts. A combination of CD1b1-2 and CD1b3 morpholinos were administrated to CD1b ortholog specific transfectant fibroblasts. After initial dosing fibroblasts were evaluated for three days for CD1 expression via flow cytometric analysis. Negative control morpholino consists of non-complementary scramble control provided from the company, Genetools, and ensure no off-target effects.

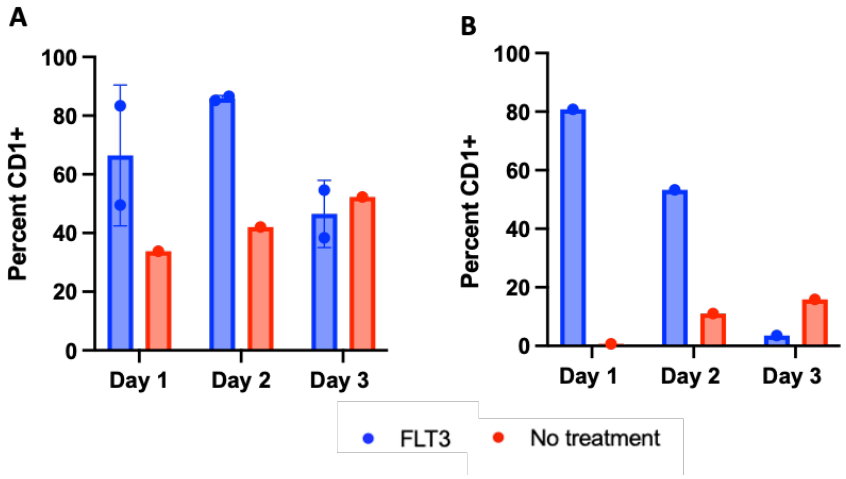

Supplemental figure S20. FLT3-L CD1 upregulation. FLT3-L was administered to bone marrow derived macrophages (A) and to Bronchioalveolar cells (B). After administration cells were evaluated every day for three days to assess CD1 expression compared to non FLT3-L treated controls.

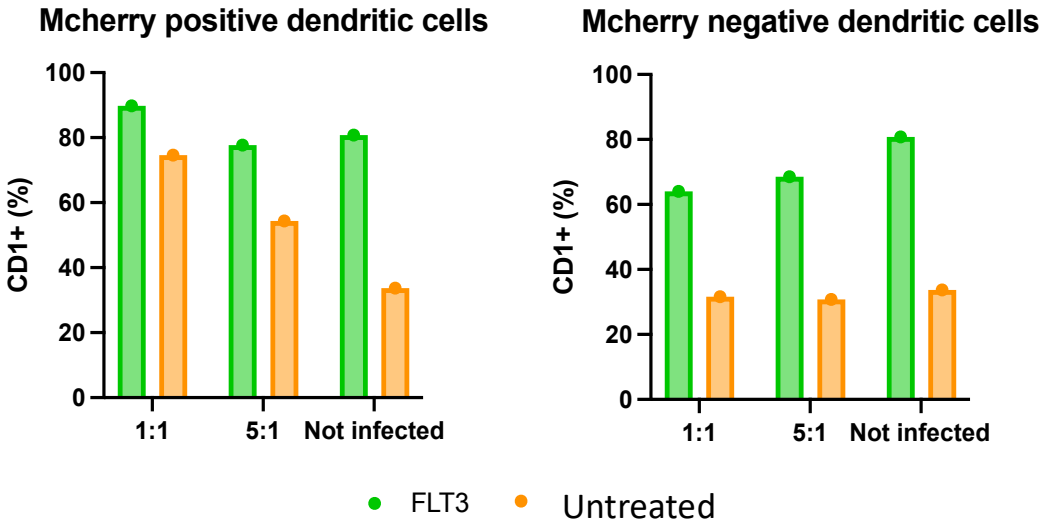

Supplemental figure S21. FLT3-L CD1 stimulation in an invitro infection. Cells were infected with mCherry Mtb and either stimulated with FLT3-L or not treated. Cells were assessed for CD1 expression via flow cytometric analysis. Cells were gated on mCherry, infected vs non-infected, and then CD1 expression was assessed based on infectious status.

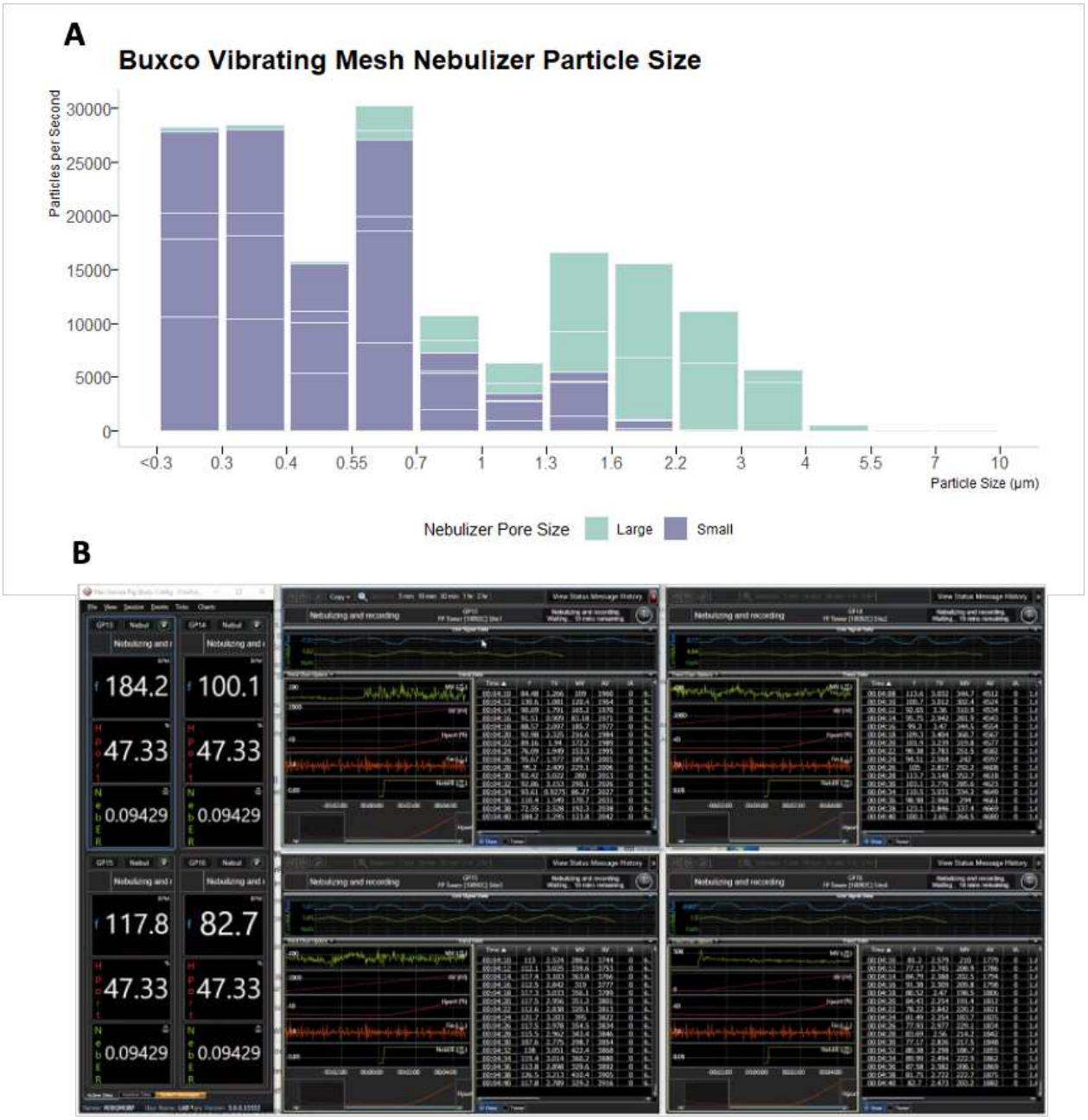

Supplemental figure S22. Particle size and parameters of Buxco inhalation tower. A) particle size distribution made by the small pore nebulizer as measured by the tower's particle size analyzer. Particles measuring an average of 1um in diameter are the correct size for penetrating into the alveolar spaces. B) Control panel of tower during an exposure. Allows for monitoring of breaths per minute, chamber humidity, particle concentration, and accumulated inhalation volume of each animal.

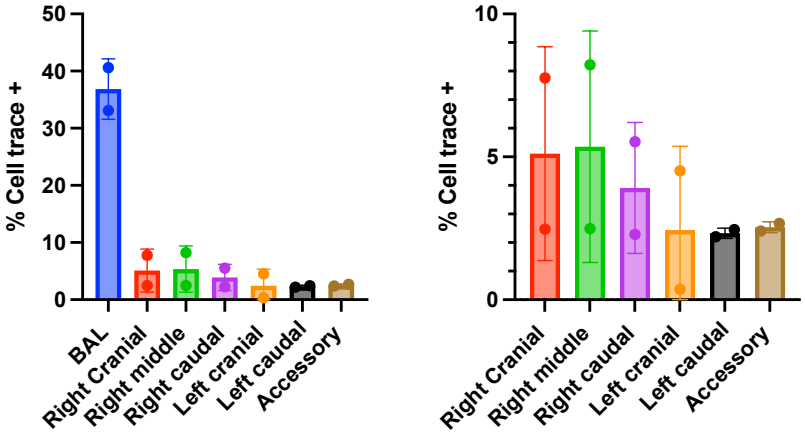

Supplemental figure S23. Cell trace violet intrapulmonary administration. CellTrace violet dye was administrated intrapulmonarily to two guinea pigs via the Buxco tower. Distribution of the dye was assessed via flow cytometric analysis for cell trace positive cells. A) Cell trace positive BAL derived cells and homogenized lung parenchyma from each individual lung lobe. B) Cell trace positive cells from only homogenized lung lobes.

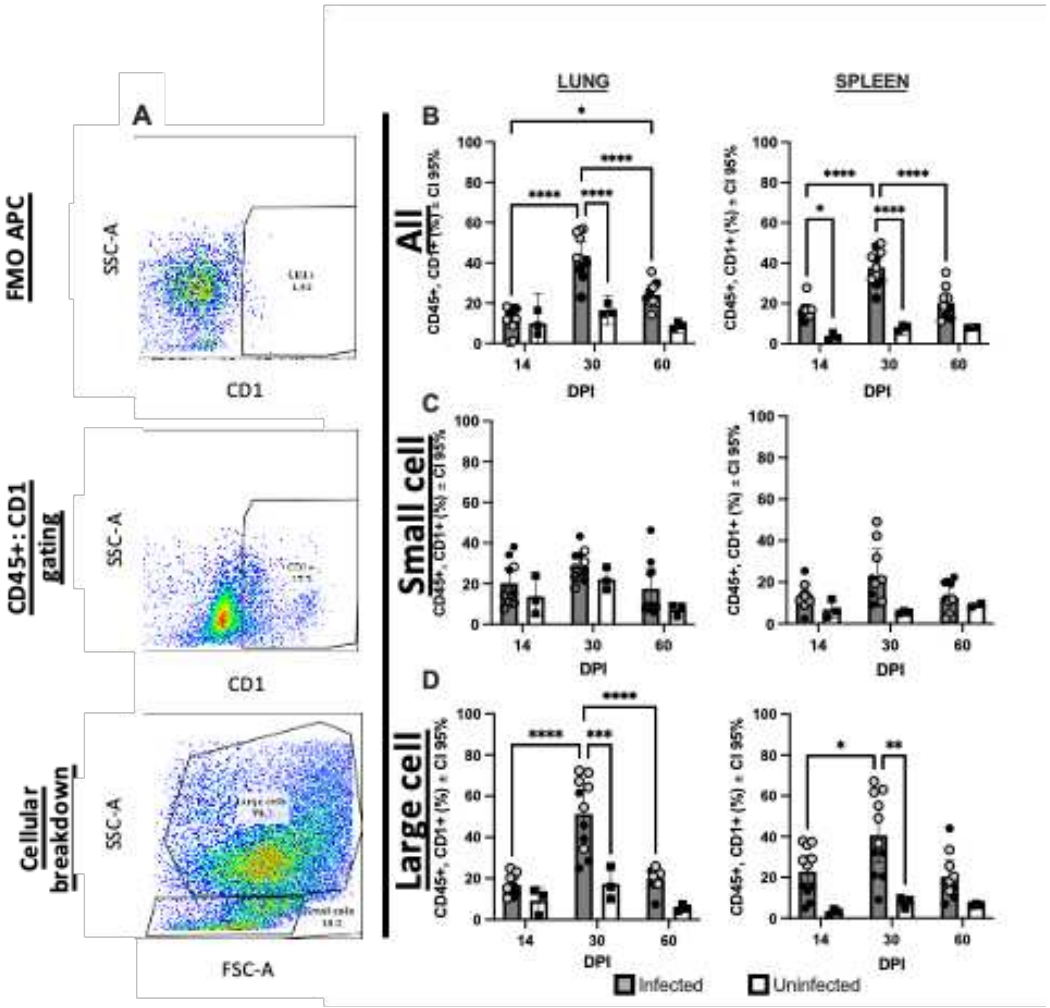

Supplemental figure S24. CD1 complex expression during Mtb infection. Flow cytometric analysis of antigen presenting cells at 14-, 30- and 60-days post infection (DPI). Cells were gated for, live, CD45 + cells and evaluated for overall CD1 expression via 1B12 CD1 antibody. Open symbols represent the first experimental set, closed symbols represent the second experimental set. Naïve time matched controls were performed only in experiment two. A) Gating of CD1 positive cells (top fluorescence minus one, middle single-color control, and lower graph strategy for segregating small vs large CD45+ cells, bottom graph. B-C) Percent CD1 positivity from both lung and spleen derived cells. Graphs represent All CD45+ cells (B), delineated large cell populations (C), and delineated small cell populations (D). Statistical significance: * P<0.05, **P<0.01, ***P<0.001, and **** P<0.0001.

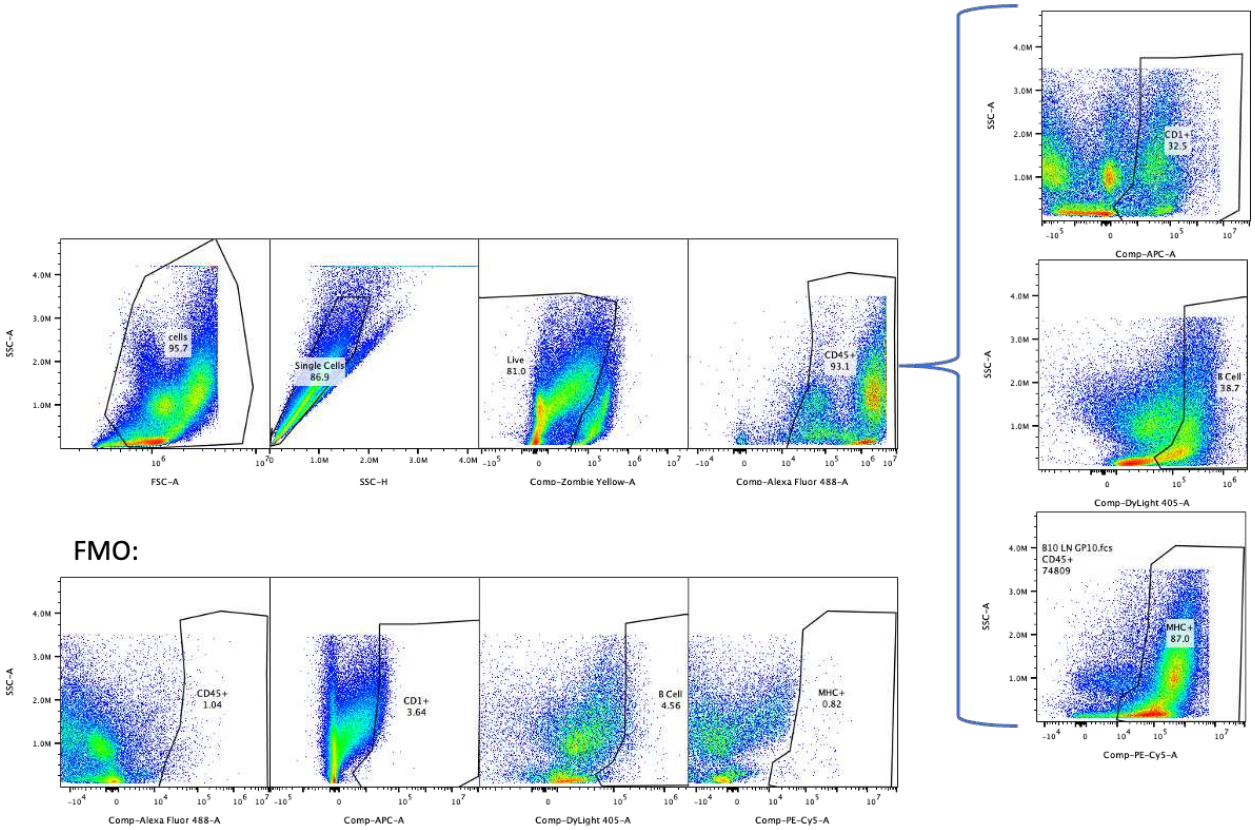

Supplemental figure S25. CD1 expression gating strategy. Initial Gating focused on isolating cells and single cells. Then utilizing FMO and single-color gating was done to isolate CD45+ and then gating on CD1, B cell and MHC II. Cellular populations were further divided by small cell and large cell populations

CD1B1 Gene block: (PCR product: 129)

```
  1 atgctgctcg tggcactggc attgcttgca tttctcttcc ctgctggtga cactcagaat
 61 gccttacagt ggccaacttc tgtccatggc atccaaatct catccttttt caaccatacc
121 atggcacaaa gtcgatgctc aggctggttg tcccgcagat ctccaggaaa tatggagctt
181 ggtagctttg acagcgacac aggcactatc atatttaaga aaccctggtc taaagcaaac
241 ttcagcaatg aagaggtttt ggagttggag gagctatttc aagtctacat gttgggattc
301 atcagagaag tacaggaacg tatgagcgat ttccagatgg aatatccctt tgagatccag
361 ggcattgcag gctgtgaact gatttctgga ggaaccattg atttcttcct gagaggagct
421 ttagagggac tagatttctt gagtattaag aattctacat gttggcctgc cccagaaggt
481 ggcaccaagg caaaaaaatt
```

CD1B2 Gene block: (PCR product: 225)

```
  1 attttggaaa tggaggagtt atttcgactc tacttcttag gatttgttaa agaagtccag
 61 gaacttgtca gtgatttcca gctggaatat ccttttgaga tccagggcat tgcaggctgt
121 gagttgcatt ctggaggagc cattgtaagc ttcttgatgg gagctataga aggactgcat
181 ttcatgagca tcaataatta ttcatgtttg tcccgcagat ctccacctgc cccagaaggt
241 ggtaccaggg cacagaaatt ctgtgcacta atcttacagt acaaaggaat ttgtgatatt
301 gtggaaaatc tcctcacaaa agtttgcccc agatatctga tgagtgtcct agaagctggg
361 aaggcagctc tgcagaagca cgtgaagcct gaggcctggc tatcccaggg acccagcccc
421 gagcctggct atctgcagct ggtgtgccac gtctctggct tctacccaaa gcctgtgtgg
481 gtgatgtgga tgagaggtga
```

CD1B3 Gene block: (PCR product: 171)

```
  1 tgggtgaaat atcaactctc aggctggttg ggagatttgc agattcatgg catggacagt
 61 gattcaggca ctgccatatt cctgaagccc tggtctaagg gcaacttcag caatgaagaa
121 atgtctgaag tggtggagct atttcgggtc tatatcgttg cattcattcg agaaacaaaa
181 gcccacgtga atgccttgca gatggaatac tcccgcagat ctccaccttt tgagatccag
241 ggcattgcag gctgtgagct gcattctgga ggtgccattg taagcttttt gcaaggagcc
301 tttggaggac tggactttgt gagtttcaag aattcttctt gtgttcctgc cccagaaggt
361 ggcagcaggg cacagacagt gtgcaaacta cttgctccat atcatgatat cttctacact
421 gtggagaagc tgctgtatga aacctgtcct caatatctct tgggtgtcct tcaagcagga
481 aaggcagatc tacacaggca
```

CD1B4 Gene block: (PCR product: 125)

```
  1 atgctgctcc tggccctggc atttttttc ccagctggtg acactcagaa cgttttgccg
 61 gggaaaattt ctttctatgg catccaaatc tcaacgtttt tcaaccatac cgtggtagag
121 aatcgaggat caggctggtt gggagatatg gagattagca gctgggacag tgaaaaagaa
181 actatcatat ttcggaaacc ctggtctaaa tcccgcagat ctccaggcaa cttcagcaat
241 gacgagattt tggaggtgga agagatattt caagtctact tctttggatt cgtcagagaa
301 gcccagaaac atatgagtga tttccaggtg gaataccct ttgagattca ggtcatctca
361 ggctgtgagg tgaactctca cagatccttt gattacttca tgagggtagc agtaaaggga
421 ttggatctcc tgagcatcaa gaatcattca tgttggcctg ccccagaagg tgtttctaga
481 gcacaggaaa tctggacatt
```

Segment gene Rv0733 in Mycobacterium tuberculosis H37Rv:

Tcccgcagatctcca

Supplementary figure S26. CD1 ortholog CD1 gene blocks. Gene block were created from NIH genebank guinea pig CD1b ortholog annotation. Gene blocks were utilized to ensure created CD1 ortholog specific primer sets had no cross ortholog amplification. Yellow highlighting indicates regions of primer sequences. Purple highlighting indicated inserted Mtb sequence to assess for any contamination of PCR run.

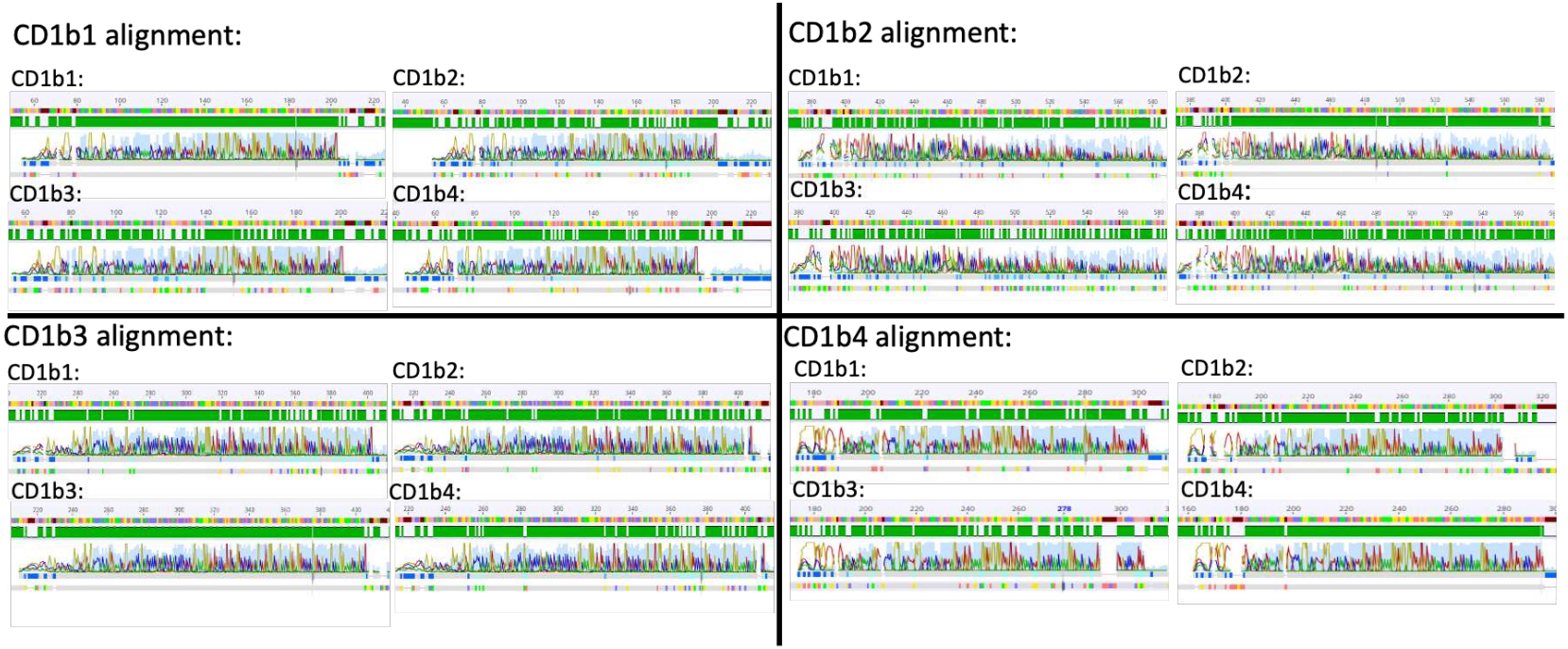

Figure S27. CD1 transfectant fibroblast amplicon product alignment to specific CD1b ortholog sequences. CD1 specific primers amplified CD1 ortholog specific transfected fibroblasts cDNA. Amplified products were run on an agarose gel, isolated and purified. Products were sent for sequencing and aligned back to annotated CD1 specific isoforms from NIH genbank.

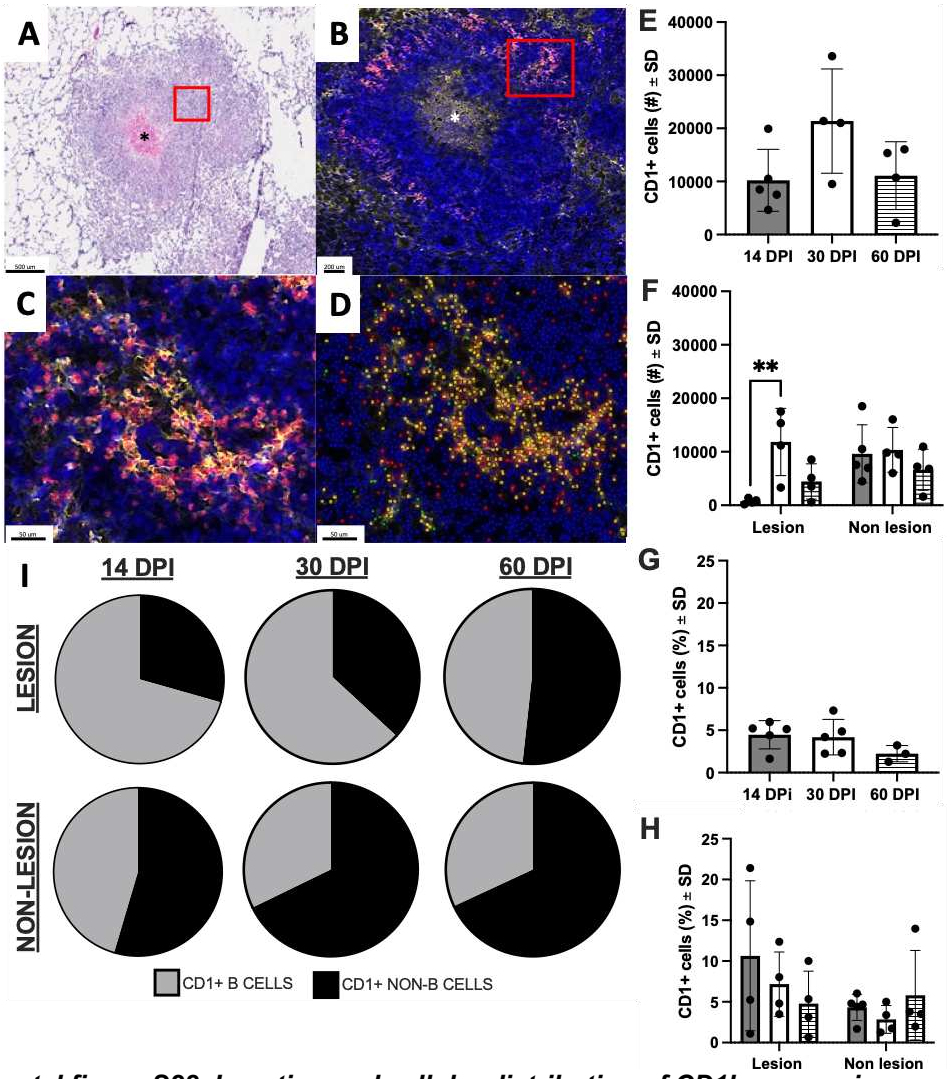

Supplemental figure S28. Location and cellular distribution of CD1b expression over the course of Mtb infection. Fresh frozen sections of lung and spleen at 14, 30 and 60 days post-infection (DPI) were labeled with antibodies targeting CD1b (6B5, Opal 520) or the B cell transcription factor, PAX5 (clone 24, Opal 690), using Opal fluorochrome chemistry and nuclear counterstain, DAPI. (A-D) Representative sections of a lung granuloma demonstrating: fresh frozen low magnification HE section (A) to low magnification serial sectioned multiplex IHC section (B) to higher magnification of CD1+, Pax5+ region (B) and the high magnification section with overlayed visiopharm analysis software (D). Asterisk in sections represent a region of necrosis, the red box indicates the region of higher magnification in C-D. For Visiopharm analysis, all nuclei in the tissue were detected and then labeled based on nuclear and membranous staining of the associated cells. Labels include: Red-B cell (pax5+, CD1-), yellow- CD1+ B cells (PAX5+, CD1+), green- CD1+ other cells (CD1+, PAX5-), and blue- negative cells (CD1-, PAX5-). (E-F) Visiopharm derived quantitative CD1+ cell numbers in (E) whole lung tissue and (F) broken into lesion and non-lesion tissue at 14, 30, and 60 days post infection. (G-H) Percentage of CD1+ cells In (G) whole lung and (H) broken into lesion and non-lesion at 14, 30, and 60 days post infection. I) Breakdown of CD1 positive B cell and non-B cells in lesion vs normal tissue **P<0.01; one-way ANOVA with a tukey correction.

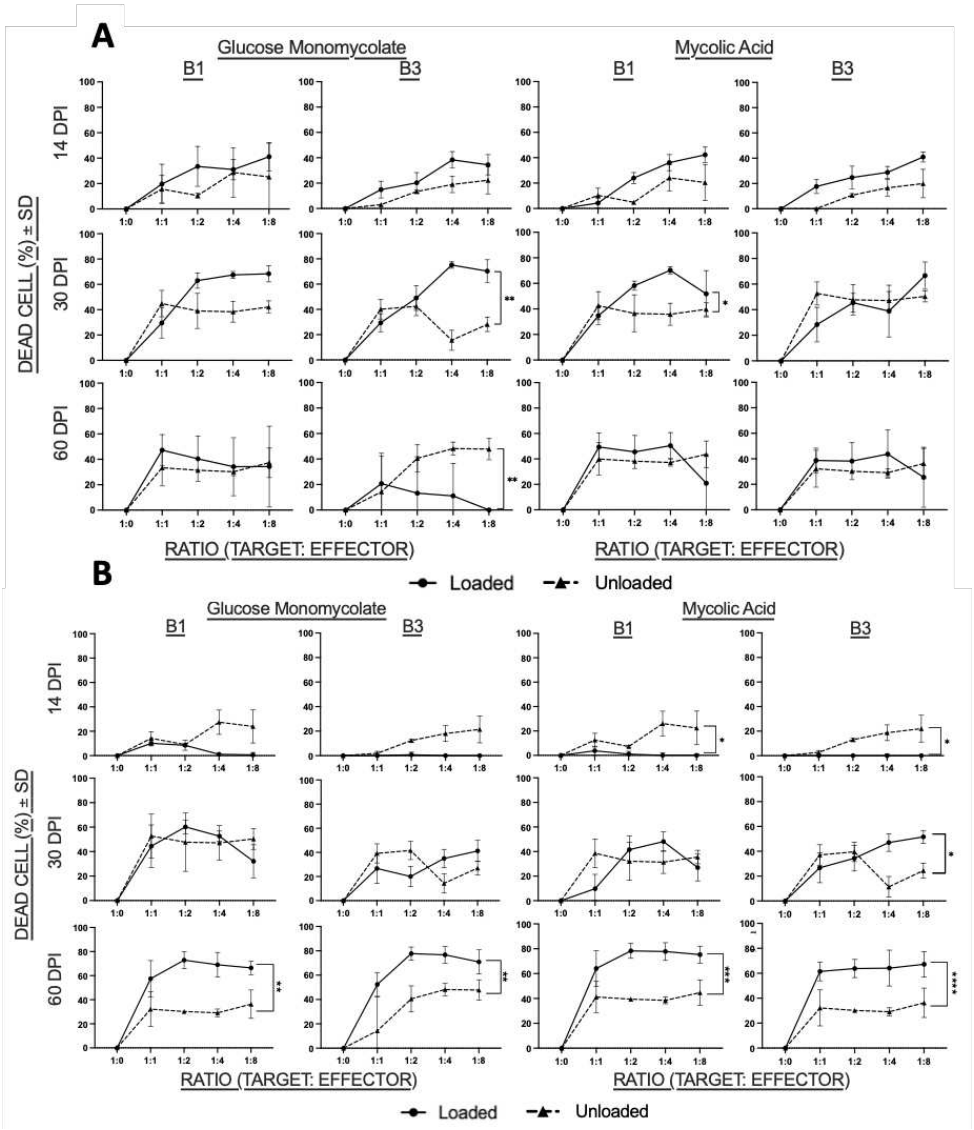

Supplemental figure S29. Lipid antigen-specific and CD1b-restricted cytotoxic activity among cells isolated from Mtb-infected lung and spleen. Guinea pig OT1 fibroblast cell line transfected with CD1b1 or CD1b3 were labeled with CellTrace Violet tracking dye then mock-loaded (unloaded) or loaded with synthetic glucose monomycolate or mycolic acid Mtb lipids to be used as target cells in this cytotoxicity assay. Target cell fibroblasts were incubated with non-adherent cells isolated from the lung or spleen of Mtb-infected or naïve guinea pigs at 14, 30 and 60 days post-infection (DPI) at ratios ranging from 1:0 to 1:8 target:effector cells. Fibroblasts in co-culture were identified by flow cytometric gating on CTV-labeled cells and viability assessed using permeability dye exclusion. Cytotoxicity is expressed as the proportion dead, permeable CTV-labeled target fibroblasts. A) Fibroblasts incubated with effector cells derived from the lung. B) Fibroblasts incubated with effector cells derived from spleen. All control measures and cytotoxicity comparisons are comprehensively shown in supplemental figure 9 & 10. * P<0.05, **P<0.01, and ***P<0.001; two-way ANOVA with a Sidak's correction.

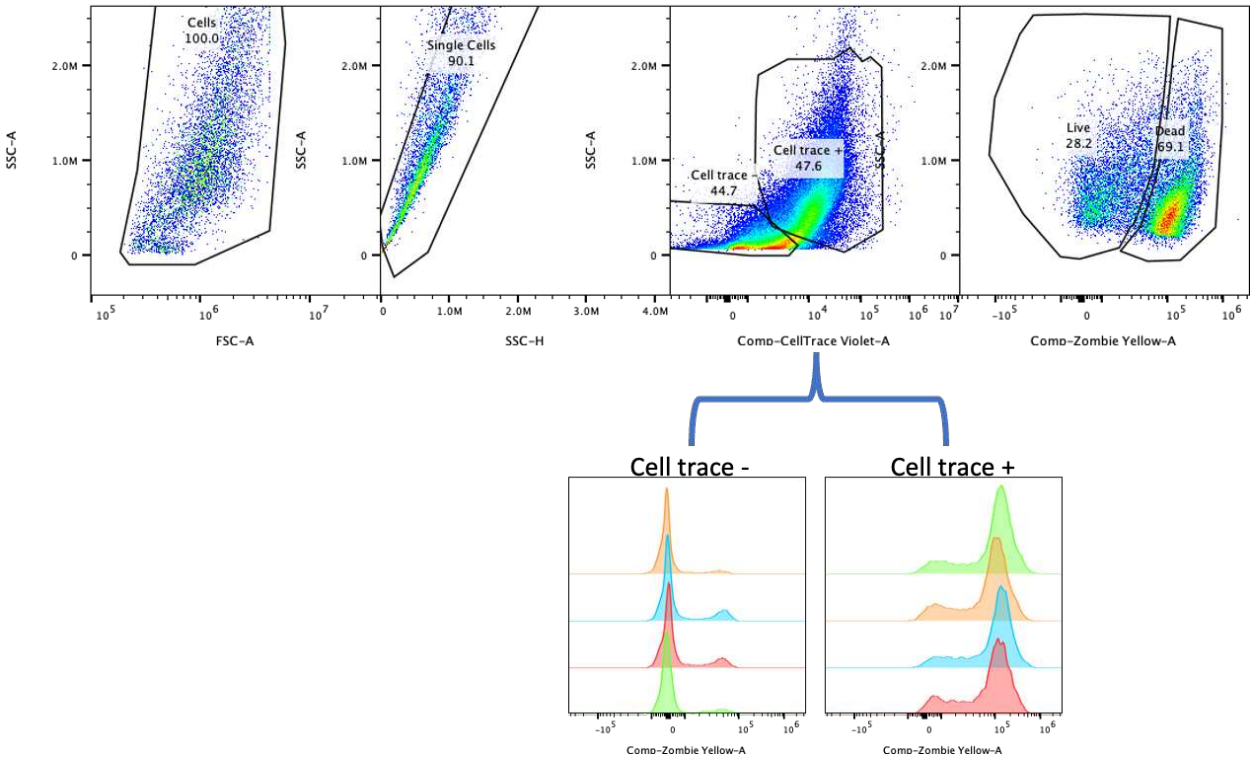

Supplemental Figure S30. CD1 cytotoxicity gating strategy. Initial Gating focused on isolating cells and single cells. Single color cell trace violet is utilized to isolate guinea pig fibroblasts transfectants. Cell trace positive cells, target cells, are assessed for overall viability in all samples. Histograms demonstrate a representative sample of viability with cell trace negative cells (effector cells) and cell trace positive cells (target cells) in differing ratio conditions.

TABLES:

Supplemental table S9. CD1 ortholog specific morpholino sequences

Morpholino	**Sequence**
CD1b1-2	5' AAAATACCAGTTCCAGCAGCAGCAT 3'
CD1b3	5' GCAATGCCAGTACCAGGAGCAGCAT 3'
Negative	5' CCTCTTACCTCAGTTACAATTTATA

Supplemental table S10. Inhalation exposure setting on Buxco inhalation tower

Parameter	**Condition**
Nebulizer	Buxco small pore nebulizer
Liters/min	300-400 L/min
Humidity	50-70% humidity at port
Particle size	Average: <1um
Run time	10-20 minutes
Volume nebulized	1.3 mls
Animal per run	6

Supplemental table S11. Flow cytometry antibodies

Antibody	Fluorophore	Company, clone
CD45	FITC or PE	Biorad, IH-1
MHC-II	PE-cy5.5	IVA12
Anti guinea B cell	Dylight 405	Biorad
CD1	PE-Texas red or APC	1B12

Supplemental table S12. PCR primers

CD1b Isoform	Sequence
CD1b1 forward	ACA GTG GCC AAC TTC TGT CC
CD1b1 Reverse	ATA GTG CCT GTG TCG CTG TC
CD1b2 Forward	GAG TTG CAT TCT GGA GGA GC
CD1b2 Reverse	CCC AGC TTC TAG GAC ACT CA
CD1b3 Forward	ACA AAA GCC CAC GTG AAT GC
CD1b3 Reserve	GTC CAG TCC TCC AAA GGC TC
CD1b4 Forward	GGC TGG TTG GGA GAT ATG GA
CD1b4 Reserve	TTC TGG GCT TCT CTG ACG AA

Supplemental table S13. Chromogenic immunohistochemistry protocol

Step number	Process	Time (mins)
1	Peroxide block	10
2-8	Bond wash solution	-
9	Block (2.5% goat serum)	10
10	Primary antibody	30
11-13	Bond wash solution	-
14	Post primary HRP antibody	10
15-25	Bond wash solution	-
26	Deionized water	-
27	Polymer (Leica)	10
28-31	Bond wash solution	-
32	Deionized water	-
33	Mixed DAB refine (Leica)	0
34	Mixed DAB refine (Leica)	10
35-40	Deionized water	-
41	Bond DAB enhancer (Leica)	5
42-44	Deionized water	-
45	Hematoxylin	5
46	Deionized water	-
47	Bond wash solution	-
48	Hematoxylin DAKO A	2
49-52	Deionized water	-

+ all volumes are dispensed at 150ul per step, all steps performed at room temp

Supplemental table S14. Opal multiplex immunohistochemical protocol

Step number	Process	Time (mins)
1		
2	Kit water (Leica)	0
3-4	Bond wash solution	-
5	H202	25
6-8	Bond wash solution	-
9	Block (2.5% goat serum)	5
10	Primary antibody	30
11-13	Bond wash solution	-
14	Secondary HRP antibody	10
15-19	Bond wash solution	-
20	Opal Fluorophore 1 (Akoya)	0
21	Opal Fluorophore 1 (Akoya)	10
22-25	Bond wash solution	-
26	Bond ER solution (Leica)	0
27	Bond ER solution (Leica)	0*
28	Bond ER solution (Leica)	20*
29	Bond ER solution (Leica)	0
30-35	Bond wash solution	-
36	H202	10
37-39	Bond wash solution	-
40	Block (2.5% goat serum)	5
41	2nd primary antibody	30
42-44	Bond wash solution	-
45	Secondary HRP antibody	10
46-50	Bond wash solution	-
51	Opal Fluorophore 2 (Akoya)	0
52	Opal Fluorophore 2 (Akoya)	10
53-59	Bond wash solution	-
60	DAPI	11
61-65	Bond wash solution	-

+ all volumes are dispensed at 150ul per step

*denotes 95C temperature incubation, all other steps are completed at room temp